PROCESSING INTEGRAL-SKIN POLYOLEFIN FOAMS IN SINGLE-CHARGE ROTATIONAL FOAM MOLDING

by

Remon Pop-Iliev

A thesis submitted in conformity with the requirements
for the degree of Doctor of Philosophy,
Graduate Department of Mechanical & Industrial Engineering,
University of Toronto

National Library of Canada
Acquisitions and Bibliographic Services
395 Wellington Street
Ottawa ON K1A 0N4
Canada

Bibliothèque nationale du Canada
Acquisitions et services bibliographiques
395, rue Wellington
Ottawa ON K1A 0N4
Canada

Your file Votre référence

Our file Notre référence

0-612-78048-1

Canada

PROCESSING INTEGRAL-SKIN POLYOLEFIN FOAMS IN SINGLE-CHARGE ROTATIONAL FOAM MOLDING

Remon Pop-Iliev
Degree of Doctor of Philosophy, 2002
Department of Mechanical and Industrial Engineering
University of Toronto

ABSTRACT

This thesis focuses on establishing the scientific and engineering foundations for gaining a fundamental understanding of the mechanisms and critical parameters governing the processing of integral-skin low-density polyolefin foams in rotational foam molding. The presented research is particularly intended to broaden the knowledge in the field of manufacturing adjacent, but clearly distinct, layers of non-cellular and cellular structures, consisting of identical or compatible plastic grades, using a single-charge processing concept. Although this technology is beneficial for the efficacy of the molding process and the structural homogeneity of the moldings, its optimization raised a fairly large number of fundamental issues that had to be resolved through further research. In this context, an attempt has been made to establish rigorous, experimentally validated, theoretical models that describe the phenomena identified as the fundamental challenges of this technology. The major contributions of this thesis include: (i) optimization of the single-charge rotational foam molding process for the manufacture of both PE/PE and PE/PP integral-skin cellular composites, (ii) development of a two-step oven temperature profile that prevents the foamable resins invading the solid skin layer and ensures that skin formation always completes prior to the activation of the foamable resin, (iii) fundamental study of the adherence behavior of powders and foamable pellets to a high-temperature rotating mold wall, (iv) fundamental study of the lifespan of CBA-blown bubbles in non-pressurized non-isothermal polymer melts using hot-stage optical microscopy and digital imaging, (v) development of a detailed theoretical model involving diffusion, surface tension, and viscosity to simulate the observed foaming mechanism, and (vi) fundamental study of the rotofoamablility of polyolefin resins using both dry blending and melt compounding based methods and characterization of rheological and thermal properties.

To Lydia and Bianca & Romina,
my beloved wife and daughters

ACKNOWLEDGEMENTS

This thesis would not have been possible to be accomplished without the support and guidance of my adviser Professor Chul B. Park, who has been supervising my academic, research, and publication work throughout both my M.A.Sc. and Ph.D studies. It is my distinct pleasure that I express my gratitude to Professor Park for his strong support, timely advice, effective consultations, encouragement, and criticism throughout the development of this work.

I would like to thank the members of my Ph.D. Thesis Committee, Prof. S. Chandra, Prof. L. Chen, Prof. J.W. Zu, Prof. J.K. Spelt, and Prof. D. Li, for the offered guidance.

My gratitude is extended to the Department of Mechanical and Industrial Engineering at the University of Toronto for providing the NSERC Postgraduate Scholarship (PGS B), the Ontario Graduate Scholarship (OGS), and the University of Toronto Doctoral Fellowship. Special thanks are due to Prof. B. Benhabib. Also thanks to Brenda Fung, Theresa Lai-Ho, and Oscar del Rio.

I would like to thank Imperial Oil and Dr. Cal Schram for sponsoring a part of this project. I would also like to acknowledge the contribution of Ingenia Polymers Corp. (former WedTech Inc.) for the supplied resins and the usage of the corporate industrial equipment. In particular, I want to thank Mr. Salvatore D'Uva and Mr. Viraj Trilokekar for the friendly support and sound advice. The assistance of Patrick and Chris, machine operators, also deserves notice. I would also like to extend my appreciation to Montell Canada and Network Polymers, Inc. for supplying the PP resins used in the experimental work.

I would like to thank all my colleagues and fellow researchers formerly and presently working in the Microcellular Plastics Manufacturing Laboratory for their friendship. I am especially thankful to Dr. Hani Naguib, Ghaus Rizvi, Dr. Xiang Xu, and Donglai Xu, for the collaboration on our common research publications and the thought-provoking discussions we had during the work. I also want to acknowledge the contribution of Donglai Xu in the computer simulation work, as well as the participation of Kyoung-Ho Lee, Qingping Guo, Yean Cheang Chew, Ning Dong, and Xiaoyan Chen in the experimental work.

Finally, I would like to thank my wife Lydia and my daughters Bianca and Romina for always being an indispensable source of motivation for me and for being very proud of me for doing what I am doing. Thanks for the diligence, tolerance, understanding, and enthusiastic encouragement you provided while enduring this long process with me.

TABLE OF CONTENTS

PRELIMINARY SECTIONS

CHAPTER 8 FUNDAMENTAL STUDY OF BUBBLE LIFESPAN IN ROTATIONAL FOAM MOLDING

LIST OF TABLES

LIST OF FIGURES

LIST OF SYMBOLS

A_{total} = total interfacial area [m^2]
A = constant of the liquid
B = constant of the liquid
b = width of a panel [cm]
c = concentration [mol/m^3]
c_i = concentration of gas in bulk of polymer melt [mol/m^3]
$(c_i)_{sat}$ = saturation concentration of gas in bulk of polymer melt [mol/m^3]
c_w = concentration of gas at bubble liquid interface [mol/m^3]
c_g = concentration of gas inside the bubble [mol/m^3]
c_p = specific heat [J/{kg K)]
$\%CBA$ = percent of CBA (by weight) in a pure resin [%]
D = diffusion coefficient [m^2/s]
D_0 = pre-exponential function (an empirical constant) [m^2/s]
$D_{nominal}$ = nominal average cell size [μm]
$D_{average}$ = average cell size [μm]
d = diameter of the nucleated bubble [μm]
E = modulus of elasticity [Pa]
E_s = heat of solution [kcal/g mole]
E_d = activation energy of diffusion [kcal/mole]
E_0 = modulus of unfoamed polymer [Pa]
f = frequency [Hz]
ΔF = free energy of system [J]
$F(\lambda)$ = a continuous function, such that, $Fd\lambda$, is the contribution to the modulus from relaxation times between, λ, and $\lambda + d\lambda$
G_0 = initial shear modulus [Pa]
$G(t)$ = relaxation modulus [dyn/cm^2]

$G(t,\gamma_0)$ = shear relaxation modulus [dyn/cm^2]

G' = storage (elastic) modulus [Pa]

G'' = loss (viscous) modulus [Pa]

dH/dt = heat flow [W/m^2]

$H(\lambda)$ = replaces, $F(\lambda)$, where, $H = F\lambda$, and $Hd\ln(\lambda) = Fd\lambda$ [dyn/cm^2]

h = thickness of a panel [cm]

h_f = thickness of foamed panel [cm]

h_0 = thickness of unfoamed panel [cm]

I = moment of inertia of foamed panel [cm^4]

I_f = moment of inertia of foamed panel [cm^4]

I_0 = moment of inertia of unfoamed panel [cm^4]

K_h = Henry's Law constant [mol/(m^3 Pa)]

k_l = thermal conductivity of the liquid [W/(m K)]

k = Boltzman's constant [J/K]

K_e = spring constant [N/m]

K_v/K_e = time constant [s]

K_1 = constant depending of temperature

K_2 = constant depending of temperature

K = stiffness [g cm]

L = die length [cm]

m_{PPfoam} = shot size of PP foam [g]

Mold rot. = rotating speed of mold [rpm]

m_{PEfoam} = shot size of PE foam [g]

m_{skin} = shot size of skin [g]

m_{foam} = shot size of foam [g]

m = melt viscosity coefficient determined using the power law model

M_e = average entanglement molecular weight [g]

M_C = critical value of molecular weight [g]

M_Z = z-average molecular weight [g]
M_W = weight average molecular weight [g]
n_{cells} = number of cells in a (1 × 1) square in the microgram
N = cell population density [cells/cm^3]
N_1 = point at the rim of the cone
N_2 = point located on the underside of the cone
n = melt viscosity coefficient determined using the power law model
$n_{critical}$ = critical size of a bubble nucleus [μm]
n_e = number of entanglements
P_f = pressure in bulk of polymer melt [Pa]
P_g = gas pressure inside the bubble [Pa]
Δp_2^1 = pressure difference between 2 bubbles having radii r_1 and r_2 [Pa]
p_2 = pressure of melt [Pa]
p_1 = pressure of gas in nucleus [Pa]
P = pressure drop rate across die [Pa/m]
$Q_{\dim}$ = dimensionless group
Q = flow rate [m^3/s]
R_g = universal gas constant = 8.3143 [Pa m^3 mol^{-1} K^{-1}]
R_D = thermal resistance of constantan disc [(K m^2) /W]
r_0 = initial radius of spherical bubble [mm]
R = time-dependent bubble radius [m]
r = radial coordinate (radius of the bubble) [m]
R_{die} = radius of die [cm]
S = equilibrium saturation concentration [mol/m^3]
S_θ = geometrical factor depending on the wetting angle θ
T = absolute temperature [K]
T_C = temperature of polymer crystallization [K]
ΔT = temperature difference between sample and reference pan [°C]

T_g = bulk temperature of the gas in the bubble [K]

T_i = bubble interfacial temperature [K]

$T_{oven\ step\ 2}$ = oven temperature for step 2 [°C]

T_{oven} = oven temperature [°C]

$T_{CBA\ decomposition}$ = temperature of decomposition of the CBA [°C]

$T_{cell\ coalescence}$ = temperature of cell coalescence [°C]

$T_{polymer\ melt}$ = temperature of the polymer melt [°C]

$T_{polymer\ sintering}$ = temperature of polymer sintering [°C]

T_{melt} = temperature of polymer melt [°C]

T_{room} = room temperature [K]

t = time [s]

$\tan\delta$ = ratio of the loss modulus to the storage modulus

t_{heat} = heating time [min]

t_{cool} = cooling time [min]

V = bubble volume [m^3]

V_{foam} = volume of the expanded foam [cm^3]

V_{skin} = volume of the skin [cm^3]

V_c = volume of CBA evolved gas at crystallization temperature [cm^3]

V_{room} = volume of CBA evolved gas at room temperature [cm^3]

VER = volume expansion ratio

V_{mold} = volume of the mold [cm^3]

V_i = volume of the initial unfoamed solid plastic material [cm^3]

v_r = velocity of the bubble wall in the radial direction [m/s]

W = spindle torque [N m]

X = thickness of solid skin layer [mm]

x = degree of gas saturation in the polymer melt

Greek Symbols:

α = angle between the cone and the plate [rad]

δr_0 = wall thickness [μm]

δ = phase angle [rad]

Δ_{ij} = ij-th components of the rate of deformation tensor [s^{-1}]

φ = gas yield per unit mass CBA [cm^3/g]

ϕ = ratio of densities

φ_{STP} = gas yield of CBA at standard temperature and pressure [cm^3/g]

Γ = surface excess of the adsorbed component

γ_0 = sudden shear strain (strain amplitude)

$\dot{\gamma}$ = shear rate [s^{-1}]

η_e = non-Newtonian elongational viscosity [Pa s]

$\eta^*(\omega)$ = complex viscosity [Pa s]

$\eta'(\omega)$ = dynamic viscosity [Pa s]

$\eta''(\omega)$ = material function [Pa s]

η = viscosity [Pa s]

η_0 = zero shear viscosity [Pa s]

λ_i = terminal relaxation time [s]

λ = relaxation time of the liquid [s]

μ = Newtonian viscosity [Pa s]

ω = angular rotation rate [rad/sec]

ψ = chemical potential

$\rho_{polymer}$ = density of polymer [g/cm^3]

ρ = density [kg/m^3]

ρ_f = density of foamed polymer [kg/m^3]

ρ_0 = density of unfoamed polymer [kg/m^3]

σ = surface tension [N/m]

$\tau_{\varphi\varphi}$ = normal viscous stress [Pa] ($\varphi\varphi$ - th components of stress tensor)

$\tau_{\theta\theta}$ = normal viscous stress [Pa] ($\theta\theta$ -th components of stress tensor)

τ_{rr} = normal viscous stress [Pa] (rr - th components of stress tensor)

τ = shear stress [Pa]

τ_0 = shear stress amplitude [Pa]

τ_{ij} = ij-th components of the stress tensor [Pa]

CHAPTER 1

INTRODUCTION

1.1 Preamble

The fascination from the properties of natural polymers (e.g., starch, cellulose, rubber, etc.) motivated the earliest studies related to the manufacture of synthetic polymers in the 1830s. Likewise, in the 1930s, naturally occurring cellular structures (e.g., animal bones, wood, etc.) and their optimally balanced strength and weight impelled the development of methods for the manufacture of foamed man-made plastics and resins. However, it was not before the late 1970s when plastics outstripped steel as the most widely used material per unit volume. Since then, plastics are increasingly regarded as the global pace-makers of progress. Currently, more plastic is used than steel, aluminum, and copper combined. Plastics have found their way into every aspect of our daily life ranging from everyday products such as beverage and food containers, medical devices, and automobiles, to completely new and advanced uses in cutting-edge technologies such as conduction and storage of electricity, heat and light, molecular-based information storage, molecular composites, separation membranes, the space program, bullet-proof vests, fire-proof garments, prosthetic limbs, and so on.

In view of the above discussion, it is clear that such a large number of current and future applications will increase the demand for plastic products over the coming years resulting in a continuous industry growth at a very rapid pace. However, the economic, ecological, and social challenges facing the globe today and in the future will continue to seek new approaches to problem-solving in terms of combining high efficiency with low energy usage and great versatility of application. Thus, there is a great need for accelerated research and development in the field of polymer science and engineering that will have to be focused towards the very highest level of achievement in product development, processing technology, and recyclability. Cellular polyolefin composites should be considered as the utmost candidates for making this goal more attainable since they provide higher quality and superior strength-to-weight and cost-to-performance ratios than their non-foamed analogs [1-3].

1.2 Plastic Foams

Plastic foams are cellular composites comprising at least two phases: a solid polymer matrix and a gaseous phase originating from at least one gas-generating substance such as a blowing agent [1-2]. “A foamed plastic or cellular plastic has an apparent density, which is decreased by the presence of numerous voids or cells dispersed throughout its mass”, (ASTM definition D883-80C) [4].

A foamed/cellular structure has the advantage of reduced weight without reduced volume. Plastics are foamed for reasons of lowering the cost (reducing the weight) and improving the properties (achieving better performance) of plastic products without compromising the structural integrity of the part [1-3].

The two major polymer classes include plastics and elastomers [5]. By definition, plastic is “a material that contains as an essential ingredient an organic substance of large molecular weight, is solid in its finished state, and, at some stage in its manufacture or in its processing into finished articles, can be shaped by flow”, (ASTM definition D883) [4]. Plastics are classified according to their characteristics at elevated temperatures into two categories: thermoplastics and thermosets [5]. Thermoplastics consist of flexible linear molecular chains that are tangled together. Thermoplastics melt and flow when heated and harden when cooled regardless of how many times the heating and cooling cycle is repeated. In contrast, thermosets consist of a highly cross-linked three-dimensional network of long chain molecules. These plastics are hardened permanently by heat and will not melt when reheated, instead they will burn [4,5].

“Polyolefins” is a generic term referring to a family of polymers which raw monomer materials, the olefins, are obtained from petroleum and natural gas [5]. Polyolefins are tough flexible thermoplastics that are resistant to chemicals and abrasion, have no toxic behaviour in fire, and are easily recyclable. Polyethylene (PE) and polypropylene (PP) are the principal representatives of the polyolefin family. Linear polymers consist of the same backbone of carbon atoms joined by one bond, but with other atoms or radicals substituted for one or more of the hydrogen [4]. The linear PE molecule is the simplest polyolefin. Ethylene C_2H_4 is a gas, which can be converted to PE by polymerization. Essentially, replacing one H by a CH_3 group produces PP. The industrial production of PP relies on polymerizing propylene, C_3H_6 ($CH_3CH=CH_2$), a gas that can be derived from two main sources: co-production with ethylene and separation from gasoline cracker streams in petroleum refineries [6].

1.2.1 Classification of Plastic Foams

Since a foamed structure has the advantage of reduced weight without reduced volume, the foam bulk density is the most commonly employed criterion for distinguishing plastic foams [3]. Thus, high-density foams assume densities of over 240 [kg/m^3], whereas low-density foams are associated with densities lower than 240 [kg/m^3] [1]. However, plastic foam densities can be reduced as low as 1.6 [kg/m^3] [1], so that the resin consumption during production can be substantially lowered. This is of great importance for plastic processors because raw material costs in the production of conventional plastic articles can often reach up to 70% [7] of the total costs. In contrast, the typical material cost for a metal part is 30%.

An equally important classification criterion for cellular structures uses the combination of the average dimension across the cell (cell size) and the number of cells per unit volume (cell density) to arrange plastic foams into three categories. These include: (i) conventional foams (cell size > 100 [μm] and cell density < 10^6 [cells/cm^3]), (ii) fine-celled foams (10 [μm] < cell size < 100 [μm] and 10^6 [cells/cm^3] < cell density < 10^9 [cells/cm^3]), and (iii) microcellular foams (cell size < 10 [μm] and cell density > 10^9 [cells/cm^3]) [7]. It is important to note here that the cell morphology of the foam (cell geometry, size, and shape) strongly affects the properties of plastic foams. In this context, the mechanical properties of foams are known to improve by decreasing the cell size and by increasing the cell-population density and uniformity [8-13]. It would be therefore highly desirable to focus on the manufacture of foams with reduced cell size structures and higher cell densities.

Yet another criterion defines rigid and flexible plastic foams. The glass transition temperature of rigid foams is above room temperature, whereas that of flexible foams is below room temperature [2].

In addition, since foamed cells may be interconnected or may be discrete and independent, open-celled or closed-celled foams are also distinguished, respectively [4].

1.2.2 Preparation of Plastic Foams

Foams could be prepared from virtually any polymer if a mechanism capable of introducing or generating gas within the polymer matrix would be put in place [1]. The first concepts for foaming plastics were established in the 1930s [14]. Since then, the commercial production of plastic foams mostly relies on the expansion process [15].

The fundamental principle of the expansion process comprises dispersing a gaseous phase throughout the fluid phase of a molten polymer. It includes three fundamental steps: (i) creation of small discontinuities or cells (cell nucleation), (ii) growth of these cells to a desired volume (cell growth), and (iii) stabilization and retaining of the expanded form obtained by physical or chemical means (stabilization) [15]. All expansion-based foam fabrication processes are deliberately designed to promote and control the sequential development of each of these three steps [15]. Bubble collapse and coalescence in polymers are not desirable [16].

The cell nucleation within the molten polymer can be generated by injected gases, introduced low boiling liquids that volatilize due to increased temperature or decreased pressure, gases resulting from a chemical reaction within the fluid polymer, and chemical blowing agents (CBAs) [15,17]. The nucleation starts to occur at an initiation site within a polymer melt that has been supersaturated with a blowing agent. Such a supersaturated state can be achieved either by a sudden pressure drop in foam processing with a physical blowing agent (PBA), or by heating a polymer containing a decomposable CBA [15].

Polyolefin foams can be produced by either a physical or chemical method. Foams made from polyolefins inherit the properties of the basic resin they are made of [15]. Table 1.1 presents the typical properties of some polyolefins as they relate to foam properties [18].

1.2.3 Application of Foamed Plastics

The industry of plastic foams is permanently growing because it is driven by an intensive development of a wide variety of applications. Plastic foams were first used in the armed services during World War II [19]. Foamed plastic articles are lighter and less expensive than equally dimensioned non-foamed analogues made of the same resin, and due to the cellular structure, plastic foams possess unique properties such as load bearing, cushioning, impact resistance, insulation, and buoyancy [1-3]. Plastic foams can successfully conserve energy and natural resources, i.e., foamed insulation products reduce energy consumption, while those used for protective shipping reduce product damage, and thereby contribute for lower manufacturing costs and less waste [20]. In transportation applications, the reduction of vehicle weight by replacing steel with structural foam decreases the fuel consumption [2].

High-density foams are basically used in furniture, wires and cables [1], automotive and structural applications, while low-density foams are used for shock mitigation, insulation, and rigid packaging [3]. Rigid high-density foams are preferred for structural and load bearing applications, whereas rigid low-density closed-cell foams are used for thermal insulation [2] and for applications where buoyancy is important [1], while rigid low-density open-cell foams are most suitable for acoustical insulation [2]. Flexible foams are used for thermal insulation, comfort cushioning, and packaging [2].

Compared to PE foams, PP foams have recently grown in importance [2]. PP foams are preferred for applications where stiffness, chemical resistance, good heat insulation, sound deadening, and higher end-use temperatures are required. Relevant fields of PP foam applications include the automotive industry ("under-the-hood" high service temperature parts, interior, and cushioning applications), the industry for home electrical appliances (hot water and air conditioner pipes insulation), and the building industry (various insulating applications).

1.3 Conventional Rotational Molding

Since extrusion, injection molding, and blow molding dominate the manufacturing industry as principal plastics fabrication technologies [1,3], the conventional rotational molding process might be still unfamiliar to many, but its products are quite visible in a variety of everyday settings. However, the rotational molding process is not in competition with any of these processes, because it is often the only available option for numerous manufacturing assignments that otherwise could not be accomplished in one piece. The conventional rotational molding (or rotomolding) process is a primary plastic processing technology deliberately designed for the manufacture of hollow, large-sized, complex-shaped, single-piece, seamless, and virtually stress-free plastic articles. It is indispensable for the production of toys, sporting equipment, containers, automotive fuel tanks, industrial storage tanks, vehicle shell, furniture, playground equipment, etc. (Figure 1.1) [21-26].

The fundamental operating principle of the conventional rotational molding process comprises four manufacturing steps. It is depicted in Figure 1.2 (a). First, a predetermined amount of a pulverized plastic resin is charged into a separable (cast or fabricated), hollow, vented, metal mold. In the second step, the mold is closed and inserted into an oven where it is externally heated (Figure 1.3 (a)) and simultaneously rotated in two perpendicular axes (Figure 1.4), or it is at least subjected to a rocking motion (Figure 1.5), until its plastic content melts and achieves even distribution on the internal mold surfaces without applying pressure or centrifugal force, thereby duplicating accurately the shape of the mold. During the third step, the mold is cooled externally (Figure 1.3 (b)) by using water mist and/or forced air while still rotating bi-axially. This allows the molded article to solidify and regain enough strength to resist the forces required to remove it from the mold. In the final, fourth step, the rotation is stopped, the mold is opened, and the hollow rotational molding is removed. A release agent is usually applied to the internal mold surfaces before the production cycle is repeated [3, 21-27].

The conventional rotational molding is a material dependent process, i.e., it is limited to those polymers that are available as a liquid, or are capable of being efficiently pulverized into fine powders (thirty-five mesh) that will flow like a liquid. Polymer materials having a melt flow index (MFI) ranging from at least three up to five or greater are desirable [26]. The most commonly rotationally molded plastics include PE, PP, polyvinyl chloride, nylon, and polycarbonate [26]. PE currently accounts for over 85% of the materials used in rotational molding operations [26]. Despite PP has been discovered in 1954 [6], PE is still the material of choice for rotomolding processors because its rheological and thermal characteristics are ideally suited to the process [23]. Although PP is lighter than water (0.9 [g/cm^3]) and PE, its major competitor, which makes it suitable for applications that require a low-density plastic material, PP has not been used extensively in rotational molding, because, until recently, most PP grades had relatively poor impact properties compared to linear low-density polyethylene (LLDPE) and high-density polyethylene (HDPE). Another reason for the domination of PE-based resins in rotomolding is the fact that, compared to PE, fewer rotomolding PP grades are available, while other kinds of PP grades are seldom readily available in a powder form, since the pulverization of PP often requires cryogenic grinding, which adds to the material cost.

1.3.1 Advantages and Disadvantages

The most important advantages of the conventional rotomolding process include the low tooling costs, the capacity to produce large-sized one-piece products that no other process can, the comfort of simultaneously running molds of different sizes and shapes on the same equipment, the convenience of almost no need for secondary operations, and the ease of molding articles with undercuts, double walls and molded inserts. Tooling is relatively simple and inexpensive because rotomolding is a low-pressure process and no cooling channels and no clamping force is required, as it is the case with injection molding and blow molding. Trimming can be eliminated because rotationally molded parts normally have very little flash. Since the produced parts are hollow, with no core, they can be deformed inward in order to free external undercuts when being removed from the mold, but the magnitude of the allowed undercut is limited by its design and the elasticity of the plastic material, whereas internal undercuts are not permissible since the shrinkage of the material will prevent the ejection of the part [24,26].

However, the greatest disadvantages of the rotomolding process are the long cycle times, the need to grind the materials before usage, the labor intensive loading/unloading operations, and the relatively limited choice of rotomolding grade resins. Cycle times are long because of the nature of the process which requires the temperature of the plastic and the mold during processing to be elevated from room temperature to beyond the melting temperature of the plastic, and than cooled back to room temperature [24,26]. In addition, since there are no cores inside the hollow moldings, surface details and dimensions can only be provided and controlled on the side of the part that is formed in contact with the cavity [26]. Also, some geometrical features such as ribs are difficult to mold [24].

1.4 Rotational Foam Molding

For end-use applications where the relatively low level of mechanical and/or insulative properties of hollow or double-walled conventionally rotomolded structures are considered as weaknesses, improvements are commonly achieved by filling their hollow shells with either polyurethane or polystyrene inner core-forming foams in a secondary operation. For example, surf boards are generally made by rotational molding to form an outer wall of PE after which the thus occupied volume is subsequently filled with polyurethane foam. If the PE coating gets damaged during use, water penetrates into the foam and can be absorbed by all the foam, thereby rendering the board useless. If there would be a good adhesion between the surface wall and foam, damages would less likely occur because with good adhesion water could only penetrate into the foam under the damaged spot. On the other hand, if polystyrene foam is desired to comprise the inner core of a rotationally molded article, after the molded article has been removed from the rotating mold, it is being filled with pre-expanded polystyrene beads while introducing steam into its hollow shell. This latter operation is usually conducted in a separate mold whose purpose is to retain the shape of the article during the expansion and fusion of the inner core by the effect of the steam, which provides the necessary heat to expand and slightly fuse the beads into a foam body. However, the above method does not guarantee that the polystyrene foam is bonded to the outer shell and thus it easily separates from it to form air pockets. Such air pockets deform the shape of the body and give an unpleasant feeling when pressed. In this context, regardless of the type of foam introduced in the cavity of the molding, this additional processing step not only reduces the productivity of the process, but also, because of the incompatibility of the dissimilar adjacent materials, produces a weak interface between the outer non-cellular skin layer and the cellular inner core structure obtained in such a way [27].

It would be therefore desirable to develop a rotational molding technology that would be able to create a foam layer or core in the interior of hollow rotational moldings adjacent to the outer solid skin layer in an uninterrupted production cycle by using identical (or compatible) materials. Thereby, the efficiency of the process and the structural integrity of the products would concurrently improve. To accommodate this concept, over the last three decades, efforts have been made to modify the conventional rotational molding process to serve as a technology for plastic foam fabrication. As a result, the redesigned process, commonly referred to as rotational foam molding, advantageously allows for the production of completely or partially foamed one-piece plastic articles with or without a non-foamed skin encapsulating the foamed core or layer [3,26].

Figure 1.2 compares the schematics of the principle of operation of the rotational foam molding process (Figure 1.2 (b)) with that of conventional rotomolding (Figure 1.2 (a)). It indicates that other than charging the mold with at least one foamable resin at Step 1 in rotational foam molding operations, the subsequent steps of these related technologies closely resemble each other. Conversely, the rotational foam molding can be carried on using ordinary rotational molding equipment that is capable of subsequently subjecting a pre-charged metal mold to biaxial rotation in both heated and cooled environments (Figures 1.3-1.5). However, since the rotational foam molding process is atmospheric by nature, and since the use of PBAs would require an elevated pressure, only CBAs are applicable [27]. Hence, the foamable resins intended for rotational foam molding have to be prepared by introducing a CBA into the polymer by means of a suitable polymer mixing technique (dry-blending or extrusion melt-compounding). At a later point, its thermally-activated decomposition will convert the polymer into a foamed (instead of a hollow) final plastic product [3,21-29].

If a skinless foam layer (Figure 1.6 (a)) or core (Figure 1.6 (b)) is desired, only a foamable resin should be used for charging the mold [3]. However, the manufacture of rotational moldings with a distinct non-foamed outer skin that encapsulates entirely a foamed core or layer requires both non-foamable and foamable resins to be charged into the mold within the same rotational molding cycle. This could be achieved either by interrupting the molding process, or continuously, without process interruptions [3,26]. Interrupted methods require molds with specially designed openings that can be used to pour the foamable resin in the mold during the interruption of the rotational foam molding process. This operation normally takes place after the initially charged non-foamable resin had sintered and formed the skin inside the mold [24]. Continuous methods can be based on a two-charge, a multi-charge, or a single-charge principle of operation. Most continuous two-charge methods use a "drop-box system", comprising of a box attached to the mold, or a "plastic bag system", which is based on using a flexible plastic bag to hold the foam charge until its rupture under certain molding thermal conditions. Both systems can be used to introduce the foamable material at the time when the non-foamed skin coating is already formed by the sintering of the non-foamable material directly charged into the mold cavity prior to processing [3]. Thereby, a foamed layer (Figure 1.6 (c)) or core (Figure 1.6 (d)) is formed on top of the non-foamed skin. Multi-charge methods are used for producing multilayered articles, i.e., if distinct skins should be developed on both the outside and the inside surface of a foamed layer, a second drop-box should be used to introduce another charge of non-foamable resins on top of the already formed integral-skin foamed structure (Figure 1.6 (e)) [3,24,26]. In contrast to the methods described above, the single-charge (also termed: single-shot or one-charge) rotational foam molding processing concept works by charging the mold with predetermined quantities of both non-foamable and foamable resins simultaneously at the outset of the cycle, so that the use of drop boxes or plastic bags becomes unnecessary [3,24,26,30-36].

1.4.1 Chemical Blowing Agents

By definition, CBAs are individual compounds or mixture of compounds that liberate gas as a result of chemical reactions, including thermal decomposition, or as a result of interactions with other components of the formulation [37]. Typically, the decomposition of nearly all CBAs is triggered by elevated temperature [3]. Most commonly used CBAs predominantly generate CO_2 or predominantly generate N_2 [29]. Most CBAs are solids [37] in a dry-powder form [3]. As such, unlike PBAs, they can be readily introduced into compositions to be foamed or be processed by using ordinary equipment. In addition, the use of CBAs reduces production costs because no specialized storage equipment is required [37].

CBAs can be exothermic or endothermic. During decomposition, exothermic CBAs generate heat, whereas endothermic CBAs consume heat. In general, once an exothermic CBA begins to decompose, it is difficult to stop it before it reaches full decomposition. This results in a faster decomposition in a narrow temperature range. In contrast, endothermic CBAs require additional heat to support their continuing decomposition. Consequently, they have a broader decomposition time and temperature range [37].

The properties that require special attention while selecting a CBA for a particular foaming application include (i) the temperature at which the expanding gas is liberated, (ii) the initial temperature of decomposition, the temperature range of the maximum rate of decomposition, the gas yield (volume of gas, in cm^3, liberated by the transformation of 1 g of CBA per unit time, usually 1 min, at the temperature of maximum gas liberation), (iii) the nature, rate, and kinetics of the liberated gases, and (iv) the pressure developed by the gas [37].

1.4.2 Rotational Foam Molding Methods

The rotational foam molding process comprises two subsequent distinct stages: foamable resins preparation and foam production. Polyolefin-based foamable resins can be prepared either in a form of blended powders or compounded pellets. In the former case, the polymer powders are mixed well with a CBA in a dry blending operation using a high-speed dry mixer, whereas in the latter case extrusion melt compounding is used to disperse the CBA particles throughout the molten polymer. Conversely, with respect to the mixing technique used for introducing the CBA into the polymer matrix during the preparation of the foamable resins, two kinds of rotational foam molding methods can be distinguished: dry blending-based and melt compounding-based [27,38-41].

1.4.3 Advantages and Disadvantages

The similarity between conventional rotomolding and rotational foam molding normally implies agreement between their advantages and disadvantages, but some exceptions exist. For instance, the rotational foam molding process requires extended total cycle times ranging between 25 to 100% [30,35] to allow the completion of the foaming process. This is so because a greater amount of material is molded and the heat transfer is retarded by the insulative effect of the cellular structure.

It should be also noted here that if molds originally designed for rotomolding were to be used for rotational foam molding, a few marginal modifications would be necessary. In this context, mold-venting enhancements would be helpful to allow for complete foaming of large parts [35], and because fully foamed parts will not normally shrink as much as conventionally rotomolded parts, greater mold draft angles should be considered to facilitate part release [30,35]. In addition, molding of articles with undercuts is not possible in rotational foam molding because the foamed core or layer does not allow inward article deformation.

1.5 Current State of the Art and Future Developments

Over the past number of years, the rotational molding process has evolved from a simple low-tech technique to the point where its advanced methods use a single operation to produce sophisticated parts, such as integral-skin cellular composites. Among these, the advent of the single-charge rotational foam molding technology for producing integral-skin cellular composites is one of the major breakthroughs in rotational molding technology [42,43]. However, although the earliest attempts for producing foamed parts using single-charge foaming go back to the early 1970s, and despite the fact that single-charge foaming materials specifically compounded for rotational molding became commercially available from Equistar and Ingenia Polymers Corp. (formerly WedTech Inc.) only in the mid 1990s [26], it is still regarded as a new technology [24,26], so that currently its potentials are not utilized to the full extent among processors and thus it enjoys a limited commercial success. It is clear, therefore, that a full-scale industrial implementation of the single-charge foaming technology requires further research focusing in understanding the relationships between its fundamental governing mechanisms, critical parameters, and optimal processing strategies.

Other recent advances presently in development or in limited use that contribute to the sophisticated new look of the rotational molding technology include: (i) temperature-sensing transmitting unit known as Rotolog, (ii) mold-in multi color graphics technology, (iii) process-simulation software for rotomolding, (iv) automated mold opening/closing, charging, and part ejection devices, (v) mold heating with infrared, microwave, or induction energy, (vi) direct (ovenless) heating/cooling of molds via delivery of heat-transfer fluids through the arm of the machine, (vii) internally pressurizing parts in the mold with gas fed through lines in the spider arm, (viii) mold-venting devices that relieve mold pressure without losing resin powder, (ix) multi-axis (at least three axes) continuous rotational molding apparatus, etc. [42-45].

1.6 Motivation for Research

The fundamental motivation for undertaking the research work that is presented in this thesis was to develop integral-skin foam-reinforced large-sized, complex-shaped, single-piece polyolefin articles that would achieve improved insulative properties, structural homogeneity, and fabrication economics in comparison with corresponding foam-filled analogs.

1.7 Thesis Objectives

The primary objective of the present thesis is to establish the scientific and engineering foundations for developing a rotational foam molding technology that would be optimized for creating adjacent layers of non-cellular and cellular structures with a controllable density out of skin-forming and foam-forming materials of identical or compatible nature in an uninterrupted single-charge production cycle. Another objective of this thesis is to understand the fundamental foaming mechanisms governing the rotational foam molding process by developing a theoretical model for simulating the lifespan of CBA-blown bubbles in non-pressurized polymer melts. Yet a further objective of this thesis is to develop a technique for preparing foamable polyolefin-based compositions that would be useful for yielding foam morphologies having the finest cell size and the highest cell population density and uniformity attainable in rotational foam molding. In particular, it is aimed to produce integral-skin PE-based foams with an average cell size of less than 300 [μm] and a cell population density below or in the vicinity of 10^6 [cells/cm^3], while the targeted foam density is below 0.185 [g/cm^3], which is equivalent to at least five-fold volume expansion ratio.

1.8 Thesis Scope and Relevance

A compounding-based rotational foam molding process for producing integral-skin cellular polyolefin composites is proposed in this thesis. It mainly deals with integral-skin foams that occupy the mold to the full capacity. However, the concepts put forward herein are equally applicable for partially foamed, hollow, integral-skin articles.

A successful completion of this research envisages the industrial implementation of a novel rotational foam molding technology which would provide foamed polyolefin articles that will possess a finer cell structure and thereby superior strength-to-weight and cost-to-performance ratios over foam-filled predecessors and non-foamed analogs.

1.9 Thesis Format and Outline

The present thesis comprises a preliminary subdivision, 9 chapters, and 2 appendices.

Chapter 1 presents a general introductory statement about plastics and plastic foams, a statement of concepts and principles associated with foamed plastics, and a summary of recent developments in the fields of polyolefin foam fabrication processes that are relevant to the thesis research topic.

Chapter 2 includes the literature review and briefly presents several distinct concepts for the production of integral-skin cellular composites by using rotational foam molding.

Chapter 3 covers the theoretical background needed to comprehend the physical meaning of the research and experimental work presented in the thesis.

Chapter 4 introduces the principal physical properties of the polyolefin resins and additives selected for experimentation and the fundamental operating principles of the analytical instruments used to characterize these materials.

Chapter 5 is primarily focused on fundamental measurements and characterization of the selected polyolefin resins and additives in terms of rheological and thermal behavior.

Chapter 6 is concerned with the investigation of the rotofoamability of polyolefin resins, i.e., identifying the suitability of PE and PP resins for manufacture of foams using rotational foam molding.

Chapter 7 investigates the technological potentials for processing integral-skin polyolefin cellular composites in rotational foam molding. It is focused on the single-step processing principle, the main feature of which is the simultaneous introduction of both the foamable and non-foamable resin into the cavity of the mold from the very beginning of the cycle. An experimentally intensive study provided the means for identifying the key processing parameters and optimal processing strategies for the manufacture of plastic articles that have a distinct layer of non-foamed PE skin encapsulating a PE or PP foamed core.

Chapter 8 is concerned with the fundamental investigation and modeling of the lifespan of CBA-blown bubbles in non-pressurized non-isothermal polymer melts such as in rotational foam molding.

Chapter 9 summarizes the major problems solved in the thesis, emphasizes the relevant conclusions, introduces a number of possible extensions that can be drawn from the work presented in the thesis, and identifies potential directions for future research.

Table 1.1: Typical properties of polyolefins [18]

Properties	Units	PP		HDPE	LDPE & MDPE	
		Homopolymer	Copolymer		Branched	Linear
Density	g/cm^3	0.900-0.910	0.890-0.905	0.952-0.965	0.917-0.932	0.918-0.940
Melting point	C^o	160-175	150-175	130-137	98-115	122-124
Tensile strength at break	MPa	31-41	28-38	22-31	8.3-31	13-28
Elongation at break	%	100-600	200-700	10-1200	100-650	100-965
Tensile modulus	MPa	1140-1550	900-1240	1070-1090	170-280	260-520

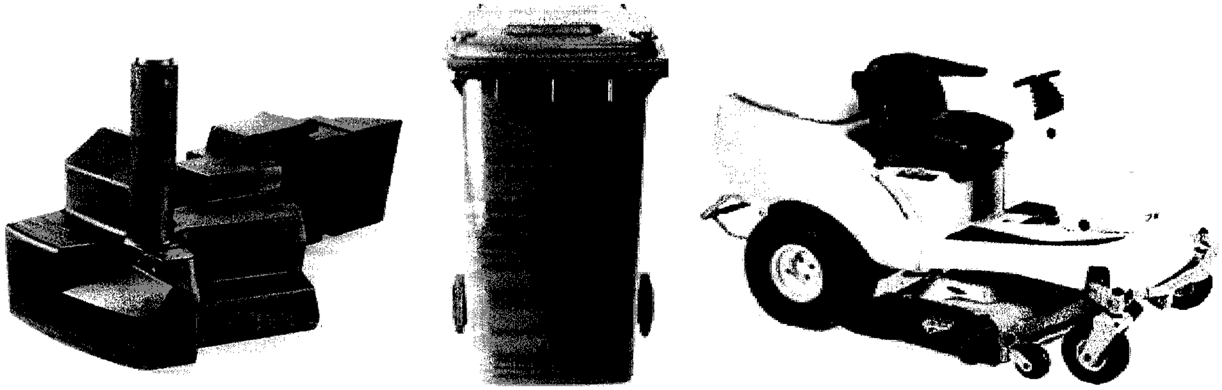

(a) Fuel tank (b) Refuse container (c) Riding mower (body)

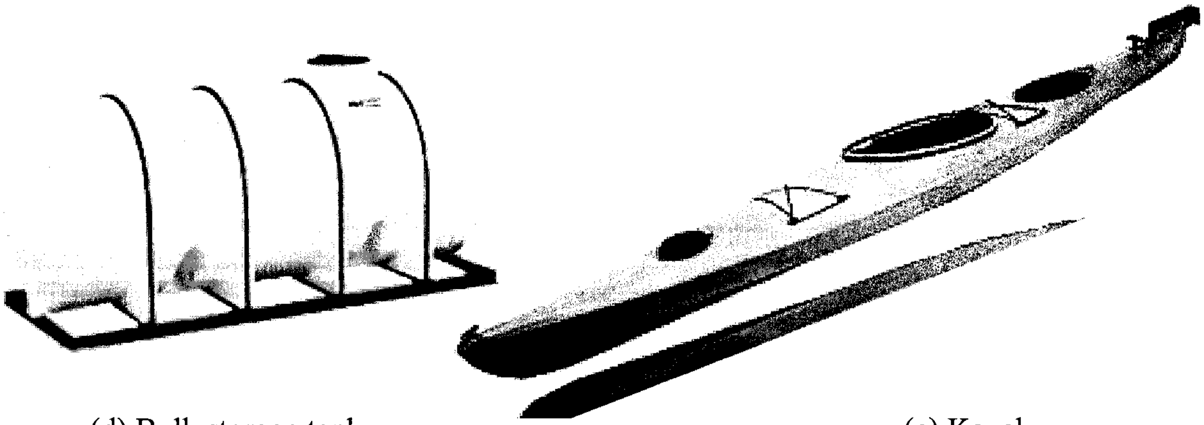

(d) Bulk storage tank (e) Kayak

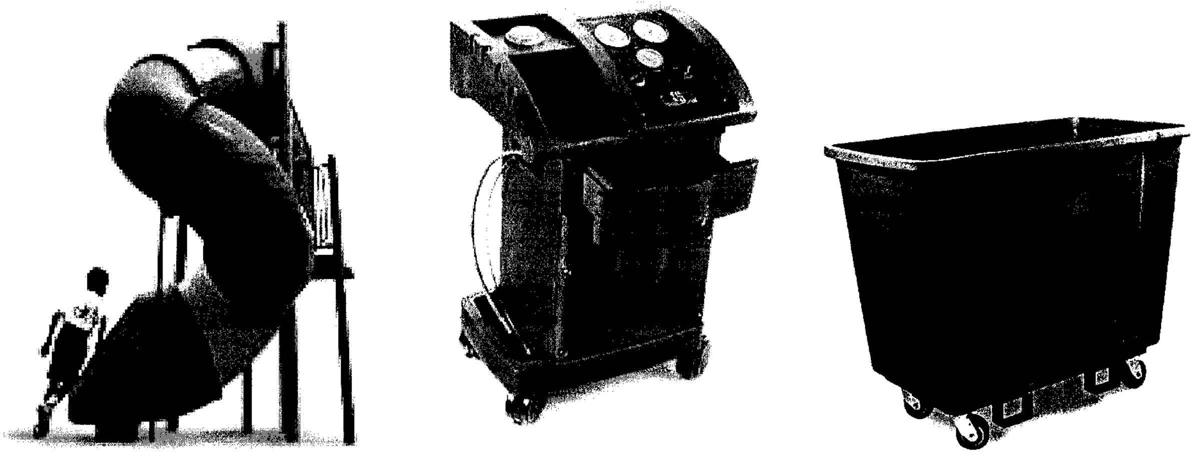

(f) Playground (g) Industrial cart (h) Utility truck

Figure 1.1: Typical rotational molding products

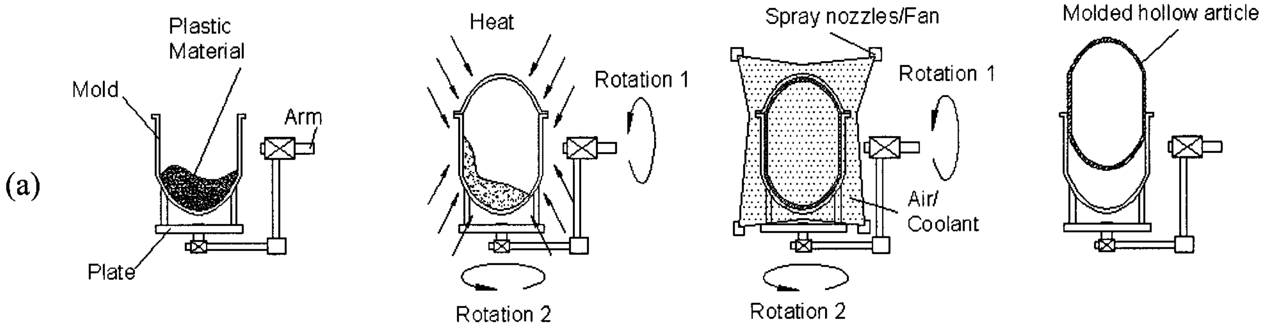

(i) Step 1:
Mold charging

(ii) Step 2:
Biaxial mold rotation and heating

(iii) Step 3:
Biaxial mold rotation and cooling

(iv) Step 4:
Molded article removal

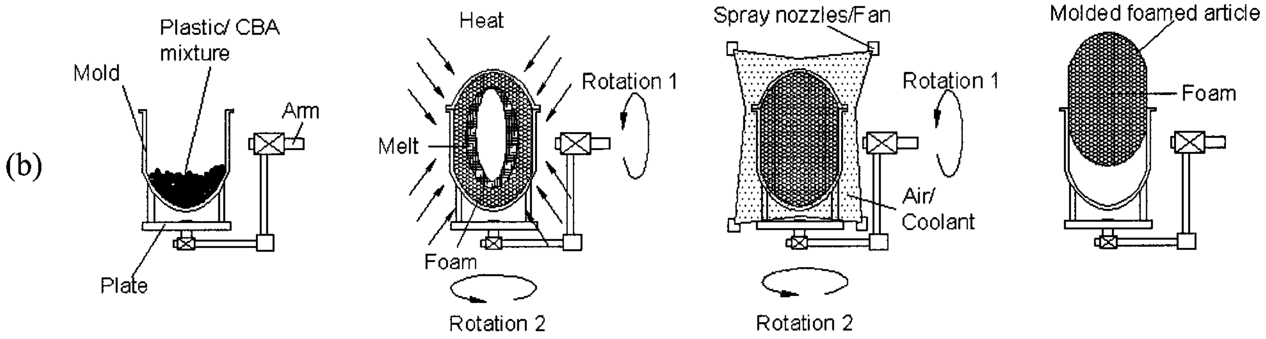

Figure 1.2: The conventional rotomolding and the rotational foam molding operating principles compared

(a) Conventional rotational molding operating principle

(b) Rotational foam molding operating principle

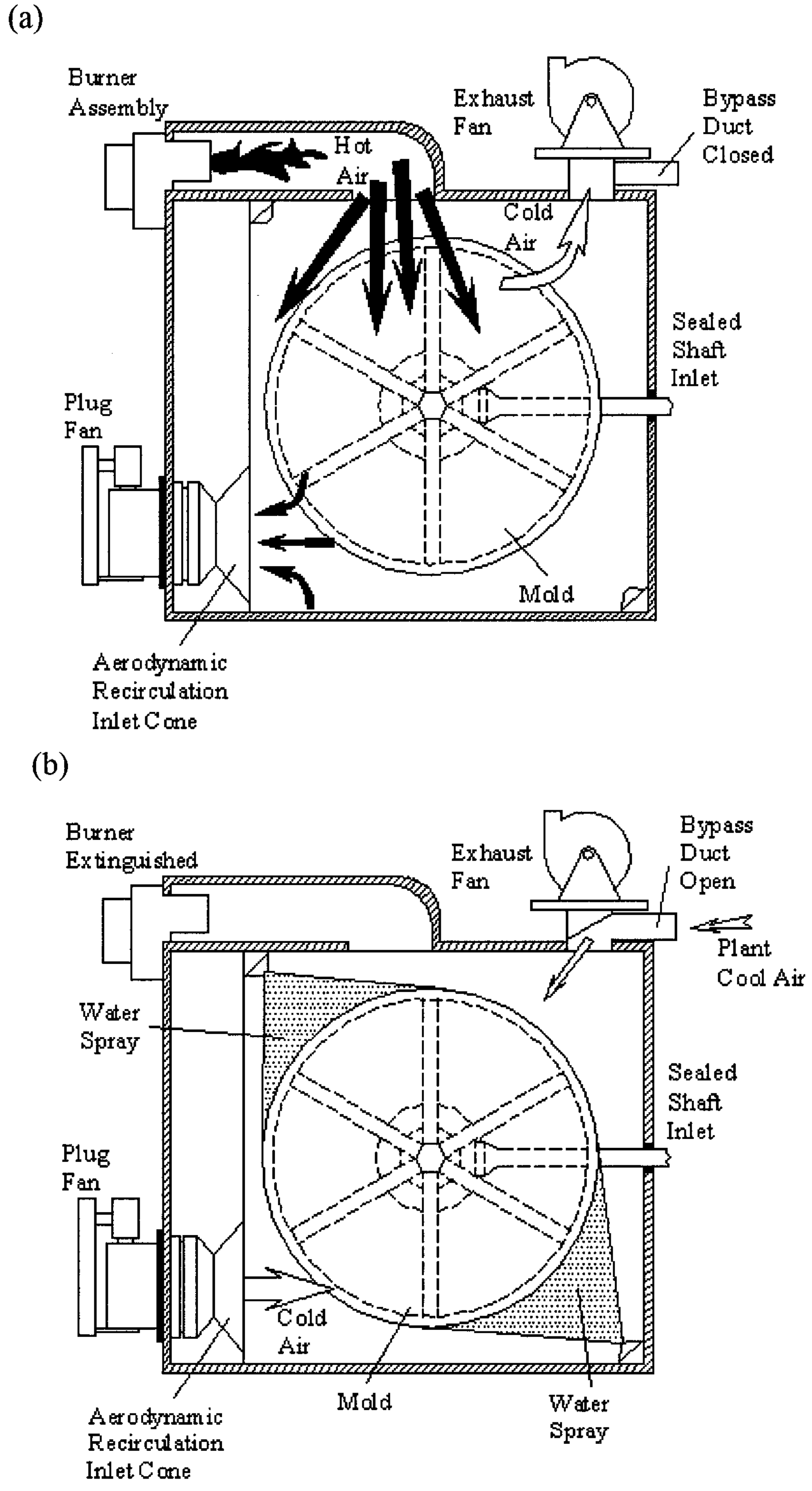

Figure 1.3: A schematic of the principle of operation of a single arm, single station, clamshell-style rotomolding machine

(a) Heating portion of the rotational molding cycle

(b) Cooling portion of the rotational molding cycle

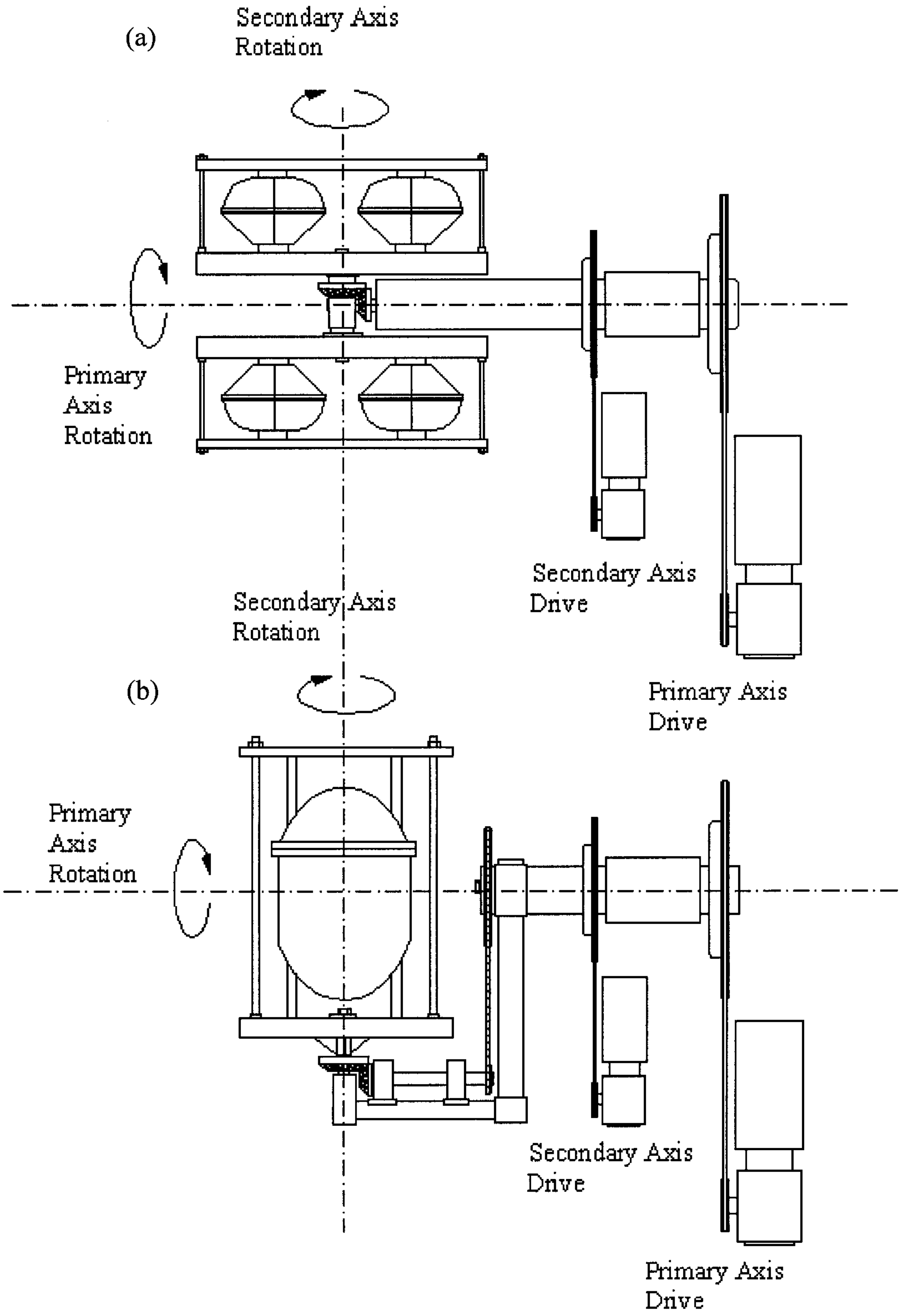

Figure 1.4: Typical configurations of mold-mounting assemblies for biaxial rotation

(a) Straight arm (or double centerline) mounting

(b) Offset arm (or cranked arm) mounting

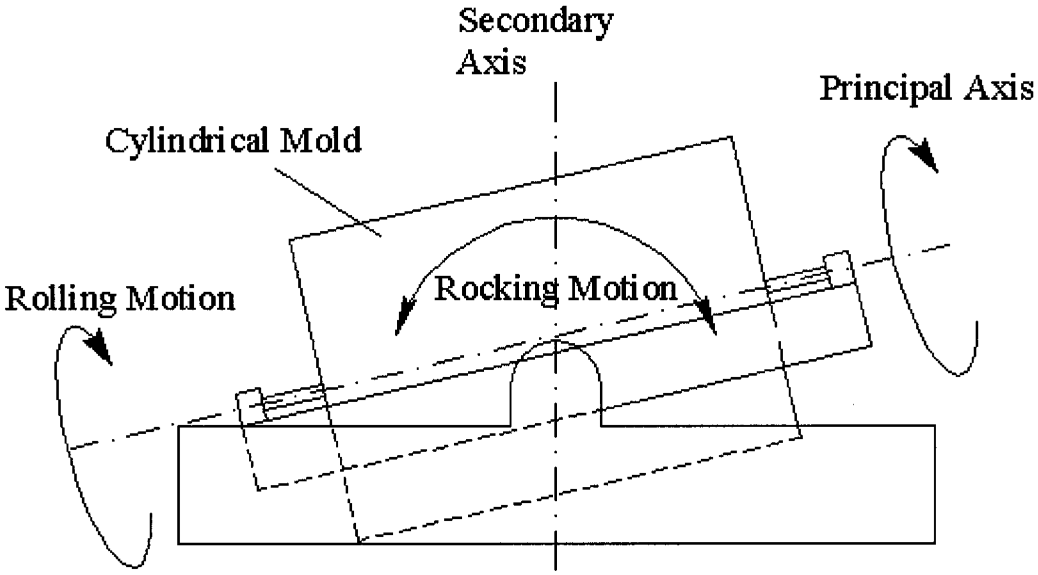

Figure 1.5: A schematic of the principle of operation of the "rock and roll" type of rotational molding machine

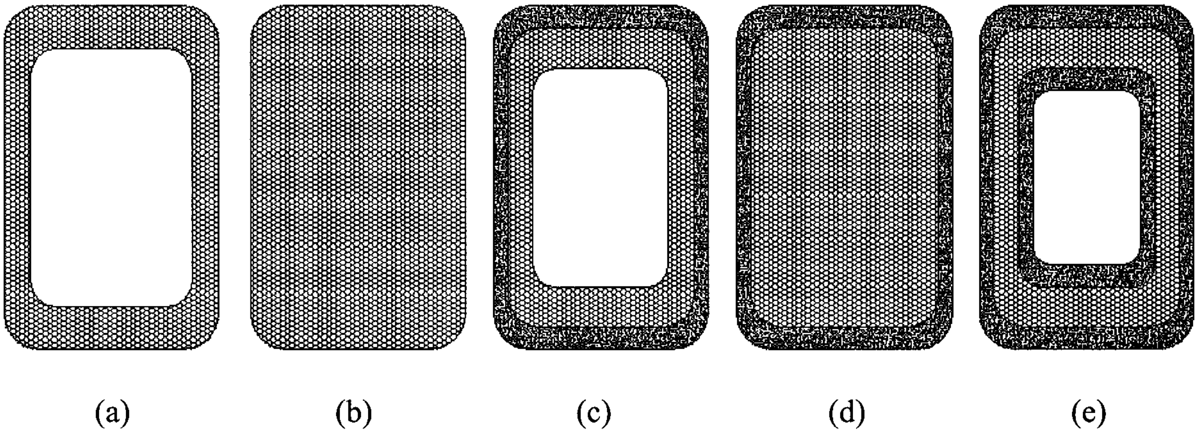

Figure 1.6: Schematics of cross sections of various types of foam-reinforced rotational moldings

(a) Skinless foam layer

(b) Skinless foam core

(c) Integral-skin foam layer

(d) Integral-skin foam core

(e) Double-sided integral-skin foam layer

CHAPTER 2

LITERATURE SURVEY

2.1 Introduction

Considering the fact that rotational foam molding is having but lately been brought into being a distinct plastic processing technology, in comparison with the relatively large volume of research studies associated with conventional rotomolding, not much work related to the rotational foam molding process has been published to date in the open literature. Particularly, very limited research has been conducted on the processing of integral-skin cellular polyolefin composites in rotational foam molding, while even a smaller body of literature [30-36] deals with the study of the single-charge rotational foam molding technology. Furthermore, while several authors have done an admirable job in studying the formation and removal of unwanted bubbles in conventional rotational molding [46-51], other than a few recent studies [52-57], no substantial work has been performed yet to explain the mechanisms governing the CBA-blown production and retention of controlled bubbles and their lifespan in non-pressurized non-isothermal polymer melts, such as in rotational foam molding.

Likewise, compared to PE foams, very little research has been accomplished to date on the production of PP foams in rotational foam molding. Unlike PE, successful processing of PP foams in extrusion melt compounding-based rotational foam molding has been reported only recently [28,38-41], whereas the production of integral-skin PP foams encapsulated with either PE or PP skins has not been reported yet. Perhaps the major reason for this is the fact that melt-compounding PP resins with a CBA is difficult because of the relatively small gap between the high melting point of PP and the decomposition temperature of a suitable CBA, so that the CBA stored in the foamable resin often decomposes prematurely while being compounded [38]. In addition, PP is not particularly favorable for foaming due to its weak melt strength, and weak melt elasticity at elevated temperatures [58,59].

2.2 Rationale of Cellular Composites

Three general types of foam structures are distinguished: (i) uniform density foam, (ii) "T-beam foam", comprising a solid skin on one side of foam, and (iii) "I-beam foam" or "sandwich foam" [53]. Stiffness, K, is the most important mechanical criterion of rotationally molded parts. It is calculated as the product of the modulus, E, and the moment of inertia, I.

$$K = EI \tag{2.1}$$

Considering uniform density foams, it can be shown that the modulus of the foamed polymer, E_f, can be determined by the relationship given below [3,24,34,53]:

$$E_f = E_0\left(\frac{\rho_f}{\rho_0}\right)^2 = E_0\phi^2 \tag{2.2}$$

where: E_0 = modulus of unfoamed polymer ρ_f = density of foamed polymer

ρ_0 = density of unfoamed polymer ϕ = ratio of densities

For instance, the moment of inertia for a panel in flexture is given in terms of its width, b, and its thickness, h, as follows:

$$I = \frac{bh^3}{12} \tag{2.3}$$

The moment of inertia is a geometric property and is independent of the density of the polymer. However, if the overall part weight remains the same, decreasing the polymer density by foaming is equivalent to increasing the part wall thickness [53] or adding a stiffening rib to the plastic [24,34]. Thus:

$$I_f = I_0\left(\frac{h_f}{h_0}\right)^3 = I_0\left(\frac{\rho_f}{\rho_0}\right)^{-3} = \frac{I_0}{\phi^3} \tag{2.4}$$

where: I_f = moment of inertia of foamed panel h_f = thickness of foamed panel

I_0 = moment of inertia of unfoamed panel h_0 = thickness of unfoamed panel

Hence:

$$K = E_f I_f = E_0 I_0\left(\frac{\phi^2}{\phi^3}\right) = \frac{E_0 I_0}{\phi} \tag{2.5}$$

Since ϕ for a foamed polymer is less than one, the stiffness of the part increases linearly with decreasing foam density at the same part weight. However, if the part stiffness is satisfactory, the foaming of the polymer results in reduced part weight and material cost at the same part stiffness. This is the primary rationale for producing cellular composites [53].

2.3 Concepts for Rotomolding Integral-skin Cellular Composites

Over the last four decades, several distinct concepts for the production of integral-skin cellular composites by using rotational foam molding as the principal process have been disclosed in the patent literature. A survey of the most relevant works is presented below.

Slapnik [60], disclosed a process which is carried out by placing particles of expandable polystyrene in a bag that is made of a thermoplastic material, inserting the bag and its contents into a stationary mold, and heating the expandable polystyrene to a temperature above the boiling point of the expanding agent but below the melting point of polystyrene. The heat causes the particles to soften, expand, and fuse together to form a cellular core that forces the bag to adhere to the fused expanded beads and conform to the shape of the mold providing an article having a skin of a thermoplastic material and a core of foamed expanded polystyrene.

Nonweiler [61,62], disclosed the earliest single-charge rotational foam molding concept by simultaneously charging the mold with a free-flowing molding composition comprising: (i) expandable polystyrene beads, (ii) nonexpendable thermoplastic resin in powder form, and (iii) retained water in the form of hydrate, such as water-glass or borax, containing at least 25% by weight chemically bound water (to provide steam when heated). This invention identified the importance of moving the mold sufficiently to cause the desired particle separation inside the mold to take place while the molds are being subjected to the action of heat.

Pitchard [63], claimed that reproducible and uniformly foamed polymer products can be obtained when a temperature control agent is first mixed with the polymer by itself, after which the dispersing agent is then added by itself and mixed with the temperature control agent and polymer composition, and the foaming agent is then added last and mixed with the combination of temperature control agent, dispersing agent, and polymer.

Mitsubishi Petrochemical Co. Ltd. [64], disclosed a single-charge foaming method based on using synthetic resins in powder form and foamable synthetic resin beads to charge a rotating heated metal mold. The pulverized resin is molded first in the absence of steam, and when the molding is almost completed, steam having a large amount of energy is blown into the mold to uniformly and completely foam the foamable synthetic resin beads. Thereby, the outer layer composed of non-foamable resin and the inner layer composed of foamable resin are distinctly defined while the foamable beads are completely foamed.

Mitsubishi Petrochemical Co. Ltd. [65], disclosed an alternative method of preparing a molded olefin polymer foam with a strong skin layer, by employing preliminary low foamed particles as a lower layer, then preliminary foamed particles having a higher amount of expansion as a middle layer, and finally, more preliminary low foamed particles as an upper layer in the mold. The process for preparing preliminary foamed particles is based on extruding a mixture comprising an olefin polymer, a first chemical blowing agent and a second blowing agent having a blowing temperature which is lower than the blowing temperature of the first blowing agent. The raw material in contact with the inner wall is foamed first, while the later foaming of the central part provides pressure on the inner wall of the mold. Because the foamed surface in contact with the inner mold is exposed to higher temperatures for a longer time, the foam cells become unstable and become ruptured by the thermal movement of the gas in the cells, thereby forming the skin layer.

Hosoda et al. [66], disclosed a method for producing foamed composite articles which comprises placing powdered plastics and granular plastics containing a foaming agent in a mold, rotating or vibrating the mold to separate the two kinds of plastics from each other, and heating and foaming the same while the rotation or the vibration of the mold is continued. It is claimed that the two kinds of materials charged simultaneously into the mold are being separated into a surface layer and a well foamed inner core owing to the difference in size of powdered and granular plastics and because of their movement within the rotating mold.

Nicholls [67], disclosed a two-step interrupted rotational foam molding method basically comprising forming a first lining layer of a synthetic plastic material in a bi-axially rotating heated mold, interrupting the process to charge the lined mold with a foamable synthetic resin material and a quantity of water, and continuing the process by rotating and heating further the mold to expand the synthetic resin material and to cause it to bond to the lining material, while the water acts as a thermal transmission agent assisting in the distribution of heat through the article being formed.

N. Shiina and K. Hosoda [68], disclosed a method which consists in heating a non-foamable powdered thermoplastic material mixed with larger particles of a foamable type of plastic material in a bi-axially rotating airtight mold with pressurized steam, followed by cooling, thereby producing a solid molding whose core is foamed. The mold is first heated from the outside with steam in a steam furnace so as to cause the plastic powder to attach itself by melting to the inner walls of the mold and thereby forming the skin of the molding, and then, steam is directly injected into the mold to expand the foamable plastic particles constituting the foamed core of the molding.

Slade [69], disclosed a single-charge rotational molding process intended for the manufacture of articles having a foamed inner layer and a solid skin substantially free of voids. According to this invention, for achieving desired particle separation, the mold should be simultaneously charged with a mixture of powdered non-foamable ethylene polymer and a pelletized foamable ethylene polymer containing a blowing agent in quantities between 0.25 to 5 wt%.

Mori et al. [70], disclosed a compounding-based single-charge method of producing composite foamed shaped articles in single-charge rotational foam molding. The key of this invention is the use of resins having different heat capacities. This concept uses a thermoplastic resin, containing a blowing agent, with a greater heat capacity than that of the thermoplastic resin not containing a blowing agent. The required ratio between the melt capacity of the foaming and the non-foaming resin must be in the range of over 50 to below 1000, with a preferable value around 100. In situations when both the foamable and the non-foamable resins are of the same class and are considered to have same heat capacities, the size of the resins can be used to set the required difference of heat capacities, because the heat capacity of the resin becomes greater as its particle size increases.

Duffy [71], disclosed a two-step non-interrupted dry-blending based rotational foam molding method for producing integral-skin cellular composites. According to this invention, both the non-foamable and foamable resins are introduced at the beginning of the operation but they are maintained separately until the non-foamable resin melts and coats the interior surface of the mold. After the outer skin is rotationally molded in the initial step, in the second step, the foamable resin is released from a specially designed two-piece container located inside the mold. An optional design, in which a flexible plastic bag is used to hold the foam charge until its rupture under certain molding thermal conditions, is also disclosed.

Needham [72], disclosed a dry-blended polyolefin-based foamable powder mixture suited for producing integral-skin hollow foamed articles in rotational foam molding. Besides the basic PE resin, the mixture includes a CBA (sodium bicarbonate), and a nucleating agent. The gas-releasing blowing agent should release gas at a temperature near the melting temperature of the polyolefin base resin. Otherwise, if the release temperature is too high, the polyolefin base resin may have inadequate melt viscosity during foaming and collapse of the foam structure may result. On the other hand, the nucleating agent may increase the containing melt strength of the polyolefin base resin and provide for controlled cellular expansion. It is claimed that if the nucleation agent would be omitted, the foamed cells would usually overexpand and rupture, producing an unsatisfactory appearance and deformed or irregular shape.

Crawford and Nugent [73], attempted to overcome the processing problems they identified in Slade's invention [69], such as the difficulty of reliably achieving a complete separation of the two layers since, typically, some of the larger particles stick to the mold, foam at the surface, and so flaw the solid skin. The key point of this invention is the proposal for coating the granules containing a blowing agent prior to subjecting them to rotational foam molding. According to the invention, during the molding process, the coating promotes separation between the granular molding material and the other molding material so that the materials form different but adjacent layers.

Graham [74], disclosed a method for improving the impact strength of rotationally molded objects, including foamed ones, without the use of cross-linking agents. The invention introduces the making and the use of heterogeneous polymer particles that incorporate a core layer and a shell layer respectively, each of which exhibits different properties. The use of such particles is recommended for eliminating common problems encountered when using the difference in polymer particle sizes (powders versus pellets or granules) for controlling the formation of two different layers in rotational foam molding.

Needham [75], claimed an improvement of his previous patent [70]. A method is disclosed that uses two resins of significantly different particle sizes for charging the mold. The principle used guarantees that the resin having the smaller particle size will form the outer skin while the powder having the greater particle size will form the inside layer or the core. If foaming of the inside core is desired the polymer having the greater particle size should be premixed with the CBA and then inserted into the mold.

Kliene [76], claimed that in order to achieve an acceptable skin thickness and uniformity using in a single-charge rotational foam molding method, in addition to providing the two main components (non-foamable and foamable) of the mold charge with differing particle sizes, it would be necessary to also provide distinct temperature stages in the process for the materials within the mold, i.e., an initial lower processing temperature high enough for completing the skin-formation phase, but not sufficiently high to melt the larger foamable pellets, followed by a higher foam-forming temperature is proposed. However, this proposal failed to provide an explanation how this kind of temperature profile improves the processing of skin-surrounded foams in single step rotational foam molding.

Strebel [77,78], disclosed a compounding-based single-charge method that uses two distinct thermoplastic resin components: foamble and non-foamble. The first component is charged into the mold in a pellet form. These pellets are obtained by mixing the ethylene polymer with a CBA in an extruder. The temperature used for mixing should be above the melting temperature of the resin but below the decomposition temperature of the CBA. The second component is charged into the mold in a powder form and is in fact a blend of ethylene polymer powders with different particle sizes and melt indexes.

Strebel [79], disclosed improved compositions for rotational foam molding that include an ethylene polymer in pellet form containing a CBA, organic peroxide and, optionally, a metal-containing activator compound, and a non-foamble ethylene polymer or copolymer in a powder form having less than 30% crystallinity.

Lee et al. [80], in a U.S. patent assigned to WedTech Inc, Toronto, disclosed novel molding compositions useful for single-charge rotational foam molding of integral-skin cellular composites consisting essentially of a mixture of a skin-forming component in a powder form and a foam core-foaming component in a form of pellets physically dry-blended together. The skin-forming component comprises two distinct phases blended together, a high zero shear viscosity material and a low zero shear viscosity material, whereas the foam core-forming component comprises a foamable polymeric material including a suitable blowing agent. This invention attempts to overcome previous problems with obtaining insufficiently smooth, thick, and uniform outer skin layers, which often fails to meet aesthetic or performance characteristics for different applications. According to the present invention, polymeric materials that exhibit a zero shear viscosity of less than 1,500 [Pa.s] at 190 °C and at a shear rate of 0.005 [s^{-1}] are referred to as "low zero shear viscosity" materials, whereas those exhibiting a zero shear greater than 2,000 [Pa.s] under the same conditions of measurement are referred to as "high zero shear viscosity" materials. A "bricks-and-mortar" analogy roughly describes the role of zero shear viscosity in the skin-forming component. The high zero shear viscosity component ("bricks") lays down along the mold inner surface, where it acts as a partitioning agent ("wall") to keep the foamable component from adhering to the inner skin surface. The low zero shear viscosity part ("mortar") of the skin-forming component completes the formation of the skin structure by melting and filling gaps in the porous structure formed by the high-viscosity component. Another way of regarding the underlying process is that the low-viscosity material is the first to deposit (melt) against the mold surface, the high viscosity part of the skin-forming component then "blocking" the particles or pellets of the foamable core-forming component so that they do not attach to the mold wall, where premature blowing/foaming action of this material could mar or thin the skin surface.

2.4 Summary

The surveyed patent literature indicates that for the manufacture of integral-skin cellular polyolefin composites using the single-charge rotational foam molding technology, it would be essential to charge the mold with predetermined quantities of non-foamable and foamable resins having a significant particle size difference [61,62,64,66,68-70,73,75-80]. The non-foamable particles intended for forming the skin should be introduced into the mold in a powder form, whereas the foamable particles intended for forming the foamed core should be first extrusion melt-compounded with an adequate quantity of CBA and then introduced into the mold in a pellet form. The powder particles would sinter earlier than the pellets because of their greater total contact area and because their smaller size would allow them to migrate towards the internal surface of the rotating heated mold where the temperature is the highest. Thereby, the powder will preferably fuse and form the skin layer before the uninterrupted heating of the mold initiates pellet sintering and subsequently trigger the decomposition of the CBA particles dispersed within the foamable pellets to form the foamed core. However, it seems that this concept may be effectively improved by selecting non-foamable resins that have a lower melting point [69], density [69], viscosity [69], and/or heat capacity [70] than the respective properties pertaining to the foamable resins. In addition, the non-foamable skin-forming resin should preferably comprise of a low and a high zero shear viscosity component [80]. Yet, the mold could be charged with a blend of non-foamable and foamable powders (usually reground compounded pellets of a polymer with a CBA) of polymers that have significantly dissimilar melting points and/or significantly dissimilar particle sizes [72]. Also, a more intensive mold rotation during the formation of the skin and an optimized oven temperature profile would be helpful in preventing the premature adherence of the foamable pellets on the skin [76].

CHAPTER 3

THEORETICAL BACKGROUND

3.1 Rheological Polymer Properties Relevant for Rotomolding

The development of quantitative relationships between deformation and force for a material of interest based on experimental measurements is considered as the principal aspect of rheology [81]. The reheological properties of polymers are related to their molecular weight and molecular weight distribution. Properties associated with large deformation such as viscosity and toughness are related to weight average molecular weight, M_W, while melt elasticity is closely dependent on the z-average molecular weight, M_Z [54].

To evaluate and understand the complex flow characteristics of polymers, it is necessary to characterize their flow properties over a wide range of deformation conditions, e.g., stress and/or rates of shear, by using proper means for extracting data describing the contribution of a polymer's viscosity and elasticity components to its overall flow properties. Dynamic measurements, where a sample is subjected to a periodic deformation of stress or strain, are particularly well suited for characterizing the viscoelastic materials because of their ability to rigorously determine both the elastic and viscous response of a sample in one experiment. In an oscillatory shear experiment, a thin sample of material is subjected to a simple shearing deformation such that the shear strain as a function of time is given by [81]:

$$\gamma(t) = \gamma_0 \sin(\omega t) \tag{3.1}$$

where: γ_0 is the strain amplitude and ω is the frequency.

If γ_0 is sufficiently small, it can be shown by using the Boltzmann superposition principle that the stress is sinusoidal in time and has the same frequency as the strain [81]:

$$\tau(t) = \tau_0 \sin(\omega t + \delta) \tag{3.2}$$

where: τ_0 is the shear stress amplitude and δ is a phase shift/lag. Namely, the applied periodic deformation causes a periodic response in the sample. This response might lag behind or lead ahead the occurrence of deformation. This phase lag, $(\delta, \tan\delta)$, represents a direct measurement of the ratio of the viscous to elastic contribution of the overall response in the sample. Accordingly, the results of an oscillatory shear experiment can be presented by the relationship given by Equation (3.3) [81].

$$\tau(t) = \gamma_0 [G'(\omega)\sin(\omega t) + G''(\omega)\cos(\omega t)] \tag{3.3}$$

where: $G'(\omega)$ is called the "storage modulus" and $G''(\omega)$ is called the "loss modulus". Using the phase lag and the magnitude of the sample's response, the signal can be decomposed into an in-phase and an 90° out-of-phase components, the in-phase representing the elastic response, whereas the 90° out-of-phase describing the viscous response. From the in-phase information, the storage modulus, G', is determined. The storage modulus is a measure of a sample's ability to store energy and is called the elastic modulus. From the 90° out-of-phase information, the loss modulus, G'', can be determined. The loss modulus is a measure of a sample's ability to dissipate energy. These two quantities can be calculated from the amplitude ratio "$G_d = \tau_0/\gamma_0$" and the phase lag δ as follows [81]:

$$G' = G_d \cos(\delta) \tag{3.4}$$

$$G'' = G_d \sin(\delta) \tag{3.5}$$

The ratio of the loss modulus to the storage modulus is called $\tan\delta$ and represents the damping properties of the sample, e.g., a low $\tan\delta$ means higher resilience and less hysteresis. A large value of, G', in comparison with, G'', indicates pronounced elastic properties of the polymer being analyzed. For such a polymer, the phase angle is also small, e.g., 20° (a phase angle of 0° means a perfectly elastic material and a phase angle of 90° means a perfectly viscous material). The frequency sweep gives information about the elastic strength, e.g., a large slope of the G' curve indicates low strength and a small slope indicates high strength [81,82].

3.1.1 Zero Shear Viscosity

The viscosity represents a measure of the material's internal resistance to deformation rate (flow/shear) [83].

Newton's law defines the viscosity, η, mathematically as the ratio of shear stress, τ, and shear rate, $\dot{\gamma}$, i.e.,

$$\eta \equiv \frac{\tau}{\dot{\gamma}} \tag{3.6}$$

Fluids are classified as Newtonian if the relation (2.11) is linear, i.e., if the viscosity is a constant independent of shear rate, and non-Newtonian otherwise. Polymeric melts are non-Newtonian fluids. Extrusion viscosimeters and capillary and parallel plate rheometers are used to measure viscosity of polymeric melts [83,84].

Cogswell et al. [85] and Barnes et al. [86], showed that the polymer viscosity is influenced by four main factors: shear rate, temperature, molecular weight, and pressure. Since pressure is not present in the rotomolding process, its effects on polymer viscosity will not be discussed further.

3.1.1.1 Effect of Shear Rate on Viscosity

Helleloid [84], described the viscosity dependence on shear rate for polymeric melts by summarizing the following important properties:

(i)

$$\lim_{\dot{\gamma} \to 0^+} \eta = \eta_0 \tag{3.7}$$

where: η_0 is the zero shear viscosity

(ii) Shear rate values below which the viscosity levels out are too small.

(iii) Experimental measurement of zero shear viscosity using available tools is not possible for most polymeric melts.

(iv) $\eta\left(\dot{\gamma}\right)$ is a decreasing function of $\dot{\gamma}$. This behavior is known as "pseudoplastic" behavior.

(v) As shown in Figure 3.1, for sufficiently low shear rate values ($\log\dot{\gamma} \le a$), viscosity becomes independent of shear rate, i.e., the material exhibits a Newtonian behavior. For ($a \le \log\dot{\gamma} \le b$) the dependence of $\log\eta$ on $\log\dot{\gamma}$ is non-linear. For ($b \le \log\dot{\gamma} \le c$), η has a power law dependence on $\dot{\gamma}$. Finally, as $\dot{\gamma}$ increases beyond c, the viscosity curve levels out, and the material tends toward a Newtonian behavior again.

(vi) $\eta\left(\dot{\gamma}\right)$ possesses a horizontal asymptote, which, for most polymeric melts, is impossible to determine experimentally due to polymer degradation at high shear rates.

The shear rate experienced during rotational molding has been estimated to be as low as 1×10^4 [s^{-1}] [87]. Since a negligible shear motion is involved during the rotational molding process, and since the mold is vented, rotational molding is considered as a virtually shear and pressure free process [24,26,88]. In this context, Barnes et al. [86], suggested that it can be assumed that the viscosity of the polymer during rotational molding is Newtonian because it is being subjected to low shear rates. However, the effect of a low shear rate on the viscosity of a polymer is not well known yet [88].

3.1.1.2 Relationship Between Melt Index and Viscosity

The molecular weight of a polymer determines its melt index so that a polymer with a high molecular weight will yield a low melt index [88]. Typically, processors use the material's MFI as a parameter that indicates the material's ability to flow and reproduce the surface of the mold, the rationale being: the higher the melt index, the better the material will flow. However, the melt index corresponds to a one point inverse viscosity measurement at a relatively low shear rate, i.e., it corresponds to a single point on a viscosity curve [83]. In addition, during the melt index test, the shear force exhibited on the polymer is significantly higher than during the rotomolding process [88]. Thus, the MFI is a very poor indicator of how a resin performs during rotomolding. Hence, the zero shear viscosity of the resin, rather than its MFI, becomes the most important property for accessing its rotomoldability [89].

Spence [88], used an extrusion plastomer to experimentally investigate the relationship between the shear rate and the apparent viscosity of a rotomolding polymer resin. These experiments revealed that the viscosity of a higher melt index (8 [g/10min]) resin increases linearly as the shear rate decreases, whereas a low melt (3.2 [g/10min]) index resins demonstrated more exponential growth as the shear rate tends towards zero. These results indicated that by reducing the rate at which polymers are being sheared the already existing differences between their viscosities get even greater. In the context of the rotomolding process, this indicates that low melt index materials are more difficult to mold because the low shear rates at which they have been subjected during the molding process have a greater influence on the viscosity of low melt index resins.

Spence [88], also found that the relationship between the material's melt index and its viscosity is reasonably linear in the range of 3.2 to 8 [g/10min] melt index, whereas as the material's melt index increases up to 25 [g/10min] the reduction in viscosity is less evident. Thus, low zero shear viscosity resins demonstrate improved surface finish due to their better sintering behavior [90] and favorable flow properties, whereas high zero shear viscosity resins result in poor surface finish and excessive amounts of unwanted bubbles [24].

3.1.1.3 Effect of Temperature on Viscosity

The temperature dependence of viscosity, η, for Newtonian fluids and for most polymer fluids above the glass-transition temperature follows the Arrhenius equation to a good approximation:

$$\eta = Ae^{B/T} \tag{3.8}$$

where: T = absolute temperature

A and B = constants of the liquid

Unlike the MFI test, which is performed at 190 °C for PE, and at 230 °C for PP when it is referred to as the melt flow rate (MFR), the rotational molding process is a dynamic process in which the temperature of the resin continually changes. In this respect, Spence [88] found that high melt index resins increase in viscosity linearly with decreasing temperature, whereas lower melt index resins display more rapid exponential growth with decreasing temperature. Thus, low melt index resins need to be heated to higher levels to achieve comparable viscosity or flow properties.

3.1.1.4 Effect of Molecular Weight on Viscosity

The zero shear viscosity, η_0, being a fundamental property of polymeric materials, has been the subject of intensive studies aimed at understanding its relationship with the polymeric structure [91-95]. Experimental and theoretical studies identified the presence of a double viscosity regime in polymers. Namely, at low average molecular weights, M_W, the relationship of viscosity with molecular weight was found to be substantially linear [91,96], but Fox and Flory [92] claimed, on the basis of measurements on narrow distribution fractions of polystyrene and polyisobutilene, that while at molecular weights higher than a critical value, M_C, the relationship follows the 3.4 power of molecular weight. These relationships are expressed as follows:

$$\eta = K_1 M_W \text{ for } M_W < M_C \tag{3.9}$$

$$\eta = K_2 M_W^{3.4} \text{ for } M_W > M_C \tag{3.10}$$

where: K_1 and K_2 = constants depending on temperature

Equation (3.10) applies to both melts and concentrated solutions for many different polymers [91,93]. However, the presence of a sharp transition between the two regimes at $M_W = M_C$, has been the subject of considerable attention in the last seven decades and especially since it was found that M_C is a characteristic constant of polymer melts equal to about 2-3 M_e, where M_e is the average entanglement molecular weight [91].

The entanglements are considered as the key factor controlling not only the melt rheology but also the solid mechanical [97-99] and adhesive properties of polymers [100]. However, the nature of the entanglements has often been discussed and criticized in the literature. For a number of years, entanglements have been considered as time fluctuating and de-localized networks [91]. However, although the entanglement concept is useful in explaining the break in the viscosity-molecular weight curve, the approach was difficult to be extended to viscoelastic effects quantitatively and has been abandoned in favor of the reptation theory [83]. The reptation model which proposed a different description of the macromolecular structure was introduced by De Gennes [101] and developed by Doi and Edwards [102,103]. In this model, the tube diameter has been introduced as an equivalent concept to the specified entanglement spacing, which allows an alternative description of the polymeric structure. Namely, reptation theory predicts that for the polymer chain to move in an entangled melt it can only do so along a tube formed by the constraints provided by the surrounding polymer chains. The time taken for a polymer chain to diffuse out of this tube is known as the reptation time.

The 3.4 power dependence of molecular weight has been extensively investigated and explained by several models of entanglements. In this context, the friction theory of Bueche [104] determines a value of 3.5 for the power dependence beyond $M_W = M_C$, whereas the reptation model of De Gennes [105] and Edwards [106] predicts a value of 3.0, but it was later modified by De Gennes to predict 3.4, invoking the effect of tube length fluctuation. Although it has been reported [107,108] that in some polymers the 3.4 dependence increases at higher molecular weight, there seems to be, at present, a consensus that the 3.4 exponent is a universal characteristic of entanglements in macromolecular chains, that it is constant, independent of temperature, pressure or stress [109].

Locati et al. [110], derived a formula for estimating the number of entanglements n_e per molecule which served for developing a mathematical model that is capable of describing the behavior of viscosity of polymeric systems over a full range of molecular weights by a single continuous function.

The effect of molecular weight distribution (MWD) on viscosity is attributed to chain entanglements during the flow of polymer molecules. Thus, when a polymer has a broad MWD short chains are present which are not involved in entanglements. This results in lower viscosity due to a reduction in friction caused by chain movement. In contrast, polymers with narrow MWD (such as metallocene polymers) appear to have a higher viscosity than respective analogs at higher shear rates [54].

3.1.2 Viscoelasticity

Ideally, materials would behave either entirely elastic and obey Hooke's Law, which states that the stress in the sample is a function of deformation only and not a function of time, or entirely viscous and obey Newton's Law of viscosity, which states that the stress in the sample is a function of the rate of deformation. However, polymers possess the properties of both elastic and viscous materials and therefore fit into a broad class of complex fluids characterized by the term viscoelastic [81]. In recent years, the melt elasticity of the polymeric resin has been also receiving importance with respect to rotomoldability [87].

The complex viscosity can be expressed via two components both of which have units of viscosity. These include the "dynamic viscosity" $\eta'(\omega)=\left(\tau/\dot{\gamma}\right)\sin\delta = G''/\omega$ and a material function $\eta''(\omega)=\left(\tau/\dot{\gamma}\right)\cos\delta = G'/\omega$ [81]. Thus, the complex viscosity is given as presented in Equation (3.11) [81],

$$\eta^*(\omega) \equiv \eta'(\omega) - i\eta''(\omega) \tag{3.11}$$

while its modulus is calculated by the relationship given in Equation (3.12) [81].

$$|\eta^*| = \tau / \dot{\gamma} = \sqrt{(\eta')^2 + (\eta'')}^2 \tag{3.12}$$

Polymeric materials are said to have a "memory", in that when deforming stresses are eliminated, they tend to return to a previous configuration. However, molten polymers are said to have a "fading memory" since the entanglement network is not permanent and is altered by flow and relaxation processes. Since the response to a sudden change in stress or strain of molten polymers is always time dependent, never instantaneous, and there is both elastic storage of energy and viscous dissipation, the combination of viscous and elastic properties endows the molten polymer with a characteristic time and makes its response time-dependent. This time is referred to as relaxation time, whereas a rheological experiment in which a sample is suddenly deformed at time, $t = 0$, and the resulting stress is measured as a function of time is called a stress relaxation experiment. In the case of a sudden shear strain of magnitude, γ_0, the quantity reported is the shear relaxation modulus, $G(t, \gamma_0)$. However, when the strain is very small, the relaxation modulus is independent of strain. In this case, the stress at any particular value of, t, is proportional to the strain. This small-strain behavior is called linear viscoelasticity. Thus, if the relaxation modulus, $G(t)$, is determined in any experiment, then the linear response to any type of deformation can be predicted [81].

However, it is more convenient to have a general functional form for $G(t)$, that contains sufficient parameters to fit experimental data for a wide range of polymeric liquids. The most popular approach to establishing such a functional form is based on the use of the Maxwell element analogy. If we take the spring constant, K_e, to be analogous to the initial shear modulus, G_0, of the polymeric liquid, and the time constant, K_v / K_e, to be analogous to the relaxation time of the liquid, λ, then in a step shear strain experiment the shear relaxation modulus can be presented as in Equation (3.13) [81].

$$G(t) = G_0[\exp(-t/\lambda)] \tag{3.13}$$

However, actual relaxation processes cannot be described by a single exponential function. A great flexibility can be obtained by use of the "generalized Maxwell model," which is the rheological constitutive equation analogous to the mechanical assembly shown in Figure 3.2. The forces in the various elements are additive, and if, G_i, and, λ_i, are the modulus and relaxation time corresponding to each Maxwell element, the relaxation modulus can be expressed as in Equation (3.14) [81]. :

$$G(t)=\sum_{i=1}^{N} G_i\left[\exp(-t/\lambda_i)\right] \tag{3.14}$$

By use of a sufficient number of elements, this equation can be made to describe almost any experimental, $G(t)$, behavior. If $G(t)$ is approximated by use of the generalized Maxwell model with a finite number of elements, the behavior of $G(t)$ at sufficiently long times will be dominated by the, $G_i - \lambda_i$, pair having the largest value of λ_i, and in the terminal zone $G(t)$ will therefore decrease exponentially with time. This largest, λ_i, is called the "terminal relaxation time." However, in the computation of one linear viscoelastic function from another, it is sometimes convenient to make use of a continuous spectrum. This can be defined by letting the number of elements in the generalized Maxwell model increase without limit so that, $G(t)$, can be represented in terms of a continuous function, $F(\lambda)$, such that, $Fd\lambda$, is the contribution to the modulus from relaxation times between, λ, and $\lambda + d\lambda$. Then, the relaxation modulus is related to the spectrum as given in Equation (3.15) [81].

$$G(t)=\int_{0}^{\infty} F(\lambda)\left[\exp(-t/\lambda)\right]d\lambda \tag{3.15}$$

However, a logarithmic time scale is normally used for the spectrum, and the continuous spectrum, $H(\lambda)$, is used in place of, $F(\lambda)$, where, $H = F\lambda$, and $Hd\ln(\lambda) = Fd\lambda$. The relaxation modulus is then related to, $H(\lambda)$, as given in Equation (3.16) [81].

$$G(t)=\int_{-\infty}^{\infty} H(\lambda)\left[\exp(-t/\lambda)\right]d(\ln\lambda) \tag{3.16}$$

Kontopoulou [111] and Kontopoulou et al. [112] used a stress relaxation measurement to determine the elasticity of various resins. The results revealed that resins with increased melt elasticity tend to manifest processing difficulties, increased part porosity, and uneven thickness [111]. Weber and Gonzales [87], also found that among two rotational molding grade PE resins having identical viscosities and similar MFI and density, the one having less elasticity demonstrates superior processability and performance. Vlachopoulos et al. [113], found that melt elasticity also plays a role in particle coalescence (sintering), fusion, and bubble removal.

During the rotational foam molding processing cycle both melt viscosity and melt elasticity affect the bubble growth dynamics in viscoelastic polymer melts [114,115], these two rheological properties should be regarded as relevant for assessing the suitability of the resin for this process, i.e., its rotofoamablity. The bubble formation and the early stage of diffusion-controlled bubble growth are favored by a low melt viscosity. As the bubble walls stretch due to the further growth of the bubble, the tensile stresses subject them to elongational deformation so that this segment of the foaming process is being controlled primarily by the elongational viscosity, melt-strength, and melt elasticity of the polymer. However, during the subsequent stage of bubble stabilization, a high elongational viscosity is preferable to achieve the desired cell size [54].

3.1.3 Melt Strength

If the melt strength of the polymer is too weak, the thickness of the cell wall decreases due to polymer drainage occurring in the cell wall at the time of volume expansion so that it becomes highly stretched and very unstable, and therefore, undesirably prone to rupture. Such processing difficulties are particularly common to foaming PP because PP has a sharp melting point and poor melt strength [116]. However, since PP has good physical properties and is a less expensive commodity resin compared to PE in recent years [117], there is a desire among processors to use PP for producing rotationally foam molded products.

The melt strength of a polymer is a measure of its resistance to extensional deformation and can be measured by using a Melt Strength Tester. It consists of a pair of rollers rotating in opposite directions that are mounted on a balance beam. A polymer melt strand extruded vertically downwards from a capillary die is drawn by the rotating rollers whose velocity increases at a constant acceleration rate. The polymer being stretched undergoes uni-axial extension. The tensile force in the strand measured by the balance beam can be plotted as a function of time or velocity of the rollers. The force at which the polymer melt breaks is called the "melt strength" [119]. Thus, the melt strength of a polymer is affected by several parameters such as melt temperature, extrusion rate, ambient temperature, and the distance between the capillary die and the melt strength tester. Regrettably, the melt strength parameter does not give a well defined rheological property because neither the strain nor the temperature is uniform in the polymer melt being stretched [120]. However, the test is still useful in obtaining meaningful comparisons of the drawing behaviors of different polymers.

Wolf [121] studied the effect of the above parameters on the melt strength of LDPE. Ghijsels et al. [122] and Micic et al. [123] studied the melt strength of ethylene-based polymers and blends in relation with the film blowing process. However, relatively few melt strength measurements have been performed on PP, possibly due to the difficulties of performing the experiment [124].

Wang et al. [125], indicated that most commercial isotactic PP resins have a linear architecture as a consequence of the Ziegler-Natta catalyzed polymerization. The absence of long chain branches leads to a deficiency in melt strength of PP. A reactive extrusion process (REX) was used to modify PP resins by introducing long chain branching to increase the apparent elongational viscosity and melt strength.

In order to overcame the melt strength drawback of PP, Scheibelhoffer et al. [126] blended PP with other polymers, whereas Sheve et al. [127] implemented post reactor long chain branching using an irradiation process.

Lau et al. [119], observed that the melt strength of conventional PP tends to increase linearly with increasing the extrusion rate at a constant temperature, whereas the melt strength of PP decreases linearly as the MFR increases. This becomes particularly significant when PP grades are subjected to foaming applications. The former could be attributed to the fact that PP grades having a lower MFR tend to have longer molecular chains and these long chain molecules can form more entanglements in the polymer structure.

Thus, polymers with higher degrees of entanglements will have higher resistance to extensional deformation and as a result, polymers having lower MFR tend to have higher melt strength. The latter implies that if the decomposition temperature of the employed CBA is too high an activator should be used. Therefore, for foaming PP applications, PP grades with low MFR should be selected, while the temperature of the melt should be preserved as close as possible to the melting point of the resin.

3.2 Thermal Polymer Properties Relevant for Rotomolding

Takacs et al. [128], suggested that not only the rheological properties but also the thermal properties of polymer resins such as melting point, crystallinity, and heat of fusion should be regarded as factors that can significantly affect their processability and the quality of the final product in rotational molding.

3.2.1 Crystallization Behavior

Since during rotational molding a vented mold rotates at relatively low speeds, there are no forces in the mold to push the material together to form the part so that the resin must be able to adhere to the hot mold surface and sinter without pressure [87]. Thus, polymers with a low melting temperature and low heat of fusion (translating into low crystallinity) can offer early onset of the adherence and sintering stages during rotational molding, resulting in reduced cycle times [128].

Crawford [24], found that the crystallinity is also correlated to the mechanical properties of the molded parts. Typically increased crystallinity results in higher stiffness, at the expense of impact properties.

Callan et al. [129], found that slower cooling produces a higher degree of crystallinity in comparison to water-cooling. In addition, it was observed that externally cooled moldings exhibit a crystallinity gradient through the thickness of the part and that the crystallinity gradient is greater from the outer to the middle surface than it is from the middle to the inner surface due to the formation of a crystal growth front. The large difference in crystallinity between the outer and middle surfaces is attributed to the fact that fast water cooling only allows small crystals to form on the outer surface. Since the middle region cools at a slower rate than the outer layer, a larger number of bigger crystals form. As the inner surface cools even slower it has more of the larger crystals throughout the thickness of the molding. The outer surface typically has 33.9% crystallinity as opposed to 42.6% and 46.4% for the middle and inner regions.

3.2.2 Degradation Behavior

The microstructure and the properties of polymers are very sensitive to the thermal treatment they have been subjected to during the molding stage [130]. Since during rotational molding the plastic is exposed to relatively high temperatures for long periods of time, this often causes polymer degradation at the inner surface of moldings which is in contact with oxygen. The resulting degraded layer deteriorates the mechanical properties of the part [131].

Cramez et al. [130], found that in rotational molding, polyethylene and polypropylene show a different degradation behavior. It was observed that if moderately overheating polyethylene, the size and perfection of the spherulites near the inside surface reduces and an inward growing layer of columnar type structure starts to appear, whereas if the heating is too severe and the temperature inside the mould goes above a certain value, the spherulitic texture disappears completely near the inside surface, and is replaced by a dark ribbon of material, apparently without any texture. However, for polypropylene, the overheating of the polymer did not prevent the crystallization of spherulites near the inner surface, but it increased their size and birefringence (double refraction). Namely, in polypropylene the thermooxidative degradation causes mainly chain scission, while in polyethylene crosslinking dominates.

In a more recent paper, Cramez et al. [131], investigated the onset of degradation of rotomolded parts using the Oxygen Induction Time (OIT) technique. They developed a model for predicting the decomposition temperature and experimentally validated the obtained data at various heating rates.

3.3 Principal Mechanisms Governing the Rotomolding Process

Fundamental research efforts have been focused on predicting the optimal rotomolding conditions by studying the heat transfer phenomenon which dominates the entire rotational molding process. However, a limited number of analytical studies are available on heat transfer in conventional rotational molding. Among these, only a few studies focus on the cooling stage of the process.

3.3.1 Heat Transfer

While several authors have presented heat transfer models for predicting the molding cycle [132-142], regrettably, there are no available studies with respect to either heat transfer or the cooling stage of single-charge rotational foam molding of integral-skin cellular composites.

Rao and Throne [132], investigated the effect of rotational speed on the time required for complete melting of the powder. They showed that this time decreases with increasing the rotational speed and asymptotically approaches a constant value at about 10-20 [rpm], which is within the range of typical rotational molding. A number of years later, Throne [133] proposed an alternate heat transfer model, in which the powder was assumed to be in a static contact with the mold surface at all times. The latter model showed better agreement with experimental data.

Nugent [134], and Crawford and Nugent [135], developed the ROTOSIM program, which examines the biaxial motion of a hollow mold containing a powder mass with a series of superimposed heat transfer models.

Nugent [134], presented numerical simulations that predicted temperature profiles of the mold and internal air during the plastic solidification and beyond. However, they deviated substantially from his experimental results, i.e., the predicted temperature profile for the internal air does not show a temperature plateau during the plastic solidification. The model required modification at the mold/plastic and plastic/internal air interfaces.

Crawford and Nugent [135], developed a numerical simulation of the heating cycle in which the movement of powder in the mold was mapped out thus allowing for the prediction of melt deposition distribution. They used a finite difference method to solve for the mold, polymer, and air temperature profiles. The temperature dependence of the polymer properties was accounted for and the density evolution of the polymer was described using an empirical relation. Nugent et al. [136], compared this model with experimental results for a wide variety of processing conditions.

Sun and Crawford [137], proposed further improvements to the above simulation by developing a model considering the internal heating and cooling in rotational molding. In this model, the powder was treated as a static layer in contact with the mold and heat transfer from the mold to the powder was analyzed much like heat transfer in a packed particle bed.

Bawiskar and White [138], presented an analytical model describing powder heating and melt deposition in rotational molding. The model predictions indicated that the mold material thermal properties and the mold thickness, combined into a single parameter, have a profound effect on the melting time.

Gogos et al. [139], recently developed a new detailed theoretical model of the rotational molding process based on the assumption that the powder is well mixed, the curvature effects in the mold are negligible, the temperature profile in the melted polymer is linear, and that the thermal properties of the materials are constant. Only the initial stages of the rotational molding process up to the end of the plastic powder deposition were analyzed. The theoretical model was employed to create differential and lumped parameter models as well as a simple closed form approximation for the time required for complete powder deposition (powder-end time). Both numerical models gave results that are in very good agreement with experimental data available in the literature, while the closed form solution gave good predictions over a wide range of processing parameters. The key dimensionless groups were identified and the effects of variations in these groups on powder-end time were evaluated. They showed that the oven temperature, the polymer melting temperature and the polymer to mold heat capacitance ration were key parameters affecting the melting time.

Throne [140] applied the Goodman method to establish a simple approximate model while investigating various factors that influence cooling rates. It was concluded that the use of a pre-cooling period before water quench seemed justified. The crystallization process of the plastic was not addressed.

Gogos et al. [141], presented a detailed heat transfer model for the entire rotational molding process (including heating and cooling stages). Additional dimensionless groups affecting the process cycle time were identified and the effects of variations on all groups on the cycle time were evaluated. This theoretical model has been employed to generate numerical results that are in very good agreement with the experimental data available in the literature. In addition, part shrinkage has been incorporated in the models, and its effect on the process cycle time was studied.

Olson et al. [142], presented a validation study comparing the mold wall temperature estimates from an axisymmetric thermal finite element simulation of the rotational molding process with temperature data obtained during experiments conducted on industrial-grade rotational molding equipment. The finite element model simulates the heat transfer process involved in rotational molding through the end of powder deposition. The simulation results for mold wall temperature agreed well with the experimental data under all of the conditions tested.

3.3.2 Polymer Particle Sintering and Melt Densification

In its most general terms, sintering is defined as the formation of a homogeneous melt from the coalescence of solid particles under the action of surface tension [143-155].

Rao and Throne [155], suggested that the formation of a homogeneous melt when polymer powder particles come in contact with each other at elevated temperatures involves two distinct steps. During the first step, the particles stick or fuse together at their points of contact and this fusion zone grows until the mass becomes a porous three-dimensional network with relatively little density change. This is referred to as sintering. During the second step, i.e., at some point in the fusion process when the network begins to collapse into the void spaces, they become filled with molten polymer that is drawn into the region by capillary forces. This is referred to as densification.

Progelhof et al. [156], observed from hot plate experiments that as the powder is heated, the particles become sticky and adhere to each other, and upon further heating, the particles fuse together or densify to form a unitized structure. As the heating process continues, the solid/melt interface moves upwards, the top of the free surface of the powder drops, and with time the powder melts completely.

Polymer powder particles tend to decrease their total surface area by coalescence, which is usually accompanied by a decrease in total volume of the particulate bed. The driving force for particle coalescence is surface tension, whereas the main factor opposing it is the resistance to flow, expressed by viscosity [148,149]. However, in semi-crystalline polymers the coalescence of polymer particles occurs at temperatures above their melting point, whereas in amorphous materials it takes place above their glass transition point [145]. Notwithstanding this fact, polymer coalescence is often wrongly referred to as polymer sintering and this terminology is widely accepted in the literature [145]. In addition, because of the increase in polymer density associated with sintering, the term "densification" is also used interchangeably with the term sintering in the material science literature [154].

In rotational molding, polymer sintering governs the transformation of a loosely packed, low density powder compact, to a fully densified polymer part, when processed at temperatures above the melting (or glass transition) point of the polymer [151-154]. This melt deposition and densification process is being governed by two bulk movements: the melt front progression and the collapse of powder particles into the melt [157]. The later movement causes the entrapment of air into the melt and thus the formation of bubbles [146]. Because it dominates a significant part of the heating time, polymer sintering is regarded as the fundamental and controlling mechanism for the rotational molding process [49]. As such, it has a profound influence on the presence of bubbles, thickness uniformity, and overall quality of the final part [89].

Although the heat transfer models mentioned in Section 3.3.1 provide predictions that are in general agreement with the experimental data presented in literature, they are restricted to simple mold geometry [146]. Moreover, none of these models have considered heat transfer combined with particle sintering and melt densification, and thus, these models do not allow for the prediction of the end product porosity for a given material and molding conditions

[49,146]. Various models have been proposed to describe the early stage of the densification process in which a neck is formed between individual particles.

Frenkel [148], derived the first analytical model for viscous sintering of two particles. Several alternatives to Frenkel's model have been suggested to overcome some of its limitations, namely the prediction of the complete process [158,159] and the considerations of material properties other than surface tension and viscosity [160,145].

In more recent fundamental and practical studies on the particle sintering and melt densification processes in rotational molding, Bellehumeur [143,144,147] and Pokluda et al. [159], put great efforts to develop suitable models for describing the sintering of two polymer powder particles. Bellehumeur et al. [145], observed that polymer sintering is not affected only by surface tension and viscosity, but also on melt elasticity, the effect of which slows down the process of polymer sintering. Using a similar approach to Frenkel [148], a viscoelstic sintering model capable of predicting the sintering rate slowdown was developed.

Also, Kontopoulou [151], Kontopoulou et al. [152, 153], and Kontopoulou and Vlachopoulos [154], modeled the early stage of the densification process which involves particle coalescence that depends on viscosity, surface tension, and powder properties, based on a formulation proposed by Scherer [161]. Importantly, they developed a model that considered the fact that the powder coalescence in rotational molding occurs in a three-dimensional compact so that it effectively describes the three dimensional shrinkage of the compact and the evolution of its density with time, as it sinters.

Kandis and Bergamn [162], proposed a model that describes the non-isothermal densification of a powder compact. Although this model can be used to predict many experimentally observed transformations of a polymer compact during sintering, since it does not consider the key features of the rotational molding process, the predictions are valid only for the densification of a stagnant compact of powder.

Bellehumeur [163], developed a model for predicting powder sintering in rotational molding based on the sintering model developed by Bellehumeur et al. [145] and the lumped parameter heat transfer formulation proposed by Gogos et al. [139]. It has been found that as the oven temperature increases, each layer of melted powder has less time to sinter before an additional layer of powder adheres to it. This proved to be beneficial for reducing the heating time, but the initial bubbles formed were larger than those formed at lower oven temperatures.

3.3.3 Bubble Formation, Evolution, and Dissolution

Research studies on the later stage of densification which comprises the dynamics of bubble formation, evolution, and removal in rotational molding showed that as the melt front progresses, the air pockets that have been entrapped inside the melt eventually become bubbles that will be subjected to diffusion controlled shrinkage and eventual disappearance [154,155]. The porosity of the molded parts depends on both the completion of the sintering and diffusion processes [49].

Rao and Throne [155], concluded that surface porosity is intrinsic to the process because the buoyancy, capillary, and hydrodynamic forces, which would cause the interior void to move away from the mold surface, are not strong enough to overcome the surface tension force required to pull the surface void away from the mold surface and into a bubble.

Progelhof et al. [156], attempted to explain the formation of voids as a result of a bound inclusion of the space between individual particles. They also observed a slow movement of voids to the free surface and some coalescence of voids, but with time the voids diminished in size.

Kelly [46], observed that the air bubbles trapped into the melt remain stationary and decrease in diameter as the melt temperature increases. This is associated to the relatively small bubble diameter, combined with the high viscosity of the melt, which prevents the movement of the bubbles into the melt [46].

Crawford and Scott [157], modeled the process based on video records of the formation and subsequent dissolution of bubbles. They observed that the initial size of the bubble has a significant effect on the rate at which it dissolves, as the surface area-to-volume ratio is inversely proportional to the diameter. They found that this initial size was dependent on the size of the particles, and that the number of bubbles was dependent on the particle size distribution and the MFI of the material.

Crawford and Xu [164], derived a semi-empirical relationship between bubble diameter ratio, temperature, and time in order to predict the bubble diameter as a function of time and melt temperature.

Spence [165] and Spence and Crawford [47], studied the effects of viscosity, powder characteristics, processing conditions, moisture, mold material, and mold release agent. It was concluded that the disappearance of bubbles depends primarily on the viscosity of the polymer used. However, the surface porosity improved when the use of a release agent was avoided.

This has been attributed to the fact that applying a release agent reduces the surface tension of the mold material, which in turn reduces the attractive force causing the polymer to wet and spread evenly over the mold surface.

Kontopoulou and Vlachopoulos [48], and Gogos [50], modeled the dynamics of bubble dissolution into the melt during rotational molding using conservation of mass and momentum. Their results revealed that within the range of viscosity typical to polyethylene rotational molding grade resins, the effect of viscosity is marginal, whereas the level of air saturation in the polymer melt is crucial. Small variations in the level of saturation were found to cause large changes in the dynamics of the bubble dissolution [48,50].

Although the above models significantly improved the understanding of the densification process in rotational molding, they are limited to predicting the densification process carried out under isothermal conditions. In an attempt to alleviate this deficiency, Bellehumeur [146], found that the size of the bubbles formed into the polymer melt is primarily controlled by powder particle size and packing arrangement, whereas the material thermal and rheological properties affect the bubble formation process to a lesser extent. Variations of the processing conditions have shown marginal effect of the initial size of the bubbles formed into the melt and a more significant impact on the bubble dissolution stage of the process.

3.4 Theory of Polymeric Foam Systems

3.4.1 Cell Nucleation

Nucleation is a thermodynamic phenomenon focusing on the first bubble formation [166]. Since a lower surface tension at the site of bubble formation would facilitate the formation of that particular bubble, the formation of bubbles in a liquid requires an increase of the free energy of the system as described by Equation (3.17) [167].

$$\Delta F = \sigma \cdot A_{total} \tag{3.17}$$

where: ΔF = Free energy of system [J]

σ = Surface tension of liquid [N/m]

A_{total} = Total interfacial area [m^2]

Sounders [167], describes three distinct bubble formation scenarios in liquid systems:

(i) ***Homogeneous nucleation.*** It can occur in an initially truly homogeneous liquid, and then the bubbles form by a self-nucleation process [167]. Surface tension depressants such as emulsifiers, wetting agents, and silicone oils are used to lower the surface tension of the liquid [167]. Homogeneous nucleation should yield foams with smaller cell sizes and more uniform cell population distribution [3].

Stewart [168] investigated the theoretical bubble size needed for homogeneous nucleation during extrusion processing of polymer foams utilizing the kinetic theory of phase transitions in one-component systems.

The critical size of a bubble nucleus is given by Equation (3.18) [168].

$$n_{critical} = \left[\frac{(2\delta/3)}{kT \ln(p_1/p_2)} \right]^3 \tag{3.18}$$

where: $\delta = 4\pi\sigma(3kT/4\pi p_1)^{2/3}$

σ = Surface tension of polymer [N/m]

T = Absolute temperature [K]

k = Boltzman's constant [J/K]

p_1 = Gas pressure inside the nucleus [Pa]

p_2 = Melt pressure [Pa]

Thus, if the nucleus dimension is greater than $n_{critical}$, the nucleus will form a bubble. If it is less than $n_{critical}$, it will dissolve into single molecules or clusters of a few molecules [3].

The nucleation rate is a kinetic mechanism indicating the speed of the bubble formation [166]. Blander and Katz [169] proposed a mathematical model for the rate of bubble nucleation which assumes that steady-state bubble formation occurs in a thermodynamic equilibrium. However, various authors [169,170] agree that the rate of self-nucleation of microbubbles is negligible and that producing desirable foams by a self-nucleation process is difficult because self-nucleation is unlikely to occur.

(ii) ***Heterogeneous nucleation.*** It can occur in presence of a second phase, especially if it is in the form of finely divided solids, the bubbles form more easily at the liquid-solid interface. Then the bubbles are said to form by a nucleation process, and the solid particles are called nucleating agents. Nucleating agents provide a significantly reduced surface tension at the interface between the liquid and a solid particle, or by actually having voids at this interface [167].

Well-dispersed materials that locally depress the surface tension of the liquid, such as by forming many "hot spots" during exothermic reactions, may serve as nucleating agents [3,166]. Unlike CBAs, which are considered active, most nucleating agents are passive, i.e., they only provide low energy wells to which gas can migrate and adsorb and in which bubbles begin to grow. In contrast, the decomposition of a CBA particle produces the gas that remains adsorbed to the foaming agent residue, while the non-decomposed CBA particles and the residue from the decomposed CBA particles act as nucleating agents [3]. It is the gaseous material that then behaves as a physical blowing agent in the plastic process [171]. The concentration and the particle size of the nucleating agent play an important role in the bubble nucleation mechanism. Bubble diameters decrease with increasing the concentration of CBA. Coarse particles provide few nucleating sites, whereas very fine particles tend to agglomerate or are quickly engulfed by the growing bubble [3].

The initial bubble size for heterogeneous nucleation can be determined from the Rayleigh equation as given by the relationship presented in Equation (3.19) [3].

$$r = \frac{2 \cdot \sigma}{p_1 - p_2} \tag{3.19}$$

where: r = Radius of the bubble [m]

σ = Surface tension at the gas/polymer interface [N/m]

p_1 = Gas pressure inside the nucleus [Pa]

p_2 = Melt pressure [Pa]

Here, the diameter of the nucleated bubble, $d \equiv 2r$, is the dimension of the nucleating agent particle pore. Equation (3.19) implies that smaller bubbles are nucleated when the internal gas pressure in the nucleus is high compared with the pressure of the melt. However, the critical bubble diameter given by the Rayleigh equation is dependent on temperature through the internal gas pressure, p_1, and the surface tension, σ. Since p_1 is essentially proportional to temperature, as melt temperature increases, the critical bubble diameter decreases. Thus, it can be implied that smaller bubbles initiate and grow at higher melt temperatures. However, higher melt temperatures reduce the melt viscosity, because of which, bubble coalescence increases. Therefore, depending on which of these relative effects is dominant, increasing the melt temperature can either increase or decrease the cell dimension, i.e., decrease or increase the bubble count (# of bubbles/cm^3), respectively [3].

(iii) ***Initially dispersed microvoids***. Successful foam systems contain either nucleating agents or dispersed microvoids [167]. In cases where a large number of microvoids is present initially, even without solid nucleating agents, they serve as sites for bubble growth, with the formation of new bubbles not being necessary. Thus, the presence of dispersed microbubbles of air eliminates the need for the foaming gas to separate liquid from itself to form a bubble. Instead, the foaming gas comes from solution, into the microbubbles, and simply grows a larger bubble without having to form a new bubble [167].

3.4.2 Bubble Growth Models

All bubble growth models published in the open literature between 1917 and 1984 focused on the growth or collapse of a single bubble surrounded by an infinite sea of fluid with an infinite amount of gas available for growth in extrusion or injection molding. Although these so called "single bubble growth models" provided several insights into bubble growth phenomena, their practical application in industry was severely limited, because in real life, the foaming process involves the growth of numerous bubbles expanding in close proximity to one another with a limited supply of gas. This led to the development of the so called "cell models" (1984-1998) [16]. Cell models can be broadly classified into two groups: (a) cell model for closed system with no blowing agent and gas loss effects and (b) modified cell model for foam extrusion with blowing agent and gas loss effects. The concept of a cell model was first introduced by Amon and Denson [172,173] in 1984. This study involved more realistic assumptions because of which the cell model yielded a final radius, while other single bubble growth models showed growth of bubble radius with time, indefinitely [16].

3.4.2.1 Inertia-controlled Cell Growth

The initial bubble growth rate is governed by external mechanical forces such as surface tension, viscoelastic, and inertial forces, but not by the gas supply to the growing bubble. However, as time goes on, the gas concentration in the polymer melt changes causing the initially dominant inertia-controlled bubble growth to be replaced by diffusion-controlled bubble growth, where supersaturation of the gas in the cooling plastic is considered to be the primary driving force for nucleation [3].

Equation (3.20) represents the general differential equation describing bubble growth in a quiescent liquid via the time-dependent bubble radius [3].

$$\rho\left[\frac{3}{2}\left(\frac{dR}{dt}\right)^2 + R\frac{d^2R}{dt^2}\right] = p_1 - p_2 - 2\sigma/R \tag{3.20}$$

where: ρ = Liquid density [kg/m^3]

R = Time-dependent bubble radius [m]

Since Equation (3.20) does not contain a viscosity term, Equation (3.21) represents the differential form of the time-dependent bubble radius for Newtonian fluids by including the effect of viscosity μ in its third term on the left [3].

$$\rho\left[\frac{3}{2}\left(\frac{dR}{dt}\right)^2 + R\frac{d^2R}{dt^2}\right] + \frac{4\mu}{R}\left(\frac{dR}{dt}\right) = p_1 - p_2 - 2\sigma/R \tag{3.21}$$

A dimensionless group Q_{dim}, (Equation (3.22)), shows the relative importance of fluid inertia and viscosity, i.e., for large values of Q_{dim}, viscous effects dominate fluid inertia during initial cell growth.

$$Q_{\text{dim}} = \left({}^{2\mu}\!/\!_{\sigma}\right)\cdot\left({}^{p_2}\!/\!_{\rho}\right)^{1/2} \tag{3.22}$$

Since external hydromechanical forces, such as inertia and viscosity, dominate the initial bubble growth [3], Yang and Street [174,175] proposed a mathematical model for describing the initial bubble growth rate in viscous-only non-Newtonian liquids, (Equation (3.23)).

$$\rho\left[\frac{3}{2}\left(\frac{dR}{dt}\right)^2 + R\frac{d^2R}{dt^2}\right] + 4m(12)^{(n-1)/2}\left[\frac{1}{R}\frac{dR}{dt}\right]^n = p_1 - p_2 - 2\sigma/R \tag{3.23}$$

where m and n are melt viscosity coefficients determined using the power law model (Equation (3.24)).

$$\eta_e = m\cdot\left(\dot{\gamma}\right)^{n-1} \tag{3.24}$$

where: η_e = Non-Newtonian elongational viscosity of the gas/polymer melt [Pa s]

$\dot{\gamma}$ = Shear rate [s^{-1}]

Viscous shear stresses are proportional to velocity gradients, with the proportionality called viscosity. The equation that relates the shear stress field to the velocity gradient field is called a rheological equation of state or constitutive equation of state [3]. It is important to note that the effect of the elastic forces is not included in the model given in Equation (3.23).

However, elastic and viscous effects can be included in the equation of initial bubble growth rate with an appropriate constitutive equation of state, such as the elastoviscous Oldroyd model [3,176].

3.4.2.2 Diffusion-controlled Cell Growth

The diffusion-controlled stage of bubble growth (maturing bubble stage) follows the initial (inertia-controlled) and precedes the final (terminal) stage of bubble growth. Once a bubble is formed, it may grow by diffusion of gas from the solution in the liquid phase into the bubble [167]. Equation (3.17) suggests that the system would be more stabile with fewer larger cells than with a greater number of smaller cells, thereby favoring the combination or coalescence of cells. However, at equilibrium, the gas pressure in a spherical bubble is larger than the pressure in the surrounding fluid, as given by Equation (3.25), and the gas pressure in a small bubble is greater than that in a large bubble, with the difference as given in Equation (3.26).

$$\Delta p = \frac{2 \cdot \sigma}{r} \tag{3.25}$$

$$\Delta p_2^1 = 2 \cdot \sigma \cdot \left(\frac{1}{r_1} - \frac{1}{r_2} \right) \tag{3.26}$$

where Δp_2^1 is the difference in pressure between the two bubbles having radii r_1 and r_2. Thus, gas will tend to diffuse from the smaller bubble into the large one, thereby favoring the loss of fine bubbles, and the increase in size of larger bubbles, given sufficient time [167].

Amon and Denson [172,173] studied the dynamics of foam growth. They indicated that as the maturing (diffusion-controlled) bubble stage progresses, the growing bubble cannot sustain growth by differential gas pressure alone any more, since mass transfer across the liquid-gas interface is no longer rapid enough to maintain inflation pressure. Consequently, the liquid region in the thin film around the growing bubble is being rapidly depleted of gas and gas is now being supplied by diffusion from liquid from some distance from the growing bubble. Thereby, although the bubbles can still be considered as isolated at this stage, the bubble sphere of influence on the liquid becomes substantially increased. Therefore, as the bubbles grow, their spheres of influence collide long before their inertial effects could be felt across the liquid membranes between them [3,177]. For bubble diameters greater than about 1 [μm], bubble oscillations are usually not influenced by the viscoelastic character of the polymer/gas melt [178].

Amon and Denson [172,173] developed a model for the growth of a spherical bubble surrounded by a thin shell of liquid. They concluded that surface tension and initial radius were of less importance than the thermodynamic driving force, mass, and momentum transfer. However, their model would apply only to high-density foams or the early stages of rise of low-density foams, because of the limitation of the spherical cell shape [167].

As long as the rate of diffusion is greater than the bubble growth rate against inertial and viscous forces, the equations used to describe initial bubble growth rate apply. Otherwise, a new set of equations that would include mass transfer is needed. In general, four equations constitute the basic framework of any analytical model describing the later stages of bubble growth. These include the continuity, momentum, energy, and species mass equations [3].

Equation (3.27) is the continuity equation for a spherical bubble of radius r in a quiescent fluid. The continuity equation represents an arithmetic statement of the law of conservation of mass. That is, the total amount of fluid in a defined volume can only change because of fluid transfer across the bounding surface [3].

$$\frac{\partial\left(r^2 v_r\right)}{\partial r} = 0 \tag{3.27}$$

where $v_r = v_r(r,t)$ is the velocity in the radial direction [3].

Equation (3.28) represents the momentum equation for a spherical bubble growing in a quiescent fluid. It relates radial velocity, v_r, to the shear field [3]. Normally, the momentum equation is a first-order tensor equation, i.e., in a proper set of position coordinates, there are three scalar equations describing time- and position-dependent velocities in each direction. For a spherical bubble growing in a quiescent fluid it reduces to a single equation [3].

$$\rho\left(\frac{\partial v_r}{\partial t} + v_r\frac{\partial v_r}{\partial r}\right) = -\frac{\partial p}{\partial r} + \frac{1}{r^2}\frac{\partial\left(r^2\tau_{rr}\right)}{\partial r} - \frac{\left(\tau_{\theta\theta} - \tau_{\varphi\varphi}\right)}{r} \tag{3.28}$$

The first term on the left of Equation (3.28) represents the time-dependent velocity of the liquid while the second represents the momentum. The first term on the right represents the thermodynamic pressure field and the last two terms on the right represent the effect of shear field on momentum. The terms τ_{rr}, $\tau_{\theta\theta}$, and $\tau_{\varphi\varphi}$ represent the normal viscous stresses [3]. It is important to note here that during simplification procedures the continuity equation is often substituted into the momentum equation. Since for this example, the velocity v_r can be written in terms of the time-dependent radius as, $v_r(r = R) = {dR}/{dt}$, when this expression is substituted into the continuity equation and the momentum equation, and the rheological equation of state for Newtonian or power-law non-Newtonian fluids is used, the results are Equations (3.21) and (3.23), respectively. These are most appropriate for describing the initial bubble growth stage [3].

Equation (3.29) is the energy equation for spherical bubble growth in a quiescent fluid [3]. The energy equation represents an arithmetic statement of the law of conservation of energy within a defined volume. That is, the total amount of energy in the defined volume can only change because of energy transfer across the bounding surface [3]. Normally, the momentum equation is a first-order tensor equation, i.e., in a proper set of position coordinates, there are three scalar equations describing time- and position-dependent velocities in each direction. However, for a spherical bubble growing in a quiescent fluid, it reduces to a single equation [3].

$$\rho \cdot c_p \frac{\partial T}{\partial t} = \frac{1}{r^2}\frac{\partial}{\partial r}\left(r^2 k_l \frac{\partial T}{\partial r}\right) - \rho \cdot c_p \left[\frac{R^2}{r^2}\frac{dR}{dt}\right]\frac{\partial T}{\partial r} \tag{3.29}$$

The term on the left of Equation (3.29) is the time-dependent change in volumetric energy with the specific heat of the liquid, c_p, as a physical measure of the sensible heat. The first term on the right presents the conduction of energy through the liquid with the thermal conductivity of the liquid, k_l, as the proportionality. The second term represents the convected amount of energy owing to bubble growth, with the term in the brackets being the radius-dependent version of the continuity equation. This equation does not include terms for viscous dissipation effects, compression effects, and decomposition of CBAs [3].

Equation (3.30) represents the mass transfer equation for a spherical bubble growing in an infinite medium owing to the inflation pressure of a single gas [3]. The mass transfer equation represents an arithmetic statement of the law of conservation of mass of a specific species within a defined volume. That is, the total amount of mass of a specific species in the defined volume can only change because of mass transfer across the bounding surface [3].

$$\frac{\partial c}{\partial t} = \frac{1}{r^2}\frac{\partial}{\partial r}\left(r^2 D \frac{\partial c}{\partial r}\right) - \left[\frac{R^2}{r^2}\frac{dR}{dt}\right]\frac{\partial c}{\partial t} \tag{3.30}$$

The term on the left of Equation (3.30) represents the time-dependent change in mass in the defined volume. The first term on the right represents the role of molecular diffusion, with D, the diffusion coefficient, as the proportionality. The second term on the right represents the amount of convected mass, where again v_r has been replaced by the equivalent rate-dependent radius, $v_r \equiv {}^{dR}\!/_{dt}$ from the continuity equation [3].

However, since mass, energy, and momentum are transmitted across the phase boundary, Equation (3.31) represents an interfacial mass transfer equation, which states that the increase in volume within the bubble is the result of mass transfer across the bubble interface [3].

$$\frac{d\left(R^2 \rho_g\right)}{dt} = 3R^2 D\left[\frac{\partial c}{\partial r}\right]_{r=R} \tag{3.31}$$

3.4.2.3 Final Stage of Cell Growth

The final (or terminal) stage of bubble growth is dominated by the internal cell gas pressure and gas permeability through the formed cells, and the ultimate tensile and elongational strength of the polymer [3]. If a stable spherical bubble of initial radius r_0 and wall thickness δr_0 is forced to expand by instantaneously dropping the external pressure from p_f to zero (there is no thermal or mass transfer to or from the bubble), then Equation (3.28) reduces to Equation (3.32) [179].

$$0 = -\frac{\partial p}{\partial r} - \left[\frac{1}{r^2}\frac{\partial}{\partial r}\left(r^2 \tau_{rr}\right) - \frac{\tau_{\theta\theta} + \tau_{\varphi\varphi}}{r}\right] \tag{3.32}$$

A three-parameter Oldroyd model can be used to represent the viscoelastic model for the final stage of cell growth describing the bubble radius as a function of time. It indicates that, for long times, the elastic character of the Oldroyd fluid acts to slow the expansion rate considerably, this implies that terminal bubble expansion rates are strongly dependent on the elastic character (or melt strength) of the polymer [3,58].

3.4.3. Cell Deterioration Mechanisms

During the initial foam rise the cells are closed. Otherwise, the blowing agent would escape without causing a normal rise. Closed cells become open when one or more membranes rupture, usually due to excessive thinning, so that the strength of the membrane cannot resist the pressure in the cell. Extensive rupture before the foam is stabilized may lead to foam collapse. However, bubbles may grow not only by diffusion of gas from the solution into the bubbles, but by expansion due to heat or pressure reduction, or by the combination (coalescence) of two or more bubbles, which may also lead to foam collapse [3,166]. Thus, successful closed cell foams are produced when the cell membranes are sufficiently strong (elastic) to withstand rupture at the maximum foam rise [167].

Bubble walls may be thinned by drainage due to gravity and also by capillary action. Capillary pressure at the junction of two or more ribs in a cell is lower than in the membrane, which of course promotes flow from the membranes into the ribs. This effect can also lead to excessive thinning of cell walls and rupture. In certain cases surfaces of a very thin film attract each other by van der Waals forces, also favouring continued thinning. The temperature of the foam strongly affects stability. An increase in temperature reduces viscosity and surface tension, making the thinning of membranes easier [167].

Once the cell nucleation has started, cells continue to grow until the gas-generation ability of the CBA is exhausted. Unlike processes that use physical expansion methods, in rotational foam molding, due to the process pressure insufficiency, the gases released from the decomposition of the CBA almost completely fail to dissolve in the polymer. Consequently, almost the total available amount of gases goes into the cells and increases the cell pressure. Since the pressure of the polymer matrix remains unchanged (i.e., remains at the atmospheric level), a pressure difference is created between the cell internal pressure and the pressure of the environment. This pressure difference controls and promotes the further growth of the cell until it eventually stabilizes (which is desirable), or ruptures due to cell coalescence, or collapses due to cell coarsening, thereby deteriorating the cell density [27, 58].

Cell coalescence occurs due to cell-wall instability that causes the common wall between two neighboring cells to rupture and thereby they become transformed into one bigger cell [27, 58].

Cell coarsening occurs due to the gas diffusion between two adjacent cells that have different cell sizes, i.e., over time, the smaller cell reduces its size and eventually collapses, while, in contrast, the larger cell increases in size over the same period. Finally, these formerly adjacent cells become one large cell [27, 58].

3.4.4 Foam Stabilization

Liquid foams are thermodynamically unstable (Equation 3.19) and their collapse is favored by gravity, pure liquids will not form stable foams, regardless of the surface tension. To obtain relatively stable liquid foams, the liquid must consist of at least two components, one of which should be preferentially adsorbed at the surface. On the other hand, when a cell expands, the concentration of adsorbed component (for example, an emulsifier) is reduced. This concentration may be restored by either the Marangoni effect or the Gibbs effect [167].

However, the above factors are likely to be important in the very early stages of rise of polymeric foam systems, when the systems are quite fluid. Therefore, the major stabilizing influence for polymeric foams is achieved by a rapid increase in viscosity. When molten thermoplastics are foamed, they are cooled immediately after foaming to provide the necessary increase in viscosity and increase the polymer modulus rapidly to a high level so that the cells are dimensionally stable in spite of the development of a partial vacuum within the cells [167].

Since the stability of the cell wall depends upon the polymer melt strength, increasing the viscosity of the molten polymer would increase its melt strength and thereby reduce the drainage effect. The increase of the viscosity may be achieved by a temperature reduction, i.e., by keeping the processing temperature as low as possible. The deterioration of cells due to coalescence should be suppressed by choosing a high melt strength material and by avoiding an unnecessarily long processing time. On the other hand, two principal strategies are commonly used for successful cell coarsening suppression. The first is based on nucleation of the cells almost simultaneously in order to induce cell growth uniformity, while the second is based on reduction of the processing time as much as possible [58].

3.5 Summary

The processing strategies for single-charge foaming should be developed after giving serious consideration to the nature of the polymer material, its relevant properties, and its behavior under the influence of the mechanisms that dominate the rotational molding process such as the heat transfer including the cooling stage, sintering and densification, unintended bubble formation, or deliberate foaming [180-183]. However, since at present there are no developed models that particularly describe the single-charge rotational foam molding technology, the issues discussed in the present chapter could serve as a good reference and a foundation for further research.

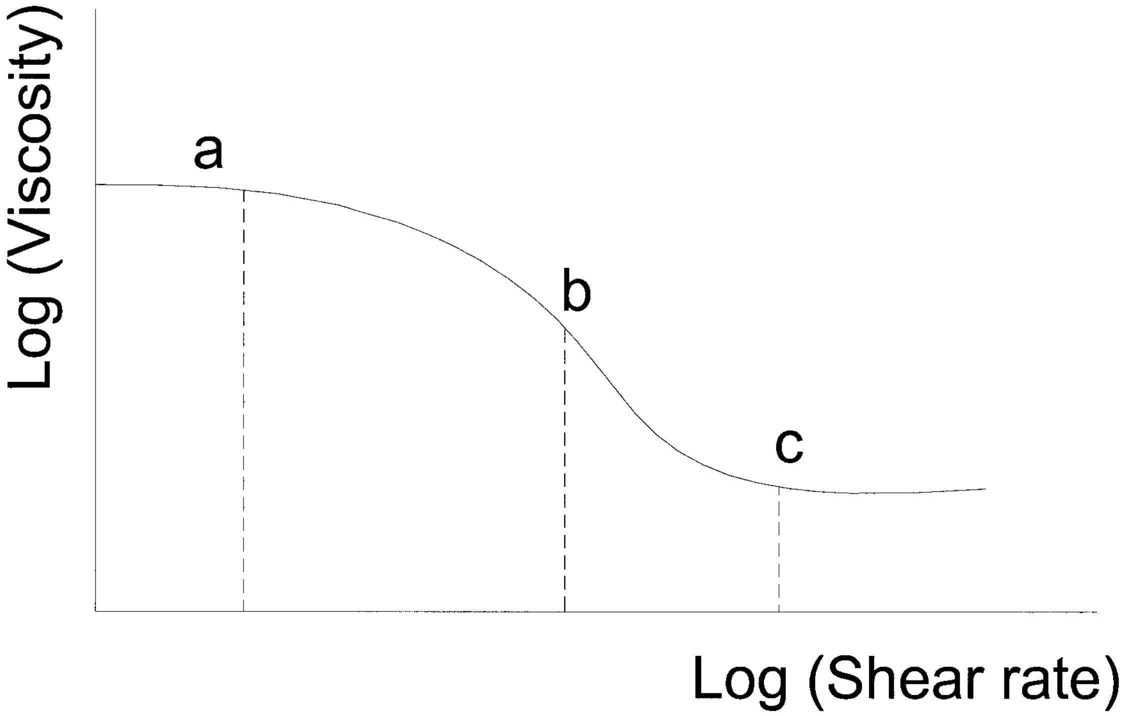

Figure 3.1: Typical Log viscosity versus Log shear rate curve for polymeric melts

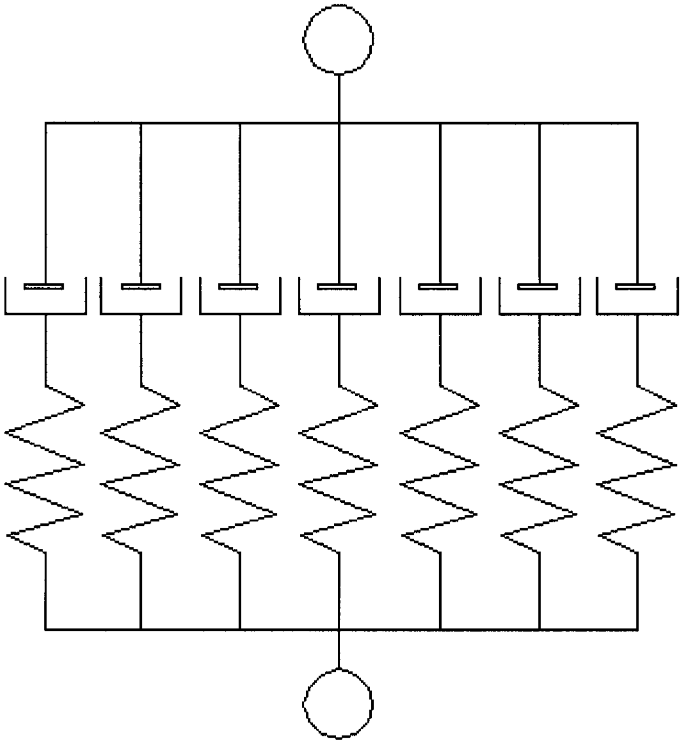

Figure 3.2: Mechanical analog of the generalized Maxwell model

CHAPTER 4

EXPERIMENTAL

4.1 Materials Used for Experimentation

4.1.1 Cellular Core-forming Materials

4.1.1.1 PE Resins

Four ethylene-based rotational molding grade resins were selected to participate in the trials conducted within the framework of the present experimental study. These include three LLDPE resins (Escorene® LL8556, LL8361, and LL8461) from ExxonMobil Chemical, and one MDPE hexane copolymer resin (Novapol® TR-0338-UG) from Nova Chemicals. All resins were used as supplied, i.e., in a ground powder form. Table 4.1 provides the principal physical properties of these PE resins and the assigned codes that will be used for referring to each grade further throughout this research, respectively [184,185].

4.1.1.2 PP Resins

Four propylene-based resins, two branched and two non-branched, were subjected to experimentation in this study. Three of these PP grades (PF633, SD812, and SD 242) were manufactured by Montell Polyolefins, while one (MT4390 HU) was manufactured by former Millennium Chemicals (currently Equistar Chemicals). PF633 is a high melt strength (HMS) PP homopolymer resin; SD812 is a HMS PP medium impact copolymer resin for extrusion coating; SD242 is a nucleated, high flow, medium impact PP copolymer resin, while MT4390 HU is a PP copolymer resin of a rotomolding grade. It was thus supplied in a powder form. The remaining three PP resins were supplied in a pellet form and have therefore been subjected to grinding prior further usage. Table 4.2 shows the principal physical properties of these PP resins and the respectively assigned codes for the purpose of this research [186,187].

4.1.1.3 CBA Used for Preparing PE Foamable Resins

Celogen OT (OT) manufactured by Uniroyal Chemical was the blowing agent selected to be used for processing PE foams. It was supplied in a form of a fine white powder. The operating temperature range of OT is reported to be between 149 and 177 °C, its decomposition temperature range is between 158 and 160 °C, while it liberates 125 [cm^3/g] of 91% N_2 and 9% H_2O. OT may be activated by triethanolamine and BIK-OT thereby reducing its decomposition temperature to 132 °C [188].

4.1.1.4 CBA Used for Preparing PP Foamable Resins

Celogen AZ-3990 (AZ) from Uniroyal Chemical was used for processing PP foams. It was supplied in a form of a yellow fine powder with an average particle size of 2.4-3.0 [μm]. The operating temperature range of AZ is reported to be between 199 and 232 °C, its decomposition temperature range is from 205 to 215 °C, while its gas-yield is around 220 [cm^3/g]. The gaseous product released by the decomposition of AZ comprises 65% N_2, 24% CO, 5% CO_2, and 5% NH_3, while its solid decomposition products, constituting approximately 68% of its original weight, comprise Urazol, Biurca, Cyamelide and Cyanuric Acid. AZ may be activated by metal organic salts, bases, and acids reducing its decomposition temperature to as low as 166 °C [188].

4.1.2 Solid Envelope-forming Materials

The non-foamble resin comprised a commercially available envelope/skin-forming ethylene-based blend Rotolite OS™ (Ingenia Polymers Corp.). It consists of two components having essentially distinct zero shear viscosities that are premixed in a predetermined proportion. Each component is a blend of two or more ethylene polymer powders with different particle sizes and melt indexes. A color pigment is often incorporated in the solid skin-forming component to make it easily distinctive from the cellular core.

4.2 Analytical Instruments

The analytical instruments used in the present research include a rotational rheometer, a differential scanning calorimeter (DSC), a thermogravimetric analyzer (TGA), and a scanning electronic microscope (SEM). These instruments were used for characterizing the selected polyolefin resins and CBAs by means of various testing techniques that measure the changes in the physical or reactive properties of a material as a function of shear rate, temperature, and/or time.

4.2.1 Rotational Rheometer

Rheometers measure the rheological character of a material in terms of its elasticity and viscosity. Understanding these rheological properties helps predicting the behavior of a material during processing and in its end use.

Rheological measurements were performed on a cone-plate type dynamic controlled stress rotational rheometer Rheometric Scientific SR200 (Figure 4.1 (a)), with a 25 [mm] plate and a 0.498 [mm] gap. The cone and plate rheometer (Figure 4.1 (b)) is the most popular method for gaining rheological information over specific shear rates. At very small angles, α, the parallel (drag flow) geometry can be approximated by the flow in the gap between a plate and a cone. Since for a body of fluid undergoing laminar flow, the shear rate it is experiencing is the ratio of the velocity difference across the fluid to the distance over which the shearing occurs, at a point, N_1, at the rim of the cone (Figure 4.1 (b)), the shear rate experienced by the sample beneath that point is the ratio of the speed of that point to the sample thickness at that point. At shallow angled cones this ratio remains constant at any radius out from the tip so that a uniform shear rate is therefore generated across the entire sample for any given rotational speed and for any point, N_2, located on the underside of the cone. In some rheometer systems the cone is often truncated by a small amount and an accurate gap setting mechanism is then employed to ensure that the "virtual" tip is in contact with the lower plate when running samples. The viscosity is then given by the ratio of the shear stress τ and the shear rate $\dot{\gamma}$ as in Equation (4.1) [83]:

$$\eta = \frac{\tau}{\dot{\gamma}} \tag{4.1}$$

where: $\tau = \frac{3W}{2\pi R^3 \omega}$ and $\dot{\gamma} = \frac{\omega}{\alpha}$

where: W = Spindle torque

ω = Angular rotation rate

α = Angle between the cone and the plate

Thus:
$$\eta = \frac{3\alpha W}{2\pi R^3 \omega} \tag{4.2}$$

Controlled stress is the basic testing mode of any stress rheometer. Creep and recovery testing, stress sweeps, and yield stress determination tests can be run in this mode. Controlled strain (shear) rate testing is useful for generating flow curves and studying the rate dependence of materials. Rate sweeps, step rate sweeps, and thixotropic loops are some of the tests that can be run in this mode. Controlled strain mode allows the rheometer to simulate the functions of a controlled strain rheometer. Strain sweeps to determine the linear viscoelastic region of a material, strain-based frequency sweeps, and time sweeps are examples of some controlled strain testing capabilities. Controlled frequency (oscillatory) mode gives the rheometer capabilities for dynamic testing. This offers the advantage of being able to simultaneously measure the elastic modulus of a material and perform viscosity measurements, a critical consideration when testing thermoplastic melts intended for foaming, as melt elasticity is often as important as viscosity in foam formation. Dynamic measurements made at high frequencies provide data corresponding to very short times, whereas measurements made at low frequencies correspond to long times [189].

4.2.2 Differential Scanning Calorimeter (DSC)

Differential scanning calorimetry is a technique in which the temperatures and heat flows associated with transitions in materials are measured as a function of temperature or time in a controlled atmosphere. This technique provides quantitative and qualitative information about physical and chemical changes that involve endothermic or exothermic processes, or changes in heat capacity. The DSC measures the heat flow into or out of a sample as a function of a desired, user pre-programmed, temperature variation over time and provides a real-time plot of the relationship. The two most commonly used methods in DSC analysis include the power compensation method and the heat flux method [190,191].

Figure 4.2 (a) presents a pictorial view of the TA 2910 DSC instrument used in this study for thermal analysis trials, Figure 4.2 (b) presents its schematic illustration, while Figure 4.2 (c) depicts schematically its cell. This DSC cell uses the heat flow flux method. The test is conducted on a sample encapsulated in an aluminum pan that is put on a constantan thermoelectric disc together with a reference pan. After the circulation of a preheated purging gas is initiated through the cell to provide a stable environment, both pans are heated. The principle of operation of the DSC cell is based on the difference between the temperature of the sample pan and that of the reference pan. The instrument software uses this difference (ΔT), and the thermal resistance of the constantan disc (R_D) to calculate and plot the heat flow (dH/dt) with respect to time or temperature by using the relationship expressed in Equation (4.3) [192].

$$\frac{dH}{dt} = \frac{\Delta T}{R_D} \tag{4.3}$$

For calibration purposes, whenever a heating rate change is being contemplated, a standard Indium specimen with a known melting point (157 °C) and heat of fusion (28.71 J/g) should be run on the DSC using a heating rate commensurate to the one that is intended to be used in subsequent experiments.

4.2.3 Thermogravimetric Analyzer (TGA)

Thermogravimetric analysis is a technique in which the mass of a substance is measured as a function of time or temperature while the substance is subjected to a controlled temperature program in a controlled atmosphere. The TGA measures the weight change of a sample with relation to the desired, user-preprogrammed, temperature variation over time and provides a real-time plot of this relationship.

Figure 4.3 (a) presents a pictorial view of the TA 2050 TGA instrument used in this study for conducting thermal analysis tests, while Figure 4.3 (c) presents a schematic illustration of the instrument. The principle of operation of the TA2050 instrument used in the present study consists of recording the weight-loss during heating the sample, in presence of a purging gas. The sample is previously loaded onto a platinum sample pan (Figure 4.3 (b)) and inserted into the heating chamber pertaining to the instrument by the sample loading assembly schematically depicted in Figure 4.3 (d). During experimentation, the sample pan is permanently hooked on an accurate balance, thereby providing data to the computer's software regarding the weight variations of the sample over time or temperature. Helium is preferred, but also nitrogen or argon could serve as purging gases for the heating chamber. Another stream of the gas selected for purging runs through the balance chamber in order to provide stabile thermal conditions, and thereby protect the accuracy of the balance. The temperature of the balance chamber is also maintained by an additional water-cooling system [193].

4.2.4 Scanning Electronic Microscope (SEM)

Scanning electron microscopy is an image formation system that uses electrons instead of light to form an image. A SEM model Hitachi S-2500 (Figure 4.4 (a)) was used for particle identification, sizing, and analysis in this research. It not only offers a significantly higher resolution than optical microscopy, but also offers an increased depth of field that gives a better presentation of the topology of the sample. Liquid nitrogen is commonly used to freeze the samples prior to fracture in order to avoid the effects of the impact during fracture. All samples have to be gold-plated before being used on the SEM. Selected microstructures can be recorded by using Polaroid imaging.

The instrumental setup of a SEM includes an electron beam source, electron lens system, scanning or deflection coils, detectors, and signal processing and display equipment (Figure 4.4 (b)). The principle of operation of the SEM is based on scanning an electron beam across the sample in the x and y direction. A beam of electrons is produced at the top of the microscope by thermionic emission, by heating a filament to a sufficiently high temperature to induce some electrons to escape. The electron beam follows a vertical path through the column of the microscope passing through electromagnetic lenses which focus and direct the beam towards the sample. Once it hits the sample, other electrons (backscattered or secondary) are ejected from the sample. The SEM detects these emissions from the upper surface of the sample and converts them to a signal that is sent to a viewing screen similar to the one in an ordinary television, producing an image. The variation of the detected signal constitutes a contrast that is utilized in the process of image formation. The resulting image reveals the surface of the sample, giving the impression of a three-dimensional view. The high resolution of an electron microscope results from the short wavelength associated with the electron beam [194].

4.3 Design of Experiments

CARD® PRO Ver.5.1, a design of experiments software package from S-Matrix Corporation, has been used to determine the best suited experiment design for evaluating the rotofoamability of polyolefin resins, identifying the optimal PE and PP resins, and selection of optimal processing strategies for various independent experimental variables, respectively. CARD® PRO consists of two work environments: CARD® Design and CARD® Analysis.

CARD® Design handles a wide range of variable types (continuous, discrete, non-numeric/categorical, mixture, and process). It contains three integrated modules: Experiment Planner, Design Generator, and Matrix Master.

The Experiment Planner module lets the user to systematically define the experiment variables and restrictions on how they can be combined (multiple constraints).

The Design generator module generates S-Matrix designs by design algorithms that create a "candidate list" of possible design points based on the defined independent variable settings and multiple constraints, and select final design points from the candidate list that contain the required cause and effect information in the minimum number of runs. The S-Matrix designs are used to study mixtures, complex variable effects, and complex experiment systems that can not be readily adapted to the restrictions of the classical designs. Model-Robust designs are more flexible than the classical designs. These designs accommodate several types of experiment variables in the same design, and must be used in the presence of multiple constraints. Model-Robust designs are adaptable to a wide range of experiment conditions. Model-Robust optimization designs have four goals. The first is uncorrelation of all experiment variable main-effects terms, simple curvilinear effects terms (squared terms), and two-way effects terms. Optimization designs thus attempt to enable estimation of all terms in a second-order quadratic model. The second goal is comprehensive coverage of the experiment design space. This means that the design algorithms will select final design points that provide data on variable effects across all allowable ranges and variable combinations. The third goal is incorporating degrees of freedom points into the final design. Degrees of freedom points allow additional model terms to be included when necessary. They also provide independence of the proposed analysis model from the experiment design points. This is critical for estimating the correctness of the analysis model estimates of variable effects. The fourth goal is inclusion of replicate runs for estimating overall experimental error. The Model-Robust design algorithms select a subset of runs for replication (R) from the final design matrix. This subset contains the minimum number of runs needed to provide an accurate estimate of overall experimental error across the design space. For optimization designs R = 3 for designs of < 15 runs, R = 4 for designs of 15 to 25 runs, R = 5 for designs of 26 to 60 runs, and R = 6 for designs of > 60 runs [195].

The Matrix Master module lets the user view the information content of each experiment design generated in CARD® Design. CARD automatically creates an analysisready data matrix from the design matrix that you can export to CARD® Analysis, or export in one of a variety of file formats compatible with spreadsheets and statistics packages. Within Matrix Master the user can edit the current design matrix to reflect actual run conditions or changes during execution of the experiment. One can then see the effects of these edits on the information content of the design matrix prior to analyzing the data using CARD Analysis [195].

CARD® Analysis provides the statistical analysis and graphics capabilities required for rigorous analysis of designed experiment results. These capabilities include nonlinear response/error analysis, experimental error analysis, ANOVA analysis, regression analysis, residuals analysis, two-dimensional graphing, three-dimensional response surface graphing, and multiple response optimization. The Optimizer compares the starting point level settings of the variables to the independent variable settings data. The starting point level settings correspond to a proposed point in an n-dimensional experiment design space, where each experiment variable contributes one dimension. The response models (equations) are next "solved" using the proposed level settings. These solutions are checked against the response variable goals. Optimizer carries out an iterative process of inputting proposed points, solving the multiple constraint and response goal equations, and comparing the response solutions to those of the previous iteration, until a solution is found that satisfies the response variable goals. Optimizer then reports the solution, or its best answer, on the optimization module sheet. Given the magnitude of overall experimental error and the model predictive error, there is a specific confidence interval around each predicted mean response in which the actual mean response resides [195].

4.4 Experimental Equipment

4.4.1 Experimental Setup for Preparing Foamable Resins

4.4.1.1 Dry Blending Experimental Setup

Dry blended polyolefin/additives foamble blends intended for subsequent processing into foams using the rotational foam molding method were prepared in a high-speed industrial-scale mixer (Gunther Papenmaier; TGAHK35) by being dry blended for 60 seconds at 2500

RPM in 4 kg batches. Except PP3, the three remaining PP resins were first frozen at – 40 °C and then ambient ground by using an industrial grinder (Wedco, SE-12-SP). Figure 4.5 presents a schematic illustration of the dry blending experimental setup consisting of a grinder (Figure 4.5(a)) and a high-speed mixer (Figure 4.5(b)).

4.4.1.2 Extrusion Melt Compounding Experimental Setup

The experimental setup and procedure described in Section 4.4.1.1 were identically used to premix the pulverized polyolefin resins with the suitable CBA into foamable blends intended to be compounded into foamable resins using the extrusion melt compounding approach. A twin-screw intermeshing co-rotating extruder (Werner & Pfleiderer, ZSK-30) was used to carry out the melt compounding operation of the dry-blended mixture and extrude these blends into foamable strands. The extruded strands were solidified by being cooled in a cooling water bath, after which a pelletizer (Automatic Apparate Machinenbau, ASG 100) was used to chop them into pellets. Figure 4.6 presents a schematic illustration of the extrusion melt compounding experimental setup.

4.4.2 Experimental Setup for Rotational Foam Molding

4.4.2.1 Conventional Uni-axial Rotomolding Machine

Figure 4.7 illustrates the uni-axial lab-scale rotomolding machine used for rotational foam molding experimentation. It consists of a sliding assembly plate, an electrically heated oven, water-cooling installation, and control units for the oven temperature and the mold rotation. The sliding plate carries the uni-axial rotating arm assembly that includes a motor, gearbox, transmission, a hollow shaft, and a removable cylindrical mold. The rotating speed of the arm, which is driven by the motor via the gearbox and the belt-transmission pulleys, can be electronically controlled from 0-30 [rpm]. The water installation provides the means for mold cooling after completion of the heating cycle.

A thermocouple, inserted into the oven, provides data to the oven temperature control unit. The hollow design of the shaft makes possible the insertion of another thermocouple inside the center of the mold in order to measure the in-mold temperature changes during processing. By connecting the thermocouple to a data acquisition device, the temperature changes over time occurring inside the mold can be recorded with a desired sampling frequency, and subsequently plotted.

The diameter of the cylindrical mold used was 31.75 [mm] (1.25"), its length was 101.6 [mm] (4.00"), and a thickness of 3.175 [mm] (0.125"), while its volume was 80 [cm^3].

4.4.2.2 Transparent Uni-axial Rotomolding Machine

Figure 4.8 (a) presents a schematic illustration of the transparent, uni-axial, lab-scale, custom-made rotational molding machine that has been specially designed to serve for the present research study. Its main features include a see-trough front oven door and front mold base. This proved to be useful for monitoring the occurrences inside the mold in real time, and for videotaping the process and conducting subsequent analysis. This machine is equipped with a see-through mold 101.6 [mm] × 101.6 [mm] × 152.4 [mm] (4" × 4" × 6") as presented in Figure 4.8 (b).

Figure 4.9 presents pictorial views of the transparent rotational molding experimental setup in different stages of conducting a rotational molding experiment. The transparent rotational molding experimental setup includes a sliding unit, an electrically heated oven equipped with a front and a rear door, water-cooling installation, and control units for the oven temperature and the mold rotation. The sliding element carries the uni-axial rotating arm assembly that includes a motor, gearbox, transmission, a hollow shaft, and a removable mold. All these assemblies are conveniently mounted on a carriage so that the rotomolding experimental setup becomes a compact standalone unit that is easy to move. The rotating speed of the arm, which is driven by a motor via the gearbox and the belt-transmission pulleys, can be electronically controlled from 0-30 [rpm]. In addition to the water-based mold cooling capability, the transparent rotational molding machine is equipped with a device for air mold cooling. The air blower is conveniently located under the sink. A thermocouple, inserted into the oven, provides data to the oven temperature control unit. In order to measure the in-mold temperature changes during processing another thermocouple is inserted trough the hollow shaft into the center of the mold.

The larger oven size, allows this rotational foam molding machine to accommodate larger molds. Therefore, it was primarily used for producing integral-skin polyolefin cellular composites using a prismatic mold 101.6 [mm] × 50.8 [mm] × 101.6 [mm] (4" × 2" × 4").

4.4.2.3 Biaxial Industrial-scale Rotomolding Machine

Since scaling-up a plastic foam manufacturing process is known to be a non-trivial task, a commercial industrial-scale biaxial roto-molding machine McNeil RC-500 (Figure 4.10) was periodically used for conducting experimental trials for the manufacture of integral-skin polyolefin cellular composites. Thereby, the validity of the developed principles and processing strategies based on experiments carried on using lab-scale experimental equipment have been evaluated in industrial environment using a large mild steel 2" × 12" × 24" flat mold. The results revealed that moderate modifications would be necessary for successful industrial implementation of the developed rotational foam molding processing strategies.

4.4.3 Experimental Setup for Pellet Adhesion on Hot Wall

Figure 4.11 presents the experimental setup that was developed for investigating the adhering behaviors of skin-forming powders and foamble pellets to a high temperature wall. It was used to simulate the adhering behaviors of the pellets to the hot mold's wall during rotational foam molding. The high temperature wall was in fact a custom made aluminum hot plate [8"×6"×5/8"] that was uniformly heated with 6 cartridge heaters the temperature of which was controlled with a ± 1 °C accuracy using a very sensitive temperature controller. The entire assembly was conveniently attached on the mold and rotating shaft pertaining to the aforementioned lab-scale transparent rotational foam molding setup so that it could rotate at a desired speed and angle thereby simulating accurately the rotation of the actual mold.

4.4.4 Experimental Setup for Hot-stage Optical Microscopy

Figure 4.12 presents a custom-build hot-stage optical microscopy computerized digital imaging experimental setup that served for investigating the transformations occurring during the cell growth of CBA-blown bubbles in non-pressurized polymer melts, such as in rotational foam molding. These experimental data have been subsequently used to identify the fundamental foaming mechanisms governing the rotational foam process and validate the respectively developed model. A Linkam HFS 91 heating and freezing stage equipped with a Linkam TP 93 precise temperature controller using Linksys software was used for heating the foamable polyolefin samples at a desired rate and temperature profile. According to manufacturer's data, its temperature range is from -196 °C up to 600 °C, its body sizes are 104

× 92 × 22 [mm], and the diameter of its centre quartz window is 2.4 [mm] [196]. The cooling capability of the stage was not used in the experimentation related to this research. A CCD camera (Costar, CV-M10BX), attached to an optical microscope (WILD, M20-50552) via an adapter (Diagnostic Instruments, HR055-CMT), was used to capture the images from the hot-stage window and transmit them for storage in the computer memory. Two kinds of digital imaging software packages were used: Sherlock™ Version 6.1.0.9 (Coreco Imaging Inc.) and Video Savant™ digital video recording software Version 4.0 (Io Industries Inc.). The former supports only manual operation for capturing images, whereas the latter is capable of continuous video recording with a frequency of at least one frame per second.

Table 4.1: Typical properties of the PE resins selected for experimentation [184,185]

Properties of the PE resins used	ASTM Method	LL8556	LL8361	LL8461	TR-0338
Assigned code		PE1	PE2	PE3	PE4
Melt Index (190 °C/2.16 kg), g/10min	D1238	6.8	5.2	3.3	3.5
Density, g/cm^3	D4883	0.936	0.932	0.938	
Density at 23 °C, g/cm^3	D792				0.938

Table 4.2: Typical properties of the PP resins selected for experimentation [186,187]

Properties of the PP resins used	ASTM Method	PF633	SD812	MT4390	SD242
Assigned code		PP1	PP2	PP3	PP4
Melt Flow Rate (230 °C/2.16 kg), g/10min	D1238	5.5	16	20	35
Density at 23 °C, g/cm^3	D792B	0.90	0.90		0.90
Density, g/cm^3	D1505			0.90	
Homopolymer/Copolymer		H	C	C	C
Branched/Non-branched		B	B	NB	NB

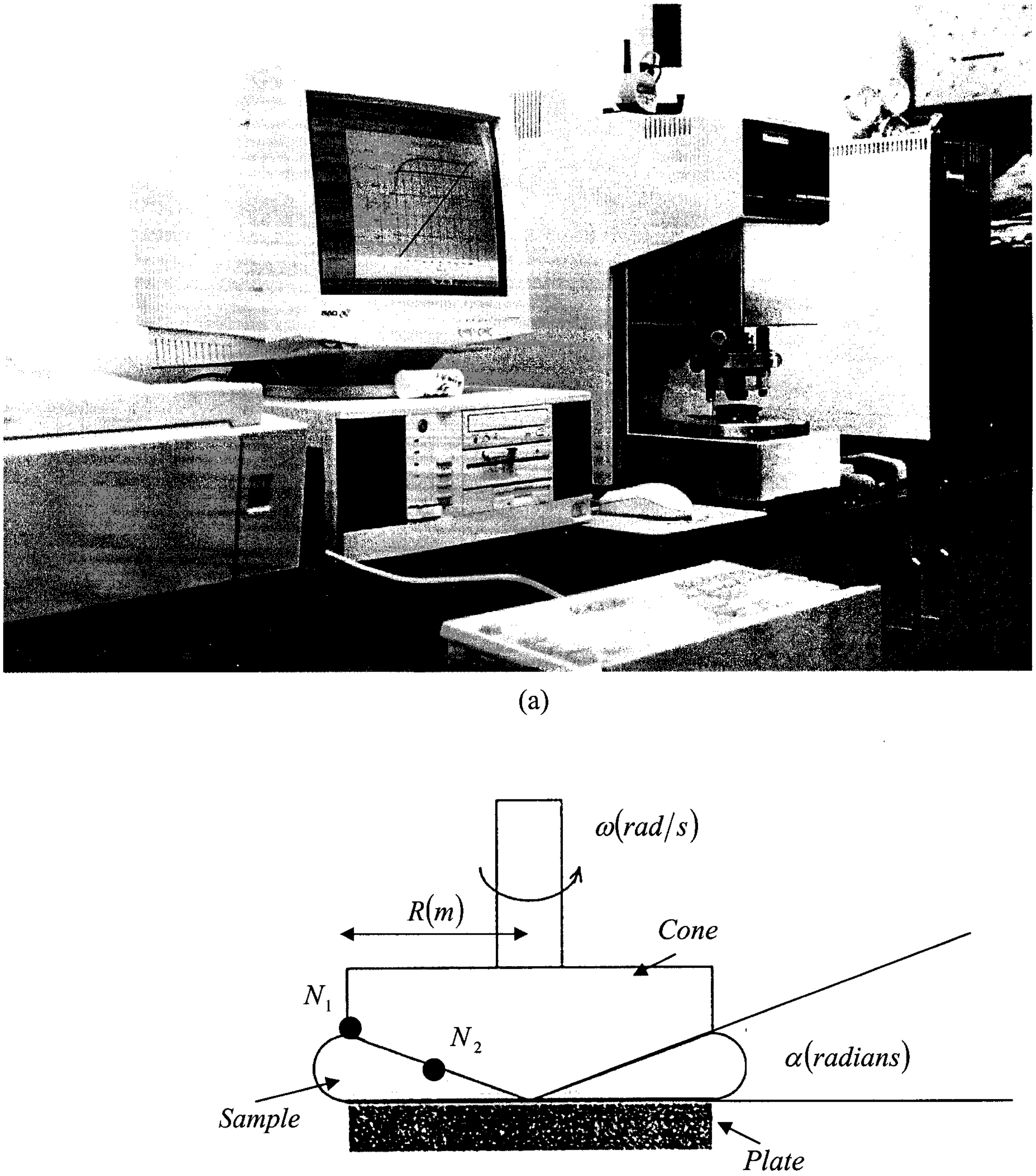

(a)

(b)

Figure 4.1: Rotational rheometer RS200

(a) Pictorial view of RS200 and host computer

(b) Schematic illustration of the cone and plate testing head

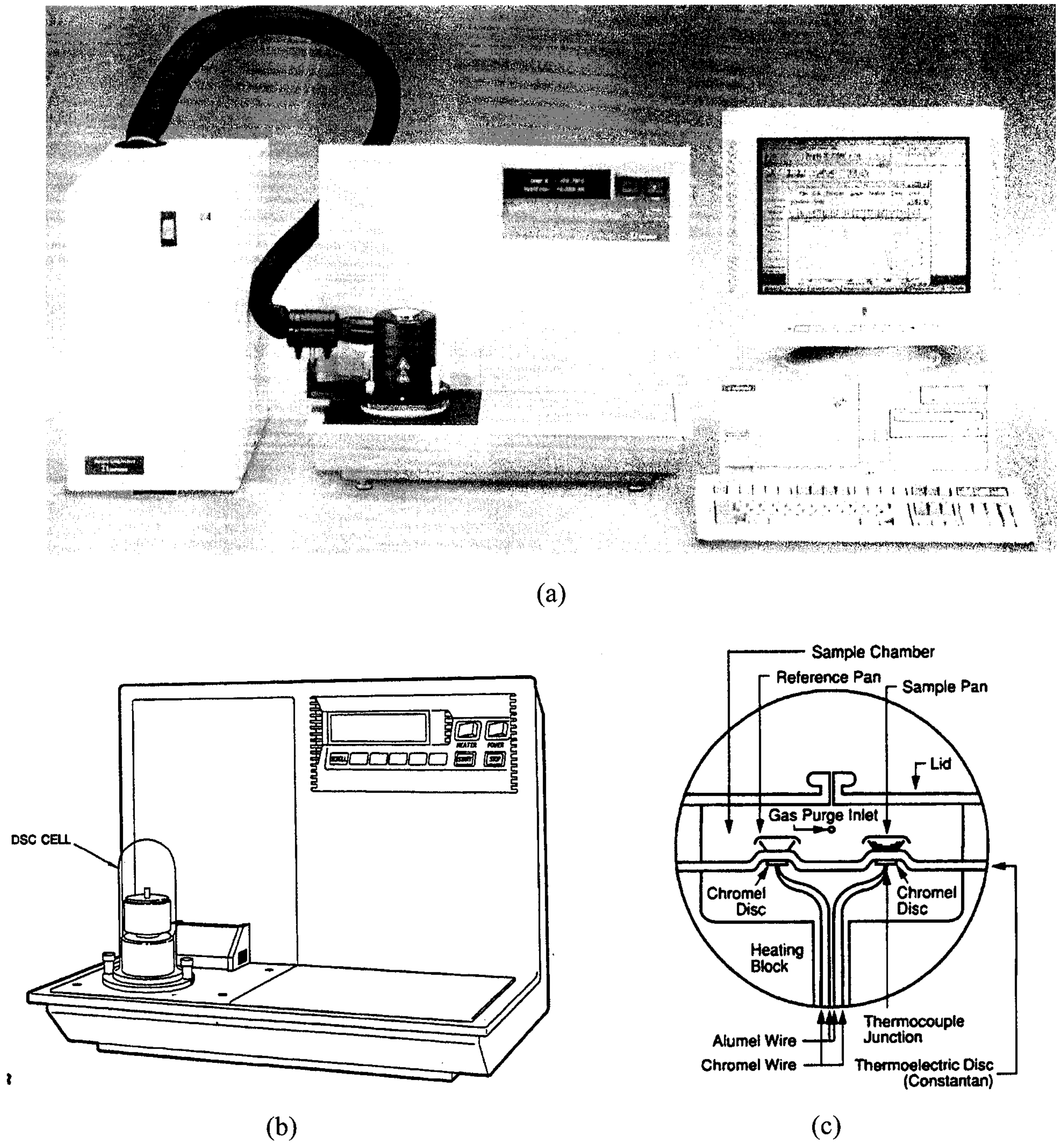

Figure 4.2: Differential scanning calorimeter DSC-TA2910

(a) DSC-TA2910, heat exchanger (left), and host computer

(b) Schematic illustration of the DSC-TA2910

(c) Schematic illustration of the DSC cell

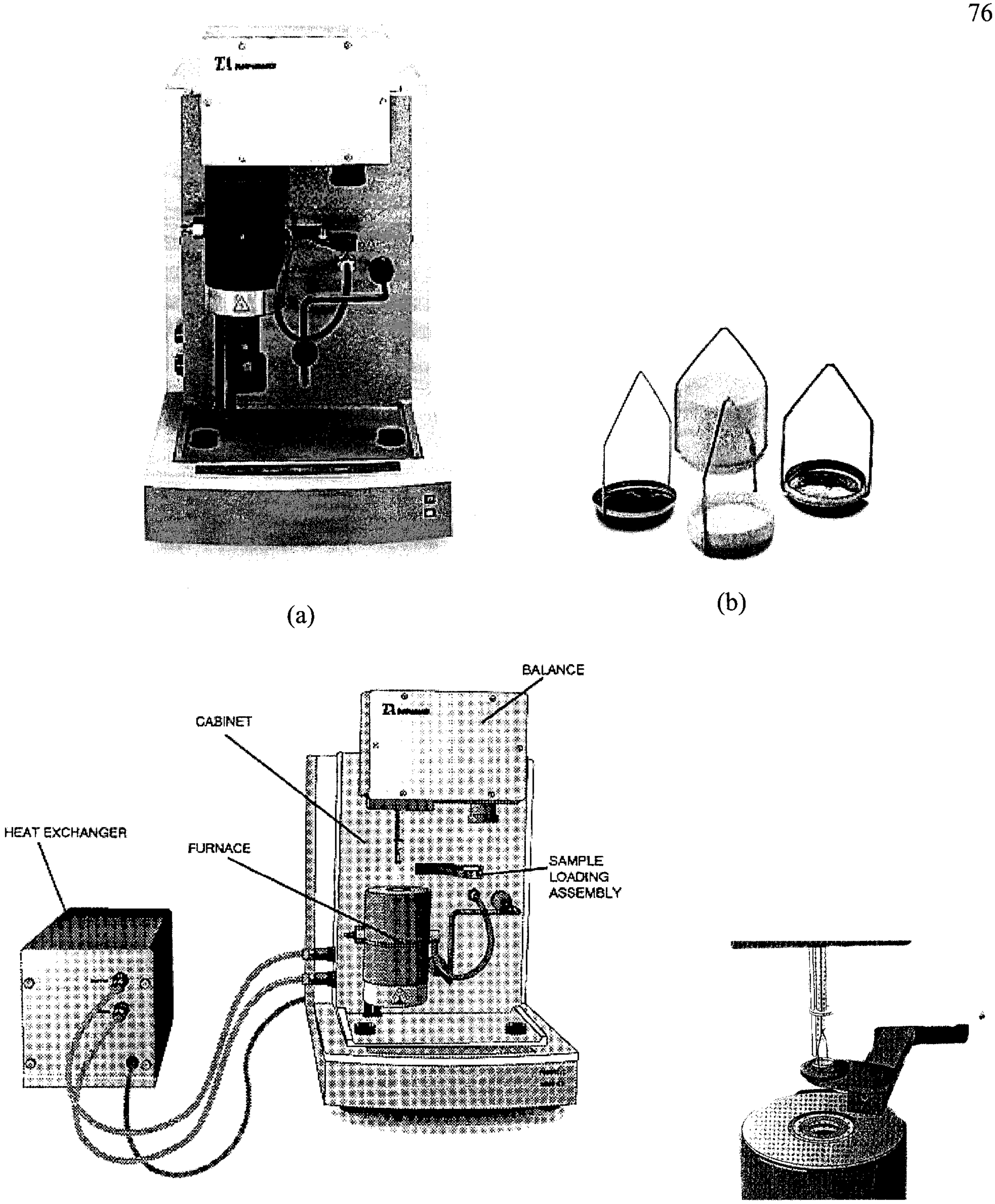

(a)

(b)

(c)

(d)

Figure 4.3: Thermogravimetric analyzer TGA-TA2050

(a) Pictorial view of TGA-TA2050

(b) Pictorial view of various types of TGA sample pans

(c) Schematic of the TGA-TA2050 and heat exchanger

(d) Magnified schematic of the sample loading assembly

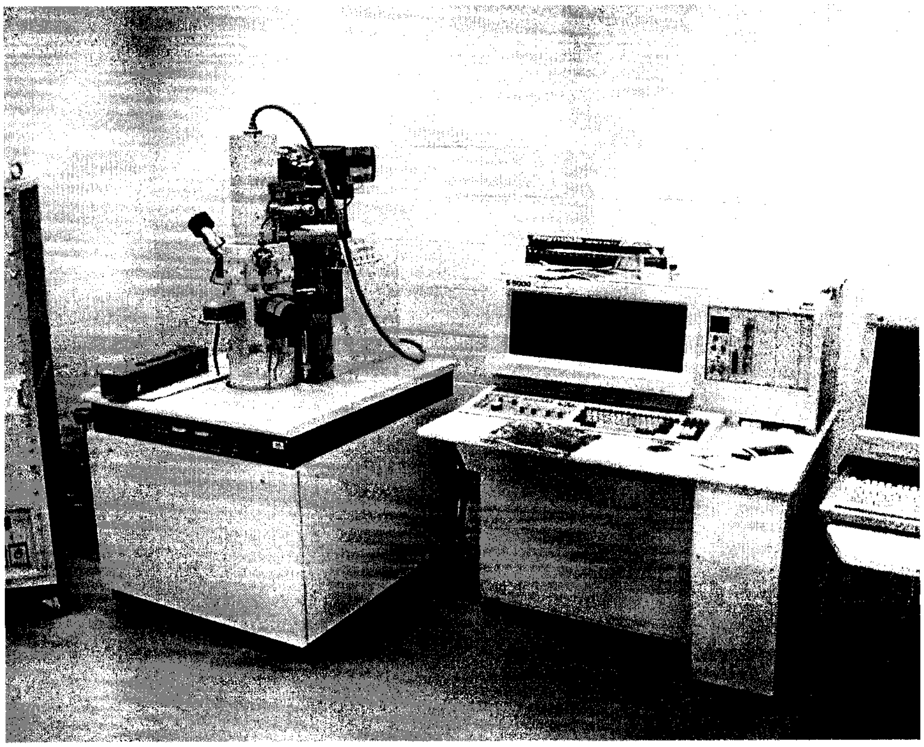

(a)

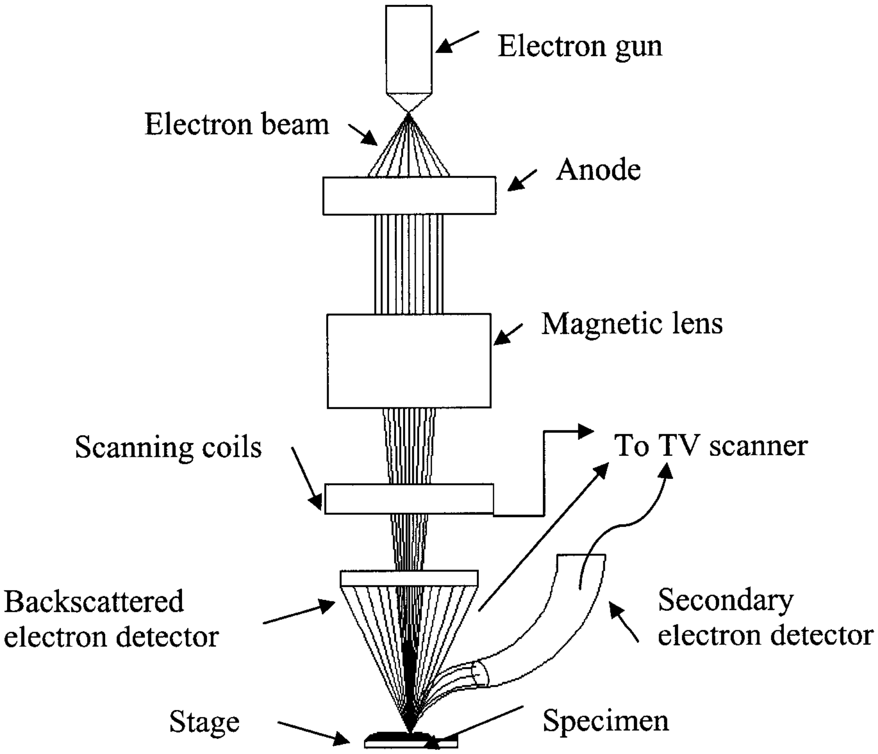

(b)

Figure 4.4: Scanning electronic microscope Hitachi S-2500

(a) Pictorial view of SEM Hitachi S-2500

(b) Schematic of the principle of operation of a SEM

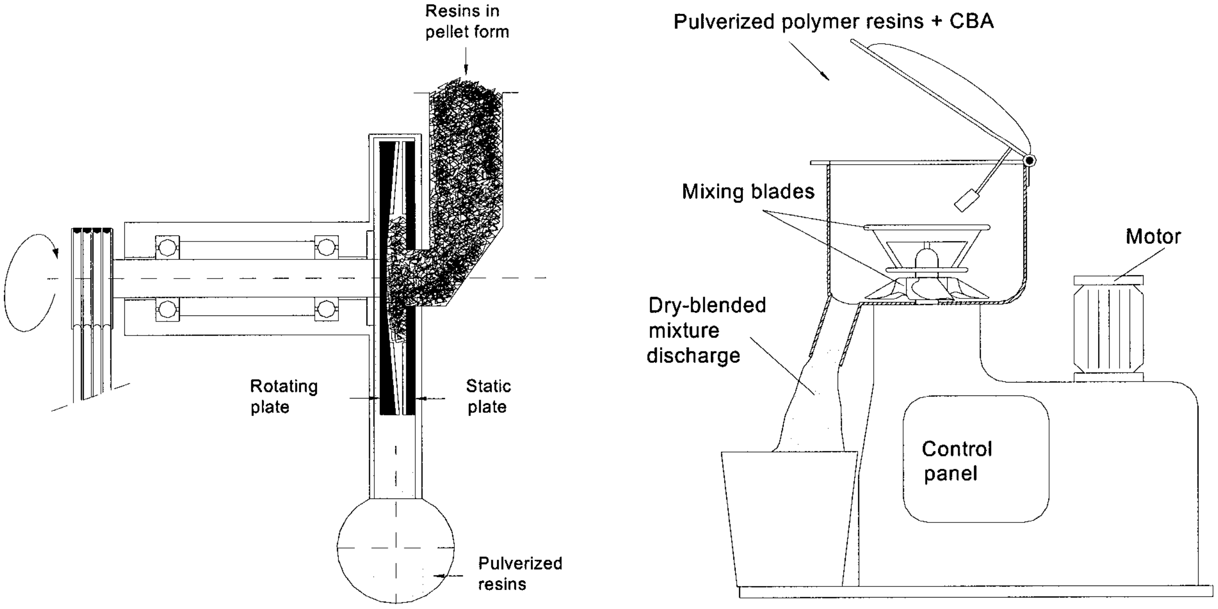

(a) (b)

Figure 4.5: Schematic illustration of a dry blending experimental setup

(a) Schematic illustration of a grinding head

(b) Schematic illustration of a high-speed mixer

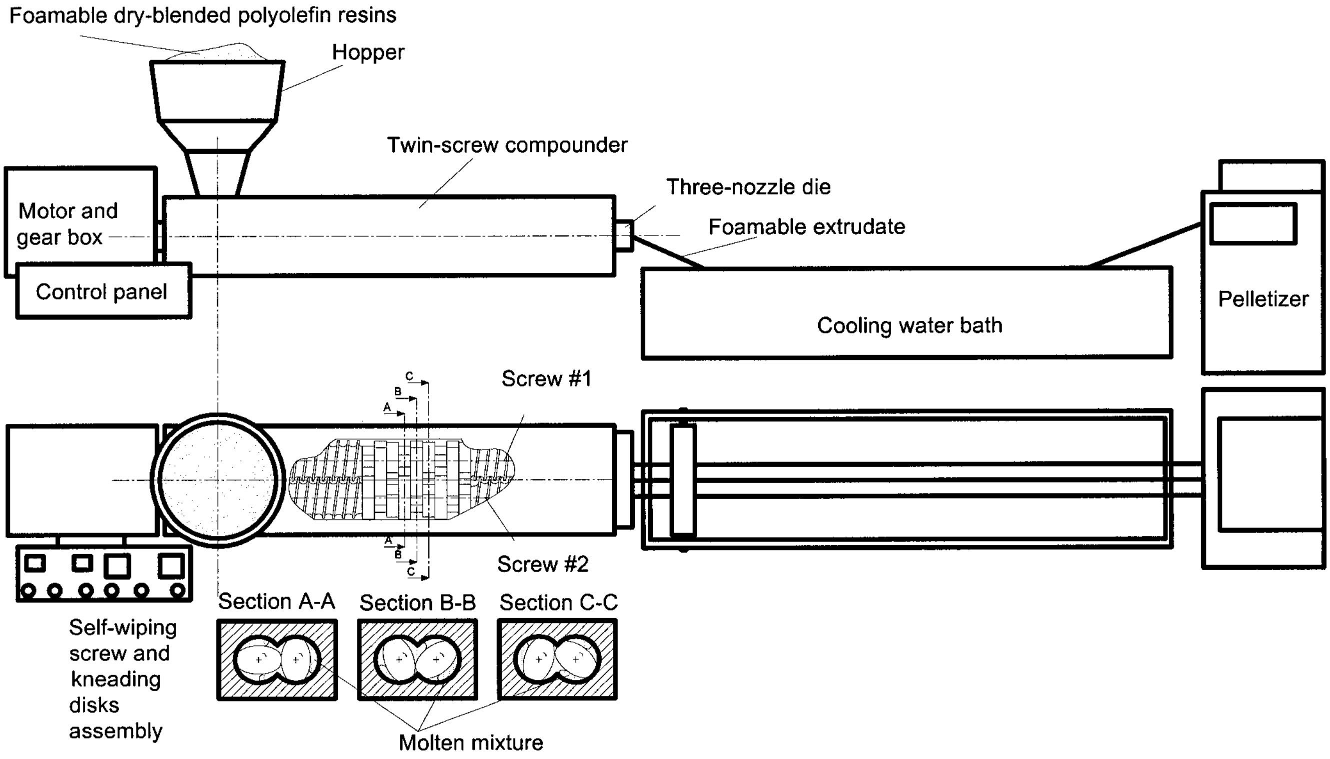

Figure 4.6: Schematic illustration of the melt compounding experimental setup

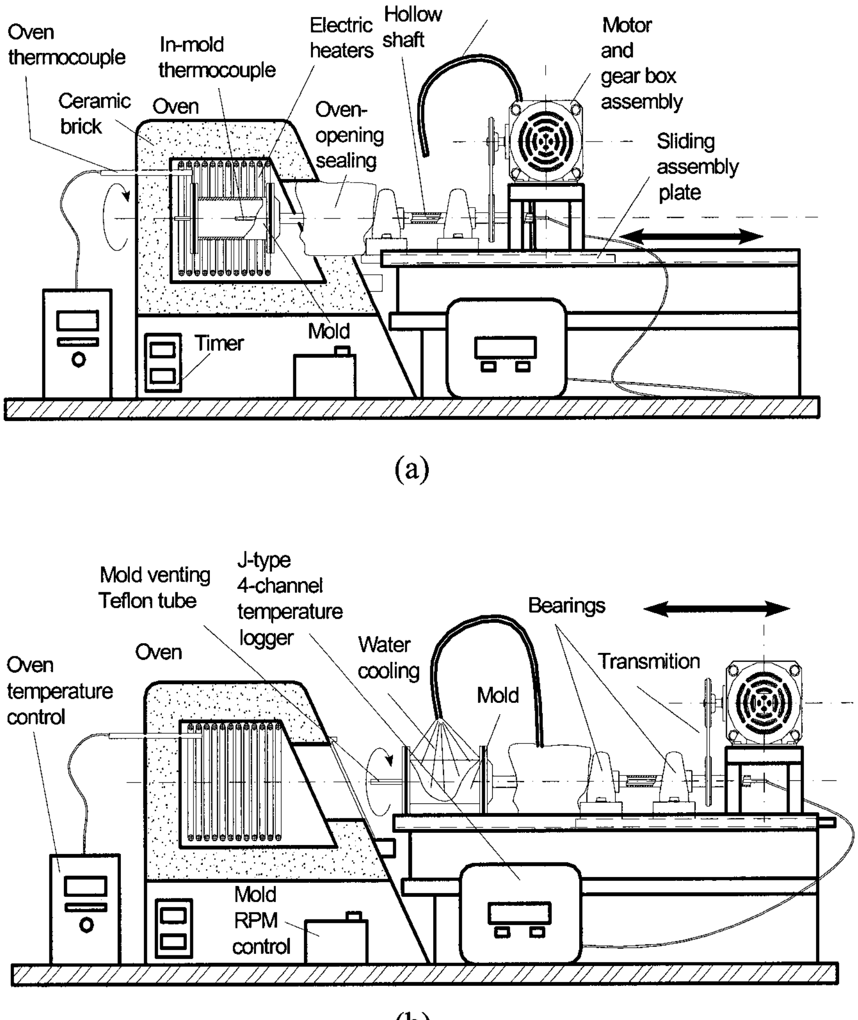

Figure 4.7: Schematic illustration of the conventional, uni-axial, lab-scale, custom-made rotational molding machine

(a) Mold heating step

(b) Mold cooling step

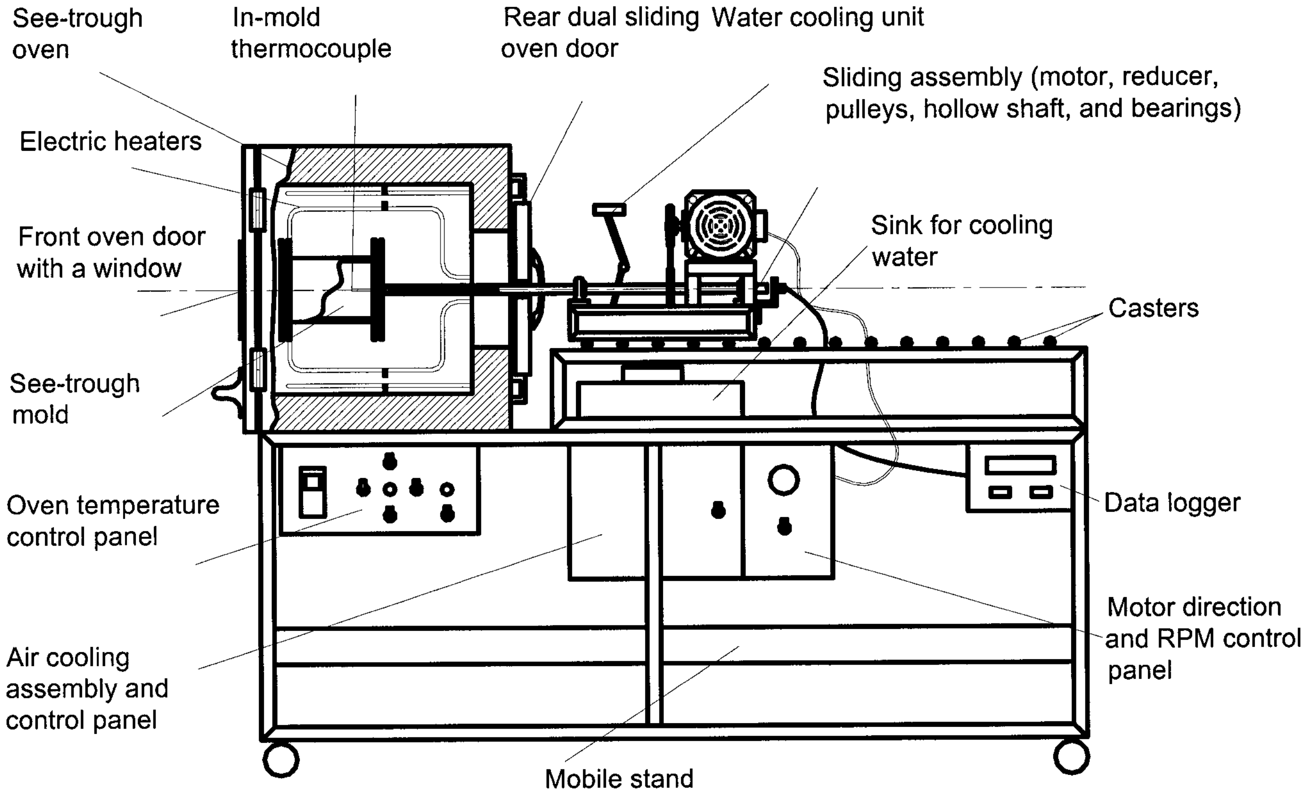

(a)

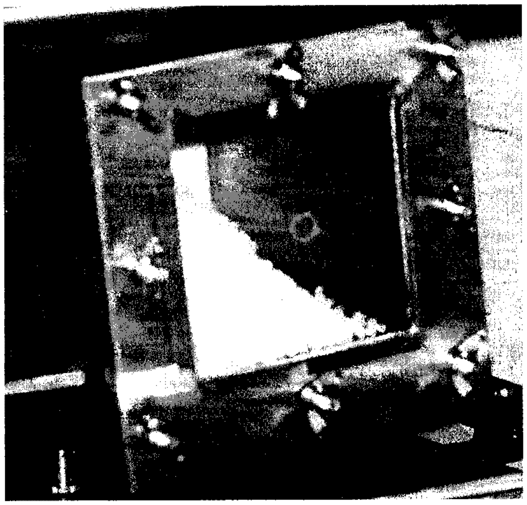

(b)

Figure 4.8: Transparent, uni-axial, lab-scale, custom-made rotational molding machine

(a) Schematic illustration of the rotomolding machine

(b) Pictorial view of the see-trough mold (4” × 4” × 6”)

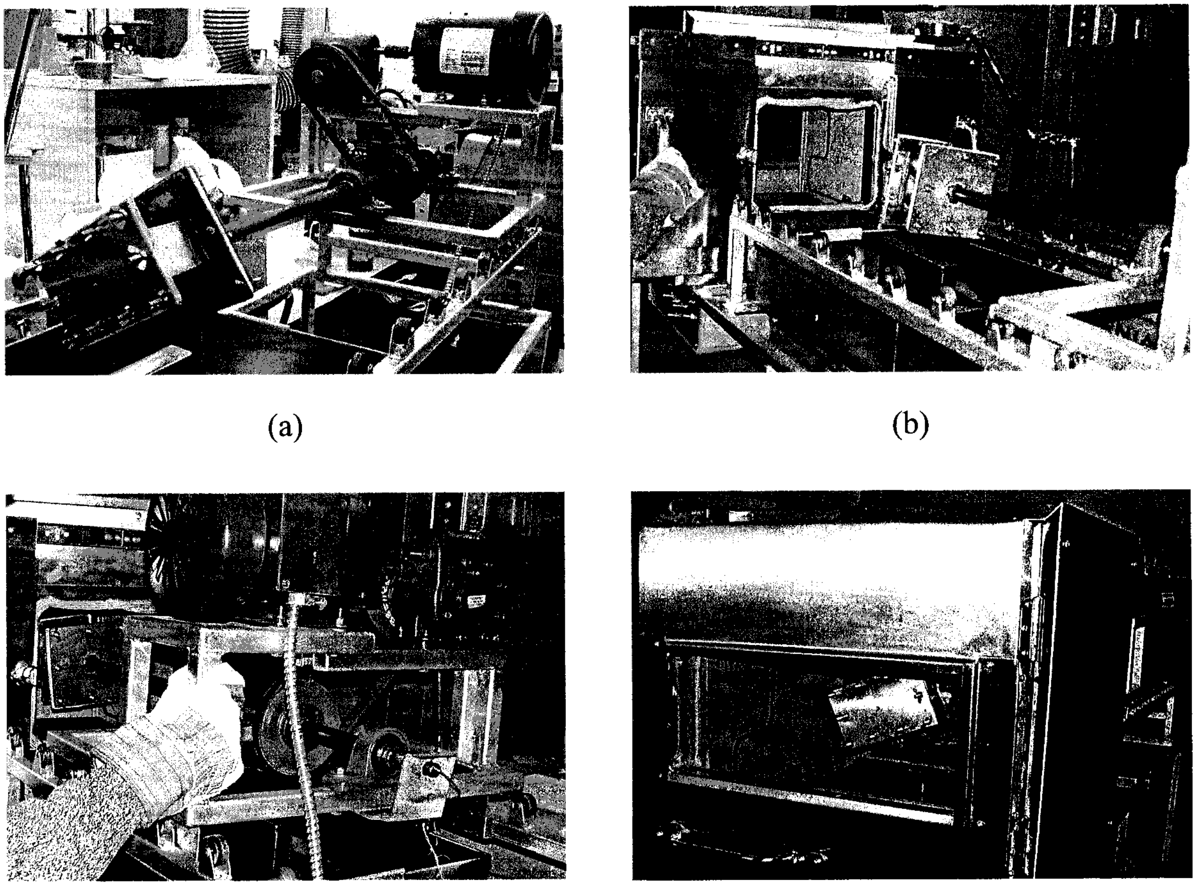

(a) (b)

(c) (d)

Figure 4.9: Pictorial view of the transparent, uni-axial, lab-scale, custom-made rotational molding machine during a rotational foam molding experiment

(a) Mold, shaft, and sliding assembly

(b) Rear sliding oven door

(c) Mold insertion in oven

(d) Front oven door with the mold inserted

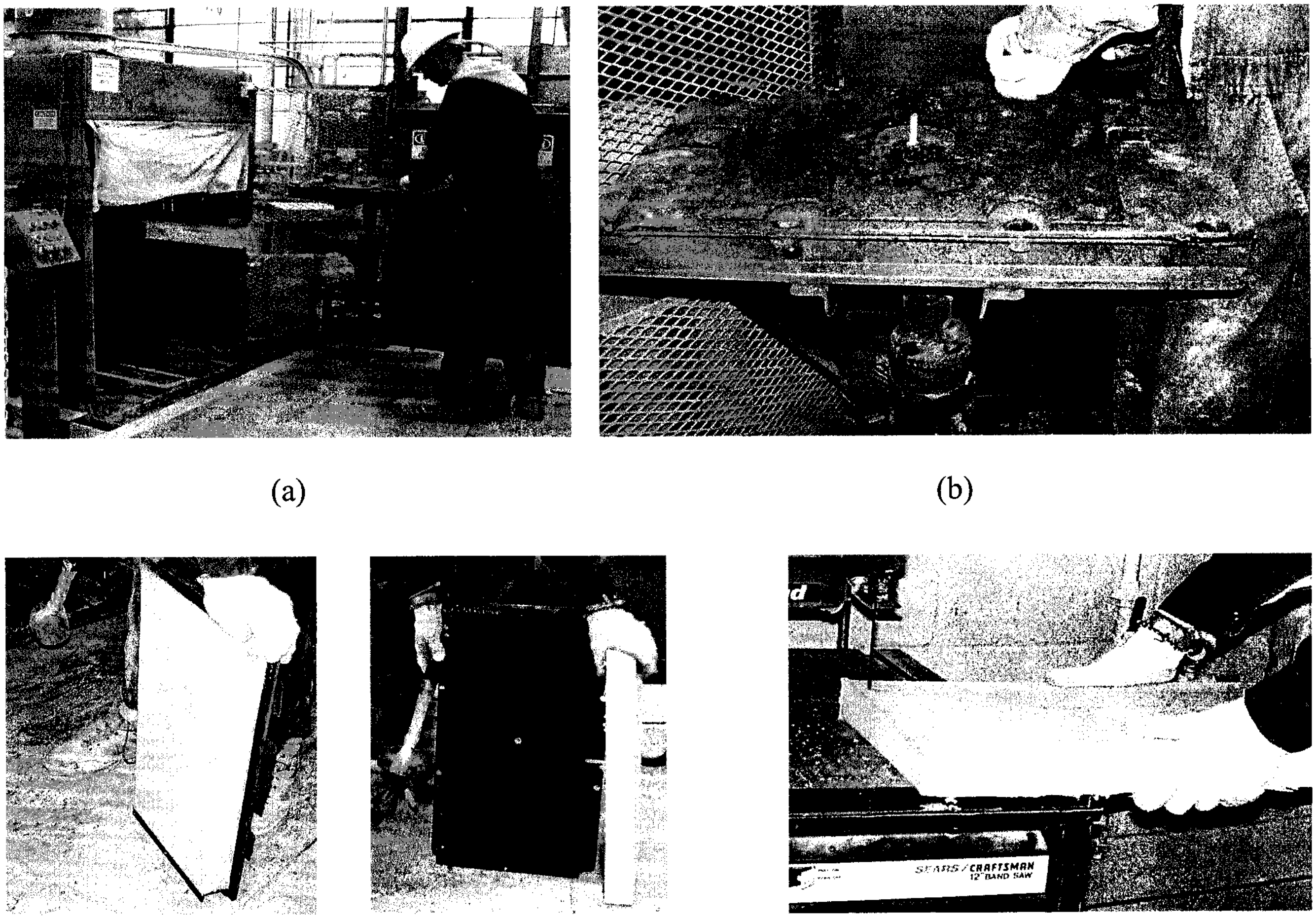

(a) (b)

(c) (d)

Figure 4.10: Pictorial view of a biaxial industrial-scale rotational molding machine McNeil RC-500

(a) Rotating arm and heating/cooling chamber

(b) Mild steel flat mold (2" × 12" × 24") and mold vent

(c) Part removal

(d) Sample cutting

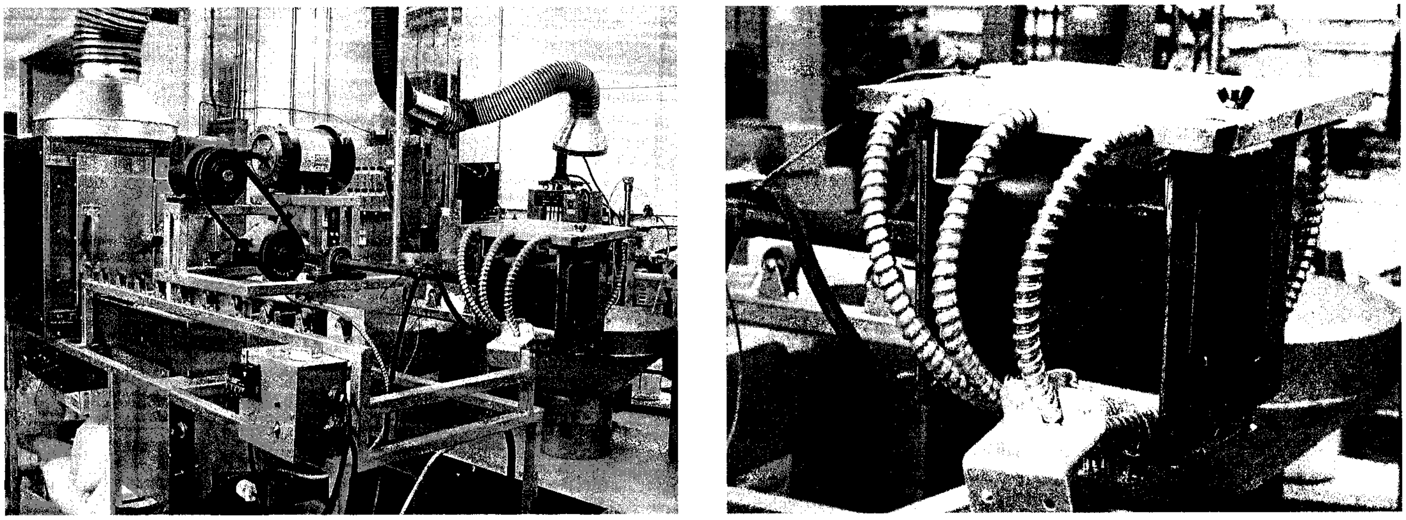

(a) (b)

Figure 4.11: Pictorial views of the rotating hot plate experimental setup conveniently attached on the uni-axial lab-scale rotational foam molding experimental setup

(a) Rotating high temperature wall experimental setup

(b) Detail of the rotating aluminum hot-plate assembly

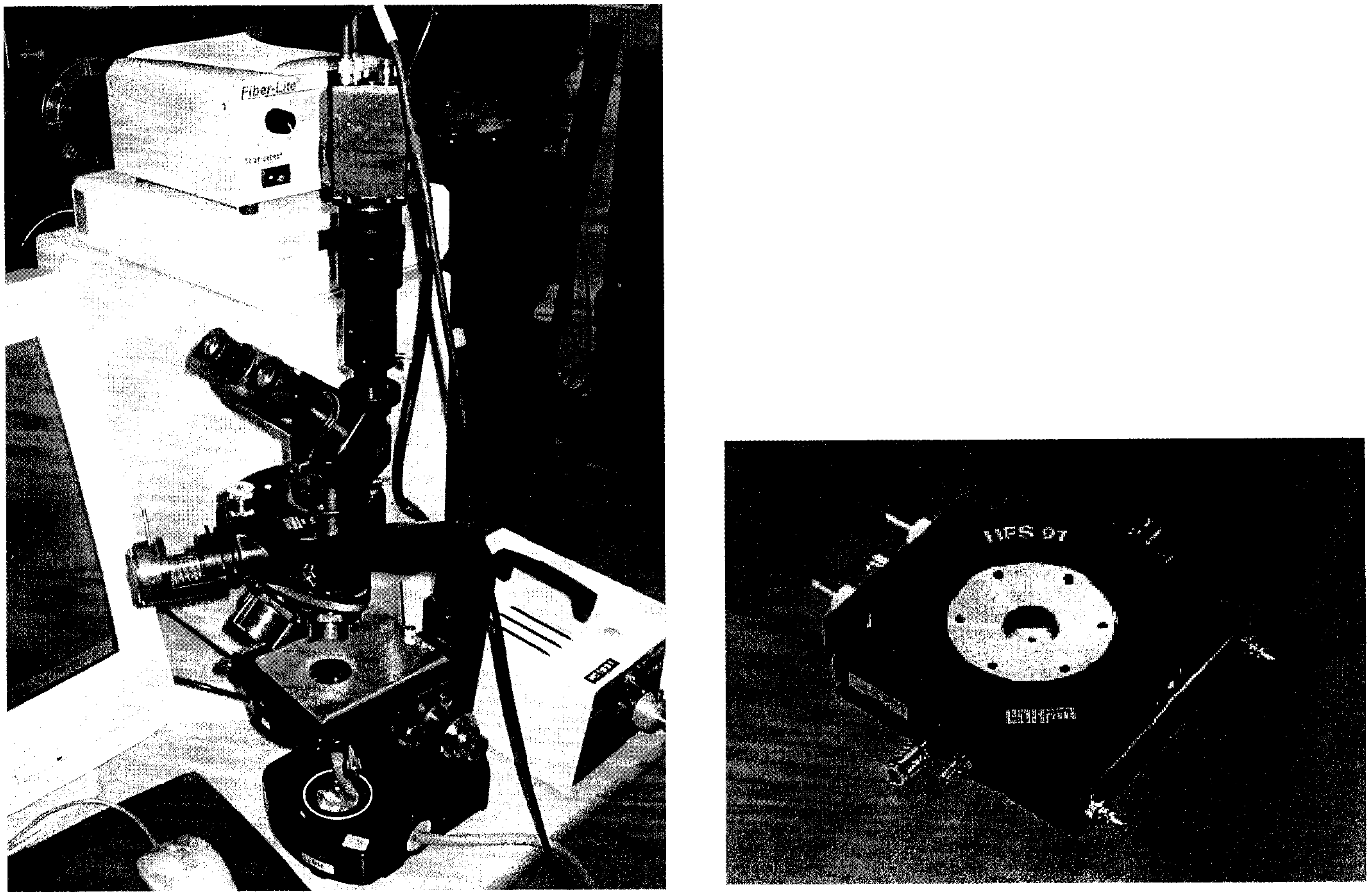

(a) (b)

Figure 4.12: Custom built hot-stage optical microscopy computerized digital imaging experimental setup

(a) Pictorial view of the optical microscope, CCD camera, light source, hot-stage controller, and computer

(b) Pictorial view of the hot-stage (Linkam HFS-91)

CHAPTER 5

CHARACTERIZATION OF POLYOLEFIN RESINS AND ADDITIVES

5.1 Introduction

Whenever plastics are processed in a molten state, the viscoelastic properties govern the flow behavior. Molten plastics are rheologically complex materials that can exhibit both viscous flow and elastic recoil [81], i.e., their behavior is a function of both shear rate and a time parameter [197].

The viscoelastic and thermal behaviors of a particular polymeric material have a controlling effect on its selection for a foaming application. Therefore, a thorough study of the fundamental rheological and thermal properties of the polyolefin resins and respective additives selected for experimentation is presented and discussed in this chapter.

The science of rheology is concerned with the way materials deform when forces are applied to them. To extract information about the rheological properties of a material, it is necessary either to measure the deformation resulting from a given force or measure the force required to produce a given deformation. The contribution of each of these components varies with time, temperature, deformation, and rate of deformation [81,197].

The simplest type of viscoelastic behavior is linear viscoelasticity. This type of behavior is observed when the deformation is sufficiently mild that the molecules of a polymeric material are disturbed from their equilibrium configuration and entanglement state to a negligible extent. However, the deformations that occur in actual plastic processing are neither very small nor very slow and because the response to an imposed deformation depends on the size, rate, and kinetics of the deformation, the linear theory does not apply. However, the principal utility of the theory of linear viscoelasticity is as a method for characterizing the molecules in their equilibrium state. This is useful in the comparison of different resins [81].

5.2 Study of Fundamental Rheological Properties of Polyolefins

A rheometric measurement normally consists of a strain (deformation) or a stress analysis at a constant frequency combined with a frequency analysis. Dynamic tests employ a method of deforming a sample by applying a sinusoidal deformation, whereas steady tests use a method of deforming a sample by applying a linearly changing or constant shear deformation. Dynamic mechanical data is used for understanding the complex behavior of polymers over a wide range of frequency or stiffness. The strain sweep gives information of the elastic (storage) modulus, G', the viscous (loss) modulus, G'', and the phase angle, $\tan\delta$ [190].

A viscometric measurement normally consists of a shear rate analysis. The shear rate sweep should preferably cover the range applied in the intended equipment [190].

5.2.1 Experimental Procedure

Considering the above, a rotational rheometer, as described in Section 4.2.1, was used to subject each of the eight selected polyolefin grades to a battery of tests comprising two rheological (dynamic frequency sweep and dynamic stress sweep) and one viscometric test (steady stress sweep).

For reasons of comparing the rheological properties of PE and PP grades at elevated temperatures, each rheological tests applied to the eight selected polyolefin grades has been conducted at multiple test temperatures. The four PE grades were tested at 160, 180, 190, and 220 °C, whereas, because of their higher melting temperature, the four PP materials were tested only at 180, 190, and 220 °C. These test temperatures were deliberately selected to match the critical temperatures identified during actual processing of foamable polyolefin resins in rotational foam molding. Namely, since the foamable PE resins are prepared with Celogen OT, a test temperature of 160 °C serves for the characterization of the rheological behavior of PE melts at temperatures close to the decomposition temperature of Celogen OT. Similarly, test temperatures of 180 and 190 °C are primarily appropriate for testing the rheological behavior of PP melts because they cover a temperature range close to the onset decomposition temperature range of Celogen AZ, especially when used at high heating rates or when the foamable formulation includes various amounts of a decomposition promoter such as ZnO [38]. Finally, since the in-mold temperature during an optimized rotational foam molding cycle seldom exceeds 220 °C, the highest test temperature for both PE and PP grades has been set at this value. Thereby, the rheological properties of the polyolefin grades within temperature regions known to reduce polymer melt strength and promote cell coalescence, which might be detrimental to the cell morphology of the final foams, could be evaluated. This test temperature was especially important for investigating the suitability of the PP grades for foaming in rotational molding.

For each rheological polymer characterization test, standard samples were made. First, the air pockets that may be trapped among the plastic powder particles were removed by melting the plastic materials using a 3/4" Brabender single screw extruder (Brabender 05-25-000), after which the obtained extrudate was charged into the standard sample maker and pressed into the designated shape. Then, the sample was loaded in the gap between the cone and plate of the testing head of the rheometer. Once the sample was molten and has reached the pre-determined testing temperature, the gap was decreased to a standard measure of 0.051 [mm] and the experiment was commenced. Nitrogen atmosphere was used to prevent the plastic from being degraded and oxidized. It is important to note that when testing high viscosity materials, the initial temperature of the heater should be set to a little higher value than the testing temperature in order to facilitate the melting process and improve the melt quality. However, the temperature should be lowered to the testing temperature before conducting the experiment.

5.2.2 Dynamic Frequency Sweep Characterization Test

The dynamic frequency sweep (strain-controlled) test applies a sinusoidal deformation of constant peak amplitude over a range of frequencies. Frequencies can be incremented or decremented. Increments can be logarithmically scaled, or a series of discrete frequencies can be generated. The logarithmic frequency sweep generates frequencies that are logarithmically incremented, resulting in equally spaced data points when plotted as a function of logarithmically-scaled frequency. Frequencies are selected by specifying initial and final frequencies, and the number of data points to measure between each decade of frequency (points per decade). The number of points per decade includes the initial frequency, but excludes the final frequency. For example, for a sweep conducted over a single decade of frequency: between 10 and 100 [rad/sec], selecting five data points to be measured per decade divides the difference of the endpoint logarithms into five equally-spaced fractional exponents.

Thus, six discrete frequencies are generated, in succession, by taking the antilogarithm of each exponent: (i) initial frequency = 10 [rad/sec], (ii) four decade frequencies = 15.9; 25.1; 39.8; 63.1 [rad/sec], and (iii) final frequency = 100 [rad/sec]. One data point is measured at each of the frequencies [189]. Standard test samples of the eight polyolefin resins selected for experimentation, were subjected to a dynamic frequency sweep test in order to investigate the effect of varying the frequency of deformation $\omega \left(\omega = 2\pi f [rad/\sec]; f = frequency[Hz]\right)$ on the storage modulus, G', loss modulus, G'', tan delta, $\tan\delta$, and complex viscosity, η *.

5.2.2.1 Effect of Deformation Frequency on Rheology of PE Melts

Figure 5.1 illustrates the typical plots of the measured rheological properties of each of the four PE resins selected for experimentation (PE1, PE2, PE3, and PE4) obtained during the dynamic frequency sweep tests conducted while the temperature of the sample melt was kept at 160 °C. This test temperature is considered to be crucial for evaluating the suitability of the rheological properties of a PE resin for being foamed with Celogen OT because it decomposes at about 158-160 °C. In all presented plots a log-log scale format was used.

Figure 5.1 (a) depicts a plot that illustrates a comparison of the measured effects of varying the frequency of deformation applied to each PE sample on its storage modulus, G', at a test temperature of 160 °C. These experimental results show that for all applied frequencies of deformation the storage modulus of all four investigated PE resins represents a monotonically increasing function of the frequency with a moderate slope. It is important to note here that a moderate slope of the G' curve indicates a moderate material strength. In particular, PE1 (the resin with the highest MFI among the selected four PE grades) exhibited the lowest storage modulus at all experimental conditions. Since the storage modulus is regarded as a measure of the elasticity of the melt and plays a significant role in particle coalescence (sintering), fusion, and bubble growth dynamics, this should be an early indication that PE1 might be the most suitable resin for foaming applications because of its lowest melt elasticity.

Figure 5.1 (b) presents comparative plots of the experimentally measured viscous response of the investigated PE resins, i.e., the loss modulus, G'', to variations of the frequency of deformation at isothermal test conditions (160 °C) as per the adopted experimental procedure. These experimental results revealed that for all applied frequencies of deformation the loss modulus curves pertaining to all four investigated PE resins are monotonically increasing. However, in comparison with the corresponding results obtained for the storage modulus, G', (Figures 5.1 (a)) the loss modulus, G'', exhibited significantly larger values, a lower slope, and a weaker dependence of the test temperature especially within the frequency region between 0.1 and 10 [rad/sec]. As a measure of the viscous/damping property of the polymer melt, the loss modulus is important for both the early stage of bubble growth and the terminal bubble stabilization stage. While a higher loss modulus is counter productive to the initial bubble growth, it is favorable for achieving the desired final cell size during the cell stabilization stage. Considering this, and because PE1 exhibited the lowest loss modulus among all investigated PE grades, PE1 seems to be the resin having the most suitable viscous behavior for foaming applications, which is sufficiently low to support the initial cell growth and sufficiently high to prevent cell coalescence and facilitate cell stabilization.

Figure 5.1 (c) illustrates the dependence of $\tan\delta$ on variations in deformation frequencies at various isothermal test temperatures for PE resins at 160 °C. Since the value of $\tan\delta$ actually presents the ratio of the loss and storage modulus $\left(\tan\delta = G''/G'\right)$, the monotonically decreasing $\tan\delta$ curve indicated that with the increase of the frequency of deformation the domination ratio of the viscous properties of the polymer over its elastic properties decreased from values of about over 40, at deformation frequencies of about 0.1 [rad/sec], to values approaching closely the range between 1 and 2, at deformation frequencies greater than 500 [rad/sec]. These results revealed that the intensity of the damping properties of the investigated PE resins almost reduce to that of their elastic properties at higher frequencies of deformation. However, for all other experimental conditions PE1 was associated with the highest $\tan\delta$ values in comparison with those pertaining to the other three investigated PE resins, it should be therefore expected that PE1 would demonstrate the lowest resilience and the highest hysteresis during foam processing, which would be especially favorable for the stage of the initial bubble growth.

Figure 5.1 (d) shows the effect of varying the frequency of PE polymer deformation on its complex viscosity, η^* at 160 °C. These experimental results revealed that for all investigated PE grades the complex viscosity tends to decrease with the increase of the frequency of deformation. Also, these plots show that the higher the MFI of a PE resin the lower its complex viscosity would be. Conversely, PE1 demonstrated the lowest complex viscosity, which indicates that it would be particularly favorable for bubble formation and the early stage of diffusion-controlled bubble growth.

Figures 5.1 (e) and 5.1 (f) illustrate the comparison of the relaxation modulus, $G(t)$ and the comparison of the relaxation spectra, $H(\lambda)$, of the investigated PE resins at 160 °C, respectively. These plots have been obtained from the dynamic frequency sweep tests discussed above. It can be also observed from the plots presented in Figure 5.1 (e) that the higher the MFI of a PE resin, the lower the relaxation modulus. PE1 demonstrated the lowest relaxation modulus at all experimental conditions. Figure 5.1 (f) demonstrates that the behavioral trends of the PE resins remained similar to those presented in the relaxation modulus plots (Figures 5.1 (e)), but the relaxation spectra provided more comprehensive information about the relaxation behavior of the PE resins at extended periods of time. Among the investigated PE grades, PE1 demonstrated the lowest relaxation values at all test conditions.

5.2.2.2 Effect of Deformation Frequency on Rheology of PP Melts

Figure 5.2 illustrates the typical rheological properties of each of the four PP resins selected for experimentation (PP1, PP2, PP3, and PP4) obtained by dynamic frequency sweep tests conducted at a test temperature of 190 °C. This test temperature is crucial for evaluating the suitability of the rheological properties of a PP resin for being foamed with Celogen AZ because its onset of decomposition is at about 190 °C. In all presented plots a log-log scale format was used.

Figure 5.2 (a) presents a comparison between the measured effects of varying the frequency of deformation on the storage modulus, G', of each PP sample at the isothermal test conditions mentioned above, respectively. For all applied frequencies of deformation the storage modulus of all four investigated PP resins produced a monotonically increasing function of the frequency. Interestingly, the PP resin with the lowest MFR (PP1) exhibited the highest storage modulus up to frequencies of about 30-40 [rad/s], however, at higher frequencies; its storage modulus dropped and reached values pertaining to the resin with the highest MFR (PP4). Since high melt elasticity is not regarded as a favorable resin's attribute for foaming applications, the actual deformation frequency at which the resin is exposed at the moment of foaming might be crucial for determining its suitability for foaming applications in rotational foam molding. However, although the curve pertaining to PP1 exhibited the smallest slope, in PP foaming, the melt strength of the resin at elevated temperatures seems to be the dominant limiting property for obtaining good quality foams, and because of its highest viscosity (lowest MFR = 5.5 [g/10min]) among the investigated PP grades, there are reasons to expect that it will exhibit the best foaming behavior.

Figure 5.2 (b) presents comparative plots of the loss modulus, G'', of the PP resins versus the frequency of deformation applied at isothermal test conditions (190 °C) as per the adopted experimental procedure. For all investigated PP resins and for all experimental conditions the loss modulus curves exhibited a monotonically increasing trend. In comparison with the corresponding results obtained for the storage modulus, G', (Figure 5.2 (a)), the loss modulus, G'', exhibited slightly larger values and a lower slope. In addition, the point at which the loss modulus of PP1 dropped and reached values pertaining to PP4 moved towards the 10 [rad/s] frequencies. Since a higher loss modulus is counter productive to the initial bubble growth, while it is favorable in achieving the desired final cell size during the cell stabilization stage, this behavior of PP1 could have twofold consequences depending on the actual deformation frequency at which it is exposed at the moment of foaming.

Figure 5.2 (c) illustrates the $\tan\delta$ curves pertaining to the investigated PP resins versus variations in deformation frequencies at an isothermal test temperature of 190 °C. The monotonically decreasing trend of the $\tan\delta$ curves indicated that with the increase of the frequency of deformation the domination of the viscous properties of the polymer over its elastic properties tend to decrease, so that the intensity of the damping properties of the investigated PP resins almost reduce to that of their elastic properties, reaching very close values for all PP resins at higher frequencies of deformation. Other than some inconsistencies at frequencies below 1 [rad/s] demonstrated by the PP3 curve, for all experimental conditions PP1 was associated with the lowest $\tan\delta$ values in comparison with its counterparts. Thus, PP1 would demonstrate the highest resilience and the lowest hysteresis during foam processing, which would not be especially favorable for the stage of the initial bubble growth.

Figure 5.2 (d) shows the effect of varying the frequency of deformation on the complex viscosity, η^*, of the investigated PP resins at 190 °C. For all investigated PP resins and for all experimental conditions the viscosity curves exhibited a monotonically decreasing trend. In particular, at lower frequencies of deformation, PP1 exhibited the highest viscosity, however, at higher frequencies (above about 10 [rad/s]) its viscosity dropped as low as that of PP3.

Figure 5.2 (e) illustrates the comparison of the relaxation modulus, $G(t)$, pertaining to the investigated PP resins, while Figure 5.2 (f) illustrates the comparison of the respective relaxation spectra, $H(\lambda)$, at a polymer melt temperature of 190 °C. It can be observed that the higher the MFR, the lower is the value and the slope of the respective relaxation modulus curve. For all investigated PP resins the relationship between the values of the relaxation modulus between the resins remained almost unchanged. Namely, PP1 demonstrated the highest relaxation modulus at all experimental conditions, while at frequencies greater than 0.1 [rad/s], it demonstrated the highest relaxation spectra.

5.2.3 Dynamic Stress Sweep Characterization Test

The dynamic stress sweep test applies a range of sinusoidal deformations (stresses), each at a constant frequency. Successive measurements are taken at each of the commanded stresses. The stress amplitude can be incremented or decremented, and scaled logarithmically or linearly. The logarithmic stress sweep generates dynamic stresses that are logarithmically incremented, resulting in equally spaced data points when plotted as a function of logarithmically-scaled stress. Dynamic stress amplitudes are selected by specifying initial and final stresses, and the number of data points to measure between each decade of frequency. Selecting five data points to be measured per decade divides the difference of the endpoint logarithms into five equally-spaced fractional exponents (10^1, $10^{1.2}$, $10^{1.4}$, $10^{1.6}$, $10^{1.8}$, and 10^2) after which six discrete stresses are generated, in succession, by taking the antilogarithm of each exponent (i) initial stress = 10 [dynes/cm^2], (ii) four decade stresses = 15.9, 25.1, 39.8, 63.1 [dynes/cm^2], and (iii) a final stress = 100 [dynes/cm^2]. One data point is measured at each of the stresses [189].

5.2.3.1 Effect of Shear Stress on Rheology of PE Melts

Figure 5.3 illustrates the effects of shear stress variations on the rheological properties of the investigated PE resins such as the storage modulus, G', the loss modulus, G'', and $\tan\delta$ at a polymer melt temperature of 160 °C in a log-log scale format.

Figure 5.3 (a) indicates that the dependence of the storage modulus of PE resins on shear stress variations in the investigated interval (10 to 10,000 [Pa]) at 160 °C was relatively weak. However, due to the increase of the PE resin's MFI, a significant decreasing trend of the value of G' could be observed. Similarly to the results obtained from the dynamic frequency sweep test, PE1 demonstrated the lowest melt elasticity among the investigated resins and thereby indicated that it should be the best suited PE resin for foaming applications in rotational foam molding.

Figure 5.3 (b) reveals that the loss modulus of PE resins was almost unaffected by the shear stress variations in the range between 10 and 10,000 [Pa] at 160 °C. Compared to the storage modulus, the increase of the PE resin's MFI, demonstrated little effect on the value of G'', while the higher the resins MFR, the higher the associated values of G'' were observed. Thus, PE1 showed the lowest loss modulus, which is favorable for achieving the desired final cell size during the cell stabilization stage.

Figure 5.3 (c) presents a comparison between the effects of the shear stress on $\tan\delta$ for each of the investigated PE resins at isothermal conditions (160 °C). Being directly dependent on the ratio of G'' and G', the value of $\tan\delta$ demonstrated that it is almost unaffected by shear stress variations. The plots indicated that the higher the MFI of a PE resin, the higher $\tan\delta$ was observed. PE1 demonstrated the highest values for $\tan\delta$ at all experimental conditions.

5.2.3.2 Effect of Shear Stress on Rheology of PP Melts

Figure 5.4 illustrates the changes the rheological properties of the investigated PP resins such as the storage modulus, G', the loss modulus, G'', and $\tan\delta$ undergo under the influence of shear stress at a polymer melt temperature of 190 °C in a log-log scale format.

Figure 5.4 (a) shows that the dependence of the storage modulus of PP resins on shear stress variations in the investigated interval was relatively weak, as was the case with the respective experimental results related to PE resins. As expected, at 190 °C, PP resins with higher MFRs demonstrated lower values for G' at all experimental conditions, so that PP1 was the resin the highest values of the storage modulus were associated with.

Figure 5.4 (b) expectedly reveals that the loss modulus of PP resins was almost unaffected by shear stress variations at 190 °C. However, the behavior of G'' associated with the investigated PP resins did not follow the expected pattern. Namely, it was observed that the values of the loss modulus of the two PP resins having the lowest MFRs (PP1 and PP2) were very close.

Figure 5.4 (c) illustrates the comparative effect of shear stress variations on $\tan\delta$ for the investigated PP resins at 190 °C. The plots indicated that $\tan\delta$ remains almost unaffected by the shear stress variations, while the higher the resin's MFR the higher $\tan\delta$ was observed. PP1 demonstrated the highest values for $\tan\delta$ at all experimental conditions.

5.2.4 Steady Stress Sweep Characterization Test

Since at sufficiently low shear rates the viscosity approaches a limiting constant value, η_0, i.e., the zero shear viscosity, the steady stress sweep test is commonly used to measure the zero shear viscosity of polymers. Normally, the viscosity decreases monotonically as the shear rate is increased, which behavior is termed "shear thinning".

5.2.4.1 Effect of Shear Rate on Rheology of PE Melts

Figures 5.5 (a) to 5.5 (d) depict the comparative effects of the shear rate variations on the zero shear viscosities of the selected PE resins at various test temperatures in a log-log scale. It could be observed that the zero shear curves pertaining to the PE resins with higher MFIs exhibited lower zero shear viscosities. However, at a test temperature of 220 °C, the curves demonstrated a shape disturbance at lower shear rates, which might be an indication of onset of polymer degradation. Among the investigated PE resins, PE1 exhibited the lowest zero shear viscosity at all experimental conditions. This should be very favorable for the early phase of bubble growth if PE1 is selected for further rotational foam molding experiments.

5.2.4.2 Effect of Shear Rate on Rheology of PP Melts

Figures 5.6 (a) to 5.6 (c) present the effects of the shear rate variations on the zero shear viscosities of the selected PP resins at respective test temperatures in a comparative manner using a log-log scale. Expectedly, the zero shear curves pertaining to the PP resins with higher MFRs exhibited lower zero shear viscosities. Thus, PP1 exhibited the highest zero shear viscosity at all experimental conditions. On one hand, this indicated a possible undesired sintering behavior of this resin and a non favorable property for the early stage of bubble growth, but oh the other, the higher viscosity might be a crucial factor for suppressing cell coalescence and retaining the desired cell size at advanced stages of the foaming process.

5.3 Study of Fundamental Thermal Properties of Polyolefins

5.3.1 Thermal Analysis Characterization of PE Grades

Figures 5.7 (a) to 5.7 (d) present the thermal analysis DSC plots pertaining to the selected PE resins, respectively. They illustrate a comparison of the initial and recristallization transition temperatures and respective degrees of crystallinity at a heating rate of 10 [°C/min]. The particular values of these thermal properties are tabulated in Table 5.1.

5.3.2 Thermal Analysis Characterization of PP Grades

Figures 5.8 (a) to 5.8 (d) illustrate the results of the thermal analysis conducted using a DSC on samples of the selected PP resins, respectively. The plots show a comparison of the initial and recristallization transition temperatures and respective degrees of crystallinity at a heating rate of 10 [°C/min]. The obtained respective experimental results are tabulated in Table 5.2.

5.4 Study of CBA Decomposition Properties

Figures 5.9 and 5.10 illustrate the decomposition behavior of samples of Celogen OT and Celogen AZ used for experimentation, respectively. These plots have been obtained by subjecting CBA samples to thermal TGA and DSC analysis, respectively. These results are in good agreement with respective data provided by the manufacturer mentioned in Sections 4.1.1.3 and 4.1.1.4.

Table 5.1: Thermal properties of the PE resins selected for experimentation measured using a DSC

		Initial curve		Recrystallization curve		
PE material	Assigned Code	Peak melting temperature [°C]	Degree of crystallinity [%]	Peak melting temperature [°C]	Degree of crystallinity [%]	Peak crystallization temperature [°C]
LL8556	PE1	127.07	45.41	126.23	47.33	111.01
LL8361	PE2	127.42	48.34	126.22	47.60	110.47
LL8461	PE3	128.94	49.76	127.55	58.75	112.14
TR0338	PE4	128.94	44.55	127.63	49.13	111.16

Table 5.2: Thermal properties of the PP resins selected for experimentation measured using a DSC

		Initial curve		Recrystallization curve		
PE material	Assigned Code	Peak melting temperature [°C]	Degree of crystallinity [%]	Peak melting temperature [°C]	Degree of crystallinity [%]	Peak crystallization temperature [°C]
PF633	PP1	160.85	43.79	159.55	50.12	125.79
SD812	PP2	167.83	50.00	163.25	41.91	125.69
MT4390	PP3	164.97	37.65	160.55	40.44	111.45
SD242	PP4	165.31	30.93	164.57	41.96	128.54

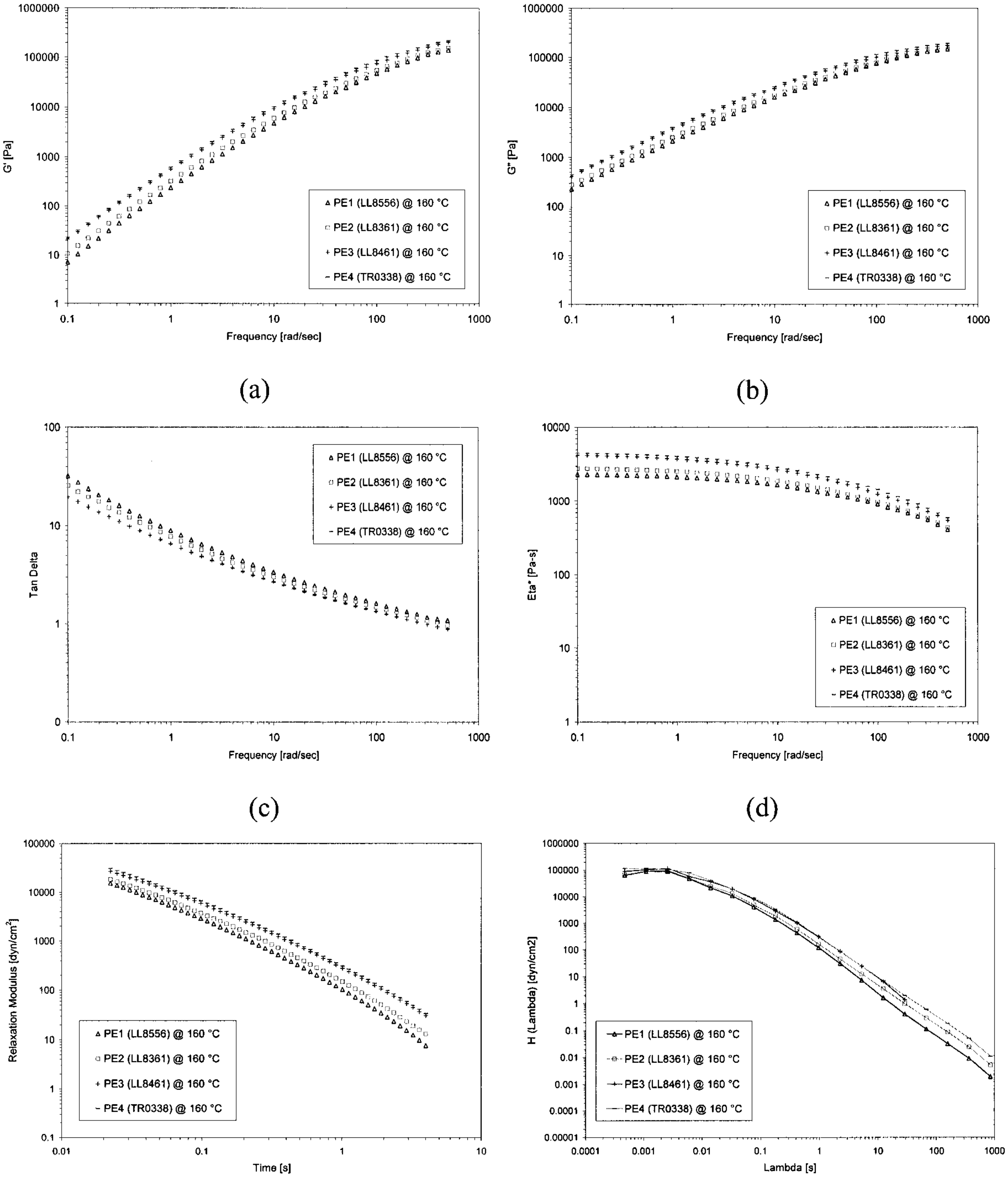

(a) (b)

(c) (d)

(e) (f)

Figure 5.1: Typical log-log scale comparative rheology plots for the selected PE grades at 160 °C

(a) Effect of frequency of deformation variations on the storage modulus, G'

(b) Effect of frequency of deformation variations on the loss modulus, G''

(c) Effect of frequency of deformation variations on, $\tan\delta = G''/G'$

(d) Effect of frequency of deformation variations on the complex viscosity, η^*

(e) Relaxation modulus, $G(t)$, obtained from respective dynamic frequency tests

(f) Relaxation spectra, $H(\lambda)$, obtained from respective dynamic frequency tests

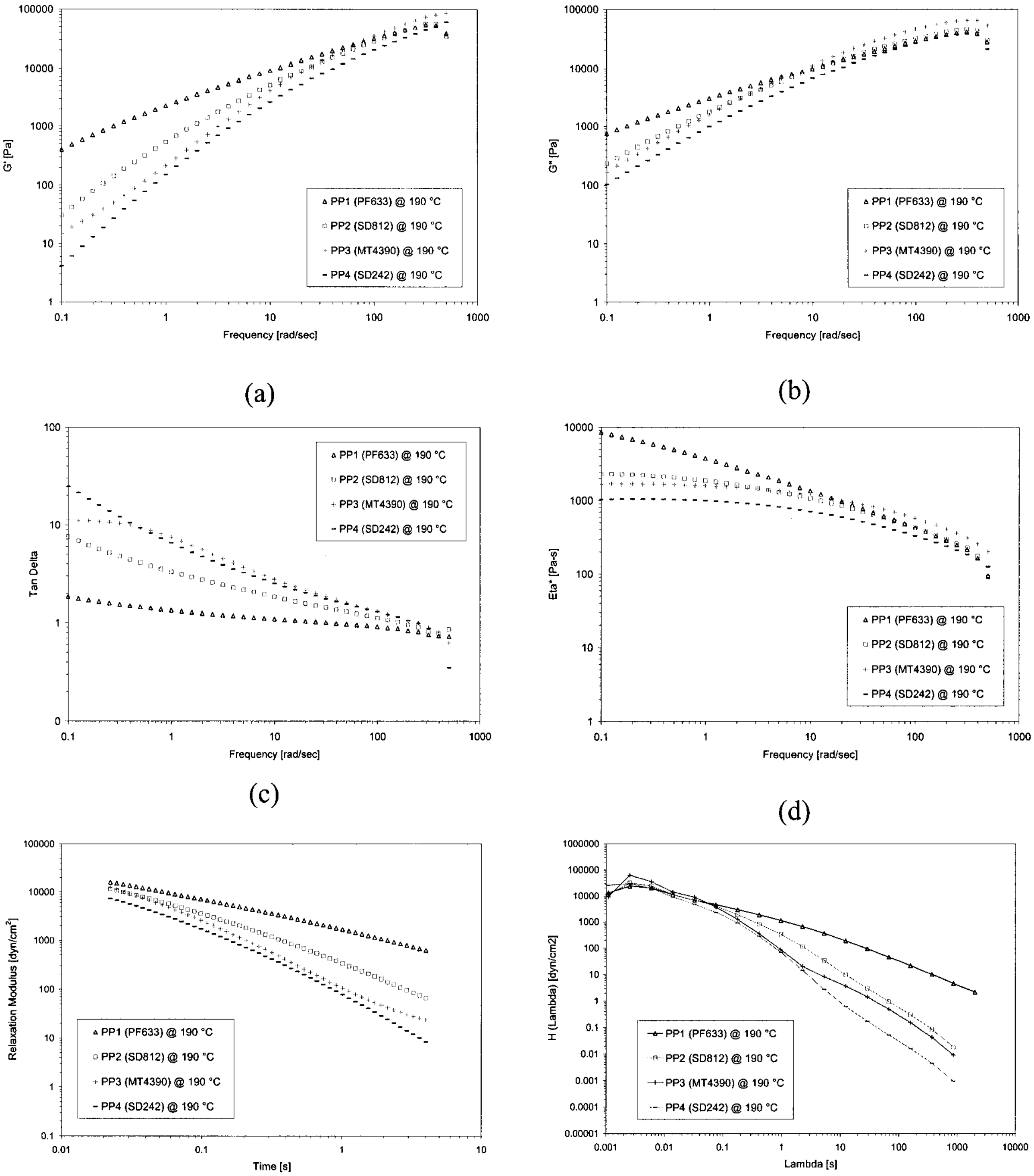

(a) (b) (c) (d) (e) (f)

Figure 5.2: Typical log-log scale comparative rheology plots for the selected PP grades at 190 °C

(a) Effect of frequency of deformation variations on the storage modulus, G'

(b) Effect of frequency of deformation variations on the loss modulus, G''

(c) Effect of frequency of deformation variations on, $\tan\delta = G''/G'$

(d) Effect of frequency of deformation variations on the complex viscosity, η^*

(e) Relaxation modulus, $G(t)$, obtained from respective dynamic frequency tests

(f) Relaxation spectra, $H(\lambda)$, obtained from respective dynamic frequency tests

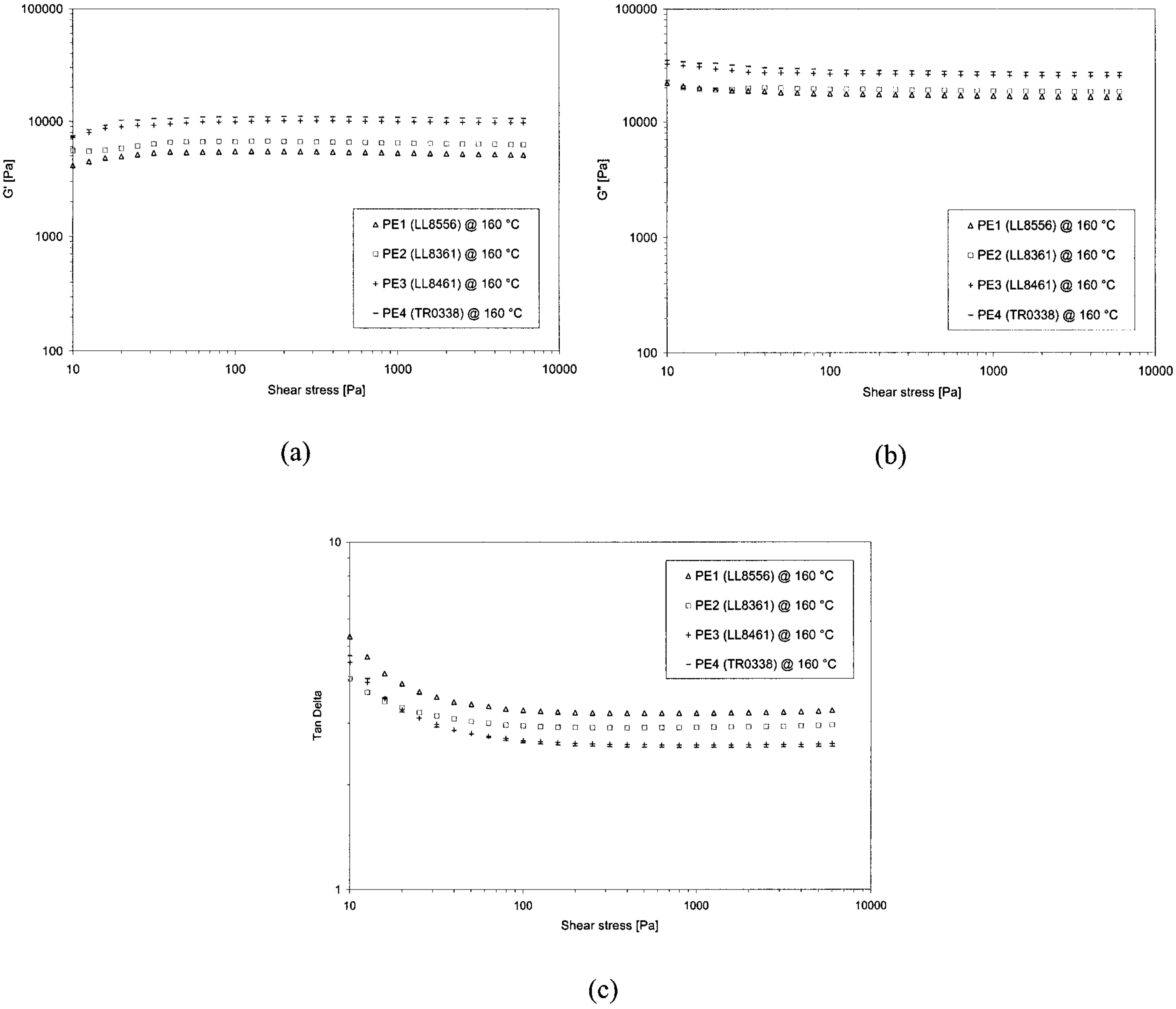

Figure 5.3: Typical log-log scale comparative rheology plots for the selected PE grades at 160 °C

(a) Effect of shear stress variations on the storage modulus, G'

(b) Effect of shear stress variations on the loss modulus, G''

(c) Effect of shear stress variations on $\tan\delta = G''/G'$

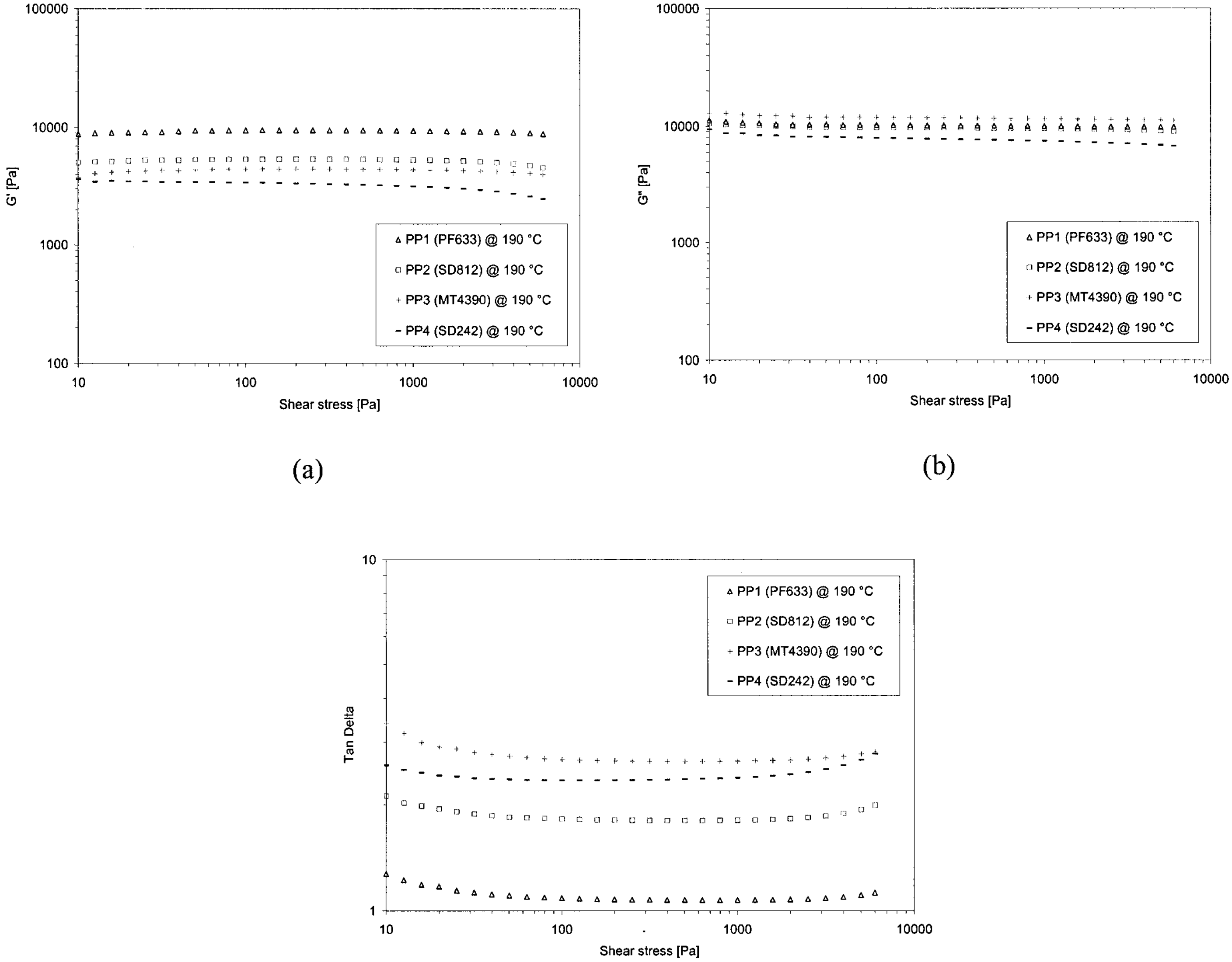

(a)

(b)

(c)

Figure 5.4: Typical log-log scale comparative rheology plots for the selected PP grades at 190 °C

(a) Effect of shear stress variations on the storage modulus, G'

(b) Effect of shear stress variations on the loss modulus, G''

(c) Effect of shear stress variations on $\tan\delta = G''/G'$

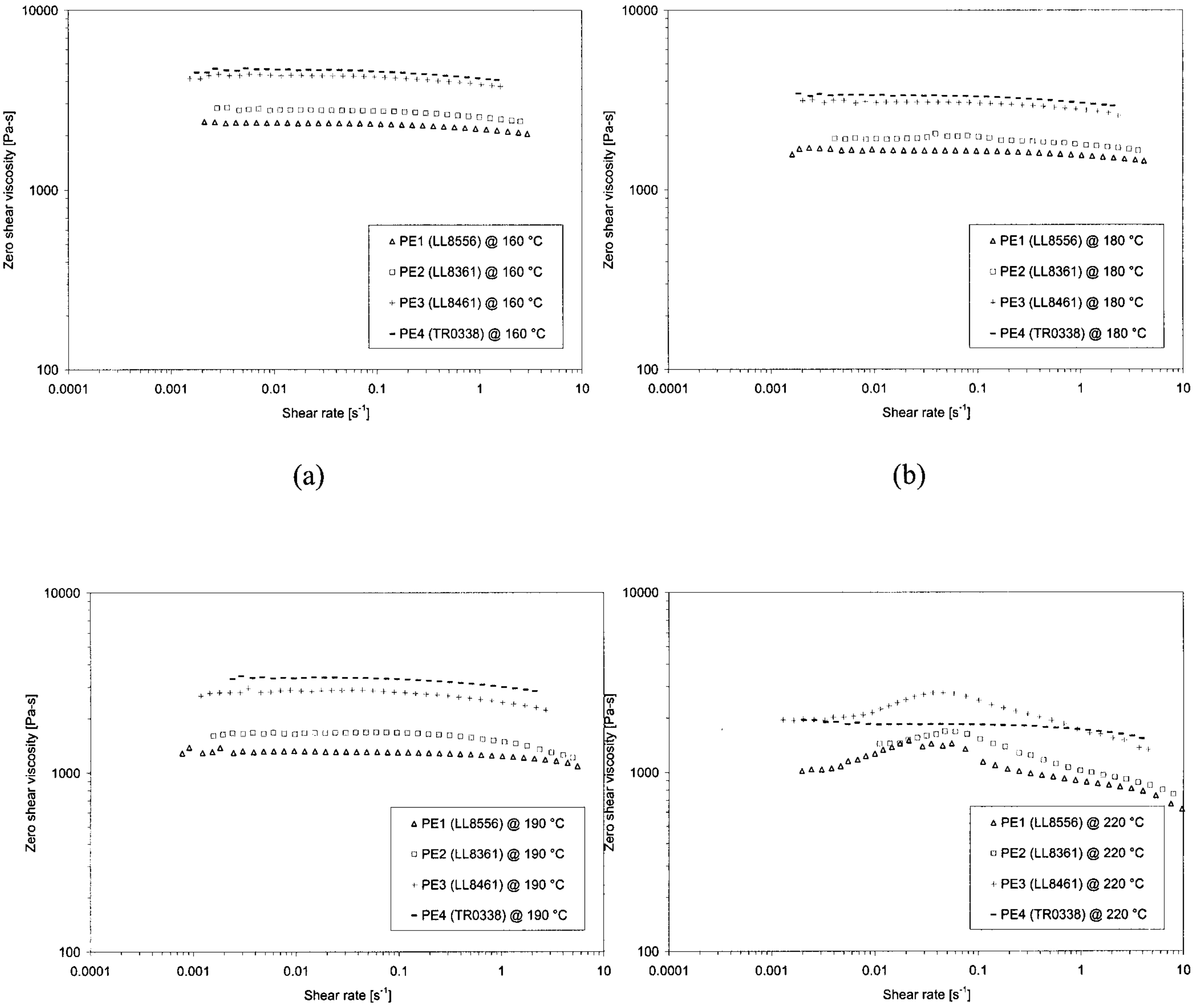

(a)

(b)

(c)

(d)

Figure 5.5: Comparison of the effect of shear rate variations on the zero shear viscosity, η_0, of the selected PE resins at various polymer melt temperatures presented in a log-log scale format

(a) Temperature of polymer melt = 160 °C

(b) Temperature of polymer melt = 180 °C

(c) Temperature of polymer melt = 190 °C

(d) Temperature of polymer melt = 220 °C

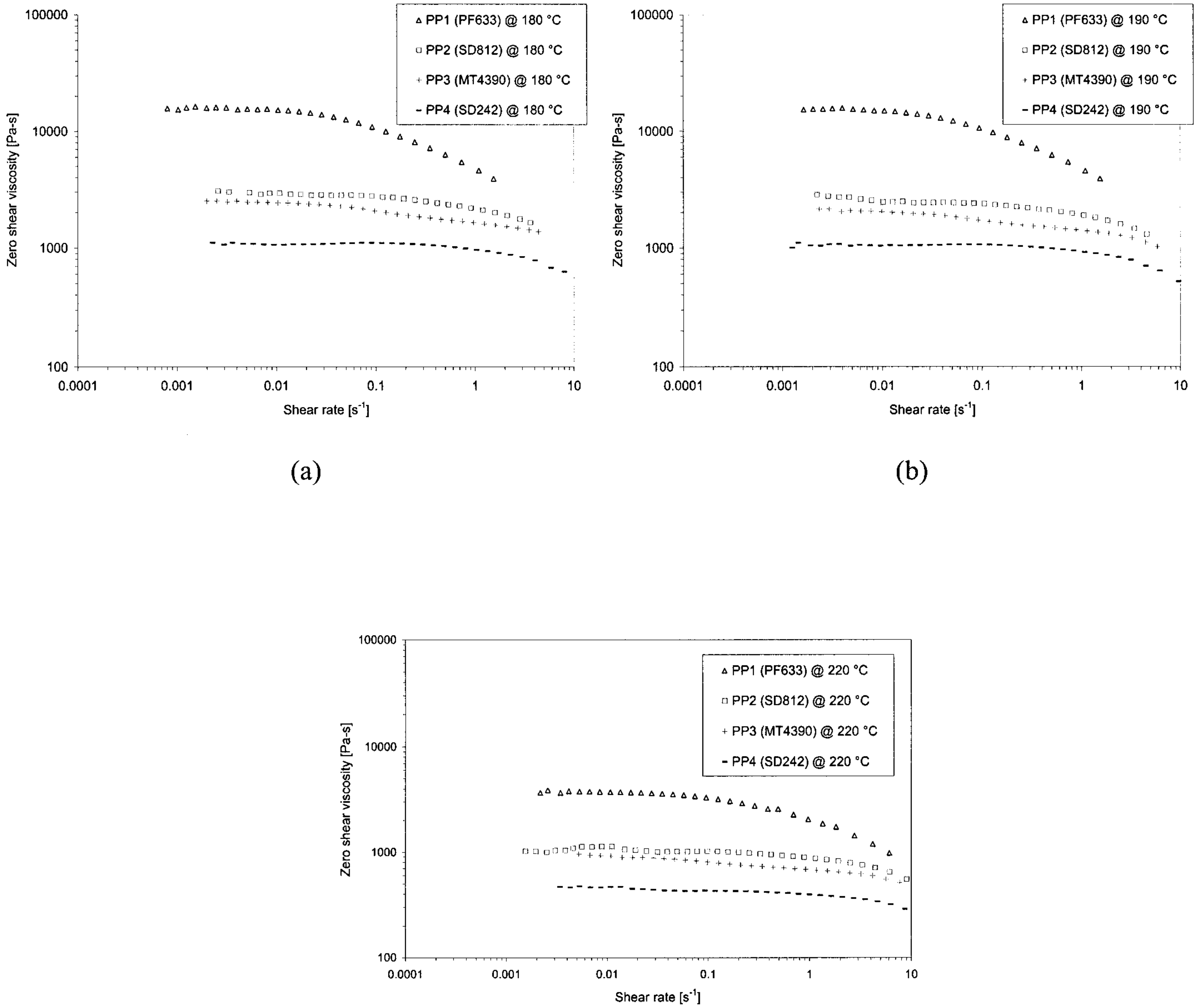

(a)

(b)

(c)

Figure 5.6: Comparison of the effect of shear rate variations on the zero shear viscosity, η_0, of the selected PP resins at various polymer melt temperatures presented in a log-log scale format

(a) Temperature of polymer melt = 180 °C

(b) Temperature of polymer melt = 190 °C

(c) Temperature of polymer melt = 220 °C

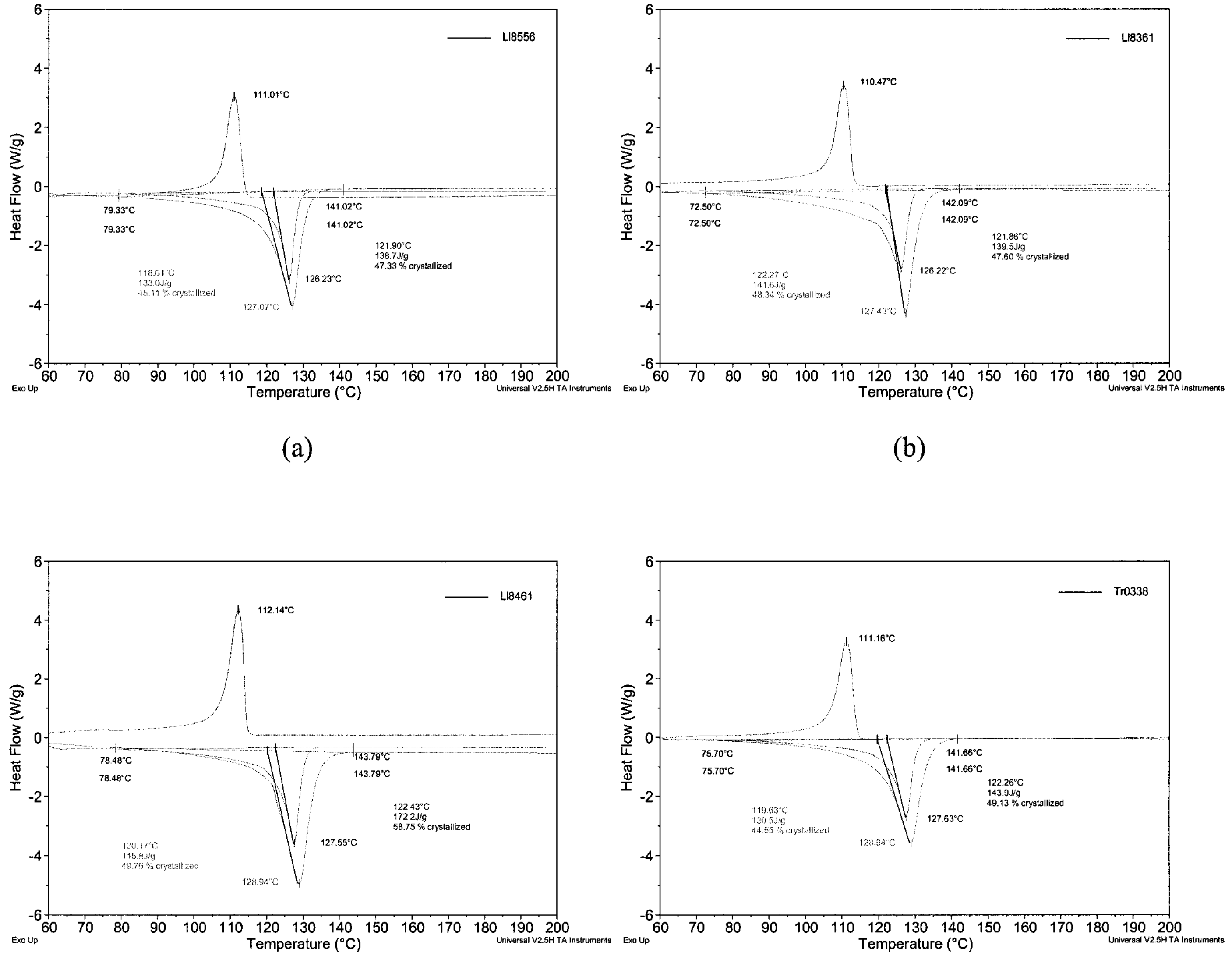

(a) (b)

(c) (d)

Figure 5.7: Comparison of the initial and recristallization transition temperatures and respective degrees of crystallinity of the selected PE grades at 10 [°C/min] heating rate

(a) PE1 (LL8556)

(b) PE2 (LL8361)

(c) PE3 (LL8461)

(d) PE4 (TR0338)

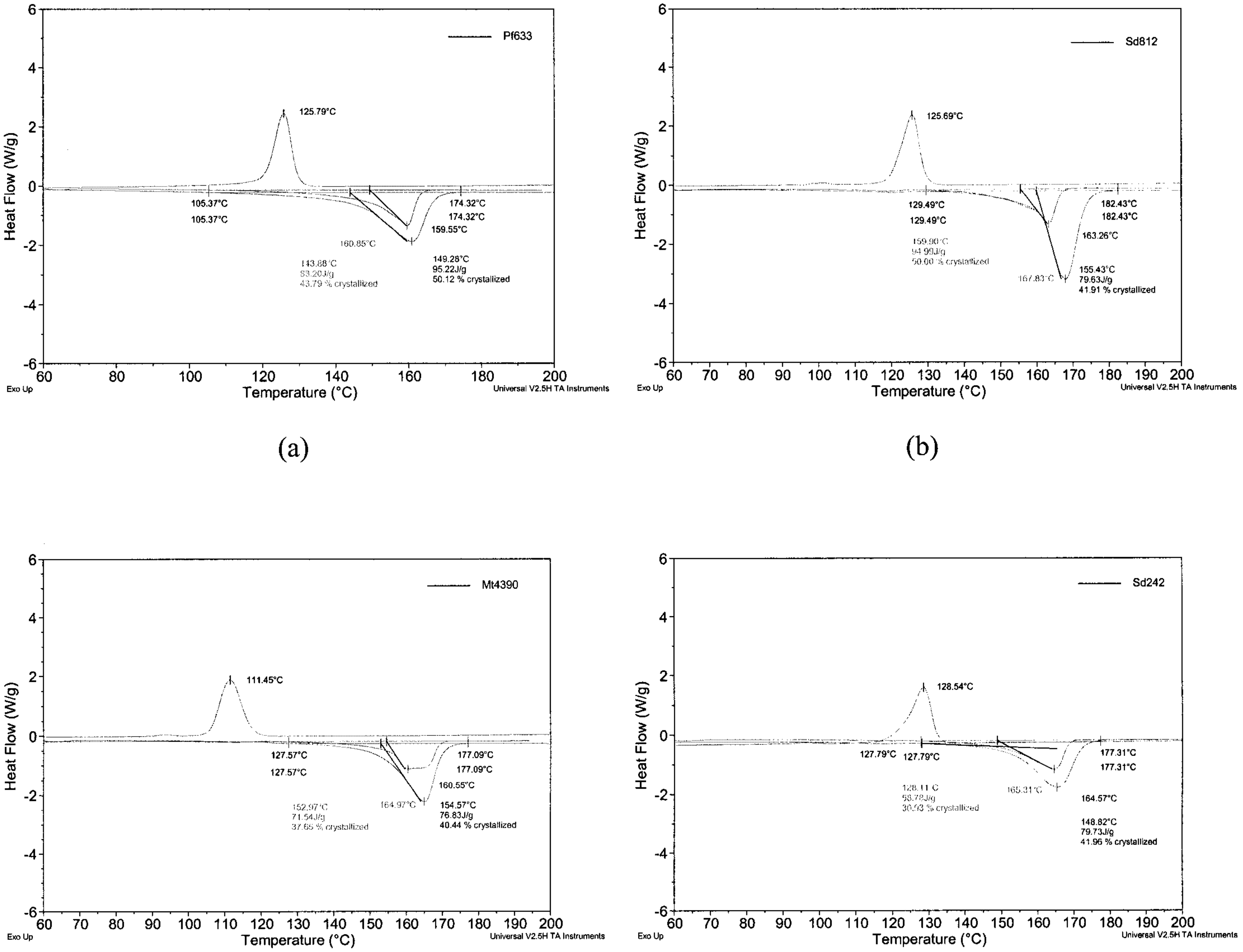

(a)

(b)

(c)

(d)

Figure 5.8: Comparison of the initial and recristallization transition temperatures and respective degrees of crystallinity of the selected PP grades at 10 [°C/min] heating rate

(a) PP1 (PF633)

(b) PP2 (SD812)

(c) PP3 (MT4390)

(d) PP4 (SD242)

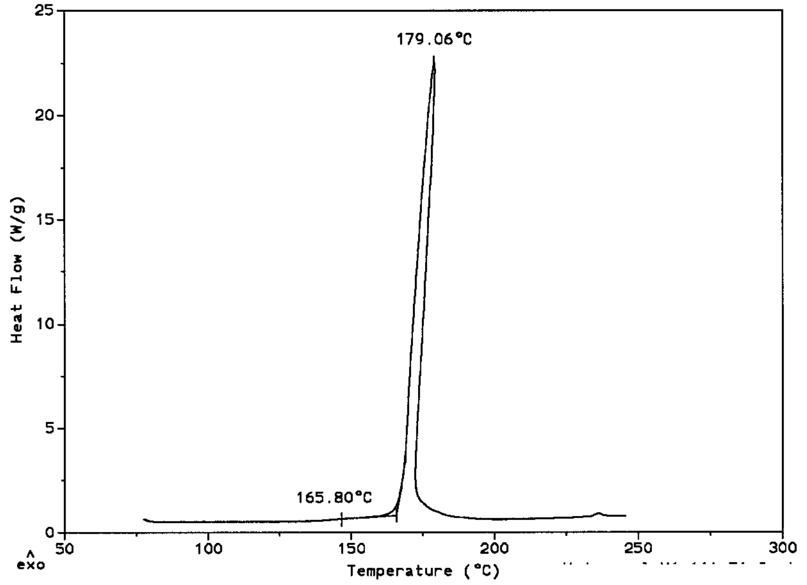

Figure 5.9: Decomposition behavior of Celogen OT at a heating rate of 10 [°C/min]

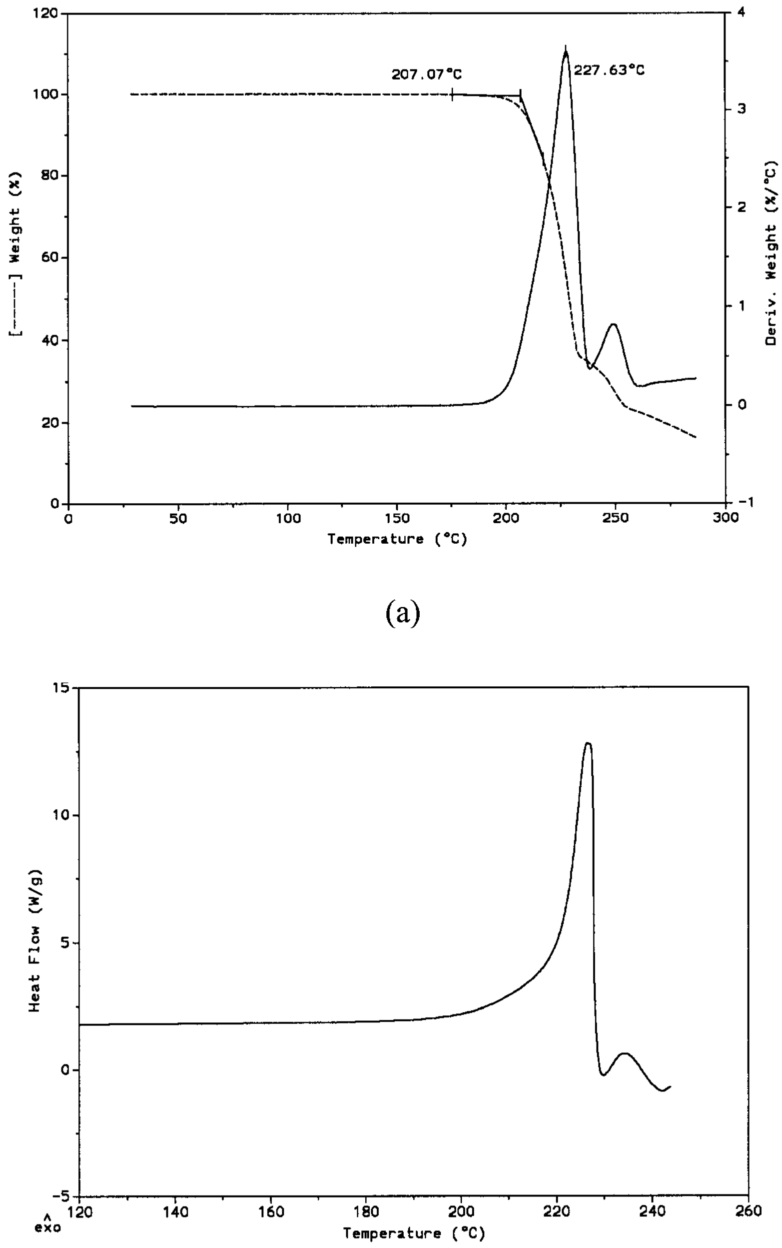

(a)

(b)

Figure 5.10: Decomposition behavior of Celogen AZ at a heating rate of 10 [°C/min]

(a) TGA plot

(b) DSC plot

CHAPTER 6

INVESTIGATION OF ROTOFOAMABILITY OF POLYOLEFINS

6.1 Introduction

The main goal of this chapter is to evaluate the suitability of each of the eight selected polyolefin resins for rotational foam molding operations. Rather than directly dealing with the complexities associated with the simultaneous processing of a dense (non-foamed) outer skin and a lower density (foamed) internal core or layer in rotational foam molding, a fundamental comparative study of the relationship between the rotational foam molding processing variables and polyolefin material parameters versus the resulting cell morphologies of the processed foams was conducted. Thereby, the number of independent processing parameters was maximized and the processing strategies were optimized.

The best suited PE and PP resins for foaming in rotational molding were identified via a specially designed plan for rotational foam molding experiments using a design of experiments software package. The structural parameters of the respectively produced skinless polyolefin foams that occupy the mold to its full volumetric capacity were used as the response for the statistical analysis of experimental results. Although, as described in Section 2.3, for the manufacture of integral-skin cellular polyolefin composites in single-charge rotational foam molding, the foamable resin should be in a pellet form, in order to obtain a broader insight in the rotofoamablity of polyolefin resins, the investigation was conducted using a more comprehensive approach that included both the dry blending and extrusion melt compounding techniques for foamable resin preparation.

The established processing concepts put forward herein have been utilized further in this thesis as a foundation for understanding the fundamental mechanisms governing the manufacture of integral-skin polyolefin foams in single-charge rotational foam molding.

6.2 Fundamental Strategies for Producing Fine-celled Foams

Although the nucleation mechanisms with CBA are not clearly known, it is believed that a strong correlation exists between the achieved degree of CBA dispersion in the polymer matrix during the preparation of the foamable resin and the subsequently obtained quality of the foamed structure [27]. However, even when a higher degree of dispersion of the CBA particles in the polymer matrix is successfully achieved, poor cell morphology can be easily obtained from the final rotationally foam molded products unless appropriate processing strategies are established.

In order to produce foams with a fine-celled structure, three major foaming strategies should be put in place during the rotational foam molding process: (i) induction of a large cell nucleus density, (ii) suppression of cell coalescence, and (iii) promotion of uniform volume expansion.

One of the most critical requirements in processing fine-celled foams is the induction of numerous cell nuclei [198,199]. Unless a large number of cells are nucleated from the outset of the foam processing, foamed products with a fine-celled structure cannot be obtained. In order to achieve a sufficient nucleus density in the low-pressure, compounding based, rotational foam molding process, it is crucial to disperse thoroughly and uniformly the CBA particles throughout the polymer matrix during compounding by intensive mixing. However, it is also crucial to simultaneously prevent the premature decomposition of the heat-sensitive CBA during the compounding operation, i.e., to preserve the well dispersed blowing agent particles throughout the pellets inactivated until needed for the subsequent rotational foam molding operation. In this context, an intermeshing co-rotating twin-screw compounder was used. Its kneading elements can provide a controlled shear input and thereby enable a sufficiently high degree of dispersion of the CBA particles without generating critical temperatures while assuring a precise control of the residence time distribution due to their self-wiping feature [200].

Even if a high cell nucleus density is achieved, this does not guarantee that the final cell density of rotomolded foams will be high: if the cells are coalesced, the initial cell density will be deteriorated. Although cell coalescence is thermodynamically favored because of the lowered free energy via reduction of the surface area of cells [201], it can be effectively suppressed by increasing the polymer melt strength [7]. Since the polymer melt strength decreases with an increase in the temperature [202], the melt temperature during rotational foam molding should be maintained as low as possible in order to minimize the negative effect of the cell coalescence phenomenon.

The distribution of the cell nuclei follows the distribution pattern of the CBA particles throughout the polymer matrix. If the distribution of CBA particles has been uniform, uniform volume expansion should be expected. However, due to the low pressure in rotomolding, the gas evolved from the decomposition of a CBA particle tends to expand rather than dissolving in the polymer melt, unless the amount of generated gas is too small and the internal pressure of bubble becomes high due to the surface tension [167].

6.2.1 Ideal Fine-cell Foaming Model

Considering the strategies presented above, an ideal fine-cell foaming model can be established. Figure 6.1 schematically illustrates this model as a sequence of desired processing steps for yielding fine-celled polyolefin foams in compounding based rotational foam molding. It is based on the assumption that during the compounding operation a uniform distribution of the CBA particles throughout the volume of the foamable pellets has been achieved. It is further assumed that the distribution could be considered uniform if the inter particle distances of the CBA contained in the foamable pellets range between 1 and 50 microns.

After charging the shot size into the mold, it is rotated (Figure 6.1, cycle time $t_0 = 0$) and exposed to elevated temperatures (Figure 6.1, cycle time $t_1 > t_0$) due to which the foamable polyolefin pellets and the air inside the mold, become gradually heated. After a while, the foamable pellets that are closest to the mold's wall begin to sinter first. As the heat propagates towards the center of the mold, it causes the neighboring pellets to sinter until a homogeneous continuous polymer melt pool is formed. In this phase (Figure 6.1, cycle time $t_2 > t_1$), it would be crucially important to complete the formation of a continuous polymer melt prior the onset of CBA decomposition. This would ensure that the amount of escaped blowing gas in the atmosphere is minimized once the CBA starts decomposing, while the number of nuclei will be maximized, thereby yielding foam with a higher cell density and a reduced and more uniform cell size. Thus, it would be desirable to establish such rotational foam molding process control that would assure completion of the sintering of the entire polymer material in the mold prior the decomposition of the CBA commences [52]. This could be accomplished by keeping the temperature of the sintered polymer melt lower than the onset decomposition temperature of the CBA until the sintering of the entire polymer material in the mold is completed. Then, the temperature of the polymer melt should be elevated above the onset decomposition temperature of the CBA to trigger its decomposition at the appropriate point in time (Figure 6.1, cycle time $t_3 > t_2$).

The gases released in the polymer melt due to the decomposition of the CBA initiate the foaming expansion process. The cell-nucleation step occurs simultaneously with the decomposition of the CBA particles, and as a consequence of the evolved gases from the decomposing CBA particles, bubbles begin to appear in the polymer melt. Due to the temperature gradient across the mold, the initiation of polymer foaming occurs first at the internal mold surface and than it extends towards the center of the mold. The cell growth step occurs at cycle time t_4 (Figure 6.1, cycle time $t_4 > t_3$), immediately after cell nucleation. The nucleated cells continue to grow until the dominant CBA gas-generation ability is exhausted, after which, depending of the nature of the liberated gases by the decomposition of the CBA, which determines their solubility and diffusivity characteristics, and the gas concentration gradient between a bubble and the molten non-pressurized polymer and/or the neighboring bubbles, gas diffusion between a bubble and the polymer melt and/or the bubbles themselves takes place and it thereby governs further cell development. Thus, due to gas diffusion in or out of the bubble, some bubbles continue to grow or begin to shrink, respectively.

However, as the temperature of the melt increases, the deteriorating effect of cell coalescence on the cell-population density becomes the major issue of concern. Therefore, a processing strategy that can suppress cell coalescence and thereby retain the expanded foam is what is required in the stabilization step. Essentially, this foam-stabilization strategy is supposed to provide increased stability of the cell wall and reduced drainage of the material from the wall that separates the cells. This is commonly accomplished by increasing the extensional viscosity of the molten polymer in order to increase its melt strength. A high extensional viscosity may be maintained if the temperature of the melt always remains below the point at which cell coalescence actively occurs. The final cell size is determined at the time when, due to the external cooling of the mold, the foamed polymer reaches the crystallization temperature because of which the polymer matrix becomes frozen.

Considering the above description of an ideal fine-cell foaming model, the temperature constraints that should be satisfied in order to establish and maintain the desired sequence of processing steps inside the mold during rotational foam molding (see Figure 6.1) could be conveniently expressed by the relationship given in Equation (6.1).

$$T_{polymer\ sintering} < T_{CBA\ decomposition} < T_{polymer\ melt} < T_{cell\ coalescence} \tag{6.1}$$

6.3 Formulation of Foamable Polyolefin Resins

In order to fill the mold with plastic foam to its full extent in a rotational foam molding operation, the concentration of the CBA in the foamable polymer/CBA mixture has to be commensurate to the desired (or required) magnitude of volumetric expansion of the material charged into the mold with respect to the volume of the mold. This parameter is referred to as the volume expansion ratio (VER) [38].

Thus, for formulating appropriately the foamble resin for achieving a given VER in rotational foam molding an appropriate relationship between the amount of CBA participating in the foamable mixture, the shot size, the volume of the mold, and the required VER has to be developed. By definition, the VER of plastic foams in rotational foam molding is defined as the ratio between the expanded volume of the foam V_{foam} and the initial volume of the solid unfoamed plastic material V_i as given in Equation (6.2) [38].

$$(VER) = \frac{V_{foam}}{V_i} \tag{6.2}$$

Since in the present study the produced plastic foam is supposed to occupy the entire free volume of the mold, the volume of the expanded foam V_{foam} will be identical to the volume of the mold used V_{mold}.

6.3.1 Calculation of CBA Amount

The most important criteria for CBA selection include its decomposition temperature, rate of gas release, gaseous composition, ease of dispersion, storage stability, toxicity, and cost [3]. However, the most important CBA properties that require special attention include the temperature at which the expanding gas is liberated, the initial temperature of decomposition, the temperature range of the maximum rate of decomposition, the gas yield (volume of gas, in cm^3, liberated by the transformation of 1 g of CBA per unit time, usually 1 min, at the temperature of maximum gas liberation), the rate and kinetics of the liberation of gas, and the pressure developed by the gas [37].

Equation (6.3) provides the formula for calculating the percentage by weight of the selected CBA relative to the weight of the polymer resin that should be introduced in the foamable mixture in order to obtain a given VER during subsequent foaming. A detailed derivation procedure for obtaining Equation (6.3) is presented in greater detail elsewhere [38].

$$\%CBA = 100\frac{(VER) - 1}{\rho_{polymer} \cdot \varphi} \tag{6.3}$$

It is important to note here that Equation (6.3) involves the VER, the density of the polymer and the gas yield of the selected CBA. However, the data describing the gas yield of CBAs, φ, provided by the suppliers are referred to room temperature conditions, while the decomposition of CBAs and thereby the expansion of polymeric foams occurs at elevated temperatures that are beyond the polymer melting temperature. As a result, during the cooling stage of the rotational foam molding process, the decreasing temperature will gradually reduce the maximum possible gas volume. Since the polymer freezing will be initiated at the onset crystallization temperature, and since the polymer will be ultimately frozen at the crystallization peak temperature, the structure of the foam will be fixed at this temperature. This indicates that the occupied gas volume at the crystallization temperature determines the void fraction of the foam [38]. Thus, the volume of the generated gas by the decomposition of the CBA at this high temperature will be significantly larger than the volume of the same gas at room temperature. Therefore, prior to introducing the gas yield data φ in Equation (6.3), the data for the gas yield provided by the manufacturer φ_{STP} should be corrected to their corresponding values at crystallization temperature by using Equation (6.4).

$$\varphi = \varphi_{STP} \times \frac{V_C}{V_{room}} = \varphi_{STP} \times \frac{T_C}{T_{room}} \tag{6.4}$$

In Equation (6.4), V_{room}, V_C, T_{room}, and T_C refer to the gas volume at room and crystallization temperature, and absolute room and crystallization temperature, respectively.

6.3.2 Calculation of Shot Size

The room temperature is 25 °C, or 298 K. If assuming an average value of 114°C for the crystallization temperature of PE resins, the absolute crystallization temperature becomes 387 K. Therefore, for the 80 [cm^3] mold that is used for rotational foam molding experiments, by implementing Equation (6.4) and than Equation (6.3), the necessary amount of Celogen OT for a given VER of PE resins can be calculated. Since the present experimentation is intended to include 3-fold and 6-fold expansion experiments, the calculated Celogen OT amount needed for 3-fold expansion of PE resins (VER=3) is 1.32%(wt), while for 6-fold expansion (VER=6) it is 3.31%(wt). The calculated shot size is 24.8 g for (VER=3) and 12.4 g for (VER=6).

Similarly, if using 138°C as the approximate crystallization temperature of PP resins, the absolute crystallization temperature becomes 411 K. Thus, for the 80 [cm^3] mold the necessary amount of CBA for a given VER for PP resins can be calculated. Thus, the calculated Celogen AZ amount needed for 3-fold expansion (VER=3) is 0.73%(wt), while for 6-fold expansion (VER=6) it is 1.83%(wt). The calculated shot size is 24 g for (VER=3) and 12 g for (VER=6).

6.4 Structure Characterization of Rotomolded Foams

Conventional foam characterization procedures include parameters such as volume expansion ratio, void fraction, foam density, cell population density, and cell size to represent the final state of foams when the cell size distribution is assumed uniform. However, for rotationally molded foams, this conventional way of foam characterization does not seem to be the best since the expansion ratio (and the void fraction/foam density) of the fully expanded rotomolded foams is fixed at the time of determining the content of polymers and CBA and the size of the mold. Although the actually rotationally molded foam samples indicated that the cell size distribution was not uniform, a uniform cell size distribution was assumed in order to employ common structure parameters such as the cell-population density and average cell size.

The cell population density per unit volume with respect to the original unfoamed polymer N was determined for each foamed sample using a magnified image of the fracture surface of the samples and by using the following equation [203]:

$$N = (n_{cells})^{3/2} \cdot VER \qquad (6.5)$$

where n_{cells} is the number of cells contained in a consistently located (1cm × 1cm) square in the image, respectively. From Equation (6.5) the average cell size $D_{average}$, regardless of the density of the foam, can be determined from the expression given in Equation (6.6) [204].

$$D_{average} = \sqrt[3]{\left[(VER-1)\cdot\frac{6}{\pi \cdot N}\right]} \qquad (6.6)$$

However, using the cell size as a structural parameter in the characterization of plastic foams should be considered with caution. It is very difficult to accurately determine the cell size using a 2D image of the fractural foam surface because the image may not indicate the actual size of the bubble. In addition, the cell size is a dependent parameter and as such it cannot solely determine the structural properties of the foam. Taking this into consideration, additional structural parameters for describing fully expanded foams in rotational foam molding, such as the "nominal" cell size distribution and "nominal" average cell size $D_{no\min al}$ could be used. Thus, unlike the average cell size calculated using Equation (6.6) that refers to a unit volume of the foam, the "nominal" average cell size is calculated with respect to a unit area of the fractured foam surface. Consequently, for equivalent rotationally molded foam samples, the "nominal" average cell size takes smaller values than the average cell size.

6.5 Variables in Rotational Foam Molding

Two principal independent sets of variables govern the single-charge rotational foam molding process: pre-processing and processing.

The set of pre-processing variables comprises the relevant physical and rheological properties pertaining to the participating polymer resins (both foamable and non-foamable) that may be deliberately designed, imparted, selected, altered, or controlled exclusively "offline", i.e., prior to actually subjecting the resins to the rotational foam molding process. This group includes but is not limited to variables related to resin properties such as particle size, density, melting point, degree of crystallinity, heat capacity, heat of fusion, while the latter includes the MFI, zero shear viscosity, melt strength, storage modulus, loss modulus, $\tan\delta$, etc.. Since these variables are controllable only during the preparation stage of the process, they represent a fixed input for the rotational foam molding process.

The set of processing variables consists of the process parameters that may be varied exclusively "online", i.e., after the mold is charged and the processing cycle has commenced. This set of variables includes: (i) oven temperature, (ii) processing time (heating and cooling), (iii) ratio (for biaxial usually 8:2 or 0.13 Hz and 0.03 Hz), and speed of mold rotation (4-20 rpm or 0.07-0.33 Hz) [24], and (v) the cooling media (water, air, or both) and rate of cooling. When the oven temperature is kept at a constant level during the entire heating segment, the heating time becomes the principal processing parameter.

6.6 Investigation of Rotofoamability of PE Resins

6.6.1 Problem Statement

In the early stage of rotational foam molding, because of the entrapped air between the powder particles, air bubbles appear throughout the polymer melt. The larger the powder particle sizes, the smaller population of air bubbles with a larger magnitude will be formed. Such a low number of large-sized air bubbles will act as cell nuclei in the later course of the rotational foam molding process [27,205]. Thus, the large size, the low density, and the uneven distribution of these bubbles would eventually result in foams having cell morphology with similar attributes that would be outside the desired fine-cell foam range [27].

In this context, previously conducted research [29,41,205], revealed that in comparison with the melt compounding based method the production of fine-celled PE foams by using the dry blending based rotational foam molding method has some inherent limits. Namely, the mixing degree of the plastic and the CBA in dry blending is limited by the quality of the plastic powder obtained by the pulverization of the basic resin. The powder properties that have the strongest limiting effect on the achievable degree of mixing and that can lead towards achieving a poor dispersion of CBA particles throughout polymer powders in dry blending include the average particle size, the particle size distribution, and the particle shape.

The consistence of the powder quality is affected by both the immediate grinding process conditions and the rate at which the powder is cooled after grinding [206]. Wrong grinding parameters can cause powder particles to be torn and shredded resulting in irregular shapes. Then, small fibrils, as shown in Figure 6.2, resembling as "tails" attached to the surface of the particles can appear. These tails obstruct the freedom of flow of the particles during dry blending [205]. Heating can reduce the presence of these fibrils, since holding the powder at a high temperature would allow the remaining fibrils sufficient time to relax back into the particles, whereas high cooling rates result in "freezing" the stretched fibrils in place preventing them from recoiling back into the particle [206].

6.6.2 Design of Experiments

Table 6.1 summarizes the formulations of sixteen PE-based foamable resins that were prepared for subsequent rotational foam molding experimentation intended for investigating the rotofoamability of the selected PE grades. Namely, these foamable resins consisted of a group of eight dry blended and a group eight melt compounded resins each of which included a 3-fold and a 6-fold expansion foamable resin from each of the four selected PE grades.

The CARD® PRO software package has been used to design the experimental plan for identifying the suitability of the PE resins for rotational foam molding operations. Table 6.2 presents the settings of the six independent process variables that have been considered as most relevant for the final cell morphology of the rotationally molded foam supplied to the software package in order to design the experimental matrix. These included: (i) the type of PE resin, which was represented by the respective MFI, (ii) the VER of the foamable composition, which could be 3 or 6, (iii) the mold heating time, which was selected to be in the range between 9 and 17 minutes, (iv) the mold cooling time, which was selected to be in the range between 20 and 25 minutes, (v) the mold rotation speed, which could be varied in the range between 10 and 15 rpm, and (vi) the preparation method for the foamable resin, which has been indicated by using the symbol 1 or 2 for melt compounded or dry blending, respectively. It is important to note here that since the melt strength of PE resins is not affected much by elevated temperatures, in order to reduce the number of necessary experiments, a uniform oven temperature of 300 °C has been used for all conducted PE foaming experiments.

Considering the research goal, type of variables, and the way they have been defined, a "Model-Robust Process" design type accompanied with a "Optimization" design sub-type has been selected as the most suitable to be implemented. This design type correctly addresses complex experiment design regions resulting from the presence of discrete variables, non-numeric (categorical) variables, and/or multiple constraints. As a result, an experiment plan consisting of a battery of 42 experimental samples with randomized variable values has been proposed by the software. Its matrix is presented in Table 6.3.

6.6.3 Experimental Procedure

The previously prepared dry blended and melt compounded foamable PE resins (Table 6.1) and the conventional uni-axial rotomolding machine and mold described in Section 4.4.2.1 (Figure 4.7), were used to conduct the designed battery of 42 rotational foam molding experiments. They were executed based on the prescribed variable values determined by the experimental matrix plan (Table 6.3). Three rotationally foamed foam samples have been prepared from each combination of variables given by the experimental plan.

The average cell size of the experimentally produced foam samples, D, as defined in Section 6.4, was selected to be the measured response for this experimental study because it is a parameter against which the evaluation of the foam quality could be carried out regardless of the density of the foam. Each of the resulting 126 (42 × 3) rotationally molded foam samples was characterized in terms of average cell size by following the procedure described in Section 6.4 while considering a consistently located fractured foam surface with respect with the length of the sample. Thereby, the matrix of responses, $D_{average}$, as shown in Table 6.4, has been created and entered into the software package for statistical analysis.

6.6.4 Statistical Analysis

Using the CARD® Analysis software package, a regression Analysis of Variance (ANOVA) has been carried out using the experimental design plan and the respective three sets of experimental responses.

Within the model term ranking Pareto Chart, the mold heating time was ranked as the variable with the highest statistical significance for the quality of the produced PE cellular morphologies. In addition, the combination of the mold heating time and the type of PE resin was ranked as the second statistically significant variable, while the combination of the mold heating time and the method used for preparation of foamable resins (dry blending or melt compounding) was ranked at the third place.

A model for calculating the average cell size of the produced PE foams involving the 6 selected variables has been established. The model was optimized for minimum response (average sell size). The optimizer suggested using a melt compounded PE1-based foamable composition for 3-fold expansion (PE1MC3) in order to obtain a minimum predicted cell size of 186.06 [μm] (Lower 2σ confidence limit = 73.02; Upper 2σ confidence limit = 299.01). According to the model prediction, for achieving this minimum predicted response at an oven temperature of 300 °C, it would be necessary to implement the following processing strategy: a mold heating time of 14.30 [min], a mold cooling time of 21.86 [min], and a mold rotation speed of 10 [rpm].

Based on the results of the regression ANOVA statistics, Table 6.5 summarizes the predicted heating times, cell densities, and average cell sizes, for all types of PE-based foamable resins, respectively.

The statistical analysis of the experimental results revealed that the melt compounding based technology is well suited for producing fine and very uniform PE foams in rotational foam molding. The effects of the preparation method on the cell population density and average cell size of the produced PE foams are presented graphically in Figures 6.3 and 6.4, respectively. These graphs indicate that the melt compounding based method is superior in terms of delivering PE foams with increased cell population densities, reduced average cell sizes, and uniform cell size distribution.

6.6.5 Summary

The main benefit of the melt compounding technique is the thorough and uniform dispersion of the CBA into the PE matrix, which cannot be achieved by using the dry-blending technique. Another benefit is the reduced sensitivity on powder quality inconsistencies. Since the pre-mixed blend is being remelted, remixed, and reshaped into pellets during compounding, the negative effects that might have been caused by the inconsistencies in powder quality in terms of particle size and shape are thereby being removed.

The experimental results revealed that among the four investigated PE grades, for all investigated foamable materials and experimental conditions, both dry blended and melt compounded PE1 based foamable compositions with Celogen OT demonstrated superior rotofoamability and preferred cell morphologies in both 6-fold and 3-fold expanded foams. Therefore, this PE resin (LL8556) has been selected for conducting further experimental studies related to the manufacture of integral skin PE-based cellular composites.

6.7 Investigation of Rotofoamability of PP Resins

6.7.1 Problem Statement

In rotational foam molding, as a result of the unavoidable thermal gradient that is created across the polymer melt, the temperature at the interface of the melt with the internal surface of the mold is the highest. As such, this temperature locally governs the cell morphology of the foams processed in rotational molding. If it is too high, it promotes either premature decomposition of the CBA with respect to the point of completion of the sintering of the foamable pellets, or severe cell coalescence. Which of these adverse outcomes will have a predominant effect on the final cell morphology of the produced foams greatly depends on the sintering behavior and the melt strength characteristics of the basic carrier polymeric grade participating in the foamable composition. Since the time required for completion of polymer coalescence controls the major part of the heating time in the molding cycle, pellet sintering is considered as the fundamental phenomenon in rotational foam molding [38,49].

In conventional rotational molding, polymer sintering is commonly described as the formation of a homogeneous melt from the coalescence of powder particles under the action of surface tension [144], whereas in compounding-based rotational foam molding of skinless foams it comprises the formation of a homogeneous melt from the coalescence of the pre-compounded foamable pellets caused to bond together by heating. However, in compounding based rotational foam molding, the task of ensuring that the sintering of the polymer always completes prior to the activation of the CBA dispersed within the foamable pellets is further aggravated by the longer time required for the completion of the coalescence (sintering) of the pellets than it would be if dry blended foamable powders have been used [90]. Such an order of thermal events leads to a premature decomposition of the CBA dispersed in the still non-sintered pellets thereby allowing a portion of the generated gases to be inevitably lost by escaping out of the pellets while the pellets are expanding. The resulting lack of blowing gas availability for carrying out the foaming process deteriorates cell morphology of the final foam and causes incomplete volume expansion. This is, therefore, considered as the fundamental problem of the compounding-based rotational foam molding technology.

The above processing anomaly is especially encountered when processing PP foams in rotational foam molding [38]. This was particularly pronounced when a CBA activator such as ZnO is included in the foamable formulation [207].

6.7.2 Highlights From Previous Research on PP Foams

It has been concluded from previously conducted research [38,40,118,207] that producing PP foams with satisfactory cell morphologies in rotational foam molding is feasible. However, the narrow interval between the melting temperature of PP and the onset decomposition temperature of the applicable CBA as well as the relatively low melt strength of PP at elevated temperatures are considered as the greatest obstacles in processing PP foams.

Experimental results revealed that the morphology of the foams obtained by processing PP pellets that have been pre-compounded with a CBA could be governed by either pellet sintering or cell coalescence. The viscosity of the basic PP resin and the processing temperature determine which of these two key factors will assume a predominating influence towards the foaming process. The influence of the VER of the foam is also important because it determines the CBA amount participating in the formulation of the foamable pellet and the shot weight. The foaming process of pre-compounded PP pellets based on high-viscosity resins (PP1 and PP2) was governed by sintering. It was characterized by a premature decomposition of the CBA with respect to the point of completion of PP pellet sintering. In contrast, the foaming process of low-viscosity PP resins (PP3 and PP4) was governed by cell coalescence. Good timing of the completion of PP pellet sintering (occurring prior to the decomposition of the CBA) and severe cell coalescence at long processing times characterized these foams. If sintering is dominant, the primary strategy for obtaining a desired sequence of events inside the mold during the molding cycle and thereby preventing the loss of blowing gasses should include reducing the pellet size. Additional measures may include decreasing (or eliminating) the CBA activator amount and/or lowering the heating rate. However, if cell coalescence is dominant, reducing the oven temperature works well as a cell-coalescence suppressing strategy. In addition, the effects of cell coalescence could be reduced by using branched PP grades and/or introducing a CBA activator (or increasing its amount if already introduced) during compounding. Both high- and low-viscosity 3-fold and 6-fold melt compounding-based expanded PP foams with improved cell morphologies have been produced by implementing these remedial processing strategies.

6.7.3 Design of Experiments

Each of the four PP-based polymer materials selected for experimentation was used for preparing four kinds of foamable compositions: two dry blended and two melt compounded respectively formulated foamable compositions, of which one for 3-fold and one for 6-fold expansion, respectively. Table 6.6 presents the assigned codes and the formulations of these sixteen foamable resins that were prepared for the rotational foam molding experimental study focused on investigating the rotofoamability of the selected PP grades.

A randomized experimental plan for identifying the suitability of the PP resins for rotational foam molding operations has been designed using the CARD® PRO software package for design and analysis of experiments. Table 6.7 presents seven independent process variables that have been considered as the most relevant for the quality of the cell morphology of rotationally molded PP foams. These independent variable settings are the prerequisite input data the CARD® Design software needs to have to be able to design the experimental plan matrix. Since PP resins are so sensitive to elevated temperatures in terms of melt strength, which makes them susceptible to cell coalescence during foaming, unlike the case of the investigation of rotofoamability of PE resins, the oven temperature becomes a significant factor for foaming PP, and thus, it has to be seriously considered when investigating the rotofoamability of PP grades. Hence, the list of independent variables for investigating the rotofoamability of PP grades included: (i) the type of PP resin, which was represented by the respective MFR, (ii) the VER of the foamable composition, which could be 3 or 6, (iii) the oven temperature, which was set to take values in the range between 250 and 300 °C, (iv) the mold heating time, which was selected to be in the range between 14 and 22 minutes, (v) the mold cooling time, which was selected to be in the range between 20 and 25 minutes, (vi) the mold rotation speed, which could be varied in the range between 10 and 15 rpm, and (vii) the preparation method for the foamable resin, which has been indicated by using the symbol 1 or 2 corresponding to melt compounding or dry blending, respectively.

For similar reasons as in the case of PE resins, a "Model-Robust Process" design type and an "Optimization" design sub-type has been selected as the most suitable for the investigation of rotofoamability of PP resins. Table 6.8 presents the resulting experiment plan matrix proposed by the software consisting of a battery of 51 experimental samples with randomized variable values.

6.7.4 Experimental Procedure

A similar procedure to that implemented during the investigation of rotofoamability of PE resins was used in the present case involving PP resins. The dry blended and melt compounded foamable PP resins (Table 6.6) were used for conducting rotational foam molding experiments using the conventional uni-axial rotomolding machine and mold described in Section 4.4.2.1 (Figure 4.7). The designed battery of 51 rotational foam molding experiments was executed based on the prescribed independent variable values determined by the experimental matrix plan (Table 6.8).

From each combination of variables given by the experimental plan three rotationally foamed foam samples have been prepared. Each of the resulting 153 (51 × 3) experimental samples was characterized in terms of average cell size by following the procedure described in Section 6.4 while considering a consistently located fractured foam surface with respect with the length of the sample. Thereby, the matrix of responses, D, as shown in Table 6.9, has been created and entered into the software package for statistical analysis.

6.7.5 Statistical Analysis

A regression Analysis of Variance (ANOVA) has been carried out using the the CARD® Analysis software package and the experimental design plan matrix including the respective three sets of measured experimental responses.

The model term ranking Pareto Chart ranked the type of PP resin as the variable with the highest statistical significance for the resulting quality of cellular structure. It was followed by the mold heating time.

A model for calculating the average cell size of the produced PP foams involving the 7 selected independent variables has been established. The model was optimized for minimum response (average sell size). The optimizer suggested using a melt compounded PP1 based foamable composition for 3-fold expansion (PP1MC3) in order to obtain a minimum predicted cell size of 679.05 [μm] (Lower 2σ confidence limit = 610.00; Upper 2σ confidence limit = 765.73). According to the model prediction, this minimum predicted response could be achieved if the following processing strategy would be put in place: oven temperature of 300 °C, mold heating time of 20.49 [min], mold cooling time of 25 [min], and mold rotation of 10 [rpm].

On the basis of the results of the regression ANOVA statistics, Table 6.10 summarizes the predicted oven temperatures, heating times, cell densities, and average cell sizes, for all types of PP-based foamable resins (at t_{cool} = 22.5 [min], and Mold rot. = 12.5 [rpm]), respectively. As expected, these results indicated that despite the increased heating times, in most cases, using a lower oven temperature of 250 °C would be more favorable for achieving acceptable cell morphologies when foaming PP resins. This is especially valid when using dry blended pulverized foamable PP resins or low-viscosity, especially 6-fold, pre-compounded foamable PP pellets [118]. This findings could be attributed to the fact that dry blended foamable PP blends are easier to melt due to their increased surface area in comparison with pre-compounded foamable PP pellets, while low-viscosity PP grades demonstrate a better sintering behavior compared to high-viscosity ones, which ensures that the sintering of the polymer is completed prior to de onset of decomposition of the CBA, thereby minimizing gas losses and achieving cellular structures of a better quality. On the other hand, a lower oven temperature reduces the deteriorating effects of cell calescence on the cell morphology of PP foams, which is one of the main drawbacks for successful foaming of PP due to the low melt strength of PP at elevated temperatures.

The effects of the foamble resin preparation method on the cell population density and average cell size of the produced PP foams are presented graphically in Figures 6.5 and 6.6, respectively. As expected, these graphs indicate that PP foams in rotational foam molding achieve significantly lower cell densities and larger average cell sizes in comparison with respective PE foams. In addition, these graphs also revealed that, unlike PE foams, the dry blending based technology is almost equally (PP1) or better (PP2, PP3, and PP4) suited than the melt compounding based technology to the production of PP foams in rotational foam molding. The reasons for this are twofold.

First, suppressing CBA pre-decomposition while compounding PP resins with Celogen AZ represents a serious processing challenge [38], which, if unresolved, causes initial losses of blowing gas in the unused foamable pellets. The relative closeness of the melting point of a PP resin (~ 165 to 175 °C for PP homopolymers and ~ 150 to 175 °C for PP copolymers) [15] to the onset decomposition temperature of Celogen AZ (~205-215 °C) [188] is the principal cause for this problem. Namely, such a narrow theoretical interval (~30 °C) between the critical temperatures that the PP melt is supposed to have to assure decomposition-free compounding of PP resins with Celogen AZ in practice seldom provides a sufficient processing window for conducting the compounding operation without activating the CBA. The reasons for this mostly lie in the fact that the rotating action of the screws in the compounder causes shear stresses throughout the polymer and thereby generates additional heat throughout the PP melt, which is further increased by the friction of the polymer against the barrel, and thus shrinks the processing temperature gap. In addition, a long residence time in the compounder may cause the CBA to prematurely decompose. Since the rotation rate of the plasticating screws is the only parameter that can control these two variables, the pre-decomposition control of the compounding is coupled and since the shear and residence time cannot be controlled independently. Therefore, an optimal range of screw revolutions capable of simultaneously satisfying both the shear stress and residence time constraints has to be established. If such an optimum cannot be determined, it would be very difficult to compound decomposition-free PP foamable resins. This indicates that even before reaching the foaming stage, the melt compounded PP foamable resins might have already inevitably lost a portion of their blowing ability during the act of melt compounding.

Second, the sintering behavior of high-viscosity PP foamable compositions (especially if the pellet size is inadequately large) is such that the CBA usually prematurely decomposes even before the completion of PP polymer sintering thereby causing additional gas losses during pellet processing. Although, the sintering behavior of low-viscosity PP compositions is favorable for foaming operations, however low-viscosity resins demonstrate a very low melt strength at elevated temperatures which makes them susceptible to cell coalescence [38,118].

As a result, although the initial dispersion of the CBA particles throughout the pre-compounded PP pellets might have been much better than what is achievable in a dry blended foamable PP blend, the final cellular structure of rotationally foam molded PP foams could be often deteriorated by the excessive blowing gas losses caused during compounding or during the polymer sintering stage in rotational foam molding or by severe cell coalescence at advanced stages of the rotational molding process involving highly elevated temperatures.

6.7.6 Summary

Successful foaming of PP in rotational foam molding can only be performed over a very narrow range of melt temperatures that are close to the melting point of the polymer and by using PP grades belonging to a limited range of MFR [38,118].

If either the temperature of the melt or the MFR of the resin is too low, the foamable polymer pellets will be softened but not fully sintered during the decomposition of the CBA so that large losses of the liberated blowing gas to the atmosphere will be incurred, and thus a poor cellular morphology will be obtained [38,118].

If either the temperature of the melt or the MFR of the resin are too high, as the nucleated bubbles grow, a further increase of the temperature of the melt will result in cell coalescence because the cell walls will loose their dimensional stability due to the excessive amount of polymer flow downward under the effect of gravity which causes polymer drainage in the cell wall and thereby critically reduces the thickness of the wall, eventually resulting in bubble rupture [38,118].

In particular, the presented experimental results involving the foamable resins based on the four selected PP grades revealed a significant advantage in the cell morphologies of the foams obtained by processing PP1-based foamable compositions. The processing of dry blended foamable compositions based on PP1 provided cell morphologies with satisfactory quality for both 6-fold and 3-fold expansion, while PP1-based foams made of melt compounded foamable resins reached a satisfactory cell morphology and adequate expansion uniformity while achieving an average cell size in the range between 700 and 740 [μm].

Desirable PP foam structures in compounding based rotational foam molding could be obtained only if pellet sintering takes place prior to the decomposition of the CBA and if the processing temperature during the foaming process is kept lower than the temperature of cell coalescence. This could be attributed to the higher melt strength of PP1 due to its branched molecular structure and the highest viscosity, i.e., lowest MFR (5.5 [g/10min]), among the investigated PP grades. Since PP1 (PF633) demonstrated a better rotofoamability and the best cell morphologies among the four investigated PP grades, this resin was selected to participate in the subsequent experimental work involving the manufacture of integral skin PP-based cellular composites.

Table 6.1: PE-based foamable resins prepared for the investigation of rotofoamability of PE

#	Assigned code		Foamable PE-based formulation	VER
	Dry blended	Melt compounded		
1	PE1DB3	PE1MC3	PE1 + 1.32%(wt) Celogen OT	3
2	PE1DB6	PE1MC6	PE1 + 3.31%(wt) Celogen OT	6
3	PE2DB3	PE2MC3	PE2 + 1.32%(wt) Celogen OT	3
4	PE2DB6	PE2MC6	PE2 + 3.31%(wt) Celogen OT	6
5	PE3DB3	PE3MC3	PE3 + 1.32%(wt) Celogen OT	3
6	PE3DB6	PE3MC6	PE3 + 3.31%(wt) Celogen OT	6
7	PE4DB3	PE4MC3	PE4 + 1.32%(wt) Celogen OT	3
8	PE4DB6	PE4MC6	PE4 + 3.31%(wt) Celogen OT	6

Table 6.2: Independent variable settings for investigating the rotofoamability of PE resins

#	Variable name	Variable symbol	Variable units	Range/ Level(s)
1	PE resin (PE1, PE2, PE3, or PE4)	PE MFI	[g/10min]	6.8; 5.2; 3.3; 3.5
2	VER of the PE foamable formulation	VER		3; 6
3	Mold heating time	t_{heat}	[min]	$9 \leq t_{heat} \leq 17$
4	Mold cooling time	t_{cool}	[min]	$20 \leq t_{cool} \leq 25$
5	Mold rotation speed	Mold rot.	[rpm]	$10 \leq$ Mold rot ≤ 15
6	Melt compounded or dry blended	MC or DB		1;2

Table 6.3: Experimental plan matrix for rotofoamability of PE resins

Sample #	PE MFI [g/10min]	VER	t_{heat} [min]	t_{cool} [min]	Mold rot. [rpm]	MC or DB
1	6.8	6	17	25.00	15.00	1
2	3.3	6	17	25.00	10.00	2
3	5.2	3	11	21.25	13.75	2
4	3.3	3	9	20.00	15.00	2
5	5.2	6	9	22.50	10.00	1
6	5.2	3	13	20.00	10.00	1
7	3.3	6	13	20.00	10.00	1
8	6.8	3	13	25.00	10.00	1
9	6.8	6	9	22.50	15.00	2
10	3.3	3	13	25.00	15.00	2
11	5.2	3	9	25.00	15.00	1
12	3.3	3	13	22.50	10.00	2
13	3.3	6	17	20.00	15.00	2
14	5.2	3	15	23.75	13.75	2
15	3.3	6	13	25.00	10.00	1
16	6.8	6	9	25.00	10.00	2
17	5.2	3	11	21.25	11.25	2
18	3.3	6	13	22.50	15.00	1
19	3.3	3	9	20.00	10.00	1
20	6.8	3	13	20.00	15.00	1
21	5.2	6	13	22.50	12.50	1
22	6.8	6	9	25.00	15.00	1
23	3.3	6	17	20.00	15.00	2
24	6.8	3	17	20.00	15.00	1
25	5.2	6	9	22.50	10.00	1
26	5.2	6	13	22.50	12.50	2
27	6.8	3	9	20.00	10.00	1
28	5.2	6	17	22.50	12.50	1
29	5.2	3	15	21.25	11.25	2
30	5.2	6	13	22.50	12.50	1
31	6.8	6	9	25.00	10.00	2
32	5.2	3	15	21.25	13.75	2
33	6.8	6	17	20.00	10.00	1
34	3.3	6	9	20.00	15.00	1
35	3.3	6	9	25.00	10.00	2
36	5.2	3	9	25.00	10.00	2
37	3.5	6	11	21.25	11.25	2
38	3.5	3	11	23.75	11.25	1
39	6.8	6	9	20.00	10.00	2
40	6.8	3	17	25.00	10.00	2
41	6.8	6	9	22.50	15.00	2
42	3.3	3	17	25.00	15.00	1

Table 6.4: Measured responses for rotofoamability of PE

	Average cell size [μm]			
Sample #	Response 1	Response 2	Response 3	Average
1	373	371	372	372.00
2	750	746	749	748.33
3	291	292	294	292.33
4	263	262	259	261.33
5	518	520	521	519.67
6	276	282	281	279.67
7	318	317	321	318.67
8	253	253	252	252.67
9	466	476	474	472.00
10	339	336	338	337.67
11	619	601	612	610.67
12	344	339	341	341.33
13	757	753	755	755.00
14	361	373	369	367.67
15	321	322	319	320.67
16	465	456	466	462.33
17	311	308	302	307.00
18	317	317	323	319.00
19	367	361	359	362.33
20	257	251	250	252.67
21	249	248	252	249.67
22	606	609	614	609.67
23	758	754	757	756.33
24	179	178	182	179.67
25	523	516	522	520.33
26	251	258	262	257.00
27	469	473	474	472.00
28	303	302	299	301.33
29	382	382	381	381.67
30	250	252	253	251.67
31	471	461	465	465.67
32	369	362	375	368.67
33	374	370	369	371.00
34	500	502	503	501.67
35	429	437	435	433.67
36	421	417	422	420.00
37	495	487	499	493.67
38	264	265	267	265.33
39	483	482	482	482.33
40	437	441	439	439.00
41	470	469	475	471.33
42	531	529	536	532.00

Table 6.5: Comparison of predicted optimized structural properties for dry blended and melt compounded PE based foams produced in rotational foam molding

(T_{oven} = 300 °C; t_{cool} = 22.5 [min]; Mold rot. = 12.5 [rpm])

Resin code	VER	$t_{heat\ pred.}$ [min]	$N_{pred.}$ [cells/cm^3]	$D_{pred.}$ [μm]
PE1DB3	3	13.0	2.77E+05	240
PE1DB6	6	13.5	4.85E+05	270
PE2DB3	3	12.5	1.57E+05	290
PE2DB6	6	12.5	2.43E+05	340
PE3DB3	3	11.5	1.42E+05	300
PE3DB6	6	11.5	1.36E+05	410
PE4DB3	3	11.0	1.57E+05	290
PE4DB6	6	12.0	1.49E+05	400
PE1MC3	3	14.8	4.81E+05	200
PE1MC6	6	15.0	1.39E+06	190
PE2MC3	3	14.0	2.76E+05	240
PE2MC6	6	14.0	5.45E+05	260
PE3MC3	3	13.0	3.16E+05	230
PE3MC6	6	13.0	3.56E+05	300
PE4MC3	3	13.0	3.14E+05	230
PE4MC6	6	13.0	3.56E+05	300

Table 6.6: PP-based foamable resins prepared for the investigation of rotofoamability of PP

#	Assigned code		Foamable PP-based formulation	VER
	Dry blended	Melt compounded		
1	PP1DB3	PP1MC3	PP1 + 0.73%(wt) Celogen AZ	3
2	PP1DB6	PP1MC6	PP1 + 1.83%(wt) Celogen AZ	6
3	PP2DB3	PP2MC3	PP2 + 0.73%(wt) Celogen AZ	3
4	PP2DB6	PP2MC6	PP2 + 1.83%(wt) Celogen AZ	6
5	PP3DB3	PP3MC3	PP3 + 0.73%(wt) Celogen AZ	3
6	PP3DB6	PP3MC6	PP3 + 1.83%(wt) Celogen AZ	6
7	PP4DB3	PP4MC3	PP4 + 0.73%(wt) Celogen AZ	3
8	PP4DB6	PP4MC6	PP4 + 1.83%(wt) Celogen AZ	6

Table 6.7: Independent variable settings for investigating the rotofoamability of PP resins

#	Variable name	Variable symbol	Variable units	Range/ Level(s)
1	PP resin (PP1, PP2, PP3, or PP4)	PE MFI	[g/10min]	5.5; 16; 20; 35
2	VER of the PE foamable formulation	VER		3; 6
3	Oven temperature	T_{oven}	[°C]	$250 \leq T_{oven} \leq 300$
4	Mold heating time	t_{heat}	[min]	$15 \leq t_{heat} \leq 22$
5	Mold cooling time	t_{cool}	[min]	$20 \leq t_{cool} \leq 25$
6	Mold rotation speed	Mold rot.	[rpm]	$10 \leq$ Mold rot ≤ 15
7	Melt compounded or dry blended	MC or DB		1;2

Table 6.8: Experimental plan matrix for rotofoamability of PP resins

Sample #	PP MFR [g/10min]	VER	T_{oven} [°C]	t_{heat} [min]	t_{cool} [min]	Mold rot. [rpm]	MC or DB
1	5.5	3	300.0	22	25.00	10.00	1
2	16.0	3	287.5	20	21.25	11.25	1
3	35.0	3	250.0	22	20.00	15.00	2
4	5.5	6	300.0	14	25.00	12.50	1
5	35.0	6	250.0	18	25.00	10.00	1
6	20.0	3	300.0	18	25.00	10.00	2
7	20.0	6	275.0	18	22.50	12.50	1
8	20.0	6	250.0	18	22.50	12.50	2
9	20.0	3	287.5	20	21.25	11.25	1
10	5.5	3	250.0	14	22.50	15.00	1
11	20.0	3	287.5	16	21.25	13.75	1
12	16.0	3	287.5	16	21.25	11.25	1
13	5.5	6	300.0	14	20.00	10.00	1
14	35.0	3	250.0	18	20.00	10.00	2
15	35.0	3	300.0	22	25.00	15.00	1
16	35.0	3	300.0	22	20.00	15.00	1
17	5.5	3	300.0	18	20.00	15.00	2
18	5.5	6	300.0	22	25.00	12.50	2
19	20.0	3	262.5	16	21.25	11.25	1
20	35.0	3	300.0	22	25.00	15.00	1
21	35.0	3	250.0	18	20.00	10.00	2
22	35.0	3	300.0	22	22.50	10.00	2
23	35.0	6	250.0	22	22.50	15.00	2
24	20.0	3	250.0	22	20.00	12.50	1
25	5.5	6	300.0	14	20.00	15.00	1
26	35.0	6	250.0	14	22.50	15.00	1
27	5.5	6	300.0	22	20.00	12.50	1
28	35.0	6	275.0	18	25.00	12.50	2
29	5.5	6	250.0	22	22.50	10.00	2
30	35.0	3	300.0	14	25.00	10.00	1
31	5.5	3	250.0	22	25.00	12.50	2
32	5.5	6	250.0	18	22.50	12.50	1
33	5.5	6	250.0	14	20.00	10.00	2
34	5.5	3	275.0	22	25.00	15.00	2
35	35.0	3	250.0	14	22.50	10.00	2
36	16.0	3	262.5	20	21.25	11.25	1
37	35.0	6	250.0	14	22.50	15.00	1
38	5.5	6	300.0	14	20.00	12.50	2
39	20.0	6	250.0	18	25.00	15.00	1
40	20.0	3	275.0	18	22.50	12.50	2
41	20.0	6	275.0	18	22.50	12.50	1
42	20.0	6	300.0	14	25.00	15.00	2
43	35.0	6	300.0	18	25.00	10.00	1
44	35.0	3	300.0	14	20.00	12.50	2
45	20.0	6	300.0	22	20.00	15.00	2
46	20.0	3	287.5	16	21.25	11.25	1
47	5.5	3	275.0	22	25.00	10.00	2
48	35.0	6	300.0	14	22.50	10.00	2
49	20.0	6	262.5	20	21.25	11.25	1
50	16.0	3	262.5	16	21.25	11.25	1
51	20.0	6	250.0	18	25.00	15.00	1

Table 6.9: Measured responses for rotofoamability of PP

	Average cell size [mm]			
Sample #	Response 1	Response 2	Response 3	Average
1	698	719	681	699.33
2	973	798	783	851.33
3	918	943	944	935.00
4	1078	1065	1112	1085.00
5	1117	1092	1078	1095.67
6	1072	1081	1097	1083.33
7	1057	1064	1025	1048.67
8	949	905	928	927.33
9	1121	1139	1129	1129.67
10	1298	1213	1274	1261.67
11	1149	1165	1173	1162.33
12	1311	1293	1304	1302.67
13	1097	1154	1111	1120.67
14	816	795	806	805.67
15	1472	1512	1423	1469.00
16	1413	1442	1501	1452.00
17	736	741	739	738.67
18	807	843	829	826.33
19	1646	1609	1684	1646.33
20	1513	1489	1423	1475.00
21	799	818	806	807.67
22	1520	1511	1487	1506.00
23	934	956	934	941.33
24	952	975	973	966.67
25	1239	1254	1248	1247.00
26	1532	1536	1502	1523.33
27	856	884	883	874.33
28	1134	1217	1197	1182.67
29	801	783	794	792.67
30	1682	1656	1684	1674.00
31	754	775	768	765.67
32	834	864	871	856.33
33	1289	1217	1265	1257.00
34	711	732	699	714.00
35	1221	1178	1254	1217.67
36	1017	1065	1013	1031.67
37	1532	1529	1521	1527.33
38	1199	1212	1278	1229.67
39	926	918	903	915.67
40	1053	1033	1044	1043.33
41	1039	1047	1052	1046.00
42	1484	1507	1529	1506.67
43	1146	1123	1149	1139.33
44	1490	1457	1441	1462.67
45	1509	1522	1564	1531.67
46	1134	1164	1141	1146.33
47	727	712	711	716.67
48	1502	1524	1505	1510.33
49	1090	1106	1095	1097.00
50	1524	1491	1498	1504.33
51	921	919	917	919.00

Table 6.10: Comparison of predicted optimized structural properties for dry blended and melt compounded PP based foams produced in rotational foam molding (t_{cool} = 22.5 [min]; Mold rot. = 12.5 [rpm])

Resin code	VER	$T_{oven\ pred.}$	$t_{heat\ pred.}$ [min]	$N_{pred.}$ [cells/cm^3]	$D_{pred.}$ [μm]
PP1DB3	3	250	20.5	9.79E+03	730
PP1DB6	6	250	20.0	2.36E+04	740
PP2DB3	3	250	20.0	5.62E+03	880
PP2DB6	6	250	20.0	1.40E+04	880
PP3DB3	3	250	20.0	4.76E+03	930
PP3DB6	6	250	20.0	1.23E+04	920
PP4DB3	3	250	19.0	4.34E+03	960
PP4DB6	6	250	19.0	1.31E+04	900
PP1MC3	3	300	21.0	1.12E+04	700
PP1MC6	6	300	20.0	2.36E+04	740
PP2MC3	3	300	20.0	4.76E+03	930
PP2MC6	6	250	21.0	1.11E+04	950
PP3MC3	3	300	20.0	3.32E+03	1050
PP3MC6	6	250	20.0	9.52E+03	1000
PP4MC3	3	250	20.0	2.69E+03	1120
PP4MC6	6	250	20.0	9.31E+03	1010

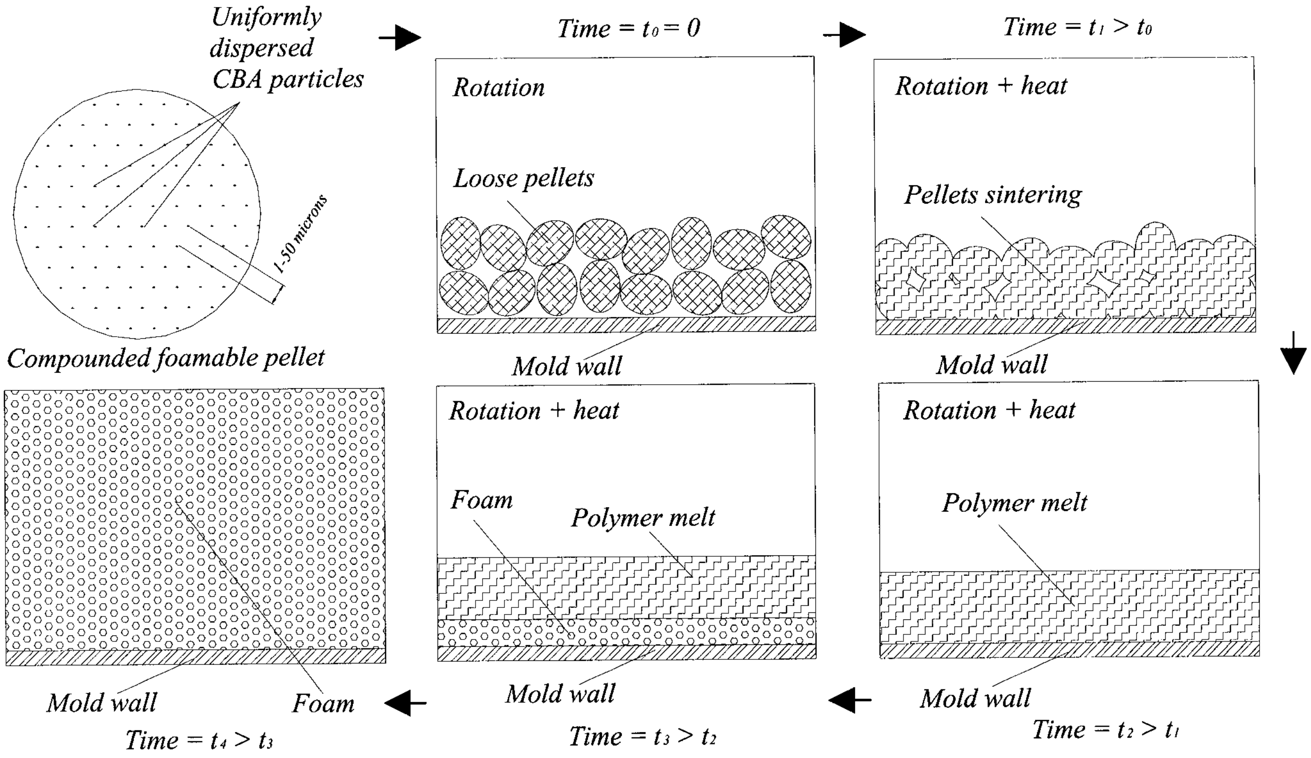

Figure 6.1: Ideal model for processing fine-celled foams in compounding based rotational foam molding

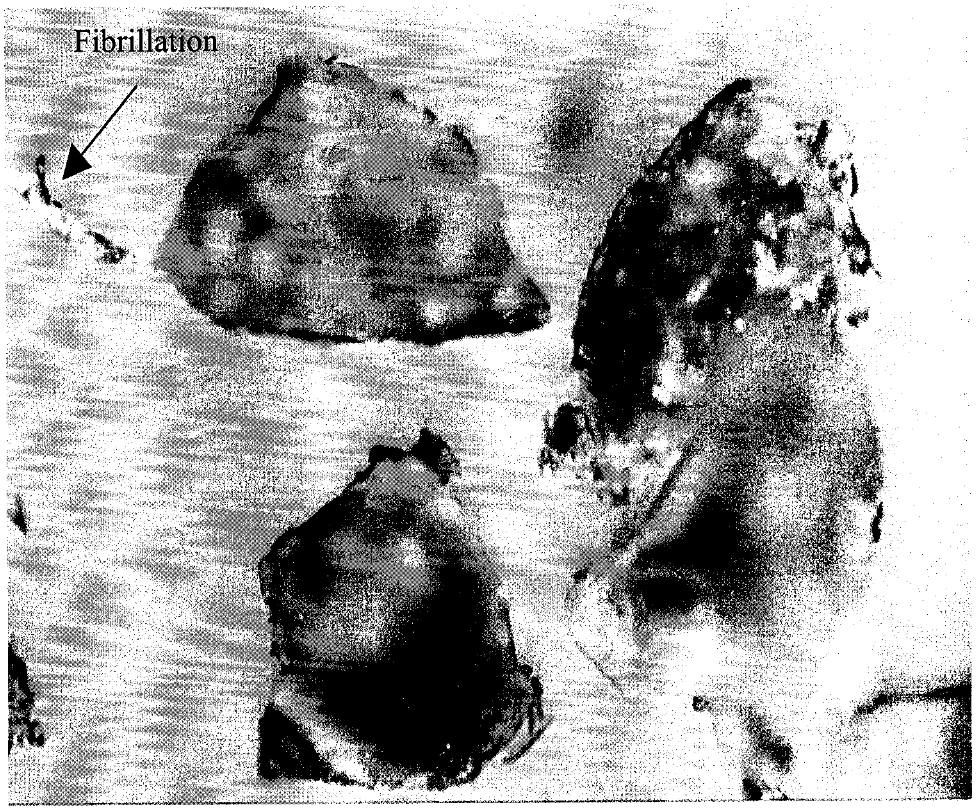

Figure 6.2: Typical PE powder particle fibrillation due to wrong grinding parameters

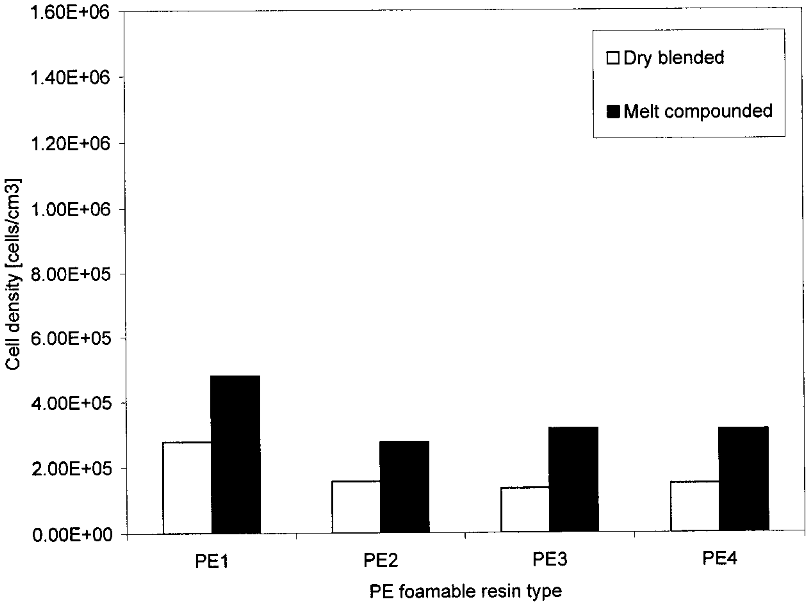

(a)

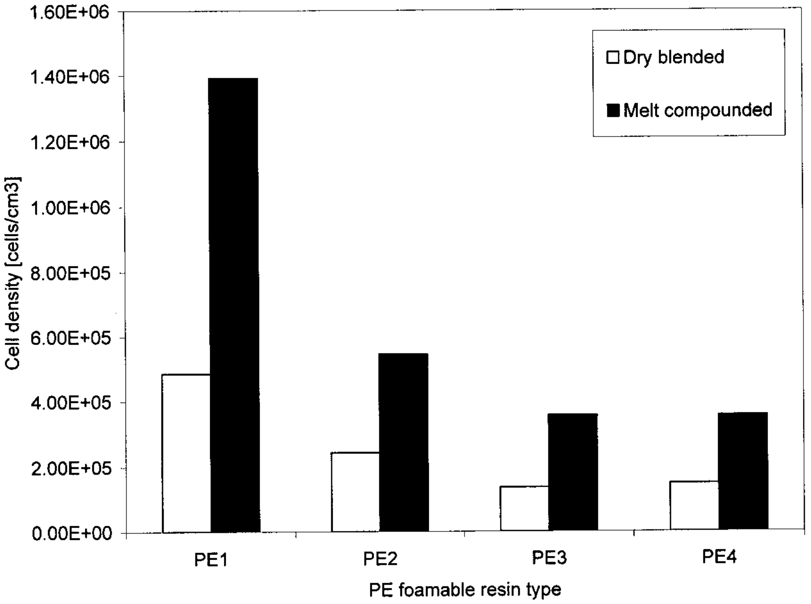

(b)

Figure 6.3: Effect of the foamable resin preparation method on the cell population density of optimized PE based foams prepared with Celogen OT

(a) 3-fold expansion

(b) 6-fold expansion

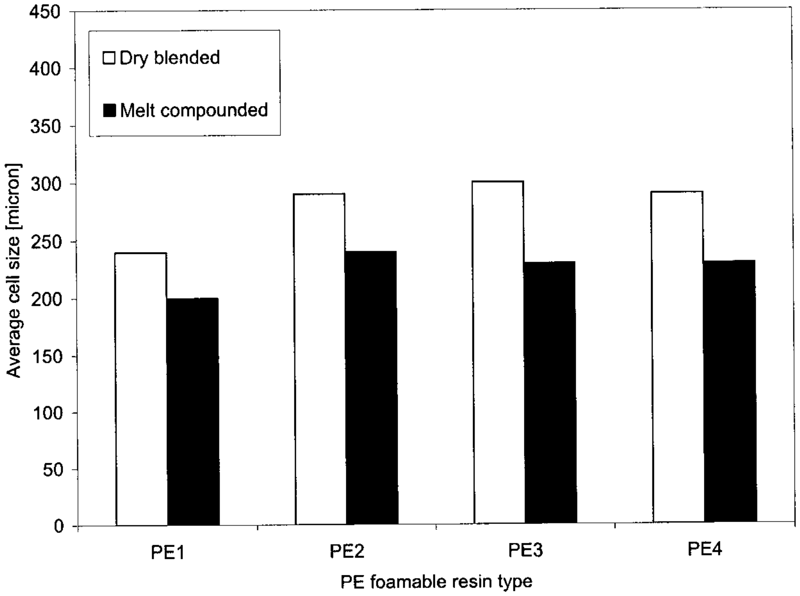

(a)

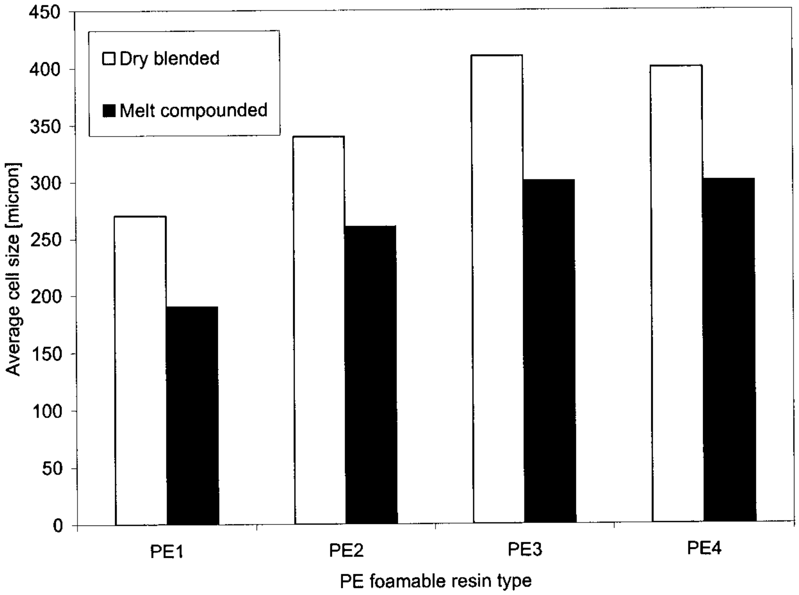

(b)

Figure 6.4: Effect of the foamable resin preparation method on the average cell size of optimized PE based foams prepared with Celogen OT

(a) 3-fold expansion

(b) 6-fold expansion

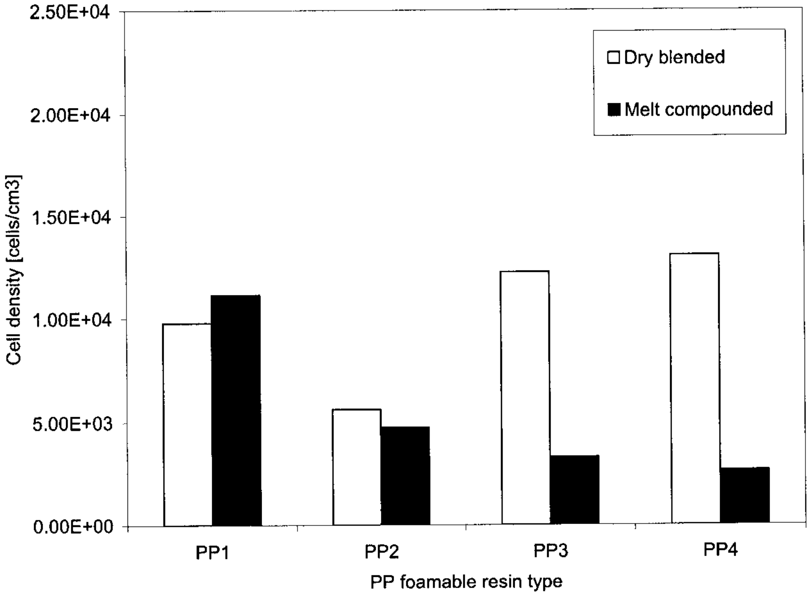

(a)

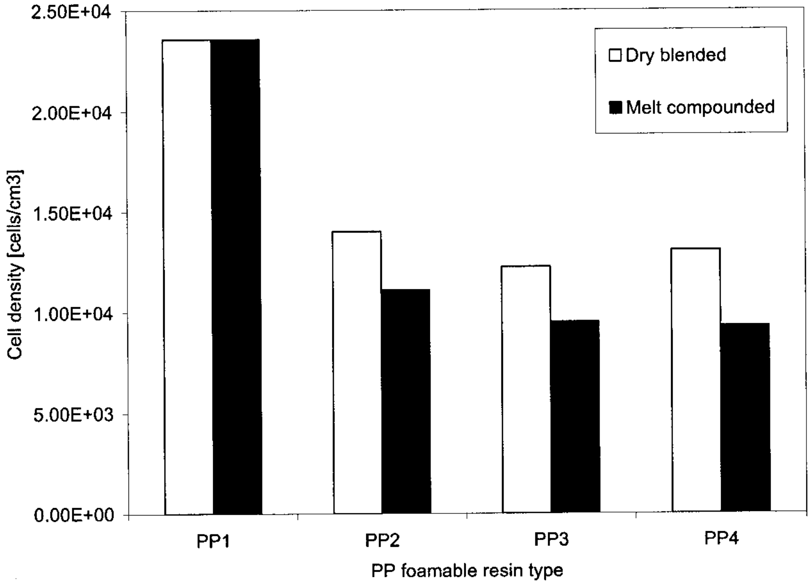

(b)

Figure 6.5: Effect of the foamable resin preparation method on the cell population density of optimized PP based foams prepared with Celogen AZ

(a) 3-fold expansion

(b) 6-fold expansion

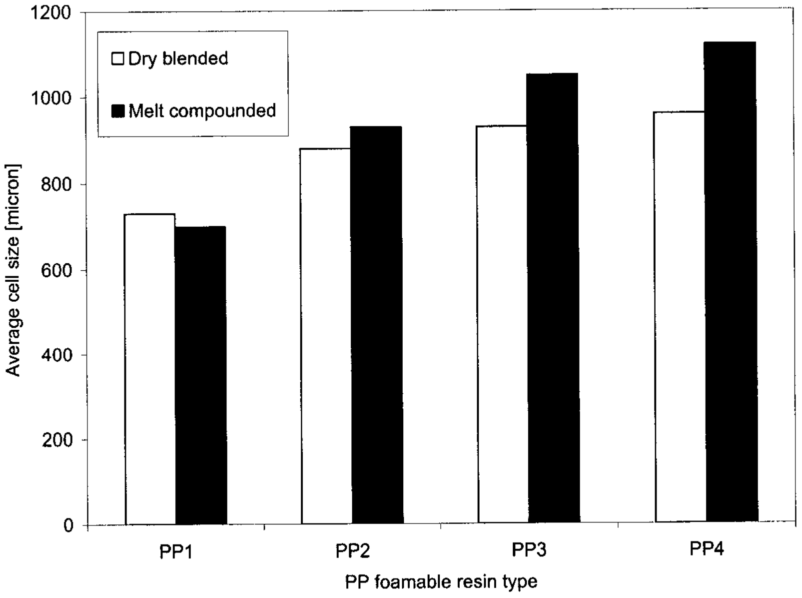

(a)

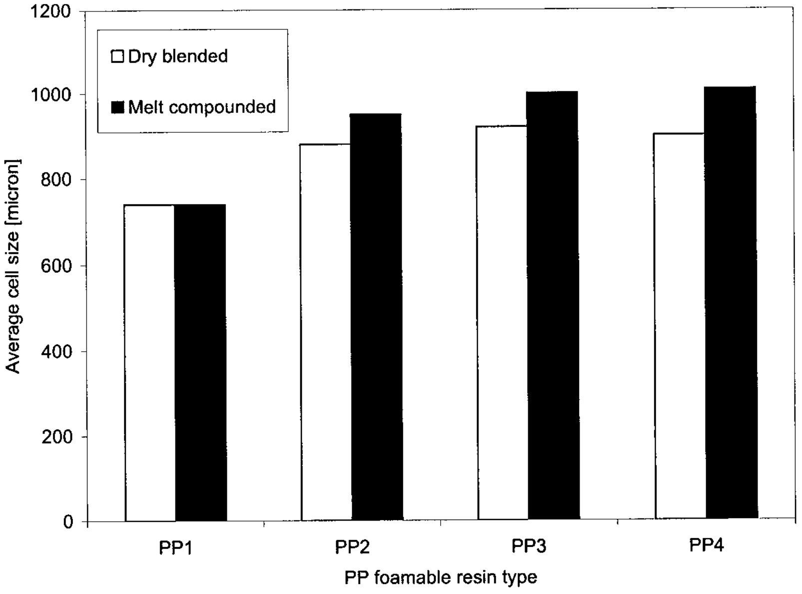

(b)

Figure 6.6: Effect of the foamable resin preparation method on the average cell size of optimized PP based foams prepared with Celogen AZ

(a) 3-fold expansion

(b) 6-fold expansion

CHAPTER 7

PROCESSING INTEGRAL-SKIN CELLULAR POLYOLEFIN COMPOSITES IN SINGLE-CHARGE ROTATIONAL FOAM MOLDING

7.1 Introduction

This chapter focuses on how the rotational molding process, the key feature of which is the production of large-sized, complex-shaped, single-piece moldings, could be employed for the manufacture of polyolefin articles that besides fulfilling the above attributes consist of a distinct layer of non-foamed skin surrounding a foamed core or layer.

The single-charge rotational foam molding processing principle assumes simultaneous introduction of both the foamable and non-foamable resin into the cavity of the mold at the very beginning of the cycle. As indicated in Section 2.3, the use of pulverized non-foamable resins to form the skin and pelletized foamable resins to subsequently form the foamed core or layer is a common practice. Ideally, as the temperature of the mold increases along the course of the rotomolding cycle, the non-foamable powders are supposed to sinter before the foamable pellets because of their greater total surface area which is in contact with the hot air in the mold and because their smaller size allows them to migrate towards the mold's internal surface where the temperature is the highest. Thereby, they should form the skin layer, on top of which, with the subsequent heating of the mold, because the core of the foamable pellets exhibits delayed heating due to the low thermal conductivity of the plastic, depending on the pellet size, the pellets are supposed to form a foamed layer or core.

In this chapter, the key issues that aggravate the single-step rotational foam molding of integral-skin polyolefin cellular composites have been identified, and by implementing an experimental investigation approach, as well as by using some specially devised experimental equipment, respective optimal processing strategies have been successfully established.

7.2 Problem Statement

The single-charge rotational foam molding process is especially suitable for the continuous manufacture of rotational moldings with improved economics and superior mechanical and insulative properties because both the non-foamable powders (for the skin) and foamable pellets (for the foamed layer or core) are charged into the mold in a single shot. However, since the thermal gradient across the polymer melt in rotational foam molding is unavoidable, for achieving satisfactory results, this basic approach requires to be accompanied with a more complex processing strategy. Namely, although this preferred processing concept significantly improves the efficacy of the molding process and the structural homogeneity of the molded product by advantageously eliminating the need for process interruptions and the use of drop boxes or plastic bags inside the mold for physically separating the foamable and non-foamable resins, it aggravates the task of ensuring that the execution of the adhesion of the non-foamable thermoplastic resin to the internal surface of the mold will always take place prior to the activation of the foaming resin. Otherwise, skin thickness insufficiency or non-uniformity and/or locally damaged skin by the premature activation of the foaming resin may render the product useless. This difficulty is being considered as the fundamental problem of the single-charge rotational foam molding technology, and thus, there is a need for establishing an appropriate processing strategy that would assure that the thermally-driven events occurring inside the mold during processing follow a desired order [32,33].

7.3 Processing Solid Skin / Foamed Core Cellular Composites

Figure 7.1 schematically illustrates the fundamental principle of the single-charge integral-skin rotational foam molding technology which is based on using two principal components for charging the mold: a skin-forming blend of non-foamable PE powders and a foam-forming component comprising melt compounded foamable PE pellets. It is intended for the manufacture of two basic typical kinds of integral-skin cellular composites which may consist of a PE solid skin either encapsulating a PE foamed layer or a PE foamed core.

Although the present study primarily focuses on the processing of PE skin / PE core type of integral-skin rotationally molded cellular composites, an attempt has also been made to produce PE skin / PP core integral-skin cellular composites. These will be referred to as “PE / PE” and “PE / PP” throughout this thesis, respectively.

7.4 Processing PE / PE Integral-skin Foams

7.4.1 Experimental Procedure

For conducting the experimental work involving single-charge rotational foam molding of PE / PE integral-skin cellular composites, Rotolite™ OS (as described in Section 4.1.2) was used as the PE-based skin-forming non-foamable component in powder form, whereas the foamable resin was prepared using PE1 (LL8556), i.e., the PE resin that was identified as the most suitable for rotofoaming applications as a result of the material characterization and rotofoamability experimental studies conducted in Chapters 5 and 6, and Celogen OT. The formulation of the foamable resin consisted of LL8556 and 3%(wt) Celogen OT, which amount of CBA is suitable for achieving 5.55-fold volume expansion. The dry-blended LL8556/Celogen OT foamable mixture obtained by using the equipment presented in Figure 4.5 (b) was extrusion melt compounded using the experimental setup presented in Figure 4.6.

The transparent uni-axial rotational molding machine presented in Figure 4.8 was used for producing integral-skin polyolefin cellular composites in a prismatic mold {A=101.6 [mm] (4"), B=50.8 [mm] (2"), H=101.6 [mm] (4")} that was rotating along its longer axis. The volume of the mold was V_{mold}=524.4 [cm^3]

It is important to note here that because the mold performs uni-axial rotation, the amount of non foamable material needed for the formation of the skin (skin shot size) should be calculated as if the front and the rear surface of the mold would not be coated with skin material. Although in practice a very thin skin film is always formed against the mold's walls that remain perpendicular to the axis of rotation at all times, this assumption proved to be useful for the accurate calculation of the remaining free volume of the mold that should be filled with foam. Considering this, for the given mold, the volume of the skin, V_{skin}, with a projected thickness of X [mm] was calculated using Equation (7.1).

$$V_{skin} = V_{mold} - V_{foam} \tag{7.1}$$

where: $V_{foam} = (A - 2X) \cdot (B - 2X) \cdot H$

Conversely, the foam shot size was calculated using Equation (7.2), whereas for obtaining a skin with desired thickness the skin shot size was calculated using Equation (7.3).

$$m_{foam} = \frac{V_{foam} \cdot \rho_{polymer}}{(VER)} \tag{7.2}$$

$$m_{skin} = V_{skin} \cdot \rho_{polymer} \tag{7.3}$$

where: m_{foam} = Foam shot size [g]

m_{skin} = Skin shot size [g]

(VER) = Volume expansion ratio

$\rho_{polymer}$ = Density of polymer/blend [g/cm^3]

The implemented experimental procedure for single-charge rotational foam molding of integral-skin cellular composites involved the following operations: (i) the mold, pre-sprayed with a release agent, was simultaneously charged with predetermined amounts of pulverized non-foamable and pelletized foamable resins, which were determined commensurately to the desired thickness of the skin and the desired volume expansion ratio (VER) of the foam, respectively, (ii) the charged mold was closed and rotated uni-axially while still out of the oven for 5 [min] in each direction at the maximum rotational speed (30 [rpm]) available to allow the non-foamable polymer powders to migrate towards the internal surface of the mold and thereby make the foamable pellets to remain tumbling on top of them, (iii) the vented rotating mold was then placed in the preheated oven to be externally heated to above the point of decomposition of its foamable contents without applying pressure or centrifugal force, (iv) after the heating time elapsed, the rotating mold was removed from the oven and externally cooled using forced air to allow the part to solidify, (v) after removing the part from the mold's cavity, the mold was sprayed with a release agent and the procedure was repeated.

7.4.2 Effect of Heating Time

A classical approach to design of experiments was chosen for this segment of the study because it provided a unique opportunity for obtaining a succession of permanent 3-D "snap-shots" of the events occurring inside the mold at systematically chosen time intervals that cannot be obtained by any process visualization technique based on using a camcorder.

Namely, the optimal heating time for 5.55-fold LL8556-based foams encapsulated with a non-foamed PE-based skin with a projected thickness of 2 [mm] in single-charge rotational foam molding was determined trough conducting multiple series of parametric search experiments over the duration of the heating time while all other parameters were kept fixed. During experimentation the heating time was varied from 13 to 30 [min]. The effect of heating time was studied by analyzing consistently cut cross sections of experimental samples obtained by deliberate and systematic process interruptions at one-minute intervals during the rotational foam molding cycle (e.g., after 13, 14 .... 29, 30 min elapsed heating time). The calculated skin shot size was m_{skin} = 56.11 [g] ≅ 56 [g], while the foam shot size was m_{PEfoam} = 77.76 [g] ≅ 78 [g]. The temperature of the oven was kept constant (T_{oven}= 300 °C). The rotation speed of the mold was kept at 10 [rpm]. The cooling of the mold was conducted using a forced air stream for 20 [min].

Figure 7.2 illustrates the effect of the heating time on the development of said PE / PE integral-skin foams. These experimental results revealed the following set of immediate observations:

(a) It was found that for the described experimental conditions the optimal heating time, i.e., the heating time at which the foam fully expanded and occupied the entire free volume of the mold, was 23 [min] (Figure 7.2 (k)). However, as presented in Figure 7.3, the morphology of the skin layer which was in permanent contact with the peripheral layer of the foamed core was unsatisfactory.

(b) At heating times shorter than the optimal time (Figures 7.2 (a) to 7.2 (j)), the foam gradually propagated inward starting from the mold's internal surface. At these times, five distinct polymer layers could be observed in the radial direction towards the mold's axis. These included: (i) a thin solid skin layer with a rough, non-uniform, thickness, (ii) a layer containing mixture of foam and solid skin elements, i.e., foam inclusions in the "supposed-to-be" solid skin layer, (iii) a fully developed foam layer without skin inclusions, (iv) a layer containing a mixture of foam and softened foamable pellets, and (v) a layer of loose non-sintered pellets. As the heating time increased the thickness of layers (i) and (ii) stagnated, while the thickness of layer (iii) rapidly increased on the expense of the decreased thickness of layers (iv) and (v). Eventually (Figure 7.2 (k)), only layers (i), (ii), and (iii) survived.

Since the ultimate goal in processing skin-surrounded foams in rotational foam molding is to achieve a distinct skin with a uniform thickness on top of which a distinct foamed layer or core with a uniform cell density will be developed, these observations raised important concerns. Namely, due to the temperature gradient and the delayed heat transfer from the mold's surface inwards by the effect of the skin and foam layers formed the foam did not expand simultaneously throughout the mold's volume, as a consequence of which, layer (ii), i.e. the layer containing a mixture of foam and solid skin elements which was located between the thin layer of rough solid skin and the foamed core was formed. This invasion of the foam in the solid skin area and vice versa indicated that the foamable pellets located in the vicinity of the mold's surface suffered a premature decomposition of their CBA content, thereby pushing a portion of the non-foamable polymer inwards. Part of the reason for this anomaly may be an inappropriately selected particle size of the non-foamable polymer resulting in a poor separation between the pulverized and pelletized phases in the mold. However, it seems that an inadequate processing temperature was the principal cause. Namely, due to a high oven temperature the temperature of the mold was also too high so that the foamable pellets located in the vicinity of the mold's surface adhered to the hot mold's wall (or the thin molten skin-forming layer) in the very early stage of the cycle, before the formation of the skin layer was completed. Thereby, instead of tumbling on the inner surface of the skin layer, some of the foamable pellets were attached to the skin and remained in a stationary position relative to the mold rotation, thereby permanently residing in the hottest region in the mold. As such, they could have been prematurely activated causing their immediate expansion, as a consequence of which, a portion of the non-foamable skin-forming melt was pushed inwards by the expanding core-forming cellular structure. This kind of outcome was clearly undesired and required establishing a remedial processing strategy.

(c) At heating times longer than the optimal time (Figures 7.2 (l) to 7.2 (s)), due to overheating, the peripheral layers near the mold's wall showed discoloration as a sign of thermal degradation of the polymer. As the heating time and mold temperature increased, the discoloration of the polymer residing near the mold corners became more pronounced and it started spreading inwards. At approximately the same time, initial cell coalescence appeared at the corners, but it was quickly propagated towards the core areas of the foam. Eventually, the entire part volume was degraded and populated with huge coalesced bubbles, while the undesired layer (ii) became even more emphasized (Figures 7.2 (p) to 7.2 (s)).

The above observations represent a clear indication that the chosen processing parameters did not ensure that the formation of the solid skin completes before the commencement of the activation of the foamable resin and that the implemented constant oven temperature profile was inadequate for controlling the appropriate order of events in the mold. This also indicated that for successful single-charge rotational foam molding of integral-skin cellular composites, both the processing time and processing temperature were to be optimized in order to avoid polymer degradation of the solid skin and the foam located at the peripheral areas of the cross section of the molding.

One way of addressing this problem was to reduce the oven temperature while still keeping it at constant level. However, this would inevitably result in prolonging the processing time which in rotational foam molding is already too long. As such, this option did not seem to be feasible. Another way of responding to this problem was to apply a variable (multi-step) oven temperature profile. However, prior attempting to determine the optimal oven temperature profile, it would be useful to investigate the effect of skin on the foam morphology, to visualize the process, and to identify the fundamental adhering behaviors of the non-foamable skin-forming powders and foamable core-forming pellets to a high-temperature rotating metal wall.

7.4.3 Effect of Skin

In order to determine the effect of the skin on the optimal processing time of 5.55-fold LL8556 foams in single-step rotational foam molding, multiple series of skinless parametric search experiments have been conducted. During this series of experiments, other than the skin shot size (which was reduced to zero) and the foam shot size (which was increased from 78 [g] to 87.87 [g] ≅ 88 [g] to keep the VER of the foam unchanged), all remaining processing parameters were kept at identical levels as during the investigation of integral-skin LL8556-based foams. The processing time was varied from 13 minutes to 25 minutes.

Figure 7.4 illustrates the effect of the heating time on the development of cell morphologies of respective skinless foams and reveals the following comparative immediate observations:

(a) The optimal heating time for the skinless foams was t = 18 [min] (Figure 7.4 (f)). Thus, the absence of the 2 [mm] thick solid skin resulted in reducing the heating time for 28%.

(b) At processing times shorter than the optimal time (Figures 7.4 (a) to 7.4 (e)), the absence of the solid skin intensified the heat transfer, as a result of which, the skinless foam propagated much faster inward starting from the mold's internal surface. However, it was still far from achieving uniform foam propagation throughout the mold's volume. In contrast to the skin-surrounded case, at these times, in the radial direction towards the mold's axis, only two distinct polymer layers could be observed. These included a fully developed foam layer and a layer containing a mixture of foam and softened foamable pellets. Eventually only the former layer survived (Figure 7.4 (f)).

(c) At processing times longer than the optimal time (Figures 7.4 (g) to 7.4 (l)), due to overheating, the peripheral layers near the mold's wall exhibit discoloration due to thermal degradation of the polymer. As the temperature increased with longer heating times, cell coalescence developed while the degradation of the polymer continued to spread further inward. Finally most of the volume of the foam became degraded and populated with coarse coalesced bubbles (Figure 7.4 (l)). In compassion with respective integral-skin foams, the skinless foams became susceptible to degradation at about 27% shorter heating times, which could be attributed to the absence of the insulative effect of the solid skin.

7.4.4 Process Visualization

The visualization of the single-charge rotational foam molding process was carried out using a transparent uni-axial rotational molding machine, a see-trough mold, and a camcorder. The oven temperature was set to $T_{oven} = 250$ °C in order to extend the cycle and slow down the process in order to allow enough time for recording the critical occurrences taking place inside the mold.

Figure 7.5 presents nine typical snap-shots that have been captured from the full motion visualization files, which characterize nine distinct subsequent phases occurring inside the mold along the course of the single-charge manufacturing cycle for integral-skin cellular composites. These include: (i) initial tumbling of the mixture of non-foamable powders and foamable pellets inside the heated mold (Figure 7.5 (a); $t_{heat} = 0$ to 4 [min]), (ii) adhering and sintering of the non-foamable powders to the hot rotating mold wall (Figure 7.5 (b); $t_{heat} = 4$ to 8 [min]), (iii) tumbling of the foamable pellets on top of the already adhered powders that have formed the initial layer of molten non-foamed skin (Figure 7.5 (c); $t_{heat} = 8$ to 10 [min]), (iv) random sticking of the foamable pellets to the molten skin layer and random pellet detachment and falling down after being rotated for ~180° to reach the highest upper position inside the mold (Figure 7.5 (d); $t_{heat} = 10$ to 13 [min]), (v) adhering of all foamable pellets to the molten non-foamed skin layer (Figure 7.5 (e); $t_{heat} = 13$ to 19 [min]), (vi) sintering of the foamable pellets (Figure 7.5 (f); $t_{heat} = 19$ to 23 [min]), (vii) expansion of the foamable pellets (Figure 7.5 (g); $t_{heat} = 23$ to 26 [min]), (viii) formation of a foam layer and its expansion inward in the radial direction (Figure 7.5 (i); $t_{heat} = 26$ to 31 [min]), and (ix) filling the mold with a foamed core that has been encapsulated by the non-foamed skin (Figure 7.5 (j); $t_{heat} > 31$ [min]).

7.4.5 Fundamental Study of Adhering Behavior

In order to check the adhesion behavior of the non-foamable skin-forming Rotolite™ OS powders and foamable core-forming PE pellets on a hot rotating metal wall a predetermined amount these materials (e.g., 1 [g] of powders or 15 pellets, respectively) originating from the same batch as those participating in the single-charge rotational foam molding experiments were dropped from a consistent vertical height (e.g., 10 cm (4")), onto a uniformly preheated metal hot plate while it was held in the upper horizontal position (Figure 4.11 (b)). Each series of experiments was conducted while the temperature of the plate was systematically held at a desired level (e.g., 104, 106,…., 120 °C). After the powders / pellets have been residing on the hot plate for each incremental predetermined period of 1, 3, 5, 10, and 20 [min], the plate was rotated for 180° using the rotating arm pertaining to the rotational molding experimental setup thereby simulating adequately the momentum occurring during actual rotational foam molding experiments. The quantity of powders/pellets falling from the plate in its reversed position was collected and measured/counted and recorded, respectively. The calculated percentage powder / pellet quantities remaining adhered on the plate was used as a quantifying parameter for describing the fundamental adhesion behavior of the powders / pellets after residing on it at a predetermined temperature for a systematically period. Then, the temperature of the plate was increased for 2 °C in order to conduct the subsequent series of experiments.

The experimental results obtained from this study revealed that all skin-forming powders were permanently adhered to the plate after 10 [min] of residence time at a temperature of 108 °C (Figure 7.6). However, even after only one minute of residence time on the hot-plate at a temperature of 118 °C, all 15 pellets remained permanently adhered on it even after it was rotated upside-down (Figure 7.7). On the other hand, it was necessary to rise the temperature of the hot plate to 116 °C in order the entire quantity of powders to remain permanently adhered on the plate after just one minute of residence time.

Thus, to maintain a desired order of thermal events inside the mold in single-charge rotational foam molding of PE / PE integral-skin cellular composites, the oven temperature profile should be designed to delay the mold wall in reaching the critical temperature of 118 °C sufficiently long (e.g., 10 [min]), in order to allow the completion of powder sintering and the formation of the first depositions of the skin layer to occur at a relatively lower temperature such as 108 °C and thereby avoid the invasion of the foamable resin into the skin layer.

7.4.6 Effect of Two-step Oven Temperature

The effect of the oven temperature on the in-mold air temperature was studied by conducting empty-mold experiments at various non-constant oven temperature profiles while keeping the remaining processing parameters unchanged. Figure 7.8 presents various measured temperature-time rotational foam molding profiles that compare the effect of a constant oven temperature of 300 °C with that of a variable two-step oven temperature on the temperature of the air in the center of the empty mold. The various two-step oven temperature profiles were obtained by initially maintaining the oven temperature at 150, 160, 170, and 180 °C for various periods after which the oven temperature was raised to 360 °C (the highest temperature at which the oven could safely operate) with the maximum heating rate of about 15 [°C/min] and kept at this level for various time periods, respectively.

The graphs presented in Figure 7.8 revealed that the measured in-mold time-temperature profiles related to a respective two-step oven temperature show that a reduced amount of heat would be transferred to the shot size at the initial stage of the molding process which corresponds with the formation of the skin. This indicated that by reducing the oven temperature to a level that would be just sufficient to melt the skin-forming resin, an uninterrupted formation of the skin layer would be allowed, while simultaneously delaying the activation of the foamable resin until the time when its effect would be beneficial for the product itself but not detrimental for the morphology of the skin layer. In addition, at lower oven temperatures, the chances that the foamable pellets adhere onto the internal high-temperature mold surface would be also lowered because they would be detached by the bending moment caused by their relatively large mass, whereas smaller particles (powders) would easily stick to the wall and form a solid skin more uniformly. Once the skin is formed, the oven temperature should be dramatically increased to trigger the CBA decomposition, and then, it should be kept constant at this high level for a relatively short time to allow a quick completion of the foaming process while avoiding the possible thermal degradation of the surface of the skin layer which is in permanent contact with the hot mold wall.

7.4.7 Design of Two-step Oven Temperature Experiments

The CARD® PRO software package was used to design the experimental plan for optimizing the two-step time-temperature profile for processing PE / PE integral-skin cellular composites in single-charge rotational foam molding while achieving a solid skin envelope without cellular inclusions and a uniform thickness. Table 7.1 presents the settings of the three independent process variables that determined the experimental matrix. These included: (i) the oven temperature during step one, which was varied between 150 and 190 °C, (ii) the mold heating time at oven temperature for step one, which was selected to be in the range between 6 and 12 minutes, and (iii) the mold heating time at oven temperature of 360 °C pertaining to step two, which was varied between 4 and 8 minutes. The remaining molding conditions were assumed to be constant and there values were: Shot weight = 56 [g] Rotolite™ OS + 78 [g] (LL8556 + 3%wt Celogen OT); $T_{oven\ step\ 2} = 360$ °C; Mold Rot. = 10 [rpm]; $t_{cool} = 20$ [min].

Using the above data as input, the software package proposed an experiment plan matrix consisting of 17 experimental samples as presented in Table 7.2. From each combination of variables given by the experimental plan three rotationally foam molded integral-skin samples have been prepared. A total of 51 (17 × 3) samples were visually characterized in terms of skin layer integrity and skin thickness uniformity at a consistently cut cross section. The matrix of responses, consisting of marks from 1 to 10 associated to each sample, is presented in Table 7.3.

7.4.8 Statistical Analysis

The detailed regression ANOVA analysis presented the Pareto Chart which ranked the oven temperature at step one as the variable with the dominant statistical significance for the quality of the produced PE / PE integral-skin cellular composites, whereas the mold heating times during step one and step two were ranked as the second and third statistically significant variable, respectively. The established model involving the 3 independent variables was optimized for maximum response (skin uniformity). In order to obtain maximum response, the optimizer suggested setting the oven temperature to 171.15 °C during the first step for 6 [min] and then rising the temperature to 360 °C and keeping it at this level for another 4 [min] (Lower 2σ confidence limit = 9.94; Upper 2σ confidence limit = 12.00).

However, during the experimental verification of the statistically optimized result it was found that best solid skin layer structures and best cell morphologies of the foamed core could be actually achieved if slightly extending the proposed duration of the steps suggested by the statistical analysis. Namely, after conducting another set of trials, it was found that for said LL8556-based cellular composites, optimum results could be obtained if the charged rotating mold would be inserted into a pre-heated oven at 170 °C for 8 [min] after which the oven temperature should gradually increase using a ramp mode with a heating rate of 15 [°C/min] up to 360 °C, at which it should remain constant for 5 [min]. By using the described rotational molding experimental setup, to increase the oven temperature from step one to step two took approximately 12 [min]. Through additional trials, it was also found that further improvements could be reached if instead of keeping the temperature constant at levels of 170 °C and 360 °C, it would be allowed to fluctuate regularly inside the boundaries of 170±15 °C and 360±15 °C, respectively. When programming the oven temperature controller in such a way, the oven temperature profile allows for subsequent cooling and heating periods along the rotational foam molding cycle, which proved to be effective in ensuring that the skin formation is completed prior to the activation of the foaming resin which in turn eliminates the invasion of the foaming resin on the solid skin layer.

Figure 7.9 presents a comparison of the thermograms of the optimized two-step oven temperature profile and the actually measured temperature of the PE foam at the center of the mold. It can be observed that the peak optimized in-mold temperature measured at the center of mold is slightly higher (175 °C) than the decomposition temperature of Celogen OT, which is exactly what is required to assure the activation of the most remote centrally located foamable pellets without overheating the melt. In this context, Figure 7.10 presents a respective PE / PE integral-skin cellular composite sample obtained using the optimized two-step oven temperature profile. It clearly shows absence of invasion of foamable pellets onto the solid skin layer and improved cell morphology of the foamed core. It is also important to note that the implementation of the pre-programmed two-step oven temperature profile extended the optimum processing time for only 8%, which is acceptable.

7.5 Processing PE / PP Integral-skin Foams

The acquired information during processing of PE / PE integral-skin foams was extensively used in attempting to produce single-charge, rotationally foam molded PE / PP integral-skin cellular composites. In this context, Rotolite™ OS was used as the PE-based skin-forming non-foamable component in powder form, whereas the foamable resin was prepared using PP1 (PF633) and Celogen AZ since, as it was described in Chapters 5 and 6, PF633 was identified as the most suitable resin for rotofoaming applications among the investigated PP grades.

The PP foamable resin intended for conducting single-charge rotational foam molding experiments for producing integral-skin foams consisted of PF633 and 1.67%(wt) Celogen AZ, which amount of CBA is suitable for achieving 5.55-fold volume expansion. The prepared dry-blended PF633/Celogen AZ foamable mixture was extrusion melt compounded using the experimental setup presented in Figure 4.6. For the identical mold as in the case of PE / PE integral-skin foams, the skin shot size for a 2 [mm] thick skin was again $m_{skin} \cong 56$ [g] of Rotolite™ OS, while the calculated foam shot size was $m_{PPfoam} = 75.26$ [g] $\cong 75.5$ [g].

With regards to the processing conditions, other than the heating times at each oven temperature step, the identical 170 °C / 360 °C two-step oven temperature profile that has been optimized for processing PE / PE integral-skin foams was implemented in the processing of PE / PP foams. The reason being that the first-step oven temperature corresponds with the formation of the skin layer for which identical materials were used in both the production of PE / PE and PE / PP integral-skin foams, whereas the second-step oven temperature should not be neither lower than 360 °C, because it would thereby unacceptably extend the duration of the production cycle, nor higher than 360 °C, because it would further decrease the already low melt strength of PP and thereby promote cell coalescence. The rotation speed of the mold was kept at 10 [rpm], while the cooling time of the mold was 20 [min].

After conducting a set of parametric search trials over the heating time per oven temperature step, it was found that for said PF633-based integral-skin cellular composites, optimum results were obtained if the oven temperature was first kept at 170 °C for 12 [min] and then increased to reach 360 °C, at which it was kept for 6 [min]. Since the increase of the oven temperature from step one to step two takes approximately 12 [min] when using said experimental equipment, the required heating time for obtaining optimal PE / PP integral-skin foams was 30 [min]. Figure 7.9 presents a comparison of the thermograms of the optimized two-step oven temperature profile and the actually measured temperature of the PP foam at the center of the mold. Similarly to the PE / PE case, the peak optimized in-mold temperature measured at the center of mold is slightly higher (225.5 °C) than the decomposition temperature of Celogen AZ, as preferred. Figure 7.11 presents a typical cell morphology of a PE / PP integral-skin foam which was produced using the optimized oven temperature profile.

7.6 Characterization of Integral-skin Polyolefin Foams

Table 7.4 presents a comparison between the calculated cell densities and the average cell size of PE / PE and PE / PP integral skin foams, while Figure 7.12 presents typical SEM micrographs of respective integral-skin polyolefin composites manufactured by using the single-charge rotational foam molding technology and a two-step oven temperature profile. In particular, Figures 7.12 (a) and (b) present the cell morphologies of the foamed core of PE / PE and PE / PP integral-skin foams, respectively, whereas Figures 7.12 (c) and (d) present the cell morphologies of the interface between the solid skin and the foamed core pertaining to PE / PE and PE / PP integral-skin foams, respectively. These experimental results revealed that the PE / PE integral-skin foams achieved cell morphologies of almost identical quality (N = 4.969 E+05 [cells/cm^3]; D = 268 [μm]; VER = 5.55) as respective skinless PE foams that have been produced by the dry-blending based rotational foam molding method (N = 4.85 E+05 [cells/cm^3]; D = 270 [μm]; VER = 6) and that have been discussed in Chapter 6. On the other hand, the PE / PP integral-skin foams achieved cell morphologies of superior quality (N = 6.708 E+04 [cells/cm^3]; D = 522 [μm]; VER = 5.55) in comparison with that of the best ranked skinless PP foams (N = 2.36 E+04 [cells/cm^3]; D = 740 [μm]; VER = 6) that have been discussed in Chapter 6. This clearly indicates that implementing the two-step oven temperature processing strategy was particularly beneficial for the PE / PP foams due to the reduced amount of heat the shot size has been subjected to during processing. In addition, the PE envelope that separated the developing PP foam from the high temperature mold wall at all times played an extremely important role in reducing the heat transfer inward and preserving the PP foamable resin from overheating and being susceptible to cell coalescence.

Table 7.5 illustrates the measured densities of the foamed core pertaining to PE / PE (0.186 [g/cm^3]) and PE / PP (0.291 [g/cm^3]) single-charge rotationally foam molded integral-skin cellular composites, respectively. The average foam densities obtained out of five measurements, indicated that the density of PE / PE foams was significantly lower than that of PE / PP foams. This can be attributed to the higher cell density achieved during the manufacture of PE / PE foams (N = 4.969 E+05 [cells/cm^3]) than that of PE / PP foams (N = 6.708 E+04 [cells/cm^3]), which indicates that the achieved void fraction in the PE-based integral-skin foams was higher. It is important to note that the achieved density of the integral-skin PE / PE foams is almost identical to the targeted one for the present research.

7.7 Process Scaling-up for Industrial Rotomolding Equipment

It is important to mention that the single-charge rotational foam molding process was successfully scaled-up for the manufacture of both PE / PE and PE / PP integral-skin cellular composites using a 2" × 12" × 24" mold to produce a flat integral-skin cellular composite article by implementing a two-step oven temperature profile. As presented in Figure 4.10, these trials were conducted by Ingenia Polymers on a biaxial industrial-scale rotomolder.

7.8 Summary

The production of integral-skin cellular composites using the single-charge rotational foam molding technology is conditioned by the timely completion of the formation of the skin layer with respect to the onset of activation of the foamable resin intended to form the cellular core or layer. Namely, the pulverized non-foamable resins should be induced to melt and coat the internal mold's surface before the rising temperature of the air inside the mold softens and sinters the foamable pellets, and then, triggers the decomposition of the CBA dispersed throughout the pellets until they eventually convert into a cellular structure. It has been demonstrated in this chapter that the oven temperature profile is the principal parameter that governs the sequence of thermal events inside the mold and thereby the compactness of the solid skin and the final foam structure. However, a constant oven temperature failed to provide a distinct solid skin layer envelope with a uniform thickness around a distinct foamed layer or core with a uniform cell density. Therefore, a two-step oven temperature profile was proposed for eliminating the invasion of the foamable resin on the solid skin layer. The two-step oven temperature profile rationale is to minimize the tendency of premature pellet sticking by maintaining the temperature of the mold in between the boundaries of the critical temperatures of powder adherence (108 °C) and pellet adherence (118 °C) after residing 10 [min] on the hot rotating mold wall, respectively. The role of the first temperature step is to promote the formation of the solid skin while substantially suppressing pellet sticking. Once the skin has been formed, since the reasons to delay the process have been exhausted, the oven temperature can be raised to the second step to promote the foaming of the sintered foamable resin. This strategy proved to be effective for PE / PE and PE / PP integral-skin foams in ensuring that the skin formation is completed prior to the activation of the foamable resin. It prolonged the processing time of PE / PE integral-skin cellular composites for only 8%.

Table 7.1: Independent variable settings for investigating the skin uniformity of PE/PE integral-skin cellular composites

#	Variable name	Variable symbol	Variable units	Range/ Level(s)
1	Oven temperature during step 1	$T_{\text{oven step 1}}$	[°C]	$150 \leq T_{\text{oven step1}} \leq 190$
2	Mold heating time at $T_{\text{oven step 1}}$	t_{step1}	[min]	$6 \leq t_{\text{step1}} \leq 12$
3	Mold heating time at $T_{\text{oven step 2}}$	t_{step2}	[min]	$4 \leq t_{\text{step2}} \leq 8$

Table 7.2: Experimental plan matrix for two-step processing temperature profile for PE/PE integral-skin cellular composites

Sample #	$T_{\text{oven step1}}$ [°C]	$t_{\text{step 1}}$ [min]	$t_{\text{step 2}}$ [min]
1	150	12.0	4.0
2	170	9.0	6.0
3	190	9.0	6.0
4	190	9.0	8.0
5	150	6.0	4.0
6	150	12.0	8.0
7	180	10.5	5.0
8	150	6.0	4.0
9	150	9.0	8.0
10	170	9.0	8.0
11	190	6.0	8.0
12	170	9.0	6.0
13	190	12.0	8.0
14	190	9.0	4.0
15	150	6.0	8.0
16	190	9.0	4.0
17	180	7.5	5.0

Table 7.3: Measured responses for skin uniformity of PE/PE intergral-skin cellular composites

	PE/PE Skin uniformity			
Sample #	Response 1	Response 2	Response 3	Average
1	3	2	1	2.00
2	10	10	9	9.67
3	2	3	2	2.33
4	2	2	2	2.00
5	4	4	3	3.67
6	2	2	3	2.33
7	8	8	9	8.33
8	4	3	3	3.33
9	3	3	1	2.33
10	9	9	10	9.33
11	4	3	4	3.67
12	9	10	10	9.67
13	2	1	2	1.67
14	3	3	4	3.33
15	3	3	3	3.00
16	4	3	2	3.00
17	9	9	8	8.67

Table 7.4: Structure characterization of PE/PE and PE/PP integral-skin cellular foams

Interal-skin cellular composite			Foam structure		
Type	Skin-forming material	Core-forming material	Cell density N [cells/cm^3]	Average cell size D [μm]	VER
PE/PE	Rotolite™ OS	LL8556 + 3%wt Celogen OT	4.969E+05	268	5.55
PE/PP	Rotolite™ OS	PF633 + 1.67%wt Celogen AZ	6.708E+04	522	5.55

Table 7.5: Density characterization of PE/PE and PE/PP integral-skin cellular foams

	Dimension of sample					
Sample code	a [mm]	b [mm]	l [mm]	Weight [g]	Density [kg/m3]	Density [g/cm3]
PE/PE-1	12.41	10.11	8.34	0.2002	191.326	0.191
PE/PE-2	11.41	9.89	8.13	0.1682	183.338	0.183
PE/PE-3	11.35	10.64	10.06	0.2314	190.471	0.190
PE/PE-4	9.86	12.63	8.47	0.2049	194.258	0.194
PE/PE-5	12.32	12.13	9.46	0.2400	169.765	0.170
				Average	185.832	0.186
PE/PP-1	11.62	13.00	9.76	0.4577	310.443	0.310
PE/PP-2	11.25	11.80	9.30	0.3257	263.815	0.264
PE/PP-3	13.45	11.58	9.57	0.4399	295.129	0.295
PE/PP-4	10.83	13.37	10.37	0.4424	294.630	0.295
PE/PP-5	10.86	13.17	9.34	0.3901	292.021	0.292
				Average	291.207	0.291

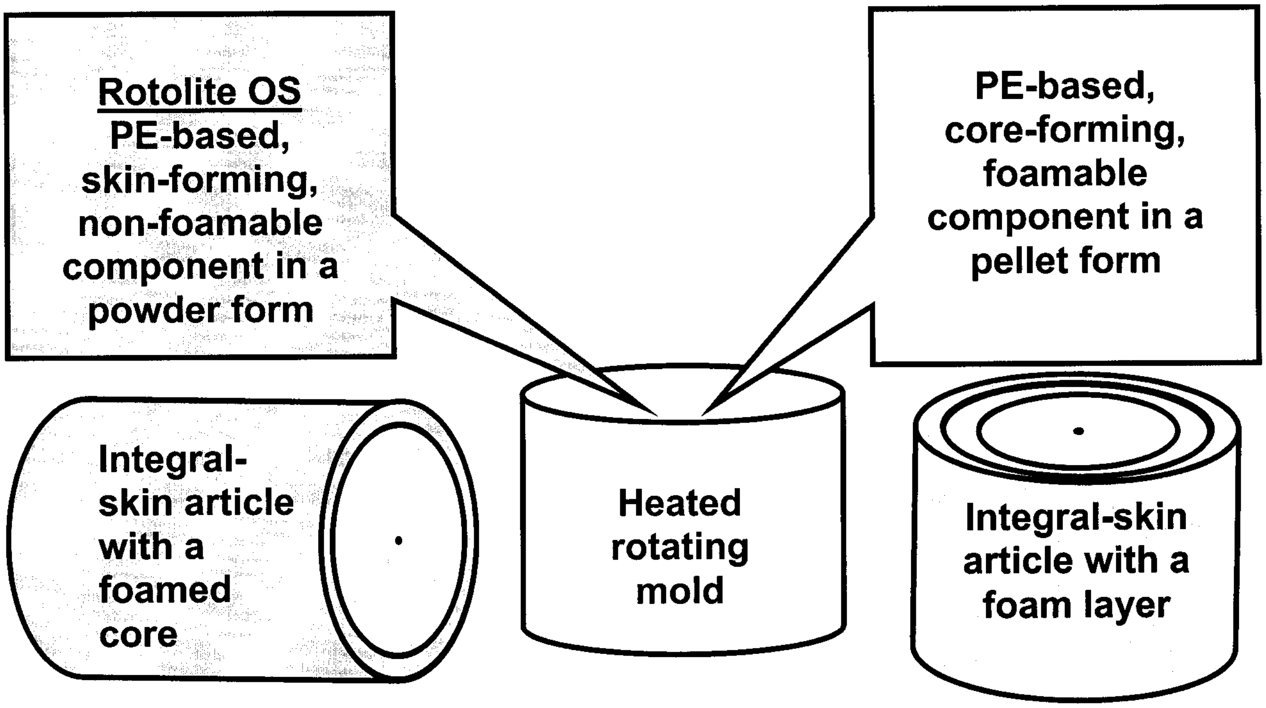

Figure 7.1: Schematic illustration of the principle of operation of the single-charge rotational foam molding process for manufacturing integral-skin cellular composites and the typical structure of its two product types: “PE skin / PE foamed core” and “PE skin / PE foamed layer”

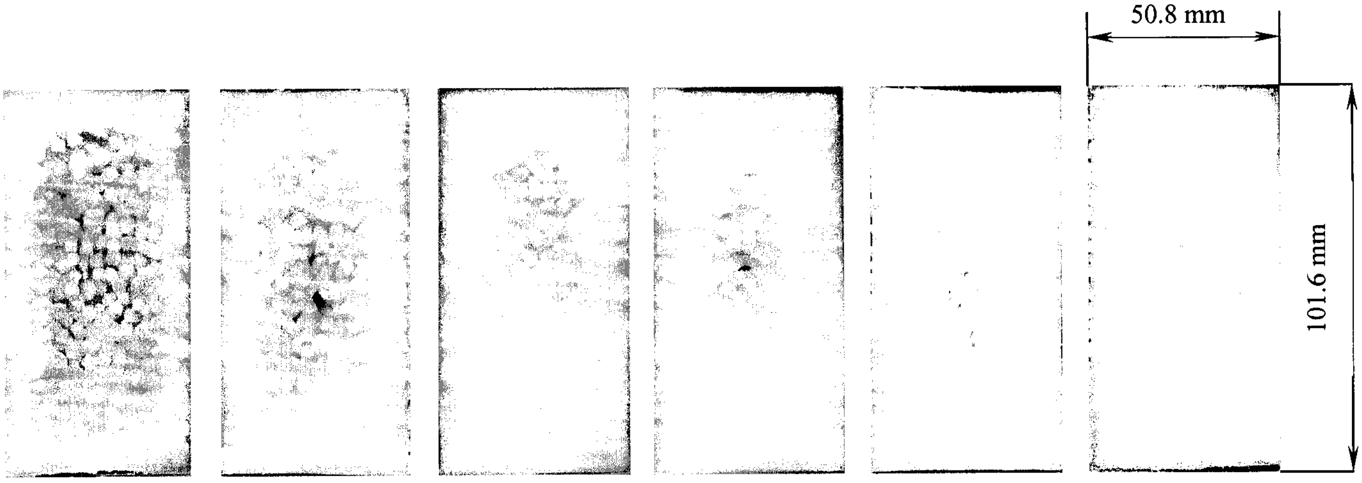

(a) t =13 min (b) t =14 min (c) t =15 min (d) t =16 min (e) t =17 min (f) t =18 min

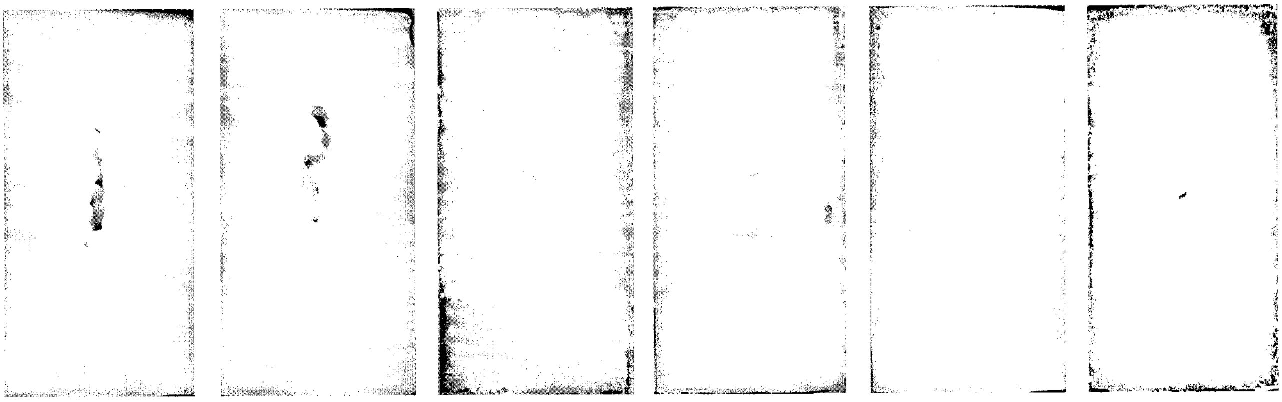

(g) t = 19 min (h) t = 20 min (i) t = 21 min (j) t = 22 min (k) t = 23 min (l) t = 24 min

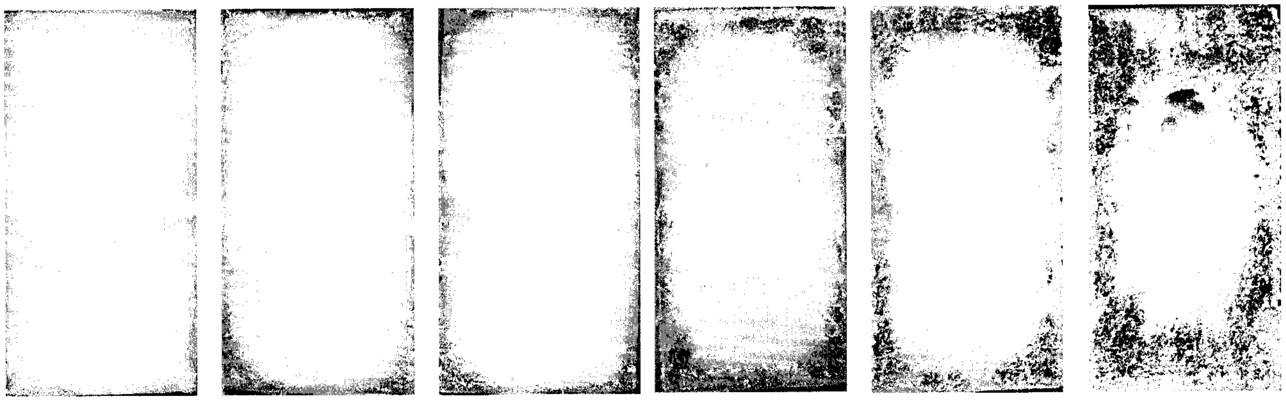

(m) t = 25 min (n) t = 26 min (o) t = 27 min (p) t = 28 min (r) t = 29 min (s) t = 30 min

Figure 7.2: Effect of heating time on cell morphology of single-charge rotationally foam molded integral-skin PE / PE cellular composites {Shot weight = 56 [g] Rotolite™ OS + 78 [g] (LL8556 + 3%wt Celogen OT); Projected skin thickness = 2 [mm]; T_{oven} = 300 °C = Const.; Mold rot. = 10 [rpm]; t_{cool} = 20 [min]}

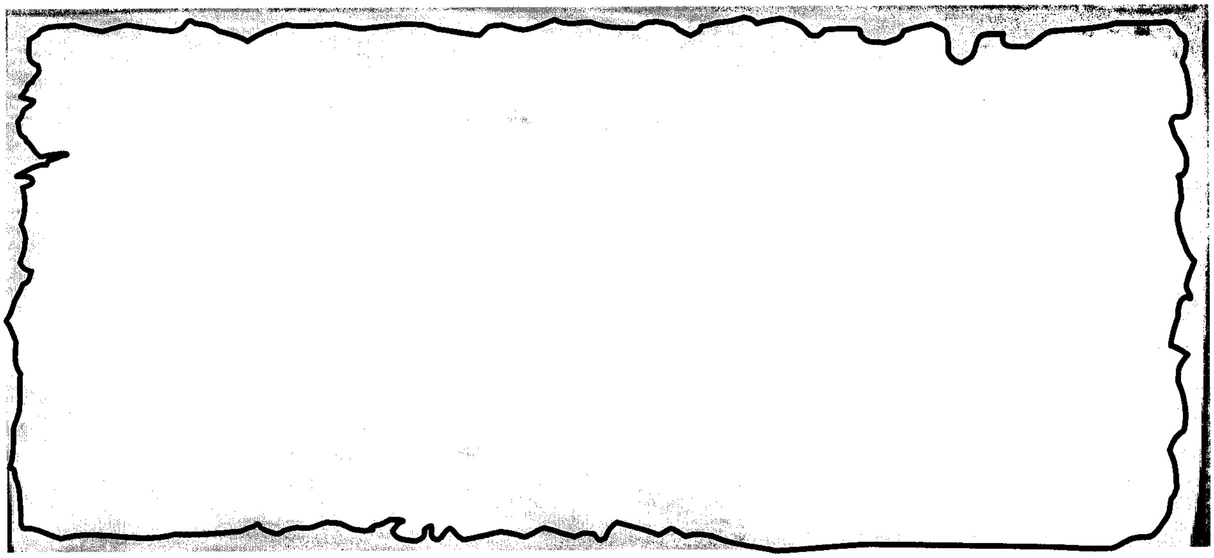

Figure 7.3: Magnified view of a typical morphology of the skin layer in optimized integral-skin PE / PE cellular composites processed at a constant oven temperature (T_{oven} = 300 °C) {t_{heat} = 23 [min]; Shot weight = 56 [g] Rotolite™ OS + 78 [g] (LL8556 + 3%wt Celogen OT); Mold rot. = 10 [rpm]; t_{cool} = 20 [min]}

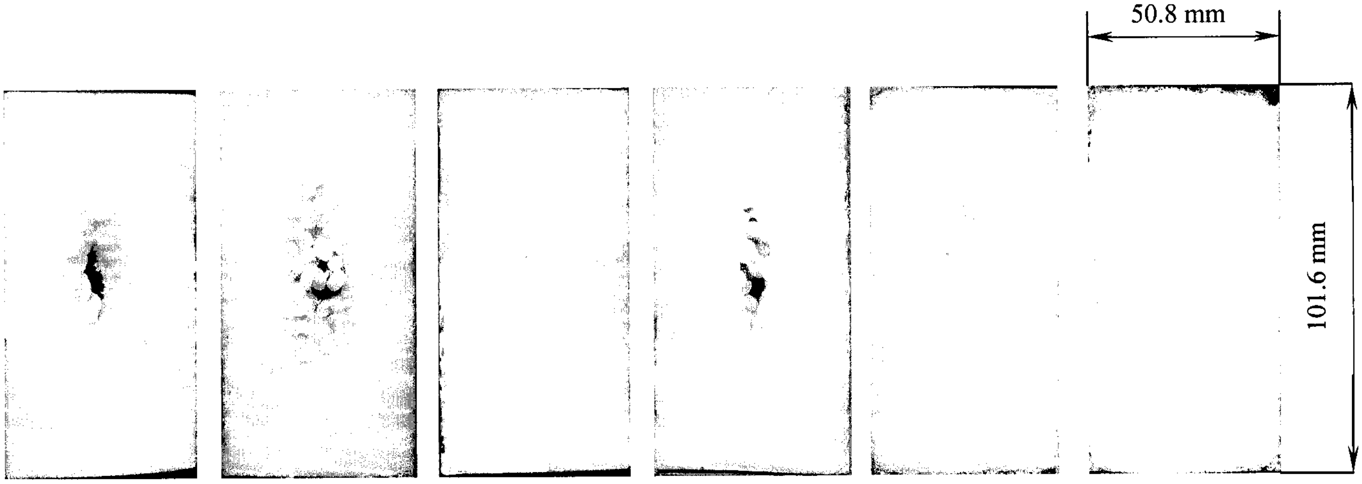

(a) t = 13 min (b) t = 14 min (c) t = 15 min (d) t = 16 min (e) t = 17 min (f) t = 18 min

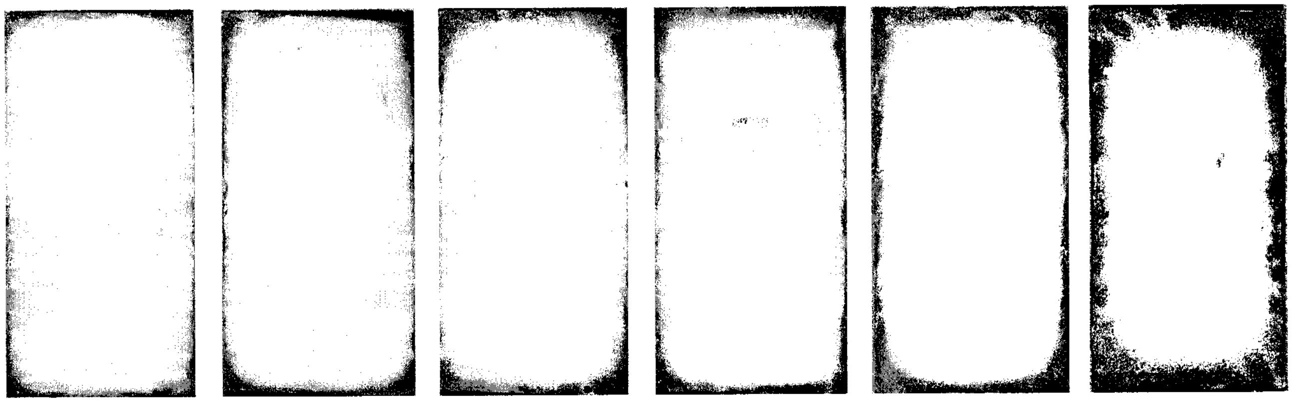

(g) t = 19 min (h) t = 20 min (i) t = 21 min (j) t = 22 min (k) t = 24 min (l) t = 25 min

Figure 7.4: Effect of heating time on the cell morphologies of rotationally foam molded skinless PE foams while implementing a constant oven temperature (T_{oven} = 300 °C = Const.) {Shot weight = 88 [g] (LL8556 + 3%wt Celogen OT); Mold rot. = 10 [rpm]; t_{cool} = 20 [min]}

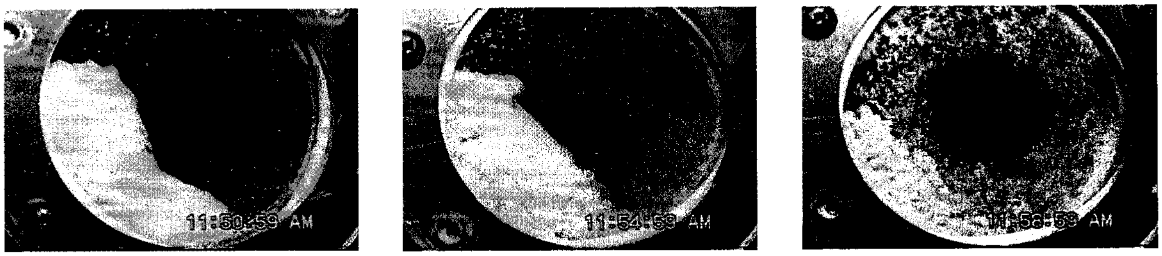

(a) t = 0 min: Powders & pellets tumbling

(b) t = 4 min: Powders adhering to wall

(c) t = 8 min: Pellets tumbling on skin

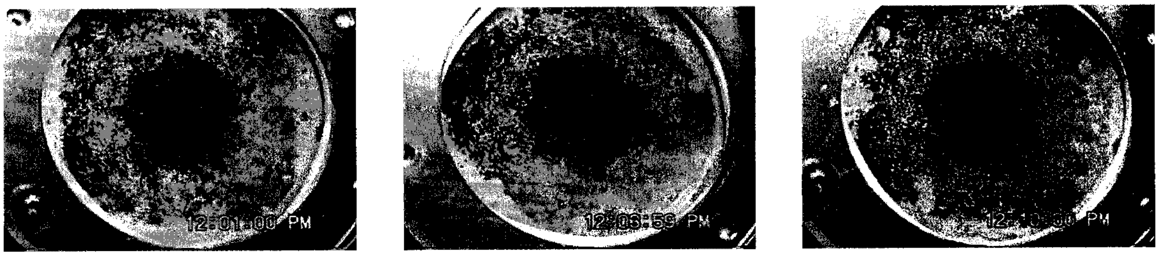

(d) t = 10 min: Pellets sticking and falling

(e) t = 13 min: Pellets adhered to skin

(f) t = 19 min: Pellets sintering

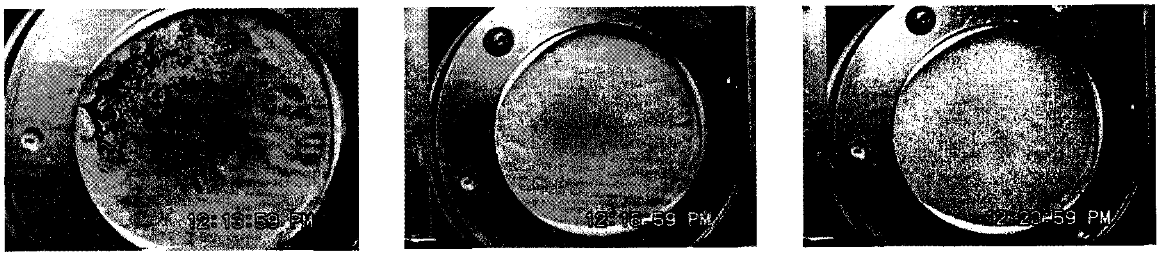

(g) t = 23 min: Pellets expanding

(i) t = 26 min: Foam layer expanding

(j) t = 31 min: Mold filled with foam

Figure 7.5: Representative snap-shots of the distinct phases of the single-charge rotational foam molding process for the manufacture of integral-skin cellular composites captured during the visualization of the process using a camcorder

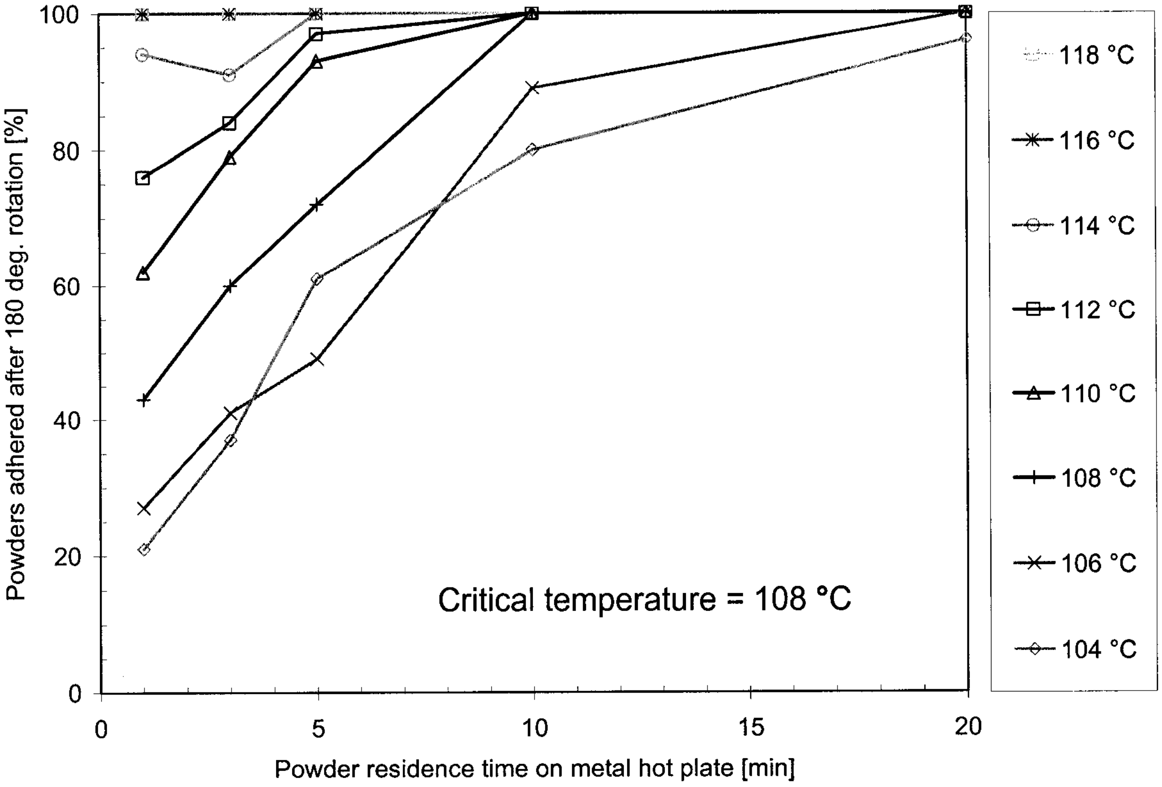

Figure 7.6: Graphical representation of the adherence behavior of non-foamable skin-forming Rotolite™ OS powders on a high-temperature rotating metal plate

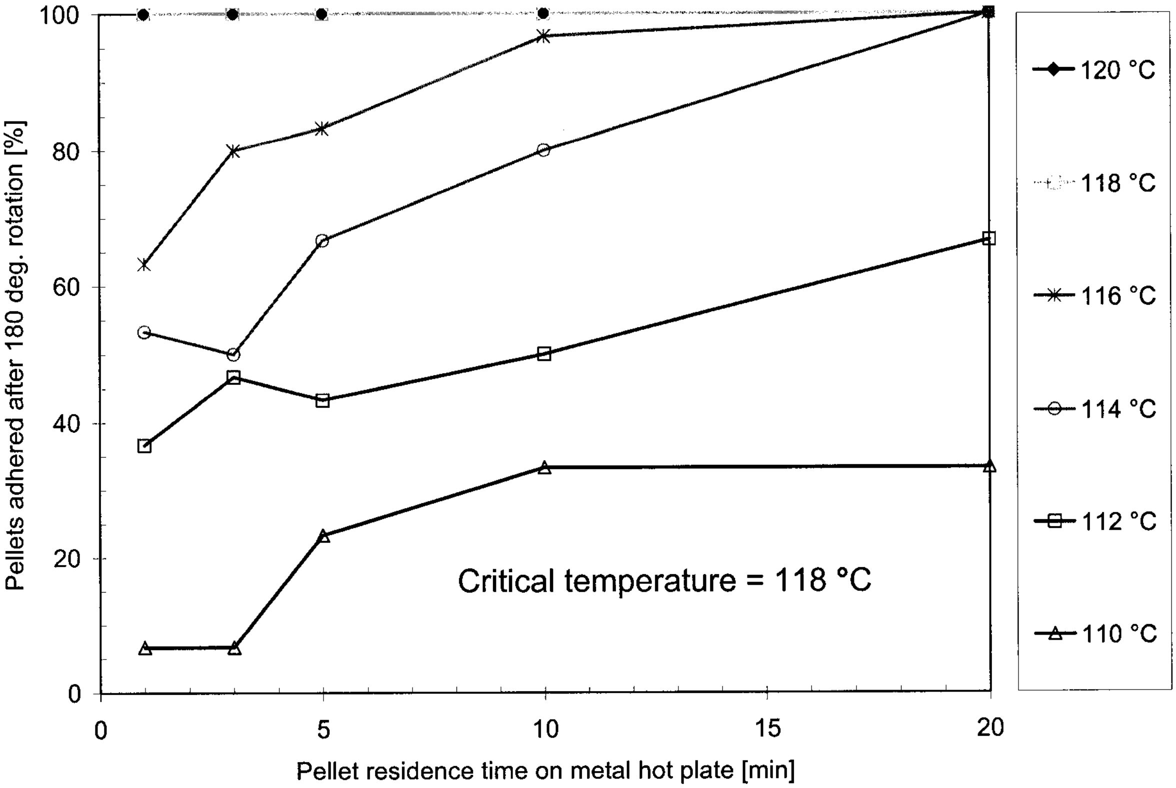

Figure 7.7: Graphical representation of the adherence behavior of foamable core-forming PE pellets on a high-temperature rotating metal plate

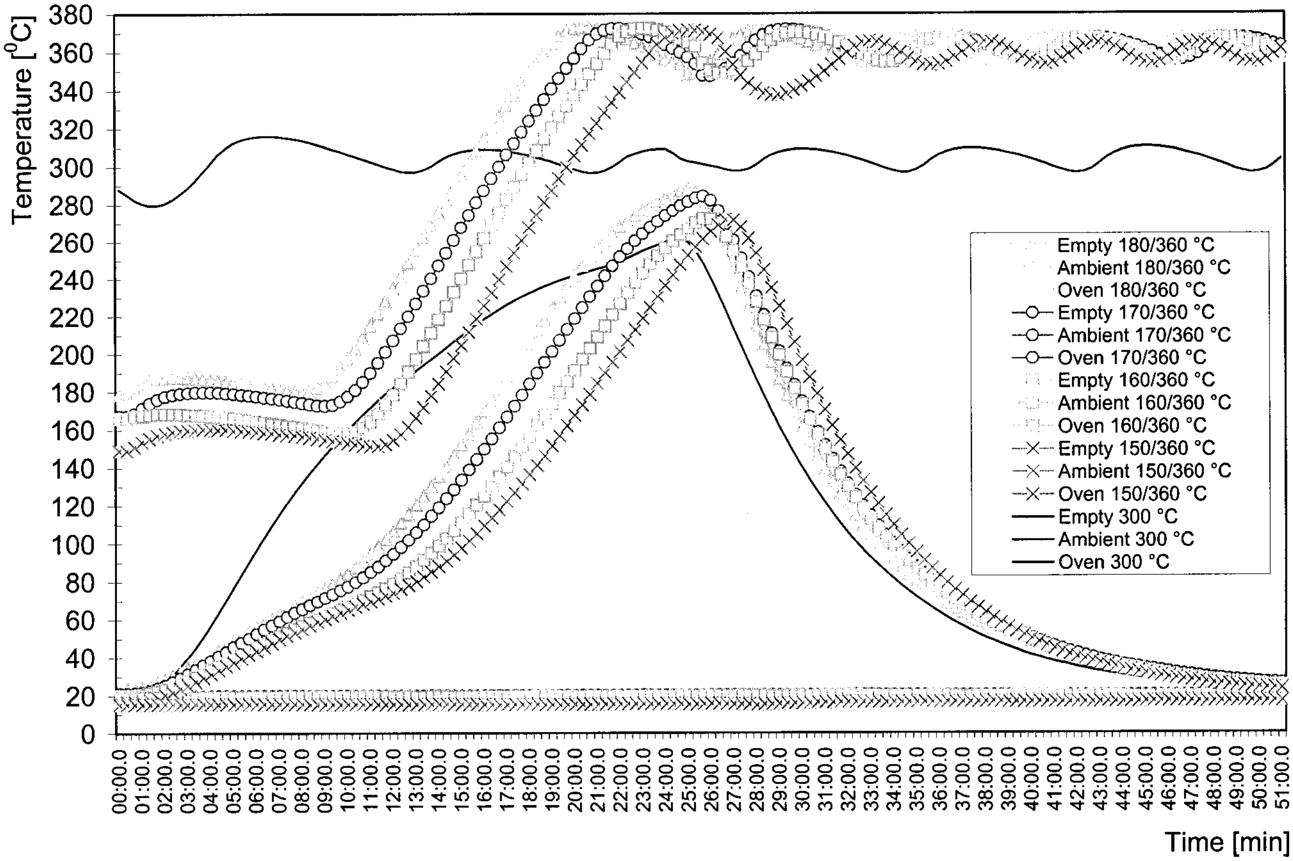

Figure 7.8: Comparison between a constant (T_{oven} = 300 °C) and various two-step oven temperature profiles and corresponding in-mold air temperatures at the center of an empty mold

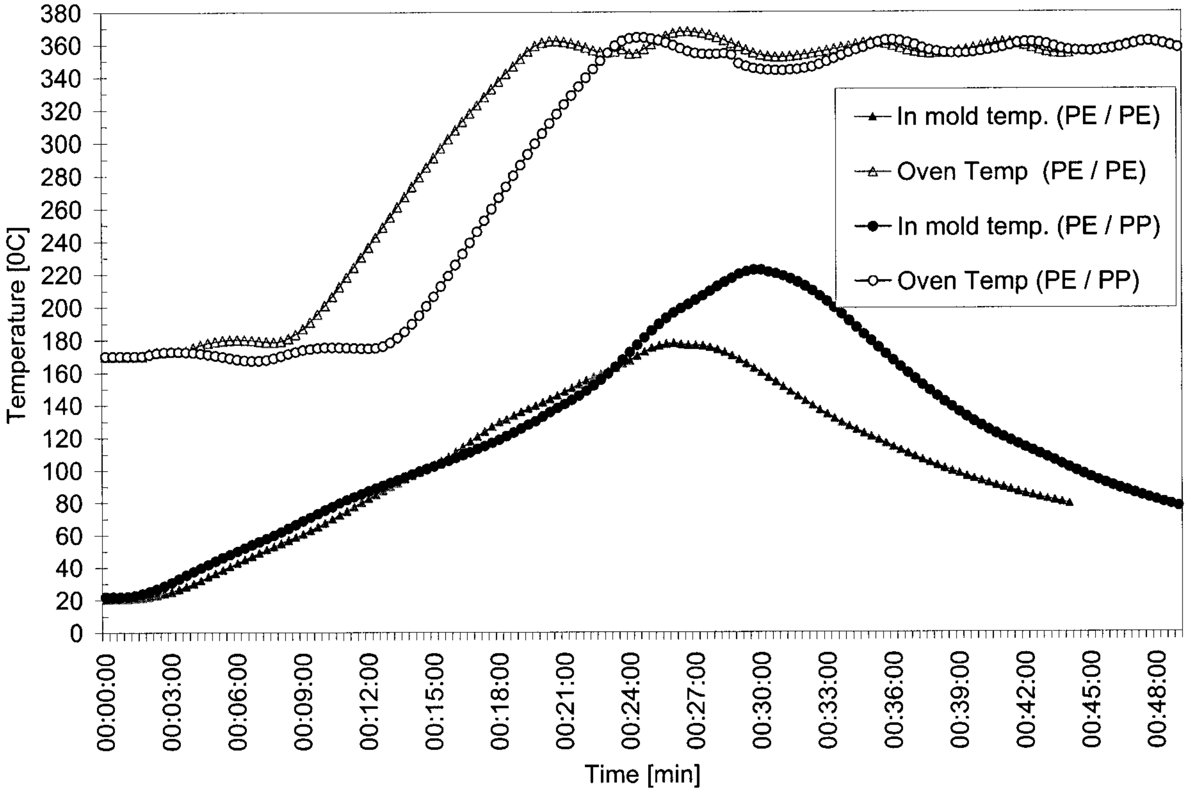

Figure 7.9: Optimized two step temperature profiles for PE/PE (8 [min] at 170 °C and 5 [min] at 360 °C; t_{heat} = 25 [min] at which T_{melt} = 175 °C) and PE/PP (12 [min] at 170 °C and 6 [min] at 360 °C; t_{heat} = 30 [min] at which T_{melt} = 222.5 °C) integral skin cellular composites

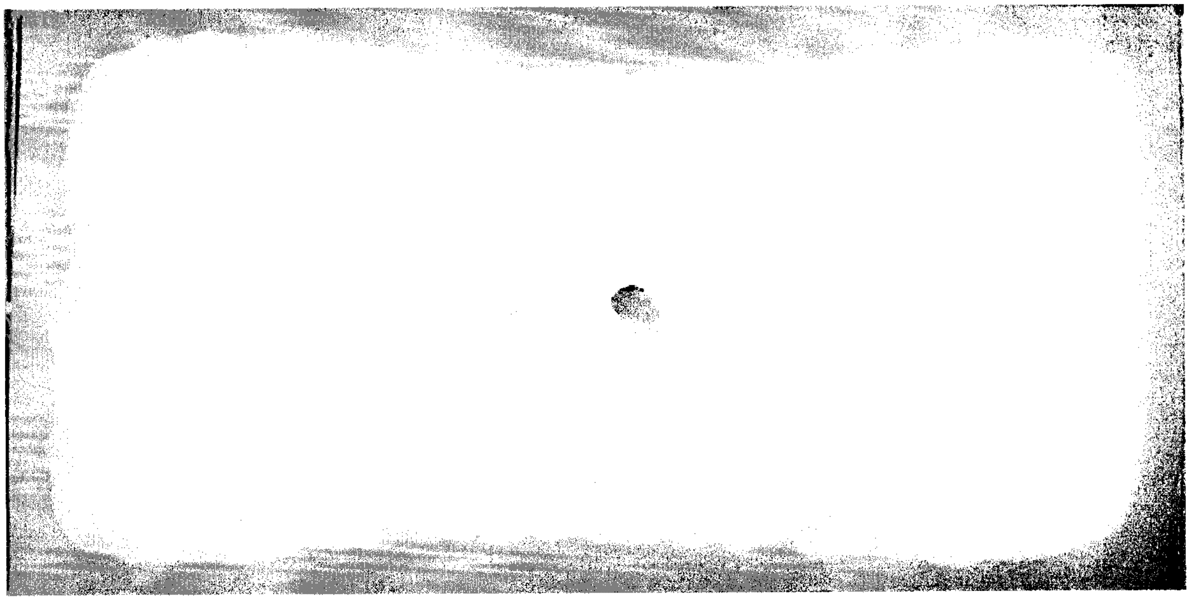

Figure 7.10: Typical improved morphology of the skin layer in integral-skin PE/PE foams processed using a multi-step temperature profile: 170 °C for 8 [min], ramp to 360 °C (~12 [min]), and 360 °C for 5 [min]

{t_{heat} = 25 [min]; Shot weight = 56 [g] Rotolite™ OS + 78 [g] (LL8556 + 3%wt Celogen OT); Mold rot. = 10 [rpm]; t_{cool} = 20 [min]}

Skin layer is missing because part of the sample was used for SEM.

Figure 7.11: Typical morphology of integral-skin PE/PP foams processed using a multi-step temperature profile: 170 °C for 12 [min], ramp to 360 °C (~12 [min]), and 360 °C for 6 [min] {t_{heat} = 30 [min]; Shot weight = 56 [g] Rotolite™ OS + 75.5 [g] (PF633 + 1.67%wt Celogen OT); Mold rot. = 10 [rpm]; t_{cool} = 20 [min]}

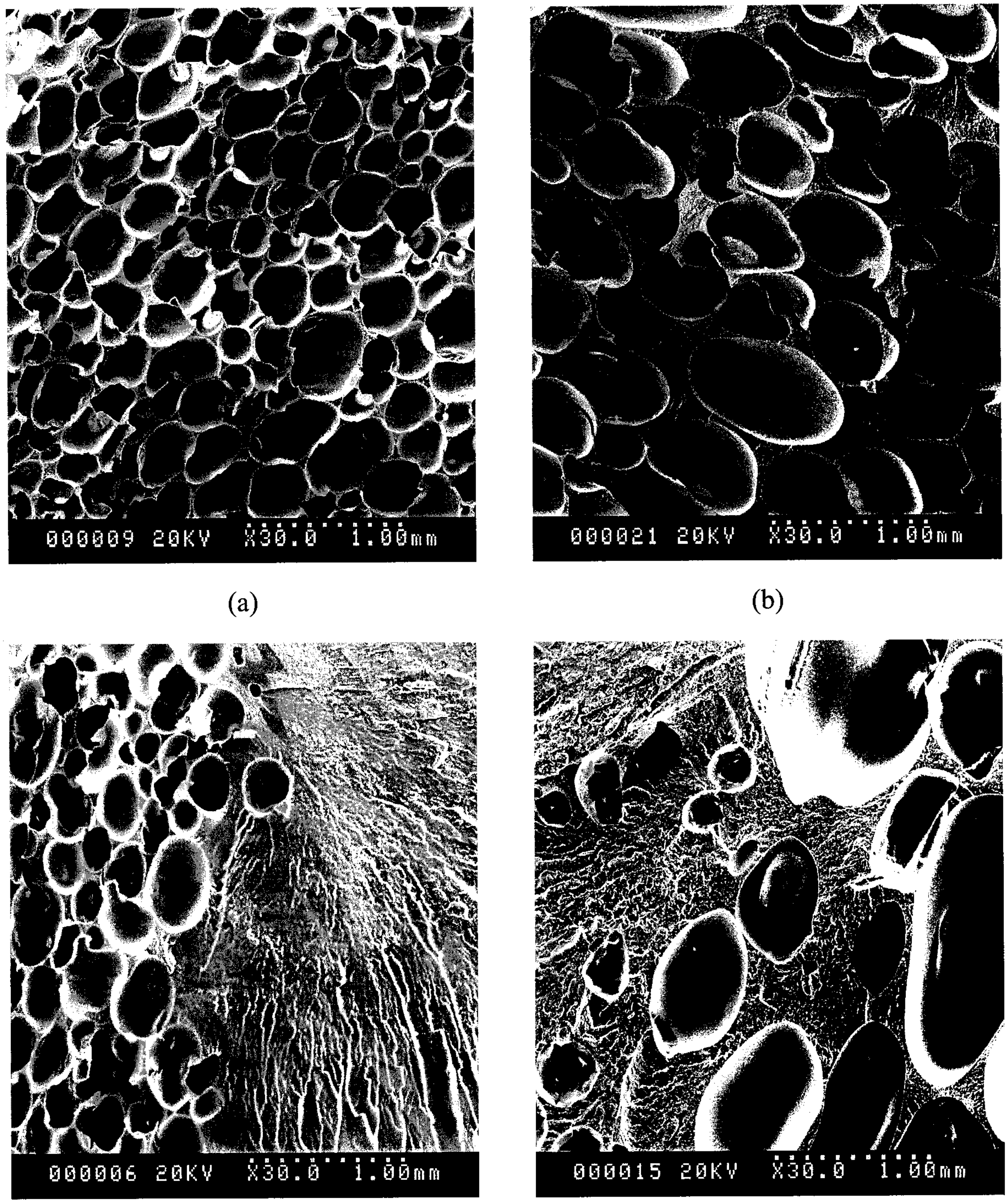

(a) (b)

(c) (d)

Figure 7.12: Typical SEM micrograms of integral-skin polyolefin integral-skin cellular composites processed using the single-charge rotational foam molding technology and a two-step oven temperature profile

(a) SEM of PE/PE foamed core

(b) SEM of PE/PP foamed core

(c) SEM of PE/PE solid skin-foamed core interface area

(d) SEM of PE/PP solid skin-foamed core interface area

CHAPTER 8

FUNDAMENTAL STUDY OF BUBBLE LIFESPAN IN ROTATIONAL FOAM MOLDING

8.1 Introduction

Conventionally rotomolded non-foamed hollow structures are susceptible to developing undesired surface pores (pin-holes) and internal voids (bubbles) on and within their walls, respectively. The former occurrence impairs the visual appearance of the product and could cause additional problems during its implementation, whereas the latter weakens the stiffness of the article [24].

To achieve article weight reduction and increased insulative properties without loss in stiffness, the rotational molding process often serves for the production of skinless cellular composites. However, instead of making voids disappear, it is then required to deliberately create controlled voids within the polymer matrix. Since this is not a trivial task, often articles of this kind exhibit unsatisfactory density reduction, inadequate cell size, or insufficiently uniform cell size and/or cell density distribution. This alters the molding's strength-to-weight and cost-to-performance ratios and limits its usefulness for a large number of applications.

For applications requiring robust moldings with additional stiffness, the rotational foam molding process may be also used for the manufacture of integral-skin cellular composites. Then, considering the above, it would be necessary to successfully manage a combination of two contrasted phenomena occurring within the same rotomolding cycle, i.e., the removal of unwanted pin-holes and bubbles formed on and within the solid skin, and the generation, growth, and retention of controlled cells throughout the adjacent foamed core. In addition, as indicated in Chapter 7, if the single-charge rotational foam molding technology would be implemented, it would be necessary to ensure that the adhesion of the non-foamable resin to the internal surface of the mold always completes prior to the activation of the foamable resin.

As it has been mentioned in Section 2.1, a considerable number of researches attempted to deal either with the bubble removal problem in conventional rotational molding or the problem of controlled cell generation and retention in rotational foam molding. Regrettably, only a few [46-57] made an effort to undertake fundamental studies that would develop an understanding of why and how bubbles are formed and what would be the optimal processing strategies for eliminating unwanted bubbles [46-51], or to explain the suitability of the rotational foam molding process to the mechanics of foaming [52-57]. However, all these works are in agreement with the statement that eliminating the unintentionally created bubbles during processing non-foamable polymers in conventional rotational molding is as difficult as to deliberately create controlled voids and then retain them during processing foamable polymers in rotational foam molding [52,53]. It is therefore clear that to process successfully non-foamable and foamable polymers in a simultaneous manner, such as in single-charge rotational foam molding production of integral-skin cellular composites, brings an even further increased level of difficulty. This may be one of the reasons why there are no published fundamental research studies focusing on the production of integral-skin cellular polymer composites in rotational foam molding.

8.2 Problem Formulation

It is well known that the ultimate goal in any closed-cell polyolefin foam production is to achieve the highest possible cell size distribution uniformity, cell size reduction, and cell density augmentation. It is also well known that the finest bubbles are formed when the gas is first dissolved in the polymer under pressure, and then allowed to form by lowering the pressure. However in atmospherically governed foaming systems the microcellular foaming technology does not work, so that the primary mechanism for producing the cells in rotational foam molding is the generation of microbubbles from decomposing CBAs. Thus, fine-celled foams (cell size < 100 [μm] and cell density $> 10^6$ [cells/cm^3]) are the most preferred cellular structures theoretically achievable in rotationally molded foams.

In deliberately developed rotationally foam molded cellular structures using a chemical blowing agent (CBA), a fine-celled morphology has been closely approached, but it has not been actually achieved yet. Also, it has never been clarified in a scientific manner whether a fine-celled morphology is actually achievable in rotational foam molding or not. This study will make an attempt to provide an answer to this fundamental scientific question.

8.3 Fundamental Barriers to Fine-cell Foaming in Rotomolding

There are four steps to bubble growth: nucleation, inertial bubble growth, diffusional bubble growth, and film-forming or terminal bubble growth [53]. In its most general terms, the polymer foaming process involves simultaneous nucleation and bubble growth in a highly non-Newtonian fluid. Any given polymer, combined with different blowing agents, and subjected to different process conditions can be foamed to produce "new cellular composites" having different densities, structures, and properties [208]. The amount of gas that can be dissolved in the polymer increases linearly with the applied pressure, and usually decreases with increasing the temperature [53]. However, polymers are poor conductors. When a polymer matrix expands to make a low-density foam, the cell walls become extremely thin, as thin as 50 μm. Thus, the gas-polymer system acts as a poor conductor [209].

The primary barrier to the development of a fine-celled morphology in rotational foam molding is attributed to the fact that the general rotational molding process is not especially favorable to efficient fine-cell foaming because of some unique inherent technical deficiencies that make it in many ways counter productive to the ideal conditions needed to establish a controlled fine-celled bubble growth and stabilization [52,53]. The most relevant reasons for this are discussed in greater detail below.

First, the polymer must be thoroughly molten and the sintering of pellets should be completed before the decomposition of the blowing agent is initiated [52,116]. Otherwise, part of the evolved blowing gas will cause premature bubble formation while the rest will escape through passages in-between the pellets and will be thereby lost to the environment so that poor or no foaming will be achieved [52,116]. However, in practice, because of slow sintering of the foamable resin that may be caused by high carrier resin viscosity or a too large pellet size, the decomposition of [52] the CBA particles dispersed throughout the foamable pellet may take place even before the sintering of the polymer material has been completed [116]. To prevent substantial blowing gas losses, it would be beneficial if the foamable pellet size could be reduced, and/or if a higher viscosity polymer could be selected [116].

Second, because the nature of the rotational foam molding process is purely atmospheric, bubbles are formed within the polymer melt as soon as the blowing agent decomposes. To prevent premature bubble formation during blowing agent decomposition, it would be beneficial if the polymer melt could remain under a sufficiently high pressure (>10 MPa or 1450 [psi]) [52].

Third, the temperature of the polymer melt continues to rise throughout the foaming process, thereby destabilizing the cellular structure and causing cell coalescence resulting in generating foams with coarser cells [52,58]. In addition, the increasing temperature intensifies the CBA gas loss to the environment thereby reducing the foaming efficiency [52]. Since the inertial rate of bubble growth is strongly dependent on polymer viscosity, it would be beneficial if the polymer melt temperature could be kept as low as possible during the foaming step in order to enhance the control of the diffusion-driven bubble growth and rapidly increase polymer melt viscosity and melt strength. Increasing the polymer melt viscosity reduces bubble growth rate and polymer drainage from the cell wall, thereby creating a favorable environment for producing fine-celled foams. This could be achieved by implementing CBA activators and/or reducing the oven temperature [52,58].

Fourth, the temperature of the polymer melt at the interface between the polymer and the internal mold surface is always significantly higher than that at the free surface. Consequently, the CBA decomposition and foaming is initiated near the mold surface rather than in the volume and the foaming process propagates inwards toward the free surface. Since bubble nucleation and initial growth do not take place simultaneously throughout the volume of the molten polymer mass, this non-uniform foaming contributes to low CBA efficiency, deteriorated cell morphology, and non-uniform cell distribution [52,210].

Fifth, the polymer close to the internal mold surface continues to be heated even after its foaming is completed simply because the interior polymer has yet to reach the decomposition temperature of the blowing agent. Consequently, in addition to cell coalescence, due to the continuing decrease in polymer viscosity, the foamed polymer at the mold surface is too hot to be stabilized by crystallization. Even when cooling is applied to the mold assembly, the recrystallization temperature takes place after several minutes, during which time bubble coalescence and collapse continuously takes place [52,58].

In summary, in rotational molding when the temperature of the melt should be decreasing to ensure ideal foaming conditions, it is increasing, whereas when elevated pressure is needed to support ideal gas generation and dissolution, there is no pressure [53].

8.4 Bubble Shrinkage

As it has been already indicated in Chapter 7, a typical, well controlled, single-charge rotational foam molding process for manufacturing integral-skin cellular composites should consist of a sequence of processing segments which include: (i) charging the mold with solid skin-forming polymer powders and foam core-forming foamble pellets, (ii) inserting the rotating mold into a hot oven, (iii) sintering and densification of the non-foamable resin introduced in a powder form to form a skin layer, (iv) subsequent sintering of the foamable resin introduced in a pellet form located on top of the formed skin, (v) decomposition of the CBA particles dispersed throughout the foamable pellets which results in nucleation of a dense population of gas clusters and growth of the nucleated bubbles in the polymer to their equilibrium size, (vi) intensive polymer foaming and foam propagation from mold's periphery towards the mold center, and (vii) quenching of the foamed material to permanently fix the structure.

Kelly [46], observed that the air bubbles trapped in the polymer during melting decrease in diameter as the melt temperature increases. The high viscosity of the melt prevents the movement of the bubbles. At a high enough melt temperature, the air in the bubbles begins to dissolve into the polymer. Since oxygen has about twice the solubility of nitrogen in polyethylene, at high temperatures, the oxygen is further depleted by direct oxidation reactions with polyethylene. The depletion of oxygen reduces the bubble diameter. The laws of surface tension dictate that the pressure inside the bubble has to increase as the diameter decreases. The increase in pressure reduced and this chain of events repeats until the bubble disappears. As the cycle time increases, the size and quantity of bubbles decrease.

Bellehumeur [49], suggested that when the mold reaches the polymer melting temperature, a layer of molten polymer appears in the mold. Once a layer of particles adheres and melts onto the mold surface, the sintering process takes place until an additional layer of powder melts onto the previous layer. At this point, air pockets are entrapped between the particles and will in turn form bubbles. The initial size of the bubbles formed in the melt is primarily controlled by the powder particle size and the degree of sintering achieved before pockets of air are trapped in the melt. The bubbles further reduce in size by the diffusion of air to the polymer melt.

Kontopoulou and Vlachopoulos [154], observed that it is inherent to the rotomolding process that, as the melt front progresses, the air pockets that have been entrapped inside the melt eventually become bubbles that will be subjected to diffusion controlled shrinkage and eventual disappearance.

8.5 Hypothesis

It has been observed that the control of the cell size of rotationally molded foams might be aggravated by some unique inherent process limitations. It is therefore hypothesized that in rotational foam molding the CBA-blown bubbles having cell sizes less than 100 [μm] shrink and ultimately dissolve before the time at which the non-pressurized viscous polymer melt is cooled to its crystallization temperature thereby precluding the formation of fine-celled foam morphologies.

8.6 Bubble Lifespan Observed in Hot-stage Optical Microscopy

The custom-build hot-stage optical microscopy computerized digital imaging experimental setup presented in Figure 4.12 served for investigating the transformations occurring during the cell growth of CBA-blown bubbles in non-pressurized PE melts. During the experimentation, pre-compounded foamable samples of LL8556 + 3%wt Celogen OT have been heated at a desired rate and temperature profile and the foam development was observed and recorded using a CCD camera. These hot stage optical microscopy experimental results revealed that the bubble lifespan consists of three distinct phases: (i) pre-CBA, (ii) CBA, and (iii) post-CBA decomposition governed.

The pre-CBA decomposition phase corresponds with melt temperatures higher than the melting point of the PE resin (e.g., ~126 °C for LL8556) but below the decomposition temperature of the CBA (e.g., ~158-160 °C for Celogen OT). In this phase, there are some randomly distributed bubbles throughout the melt, which origins might be either entrapped air pockets during sintering and polymer densification or CBA pre-decomposition during melt compounding, or both. Also, it is believed that some of the initial bubbles are being nucleated due to the presence of the CBA particles in this phase acting as a nucleating agent. As the temperature increases, bubbles begin to interact, gas concentration gradient driven diffusion takes place, and thus, some of the bubbles grow on the account of the shrinkage and eventual disappearance of the surrounding ones. Thereby, a reduced number of larger bubbles live long enough to participate in the second phase. Figure 8.1 illustrates this phase.

The CBA decomposition phase commences at the time when the CBA becomes activated and the CBA particles dispersed throughout the melt begin to decompose. Since their sizes vary, and since some are agglomerated, they have different bubble-generation abilities so that while some particles form new bubbles some of them only increase the concentration of gas in the molten polymer matrix which busts further the growth of the surviving bubbles from the first phase. For the newly created bubbles, since the time of CBA gas evolution is very short (comparable to a small explosion), the volume of the bubble almost doesn't change at all for this short time period due to the resistance to bubble volume changes caused by the viscoelastic response of the surrounding polymer melt acting on the bubble wall. As the time progresses, the pressure-governed bubble overcomes this resistance. The resulting effect is an oscillatory bubble behavior, which is exposed to dissipative losses caused by the viscosity of the polymer melt, while the elasticity is associated with the gas contained in the bubble [178]. The effect of viscosity is most pronounced for small bubbles [178]. As the bubble volume increases, the gas concentration and inside pressure in the bubble drops until a temporary equilibrium is reached. Then the third and last phase of bubble growth commences. Figure 8.2 illustrates this phase.

The post-CBA decomposition phase includes the continued rise of the temperature of the polymer melt to the maximum process value (e.g., ~220 °C) and lasts up to the time when the polymer cools up to its temperature of crystallization (e.g., ~114 °C). The gas diffusion in or out becomes dominant during this phase. As a result, initially, the bubble continues to grow thereby depleting the gas concentration of the surrounding polymer up to the point at which the direction of gas diffusion is directed out of the bubble. As a consequence, the bubble shrinks. The reduced temperature of the polymer stabilizes the bubble after which it becomes permanently frozen at the peak crystallization temperature of the polymer. Figure 8.3 illustrates this phase.

8.7 Modeling Bubble Lifespan

The bubble growth mechanism in an infinite polymeric liquid can be described by a standard group of governing equations that include: (i) the momentum equation (ii) the mass balance equation over the bubble, and (iii) the gas diffusion equation in the surrounding polymer melt [48,50,100,178,197,211-217]. Based on the bubble dissolution model developed by Kontopoulou and Vlachopoulos [48], two simplified models, a Newtonian and a viscoelastic, have been developed to describe, simulate, quantify, and compare the lifespan of CBA-blown bubbles in rotational foam molding. To facilitate the development of these models the following basic assumptions had to be made beforehand:

1) Although in reality a great number of bubbles are formed in the polymer melt during rotational foam molding, this model will be related to a single CBA-blown gas bubble in an infinite isothermal non-pressurized PE melt. Figure 8.4 illustrates the bubble geometry.

2) It is assumed that the bubble has a spherical geometry.

3) A unidirectional flow in the direction of the bubble radial coordinate, r, is assumed.

4) A constant polymer density, ρ [kg/m^3], is assumed.

5) The kinematics of the problem are satisfied by the continuity equation, which for spherical symmetry, unidirectional flow in the r direction, a constant density, ρ, and by using the boundary condition that the bubble wall velocity, v_r [m/s], at $r = R$ is $v_r = dR/dt$ can be simplified to the relationship expressed as: $v_r = \frac{R^2}{r^2}\dot{R}$.

8.7.1 Momentum Equation

The dynamics of the system assumed above are governed by the conservation of momentum in the radial direction. The integrated momentum equation can be written as follows [48]:

$$P_g - P_\infty - \frac{2\sigma}{R} + 2\int_R^\infty \frac{\tau_{rr} - \tau_{\theta\theta}}{r}dr = 0 \qquad (8.1)$$

8.7.1.1 Momentum Equation for Newtonian Fluid

For a Newtonian liquid, since the stress components depend on the rate of deformation, the following equations are valid [48]:

$$\begin{aligned} \tau_{ij} &= \mu\Delta_{ij} \\ \Delta_{rr} &= -\frac{4R^2\dot{R}}{r^3} \\ \Delta_{\theta\theta} &= \frac{2R^2\dot{R}}{r^3} \end{aligned} \qquad (8.2)$$

Where, τ_{ij}, represents the ij-th components of the stress tensor [Pa], whereas, Δ_{ij}, represents the ij-th components of the rate of deformation tensor [s^{-1}]. Thus, the momentum Equation (8.1) after rearranging and naming $P_\infty = P_f$ will become [48]:

$$\dot{R}=\frac{1}{4\mu}\left[\left(P_g-P_f\right)R-2\sigma\right] \tag{8.3}$$

where: R = Radius of the bubble [m]

μ = Viscosity of the polymer [Pa s]

P_g = Gas pressure inside the bubble [Pa]

P_f = Pressure in bulk of polymer melt [Pa]

σ = Surface tension [N/m]

8.7.1.2 Rheological Equation for Viscoelastic Fluid

Maxwell model [214-216]:

$$\tau+\frac{\eta}{G}\frac{d\tau}{dt}=-\eta\dot{\gamma} \tag{8.4}$$

Dewitt Model [218,219,221]:

$$\underset{\approx}{\tau}+\lambda\frac{D\underset{\approx}{\tau}}{Dt}=2\eta_0\underset{\approx}{d} \tag{8.5}$$

The Dewitt viscoelastic model has been selected to be included in the further development of the model. Appendix 1 provides derivation details of how it can be used for the calculation of the radial and θ direction stresses participating in Equation (8.1).

8.7.2 Mass Balance Equation

In order to determine the rate of growth/dissolution of the bubble from Equation (8.3) it is necessary to obtain a relationship for the gas pressure inside the bubble. For this purpose, the principle of conservation of mass has to be applied for the gas inside the bubble. By assuming that the buildup of adsorbed gas on the bubble wall is negligible, the rate of change of the amount of gas within the bubble can be equalized with the rate of diffusion of gas from/into the bubble across its wall towards/from the liquid. Hence, by assuming that the gas inside the bubble is ideal, i.e., $P_g=\frac{nR_gT}{V}$, Equation (8.6) can be obtained [48,50,213-217]:

$$\frac{4}{3}\pi\frac{d}{dt}\left(\frac{P_g}{R_gT}R^3\right)=4\pi R^2D\left(\frac{\partial c}{\partial r}\right)\Big|_{r=R} \tag{8.6}$$

Where: R_g = Universal gas constant = 8.3143 [Pa m^3 mol^{-1} K^{-1}]

T = Temperature [K]

D = Diffusion coefficient [m^2/s]

V = Bubble volume [m^3]

c = Concentration [mol/m^3]

8.7.3 Diffusion Equation

To solve Equation (8.6) the concentration profile in the liquid has to be known. This can be determined by solving the complete diffusion equation for the liquid surrounding the bubble, which for spherical coordinates reduces to the following relationship [48]:

$$\frac{\partial c}{\partial t}+\dot{R}\frac{R^2}{r^2}\frac{\partial c}{\partial r}=\frac{D}{r^2}\frac{\partial}{\partial r}\left(r^2\frac{\partial c}{\partial r}\right) \tag{8.7}$$

Equation (8.7) can be solved subject to the boundary and initial conditions below [48]:

$$c(r,0)=c_i, r>R$$
$$c(\infty,t)=c_i, t>0$$
$$c(R,t)=c_w=K_hP_g$$

The concentration of gas dissolved initially in the polymer melt can be assumed [48]:

$$c_i=x(c_i)_{sat}=xK_hP_f$$

Where: t = Time [s]

c_i = Concentration of gas in bulk of polymer melt [mol/m^3]

c_w = Concentration of gas at bubble liquid interface [mol/m^3]

$(c_i)_{sat}$ = saturation concentration of gas in bulk of polymer melt [mol/m^3]

x = Degree of gas saturation in the polymer melt

K_h = Henry's Law constant [mol/(m^3 Pa)]

8.7.4 Estimation of Physical Constants

1) Diffusivity [197]:

$$D=D_0\exp\left(-\frac{E_d}{R_gT}\right) \tag{8.8}$$

Where: D = Diffusion coefficient [m^2/s]

D_0 = Pre-exponential function (an empirical constant) [m^2/s]

E_d = Activation energy of diffusion [kcal/mole]

D_0 and E_d for nitrogen in PE are [197]:

$$D_0 = 53.414\times10^{-9}\left[m^2/s\right]$$
$$E_d = 2.0\left[kcal/mol\right]$$

Then, the diffusion coefficient, D ,of nitrogen in PE at 190 °C can be calculated as follows:

$$D = D_0\exp(-\frac{E_d}{R_gT}) = 53.414\times10^{-9}\times\exp\left(-\frac{2000\times4.187}{8.314\times463.15}\right) = 6.04\times10^{-9}\left[m^2/s\right]$$

2) Henry's law constant [197]:

$$K_h = H_0\exp(-\frac{E_s}{R_gT}) \qquad (8.9)$$

Where: E_s = Heat of solution [kcal/g mole]

For nitrogen in PE, the Henry's law constant, K_h, is: 0.111 [cm^3(STP) /g atm] [197]. Hence, at 190 °C, it would be:

$$K_h = \frac{0.111\times10^{-3}/22.4}{1.01325\times10^5}\times\rho_{PE,190^\circ C} = 3.71\times10^5\left[{mol}/{m^3Pa}\right]$$

3) Surface Tension [42]:

$$\sigma = 0.026\left[N/m\right]$$

4) Zero Shear Viscosity:

By using experimental data for LL8556 at 190 °C the zero shear viscosity is determined to be: $\eta_0 = 1431.99\left[Pa\cdot s\right]$

8.7.5 Initial Conditions

1) Initial Bubble Diameter

Since in rotational foam molding the bubbles are generated by the blowing gases evolved as a result of the decomposition of the CBA particles dispersed throughout the polymer matrix, the initial diameter of the bubble is determined by the CBA particle size. The average particle size of Celogen OT that was used in the experimentation was 3 [μm]. Thus, if the geometry of the CBA particle is assumed to be cubic, than the bubbles that have been generated by a single (3×3×3 [μm]) CBA particle would assume an initial diameter of 3.72 [μm]. Similarly, the bubbles that have been generated by a medium agglomerated (9×9×9 [μm]) CBA particle would assume an initial diameter of 11.16 [μm], while bubbles that have been generated by a largely agglomerated (15×15×15 [μm]) CBA particle or a cluster of particles would assume an initial diameter of 18.61 [μm].

2) Gas Releasing Ability of CBA Particles

It has been assumed that the gas releasing ability of the CBA particle is proportional to its mass. Thus:

(i) For a single (3×3×3 [μm]) CBA particle it can be calculated that:

$$n = \frac{PV}{R_g T} = \frac{1.01325 \times 10^{5} \times 6.70 \times 10^{-15}}{8.3143 \times 433.15} = 1.884 \times 10^{-13} [mole] \qquad (8.10)$$

(ii) For a medium (9×9×9 [μm]) CBA particle $n = 5.087 \times 10^{-12} [mole]$

(iii) For a large (15×15×15 [μm]) CBA particle $n = 2.355 \times 10^{-11} [mole]$

3) Initial Bubble Pressure

It has been assumed that the CBA particle decomposes and evolves the respective amount of gas instantaneously. As a result, the pressure of the gas within the bubble will suddenly increase. This increase can be calculated by using the gas state equation:

$$P_g = \frac{nRT}{V} = \frac{1.884 \times 10^{-13} \times 8.3413 \times 463.15}{\frac{4}{3}\pi \times \left(1.5 \times 10^{-6}\right)^3} = 5.13 \times 10^{7} [Pa] \qquad (8.11)$$

Due to this sudden increase of the pressure inside the bubble, the concentration of gas inside the bubble will also suddenly increase to a very high level. As a result, the gas will tend to diffuse out of the bubble towards the lower concentration area, i.e., in the surrounding polymer. However, with the previously assumed boundary condition based on Henry's law, the gas concentration at the interface of gas-liquid will be extremely high. If we still use the diffusion-dependent equation to solve the gas concentration in the polymer melt, the gas concentration in the polymer near the boundary might be very high, i.e., much higher than its saturation level at atmospheric pressure. Therefore, it might be necessary to determine the pressure profile from the bubble wall to a certain arbitrary located boundary within the polymer melt. Appendix 2 clarifies the significance of the pressure profile of the polymer on the accuracy of the model prediction. It indicates that for a Newtonian fluid taking into account the pressure profile would not improve the accuracy of the model prediction.

8.7.6 Numerical Solution and Model Implementation

A numerical method, using a finite difference discretization and a forward Eulerian scheme is implemented to solve the partial differential equation (Diffusion equation). Also, the Runge-Kutta method was used to solve the differential equation group.

8.7.6.1 Solution Procedure for Newtonian Model

Step 1) Establishing the equation group:

$$\dot{R} = \frac{1}{4\mu}\left[\left(P_g - P_f\right)R - 2\sigma\right] \tag{8.12}$$

$$\frac{4}{3}\pi\frac{d}{dt}\left(\frac{P_g}{R_g T}R^3\right) = 4\pi R^2 D\left(\frac{\partial c}{\partial r}\right)\Big|_{r=R} \tag{8.13}$$

$$\frac{\partial c}{\partial t} + \dot{R}\frac{R^2}{r^2}\frac{\partial c}{\partial r} = \frac{D}{r^2}\frac{\partial}{\partial r}\left(r^2\frac{\partial c}{\partial r}\right) \tag{8.14}$$

Step 2) The concentration gradient $\frac{\partial c}{\partial r}\big|_{r=R}$ can be determined for the first time increment by solving the diffusion equation, i.e., Equation (8.14).

Step 3) Once $\frac{\partial c}{\partial r}\big|_{r=R}$ has been set, the new values of the pressure inside the bubble as well as the bubble diameter at the end of the time increment can be determined by solving Equations (8.12) and (8.13) simultaneously.

Step 4) Using the most recent value of bubble pressure, the gas concentration at the liquid-gas interface can be calculated by using Henry's law. Then, the new bubble diameter and gas concentration profile in the polymer melt can be calculated by repeating Steps 2 and 3 till the bubble diameter reaches values that tend to zero.

8.7.6.2 Solution Procedure for Viscoelastic Model

Step 1) Establishing the equation group:

$$P_g = P_\infty + \frac{2\sigma}{R} - 2\int_R^\infty \frac{\tau_{rr} - \tau_{\theta\theta}}{r}dr \tag{8.15}$$

$$\frac{4}{3}\pi\frac{d}{dt}\left(\frac{P_g}{R_g T}R^3\right) = 4\pi R^2 D\left(\frac{\partial c}{\partial r}\right)\Big|_{r=R} \tag{8.16}$$

$$\frac{\partial c}{\partial t}+\dot{R}\frac{R^2}{r^2}\frac{\partial c}{\partial r}=\frac{D}{r^2}\frac{\partial}{\partial r}\left(r^2\frac{\partial c}{\partial r}\right) \tag{8.17}$$

Step 2) The concentration gradient $\frac{\partial c}{\partial r}|_{r=R}$ can be determined for the first time increment by solving the diffusion equation, i.e., Equation (8.17).

Step 3) It is now necessary to solve rheological equations that have been introduced and discussed in Appendix 1 to get the radial and θ direction stress at every grid. Then, by integrating, the bubble pressure can be calculated from Equation (8.15). It is useful that for the first time increment the bubble changing speed is assumed to be zero. The pressure change rate, i.e., the difference between the newly calculated pressure and the pressure pertaining to the previous time interval divided by the time interval, could be then readily calculated. .

Step 4) Knowing the value of $\frac{\partial c}{\partial r}|_{r=R}$ and the pressure change rate the new bubble diameter could be calculated by solving Equation (8.16).

Step 5) Steps 2 to 4 should be repeated till the bubble diameter approaches zero.

8.8 Results and Discussion

Figures 8.5 and 8.6 illustrate graphically a comparison between the typical trends exhibited during the simulation of the lifespan of CBA-blown bubbles in rotational foam molding referring to a PE (LL8556) foamable resin that has been pre-compounded with 3%wt of Celogen OT. In particular, each of these figures demonstrates a comparison of the lifespan of three bubbles generated by three differently sized CBA particles, i.e., (3 × 3 × 3) [μm], (9 × 9 × 9) [μm], and (15 × 15 × 15) [μm], that has been simulated by implementing both the Newtonian and viscoelstic models developed for this purpose. It is important to note that both the Newtonian and viscoelastic models simulated for all three distinct CBA particle sizes that are presented in Figure 8.5 assume a lower concentration of gas in the surrounding polymer (e.g., x = 0.95) than that of the respective models simulated for respective CBA particle sizes presented in Figure 8.6 (e.g., x = 0.995).

As it was already indicated by the observation of the experimental result obtained by hot-stage optical microscopy, regardless of the conditions assumed the typical curve of the bubble lifetime consists of two characteristic parts and a peak. The first monotonically increasing part of the curve with a very high slope corresponds with the growth of the bubble diameter as a result of the evolved blowing gas by the decomposition of the CBA particle. This part of the curve is barely visible on the plots, especially those curves referring to smaller particle sizes, because the time of blowing gas generation is extremely short (less than 1 [s]). The peak indicates that the gas-generation ability of the CBA has been exhausted and that equilibrium has been reached so that from that point the bubble diameter would not increase any more and the bubble should start to shrink. The shrinking behavior of the bubble represents the second monotonically decreasing part of the curve which slope depends on the CBA particle size, the gas concentration in the surrounding polymer and the nature of the polymer melt (Newtonian or viscoelastic).

In this context, it can be observed from the plots shown in Figures 8.5 and 8.6 that:

1) For all investigated simulation conditions, the lifetime of the respective bubbles was significantly longer when assuming the higher gas concentration because thereby the difference in gas concentration between the bubble and the surrounding polymer, which is the driving force for diffusion, was slowed down so that the diffusion of the gas out of the bubble during the shrinking stage was taking more time.

2) For both cases of assumed gas concentration in the surrounding polymer the smaller the CBA particle the shorter the lifespan of the bubble was.

3) For all investigated simulation conditions, the viscoelastic nature of the polymer melt was detrimental to the bubble lifespan in comparison with the respective lifespan if assuming a Newtonian fluid.

4) Even if assuming the most favorable conditions (Newtonian fluid and $x = 0.995$) the lifetime of a ~100 [μm] bubble would be less than 140 [s], which prevents fine-celled foams to be preserved till the end of any kind of rotomolding cycle.

8.9 Summary

Both optical microscopy and simulation results indicated that it would be very difficult to generate the preferred fine-celled bubbles in rotational foam molding. It has been shown that the lifespan of fine-celled bubbles is significantly shorter than the inherently lengthy heating portion of the rotational molding process, so that fine-celled bubbles seldom reach the solidification stage of the cycle, which implies that only coarser-celled bubbles live long enough to participate in the final cellular structure. Thereby, the hypothesis established in Section 8.5 should be accepted as valid.

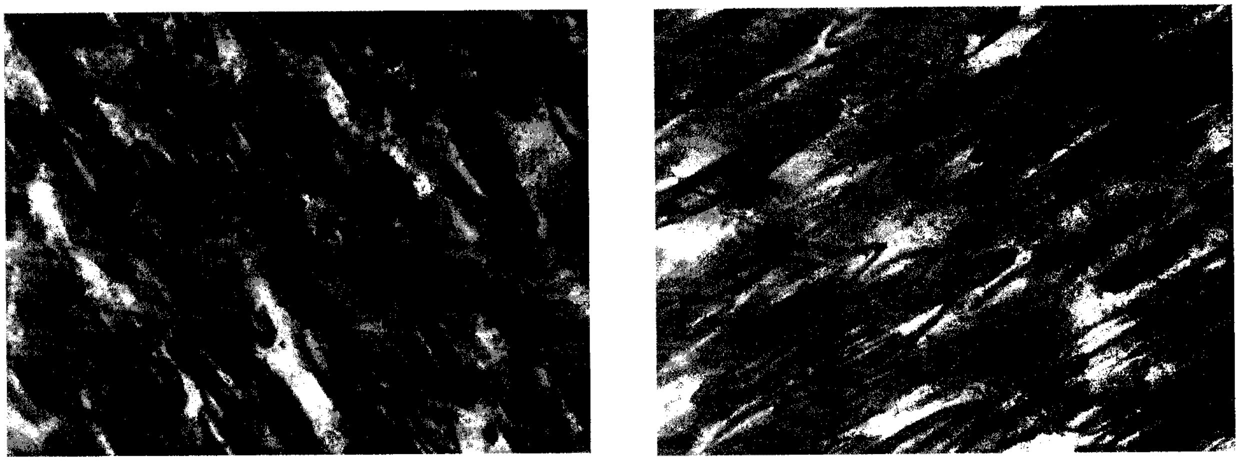

(a) T = 120 °C

(b) T = 130 °C

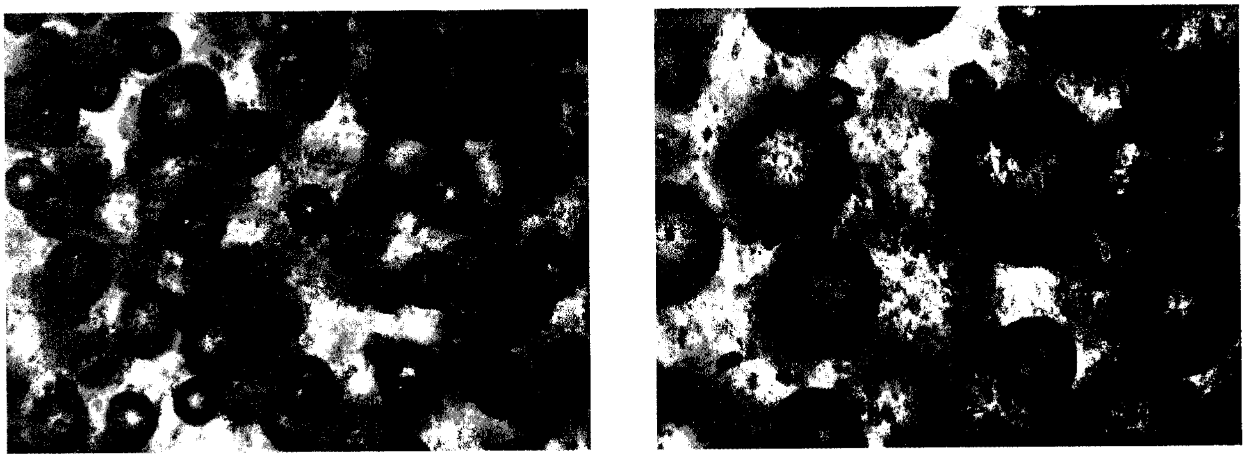

(c) T = 140 °C

(d) T = 145 °C

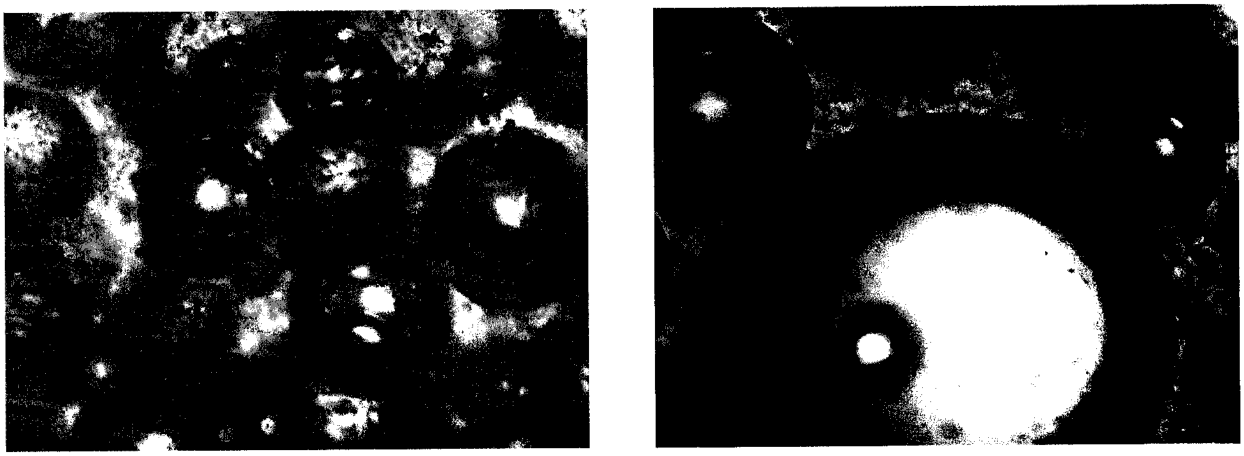

(e) T = 150 °C

(f) T = 155 °C

Figure 8.1: Typical hot-stage optical microscopy images of the pre-CBA decomposition governed phase of pre-compounded PE (LL8556 + 3%wt Celogen OT) foamable resins

Sample size = 0.75 × 0.55 [mm]

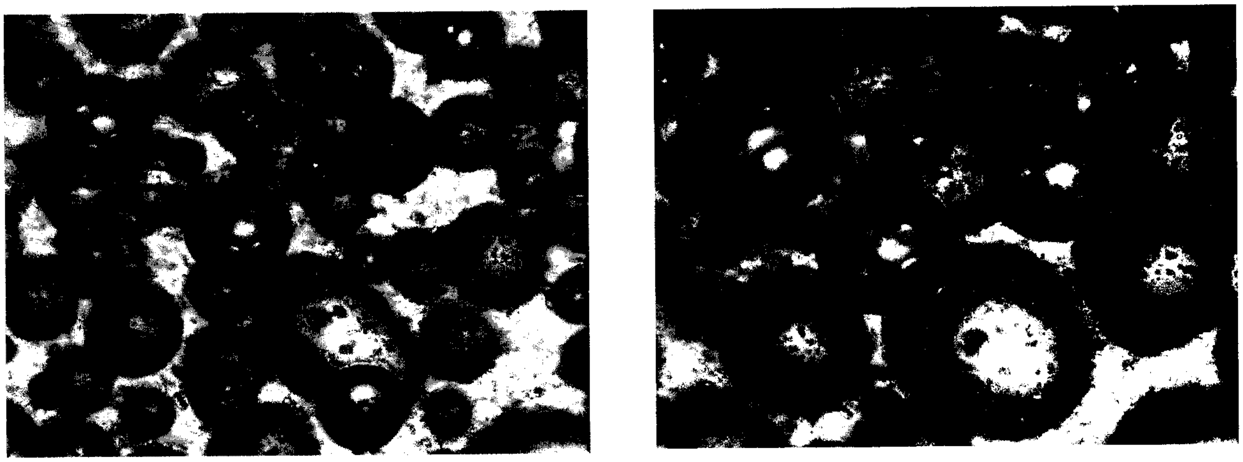

(a) T = 160 °C; t = 1 [min]

(b) T = 160 °C; t = 2 [min]

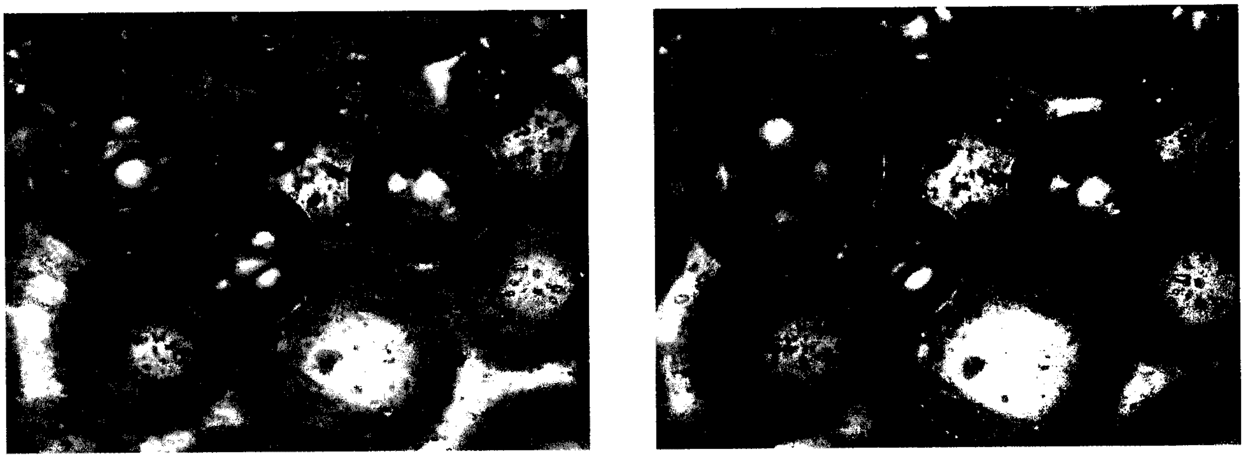

(c) T = 160 °C; t = 3 [min]

(d) T = 160 °C; t = 4 [min]

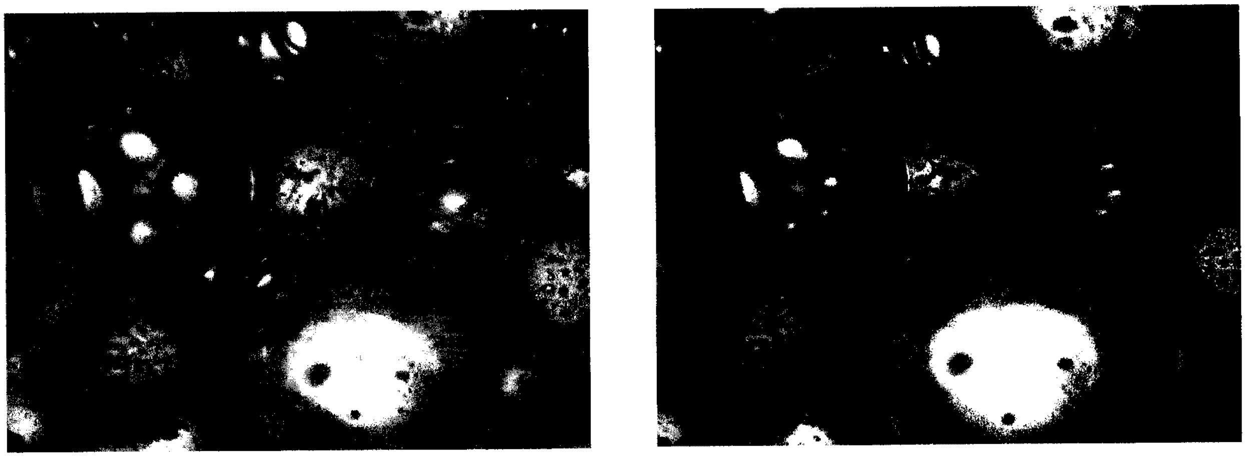

(e) T = 160 °C; t = 5 [min]

(f) T = 160 °C; t = 6 [min]

Figure 8.2: Typical hot-stage optical microscopy images of the CBA decomposition governed phase of pre-compounded PE (LL8556 + 3%wt Celogen OT) foamable resins

Sample size = 0.75 × 0.55 [mm]

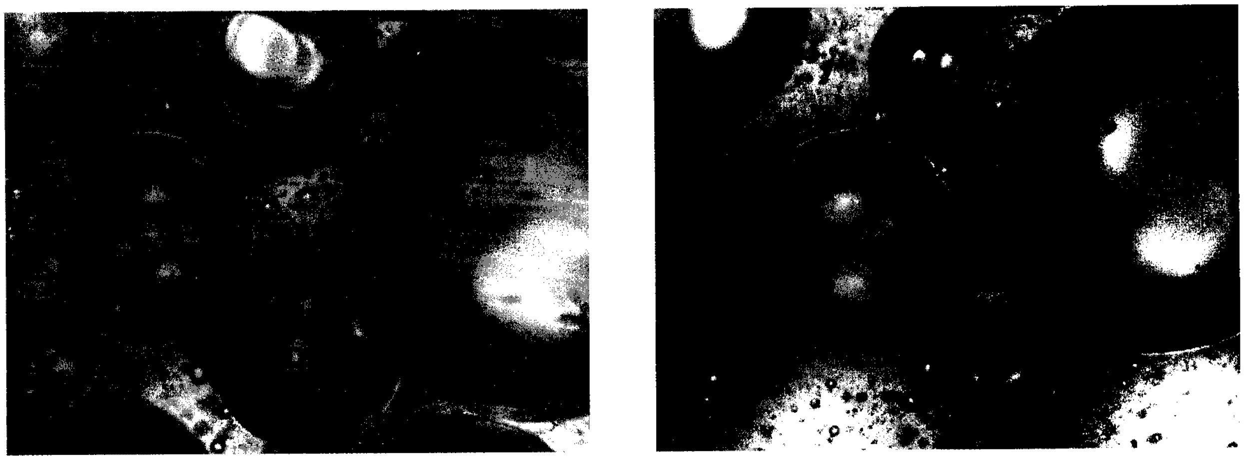

(a) T = 165 °C

(b) T = 170 °C

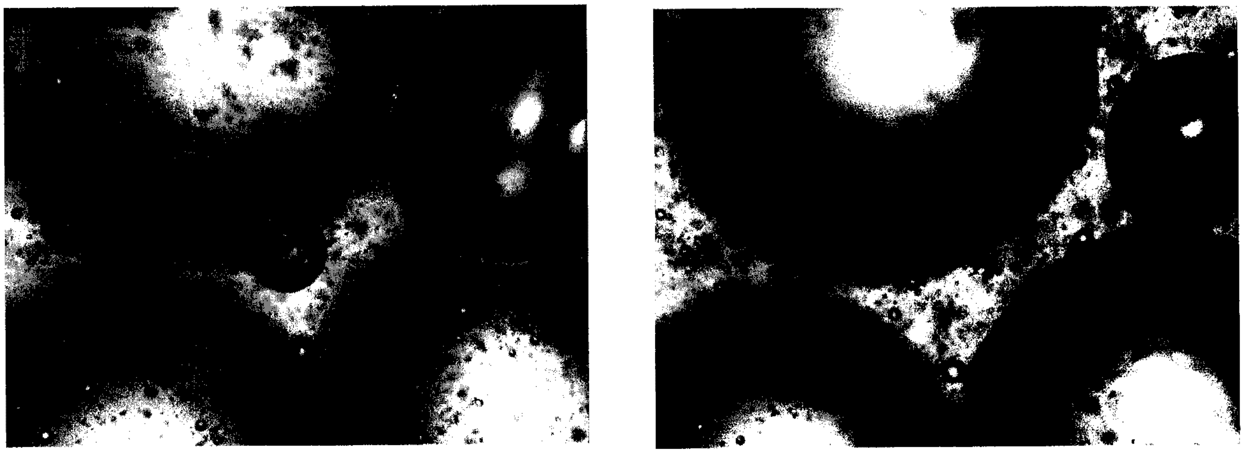

(c) T = 175 °C

(d) T = 180 °C

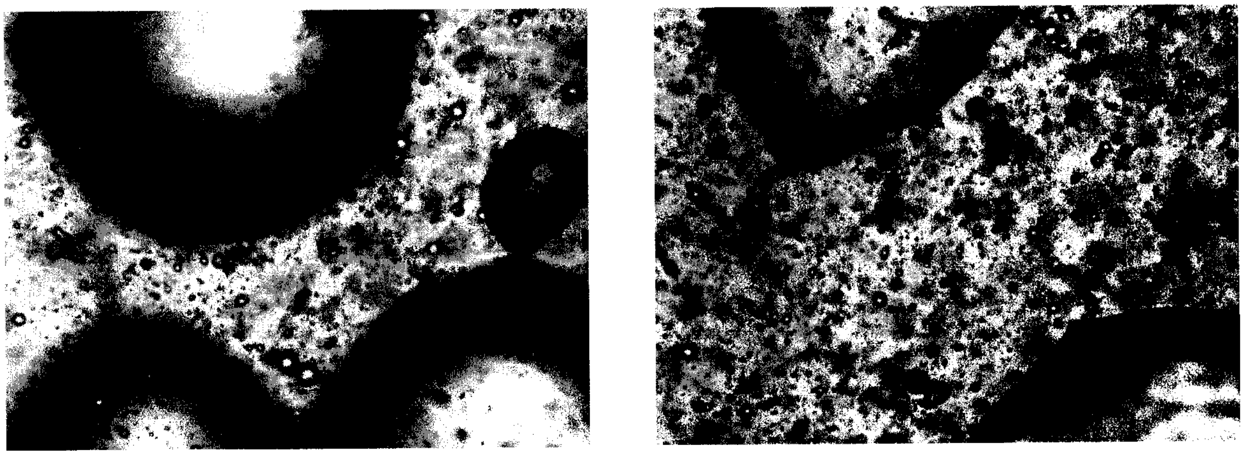

(e) T = 185 °C

(f) T = 190 °C

Figure 8.3: Typical hot-stage optical microscopy images of the post-CBA decomposition governed phase of pre-compounded PE (LL8556 + 3%wt Celogen OT) foamable resins

Sample size = 0.75 × 0.55 [mm]

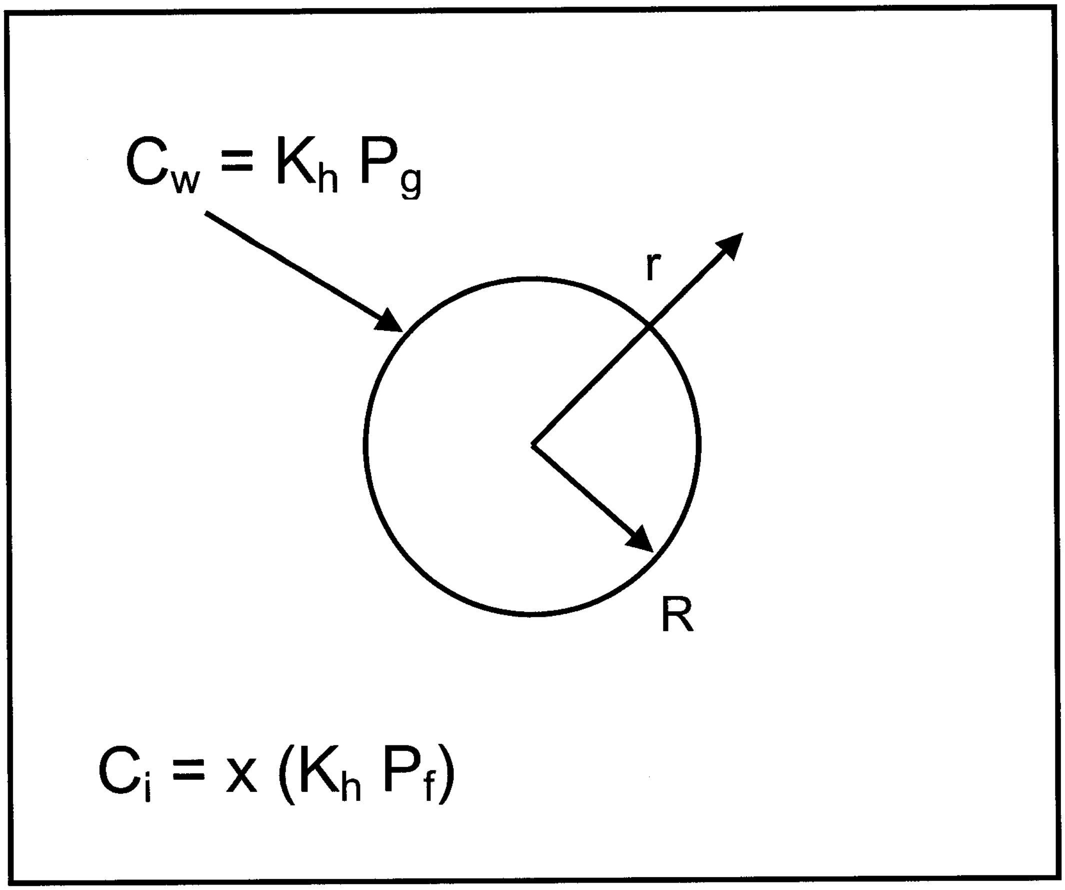

Figure 8.4: Geometry of a single spherical bubble surrounded by an infinite amount of polymer melt

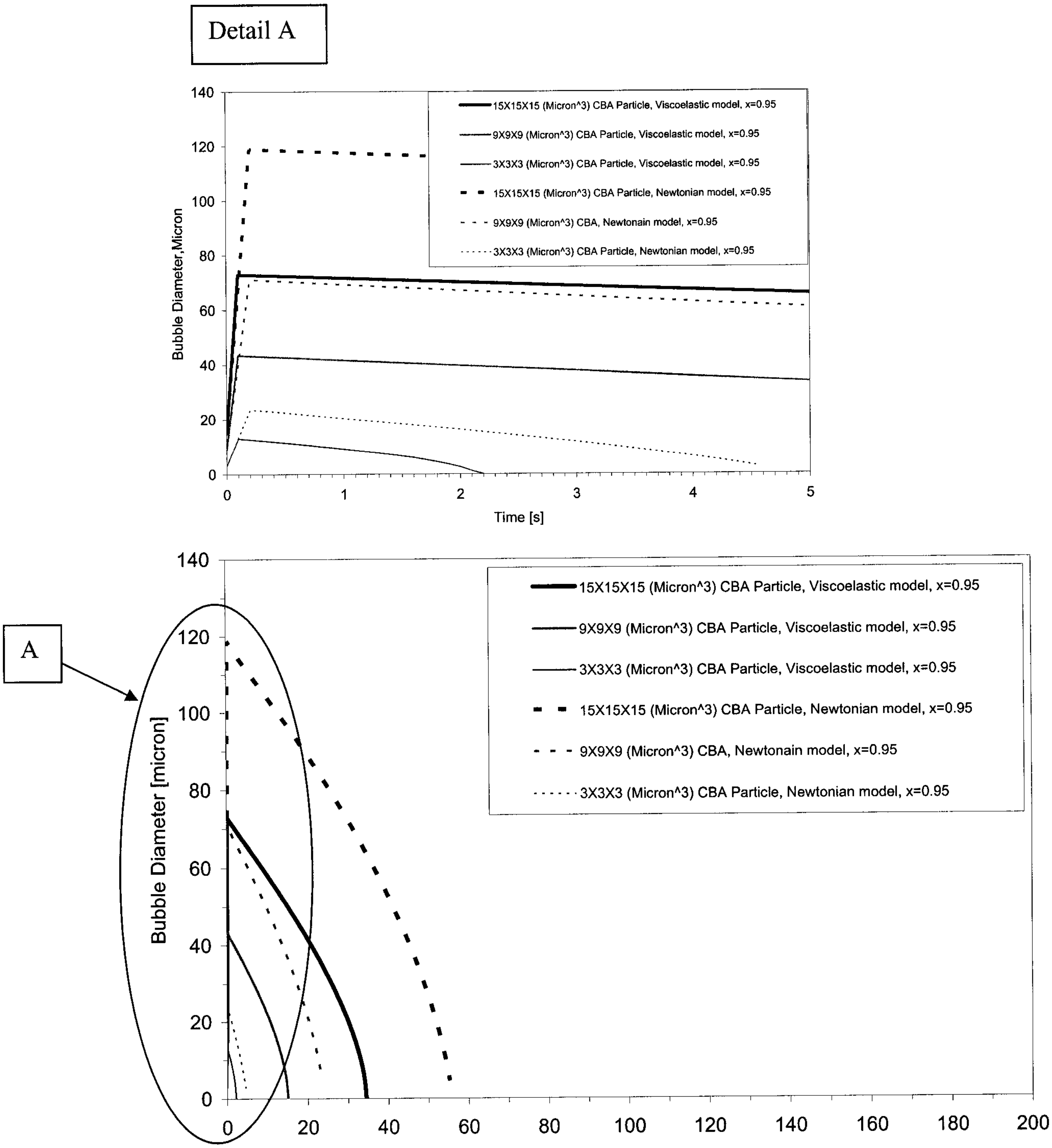

Figure 8.5: Comparison between the computer simulations of the lifespan of three CBA-blown bubbles formed by three differently sized CBA particles in rotational foam molding obtained by implementing the developed viscoelastic and Newtonian models at an assumed concentration of gas in the surrounding polymer melt of x = 0.95

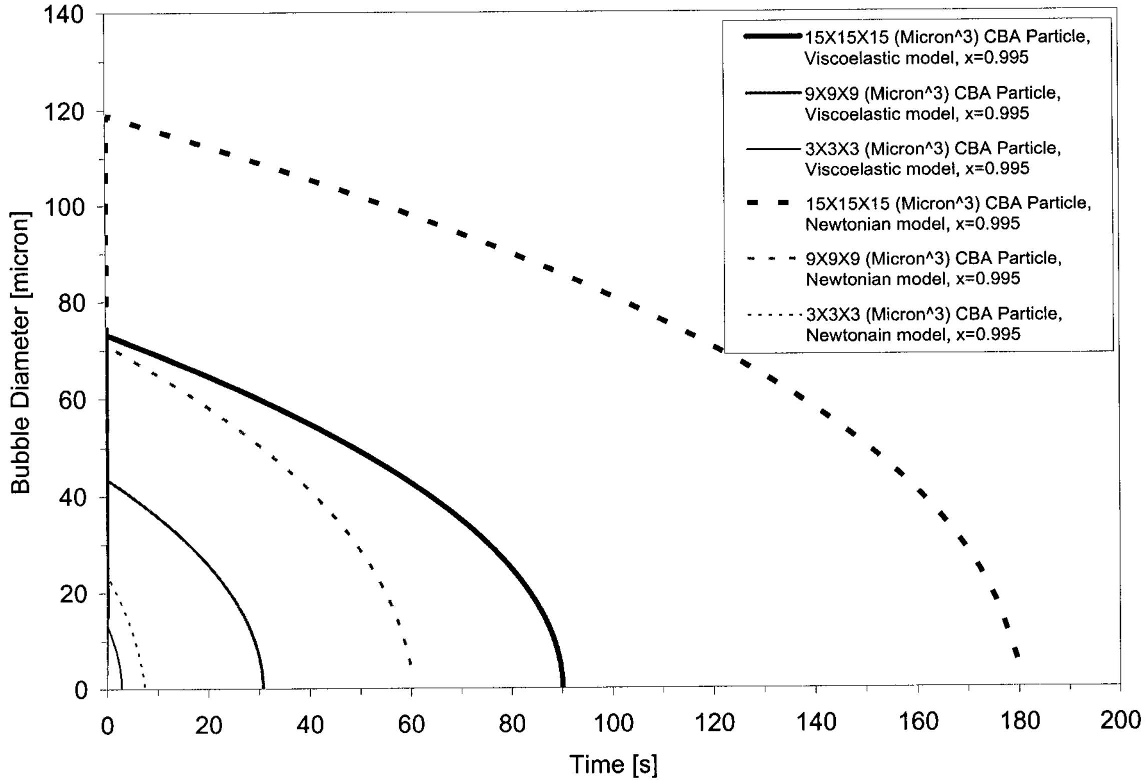

Figure 8.6: Comparison between the computer simulations of the lifespan of three CBA-blown bubbles formed by three differently sized CBA particles in rotational foam molding obtained by implementing the developed viscoelastic and Newtonian models at an assumed concentration of gas in the surrounding polymer melt of x = 0.995

CHAPTER 9

CONCLUDING REMARKS AND FUTURE WORK

9.1 Concluding Remarks

The theoretical and experimental studies conducted within the framework of this thesis lead to the following conclusions:

1) It has been found to be essential that for the successful manufacture of integral-skin cellular polyolefin composites using the single-charge rotational foam molding technology the mold should be charged with predetermined quantities of non-foamable and foamable resins having a significant particle size difference. The non-foamable particles intended for forming the skin should be introduced into the mold in a powder form, whereas the foamable particles intended for forming the foamed core should be introduced into the mold in a pellet form after being extrusion melt-compounded with an adequate quantity of CBA.

2) A rigorous Newtonian and a viscoelastic model have been developed in this thesis to describe the lifespan of CBA–blown bubbles in rotational molding. These are the first published CBA-blown bubble growth models for rotational foam molding. They have been experimentally verified and used to prove that the fundamental reason why fine-celled foams cannot be produced in rotational foam molding is the fact that the CBA-blown bubbles having cell sizes less than 100 μm, even when subjected to most favorable processing conditions, shrink and ultimately dissolve in less than 140 [s] thereby precluding the formation of fine-celled foam morphologies.

3) In this thesis, the single-charge rotationally foam molded technology has been successfully extended to the production of PE skin / PP foamed core integral-skin cellular composite articles.

4) It has been demonstrated in this thesis that the processing temperature profile is the principal parameter that governs the sequence of thermal events inside the mold and thereby

the compactness and uniformity of the solid skin and the final foam structure in single-step rotational foam molding. A specially programmed two-step oven temperature profile was proposed in this thesis for eliminating the invasion of the foamable resin on the solid skin layer. It proved to be effective for PE / PE and PE / PP integral-skin foams in ensuring that the skin formation is completed prior to the activation of the foaming resin. This is a crucial remedial processing strategy for the production of integral-skin cellular composites using the single-charge rotational foam molding technology which is known to be conditioned by the timely completion of the formation of the skin layer with respect to the onset of activation of the foamable resin intended to form the cellular core or layer.

5) The developed single-charge rotational foam molding method was successfully scaled-up for the manufacture of both PE / PE and PE / PP integral-skin cellular composites using a two-step oven temperature profile and a biaxial industrial-scale rotomolder.

6) Full visualization of the single-charge rotational foam molding process has been achieved using a transparent uni-axial rotational molding machine (specially designed and built for the experimental work conducted in this thesis), a see-trough mold, and a camcorder.

7) A fundamental study of the adhesion behavior of non-foamable skin-forming Rotolite™ OS powders and foamable core-forming PE pellets with 3%wt Celogen OT on a high-temperature rotating metal wall experimental setup (specially designed and built for the experimental work conducted in this thesis) has been successfully accomplished. Importantly, it has been found in this thesis that to maintain a desired order of thermal events inside the mold in single-charge rotational foam molding of PE / PE integral-skin cellular composites, the oven temperature profile should be designed to delay the mold wall in reaching the critical temperature of 118 °C sufficiently long (e.g., 10 [min]), in order to allow the completion of powder sintering and the formation of the first depositions of the skin layer to occur at a relatively lower temperature such as 108 °C and thereby avoid the invasion of the foamable resin into the skin layer.

8) As a part of a fundamental research study conducted in this thesis on the rotofoamability of polyolefins, it has been found that PP foams in rotational foam molding achieve significantly lower cell densities and larger average cell sizes in comparison with respective PE foams. In addition, it has been found that the melt compounding based technology is well suited for producing fine and very uniform PE foams in rotational foam molding, whereas the dry blending based technology is almost equally (or better) suited than

the melt compounding based technology to the production of PP foams in rotational foam molding.

9) As a part of a fundamental material characterization study, the most relevant rheological and thermal properties of four PE and four PP grades have been identified and experimentally determined. These proved to be very useful in optimizing single-charge rotational foam molding processing strategies.

9.2 Recommendations for Future Work

As a direct extension of the research work conducted in this thesis, it would be necessary to conduct an experimental verification of the developed Newtonian and viscoelastic models for the lifespan of a CBA-blown bubble in rotational foam molding by using specially designed and prepared experimental samples that will allow the observation and investigation of the decomposition behavior and blowing ability of a literarily single CBA particle in a molten non-pressurized PE melt using hot-stage optical microscopy.

9.2.1 Modeling of Governing Mechanisms

Since at present there are no developed and experimentally validated models that treat and describe the fundamental mechanisms that govern the processing of non-foamable powders and foamable pellets that have been simultaneously charged into a rotating heated mold with a deliberate intention to produce integral-skin cellular composites, and since these single-charge mechanisms differ significantly from the already established ones with respect conventional rotational molding, it would be desirable to establish research programs that would aim towards the modeling of the: (i) heat transfer, (ii) cooling stage, (iii) sintering and densification phenomena, and (iv) foaming mechanism by considering the interaction of multiple-bubbles in non-pressurized non-isothermal viscoelastic polymer melts. In addition, a better parameter estimation would be required.

9.2.2 Innovative Processing Concepts

1) Since the lifespan of CBA-blown bubbles in rotational molding strongly depends on the gas concentration in the surrounding polymer melt, and since it is considerably longer if the concentration is higher, in order to extend the lifespan of the preferred fine-celled bubbles

it would be important to check the feasibility of a new concept based on the use of two CBAs. The one of these CBAs should preferably have a lower decomposition temperature than the other and both should be extrusion melt compounded with a polyolefin resin (e.g., PE). During rotational foam molding, the CBA with the lower decomposition temperature will be the first to generate bubbles. These bubbles will most probably shrink and eventually dissolve in the polymer melt along the course of the cycle, thereby increasing the gas concentration within the polymer melt and creating a favorable environment for extended lifespan of the bubbles that would be generated by the decomposition of the second CBA. This concept could be referred to as two blowing agents “suicide” bubbles concept.

2) Since rotomolding production cycles are in general inherently, but undesirably, lengthy because the plastic material has to be indirectly heated to beyond its melting point and than cooled back till it solidifies, it would be desirable to displace the heating part of the process by using more efficient plastic fabrication methods such as extrusion. Namely, the end of an extrusion system should be adequately connected via a specially designed injection port with a preheated rotational mold (especially economically feasible for large molds) in order to directly charge the mold with molten plastics instead of solid resins and then use the mold rotation to shape and then solidify the plastic into a useful product. This concept could be referred to as extrusion-assisted rotational molding.

3) An effort should be made also in the future to transfer the developed concepts and principles in this thesis to other plastic fabrication processes such as compression foam molding.

REFERENCES

[1] D. Klempner and K.C. Frisch, eds., Handbook of Polymeric Foams and Foam Technology, Hanser Publishers, New York (1991)

[2] A.H. Landrock, Handbook of Plastic Foams, Types, Properties, Manufacture and Applications, Noyes Publications, New Jersey (1995)

[3] J.L. Throne, Thermoplastic Foams, Sherwood Technologies, Inc., Sherwood Publishers, Ohio (1996)

[4] K. Budinski, Engineering Materials Properties and Selection, Second Edition, Reston Publishing Company Inc. (1983)

[5] F.W. Billmeyer, Textbook of Polymer Science, John Wiley & Sons, New York (1984)

[6] E.P. Moore Jr., Polypropylene Handbook, Hanser/Gardner Publications Inc., (1996)

[7] K.C. Frisch and J.H. Saunders, Plastic Foams, Part I, Marcel Dekker, Inc., New York (1972)

[8] K.A. Seeler and V. Kumar, *J. Reinforced Plast. Comp.*, **12**, 359 (1993)

[9] D.I. Collias, D.G. Baird, and R.J.M. Borggreve, *Polymer*, **25**, 3978 (1994)

[10] D.I. Collias and D.G. Baird, *Polym. Eng. Sci.*, **35**, 1167 (1995)

[11] D.I. Collias and D.G. Baird, *Polym. Eng. Sci.*, **35**, 1178 (1995)

[12] S. Doroudiani, C.B.Park, and M.T.Kortchot, *Polym. Eng. Sci.*, **38**, 1205 (1998)

[13] L.M. Matuana, C.B.Park, and J.J. Balatinecz, *Cellular Polymers*, **17**, 1 (1998)

[14] S. Ham, "Structural Foam", 1309, in I.I. Rubin, Handbook of Plastic Materials and Technology, 1309, John Wiley and Sons Inc. (1990)

[15] C.P. Park, "Polyolefin Foam", 187, in Handbook of Polymeric Foams and Foam Technology, D. Klempner and K.C. Frisch, eds., Hanser Publishers, New York (1991)

[16] N.S. Ramesh, "Foam Growth in Polymers", 125, in Foam Extrusion Principles and Practice, Lee S.-T., ed., Technomic Publishing Company Inc., Lancaster, Pennsylvania (2000)

[17] C.J. Benning, Plastic Foams, Volume I: Chemistry and Physics of Foam Formation, John Wiley & Sons, Inc. (1969)

[18] R. Juran, ed., *Modern Plastics Encyclopedia*, ***66*** (11), McGraw-Hill Book Co., New York (1989)

[19] J.H. Dubois, Plastics History U.S.A., Cahners Publishing Company (1972)

[20] Y.L. Meltzer, Foamed Plastics Recent Developments, Noyes Data Corporation, New Jersey (1976)

[21] Modern Plastics Encyclopedia, 318 (1983-1984)

[22] Modern Plastics Encyclopedia, 317 (1990)

[23] P. Dodge, *Modern Plastics*, D-158 (Mid-November 1994)

[24] R.J. Crawford, Rotational Moulding of Plastics, Second Edition, John Wiley and Sons Inc. (1996)

[25] R.J. Crawford, Plastics Engineering, Third Edition, Butterworth Heinemann (1998)

[26] G.L. Beall, Rotational Molding: Design, Materials, Tooling, and Processing, Hanser/Gardner Publications, Inc., Cincinnati (1998)

[27] G. Liu, C.B. Park, and J.A. Lefas, *Polym. Eng. Sci.*, ***38***, 1997 (1998)

[28] R. Pop-Iliev, G. Liu, F. Liu, C.B. Park, S. D'Uva, and J.A. Lefas, *SPE RETEC, Technical Papers*, Strongsville, Ohio, 95 (1999)

[29] R. Pop-Iliev, G. Liu, F. Liu, C.B. Park, S. D'Uva, and J.A. Lefas, *SPE ANTEC, Technical Papers*, ***45***, 1457 (1999)

[30] Equistar Chemicals Company, Equistar Rotomolding Technical Topics #2-#5 (2001)

[31] S.-J. Liu and C.-H. Yang, *SPE, ANTEC, Technical Papers*, ***46***, 1309, (2000)

[32] R. Pop-Iliev and C.B. Park, *"Single-step Rotational Foam Molding of Skin-surrounded Polyethylene Foams"*, *Journal of Cellular Plastics*, accepted (Sept. 2002), and R. Pop-Iliev and C.B. Park, *SPE ANTEC, Technical Papers, **48*** (2002)

[33] R. Pop-Iliev, C.B. Park, and S. D'Uva, *SPE RETEC, Technical Papers,* Independence, Ohio, 85 (2002)

[34] M.P. Kearns and R.J. Crawford, *Rapra Technology Ltd.,* Heidelberg, Germany, Paper 12, 123 (2002)

[35] S.-J. Liu and C.-H. Tsai, *Polym. Eng. Sci.*, ***39***, 1776 (1999)

[36] S.-J. Liu and C.-H. Yang, *Adv. Polym. Tech., **20***, 108 (2001)

[37] F.A. Shutov, "Blowing Agents for Polymer Foams", 375, in Handbook of Polymeric Foams and Foam Technology, D. Klempner and K.C. Frisch, eds., Hanser Publishers, New York (1991)

[38] R. Pop-Iliev, *"Processing of Fine-cell Polypropylene Foams in Compounding-based Rotational Foam Molding"*, M. A. Sc. Thesis, University of Toronto (1999)

[39] C.B. Park, G. Liu, F. Liu, R. Pop-Iliev, S. D'Uva, and B. Zhang, *"Production of Foamed Low-density Polypropylene by Rotational molding",* U.S. Patent 6,103,153 (August 15, 2000)

[40] R. Pop-Iliev, and C.B. Park, *J. Reinforced Plast. Comp.*, ***21***, 101 (2002)

[41] R. Pop-Iliev, G.M. Rizvi G.M., and C.B. Park, *Rapra Technology Ltd.*, Frankfurt, Germany, Paper 4, 11 pages (2001)

[42] M. Knights, *Plastics Technology*, ***45***, 100 (1999)

[43] M. Knights, *Plastics Technology*, ***41***, 26 (1995)

[44] M. Shortt, *Job Shop Technology Magazine* (2002)

[45] L.R. Payne, *"Multiaxis Rotational Molding Apparatus",* U.S. Pat. 4,956,135 (January 6, 1998)

[46] P.Y. Kelly, *"A Microscopic Examination of Rotomolded Polyethylene",* DuPont Canada Inc., unpublished report (1981)

[47] A.G. Spence and R.J. Crawford, *Polym. Eng. Sci.*, ***36,*** 993 (1996)

[48] M. Kontopoulou and J. Vlachopoulos, *Polym. Eng. Sci.*, ***39,*** 1189 (1999)

[49] C.T. Bellehumeur and J.S. Tiang, *SPE ANTEC, Technical Papers*, ***46***, 1356 (2000)

[50] G. Gogos, *SPE ANTEC, Technical Papers*, ***45***, 1433 (1999) and *SPE RETEC, Technical Papers*, Strongsville, Ohio, 121 (1999)

[51] A.G. Spence and R.J. Crawford, *Rotation,* 17 (1995)

[52] J. Throne, *SPE ANTEC, Technical Papers*, ***46***, 1304 (2000)

[53] J. Throne, *SPE RETEC, Technical Papers*, Independence, Ohio, 79 (2002)

[54] E. Takacs, J. Vlachopoulos, and C. Rosenbusch, *SPE ANTEC, Technical Papers*, ***48***, (2002)

[55] E. Archer, E. Harkin Jones, M.P. Kearns, R.J. Crawford, and A-M Fatnes, *Rotation*, ***XI (2),*** 27 (2002)

[56] R.J. Crawford, *Rotation*, 30 (1997)

[57] E. Takacs, J. Vlachopoulis, and S. Lipsteuer, *SPE, RETEC, Technical Papers*, Strongsville, Ohio, 15 (1999)

[58] R. Pop-Iliev, C.B. Park, G. Liu, and F. Liu, *SPE, ANTEC, Technical Papers*, ***46***, 1896 (2000)

[59] C.B. Park and L.K. Cheung, *Polym. Eng. Sci*, ***37***, 1 (1997)

[60] J. Slapnik, *"Plastic Process",* U. S. Pat. 2,989,783 (June 27, 1961)

[61] R.A. Nonweiler, *"Method of Producing an Expanded Polystyrene Foam Having a Dense Surface"*, U.S. Pat. 3,309,439 (March 14, 1967)

[62] R.A. Nonweiler, *"Composition for making Coated Expanded Polystyrene Foam"*, U.S. Pat. 3,457,205 (July 22, 1969)

[63] J.E. Pitchard, *"Method of Making a Foamable Polymer and Foamable Composition Obtained Therefrom"*, U.S. Pat. 3,461,087 (August 12, 1969)

[64] Mitsubishi Petrochemical Co. Ltd., *"Process for Manufacturing a Synthetic Resin Foam Having a Skin"*, British Pat. GB1,308,716 (March 7, 1973)

[65] Mitsubishi Petrochemical Co. Ltd., *"Process for Preparing Molded Olefin Polymer Foam"*, British Pat. GB1,321,341 (June 27, 1973)

[66] K. Hosoda, N. Shiina, Y. Kadowaki, M. Hashimoto, N. Suzuki, and T. Sugita, *"Method for Producing a Composite Foamed Article"*, U.S. Pat. 3,814, 778 (June 4, 1974)

[67] B.F. Nicholls, *"Improvements in or Relating to Buoyant Articles"*, British Pat. GB1,368,743 (October 2, 1974)

[68] N. Shiina and K. Hosoda, *"Method for Rotational Molding of Composite Foamed Plastic Articles"*, U.S. Pat. 3,914,361 (October 21, 1975)

[69] C.E. Slade, *"Rotational Molding of Articles with Foamed Inner Layer"*, Canadian Pat., CA983226 (February 10, 1976)

[70] H. Mori, E. Adachi, and Y. Nogichi, *"Method of Producing Composite Foamed Shaped Articles from Thermoplastic Resins"*, U.S. Pat. 3,962,390 (June 8, 1976)

[71] K. Duffy, "Method for Forming Expanded Foam Rotomolded Products", U.S. Pat. 4,952,350, (August 28, 1990)

[72] D.G. Needham, *"Foamable Polyethylene-based Composition for Rotational Molding"*, U.S. Pat. 5,366,675, (November 22, 1994)

[73] R.J. Crawford and P.J. Nugent, *"A Method of Rotational Molding and Rotationally Molded Products"*, International Pat., WO 95/19877 (January 20, 1995)

[74] B.A. Graham, *"Multi-layer Particles for Rotational Molding"*, International Pat., WO 96/15892 (November 17, 1995)

[75] D.G. Needham, *"Polyolefin-based Composition for Rotational Molding"*, U.S. Pat. 5,532,282 (July 2, 1996)

[76] R.I. Kliene, *"Rotational Molding of Articles Having Cellular Interiors"*, British Pat. GB2,311,245 (September 24, 1997)

[77] J.J. Strebel, *"Compositions and Process for Rotational Molding Foamed Articles"*, U.S. Pat. 5,783,611 (July 21, 1998)

[78] J.J. Strebel, "*Compositions and Process for Rotational Molding Articles*", U.S. Pat. 5,830,392 (November 3, 1998)

[79] J.J. Strebel, *"Rotational Molding compositions and Process for Producing Foamed Articles Therefrom"*, U.S. Pat. 5,922,778 (July 13, 1999)

[80] C.C. Lee, *"Foamble Compositions for Rotational Molding"*, U.S. Pat. 5,928,584 (July 27, 1999)

[81] M. Dealy and K.F. Wissbrun, Melt Rheology and Its Role in Plastics Processing, Theory and Applications, Chapman & Hall, London, UK (1995)

[82] S.M. Colo, K. Hedman, and B.K.S. Rudolph, ATS RheoSystems Application Note (1997)

[83] J. Vlachopoulos, Lectures on Polymer Rheology and Extrusion, Polydynamics Inc. (1997)

[84] G.T. Helleloid, *Morehead Electronic Journal Of Applicable Mathematics,* Issue I (2001)

[85] F.N. Cogswell, *Plastics and Polymers,* 39 (February 1973)

[86] H.A. Barnes, J.F. Hutton and K. Walters, An Introduction to Rheology, Oxford: Elsevier (1989)

[87] M. Weber and R. Gonzales, *SPE, ANTEC, Technical Papers, **45***, 1468 (1999)

[88] A. Spence, *SPE, ANTEC, Technical Papers, **45***, 1482 (1999)

[89] M. Bisaria, E. Takacs, C.T. Bellehumeur, and J. Vlachopoulos, *Rotation*, ***3***, 12 (1994)

[90] C.T. Bellehumeur, M. Bisaria, and J. Vlachopoulos, *Polym. Eng. Sci*, ***36***, 2198 (1996)

[91] D.J. Ferry, Viscoelastic Properties of Polymers, 3rd Ed., john Wiley & Sons, New York (1980)

[92] T.G. Fox and P.J. Flory, *Phys. Colloid. Chem.*, ***55***, 221 (1951)

[93] T.G. Fox and P.J. Flory, *J. Am. Chem. Soc.*, ***70***, 2384 (1948)

[94] G.C. Berry and T.G. Fox, *Adv. Polym. Sci*, ***6***, 261 (1968)

[95] W.W. Graessley, *Adv. Polym. Sci.*, ***16***, 1 (1974)

[96] P.E. Rouse, *J. Chem. Phys.*, ***21***, 1272 (1953)

[97] H.H. Kaush, Polymer Fracture, 2nd Ed., Springer Verlag, Berlin (1987)

[98] A.M. Donald and E.J. Kramer, *J. Pol. Sci., Polym. Phys. Ed.,* ***20***, 899 (1982)

[99] A.M. Donald and E.J. Kramer, *J. Mater. Sci.,* ***17***, 1871 (1982)

[100] S.Wu, Polymer Interfaces and Adhesion, Marcel Dekker, New York (1995)

[101] P.G. De Gennes, Scaling Concepts in Polymer Physics, Cornell University Press, Ithaca, N.Y. (1979)

[102] M. Dol and S.F. Edwards, *J. Chem. Soc., Faraday Trans. II,* ***74***, 1789, 1802, 1818 (1978)

[103] M. Dol and S.F. Edwards, *J. Chem. Soc., Faraday Trans. II,* ***75***, 38 (1979)

[104] F. Bueche et.al., *J. Chem. Phys.,* ***20***, 1956 (1952)

[105] P.G. De Gennes, *J. Chem. Phys.,* ***55***, 572 (1971)

[106] S.F. Edwards and J.W.V. Grant, J. Phys. A: Math. Nuclear. Gen, ***6***, 1169 (1973)

[107] S. Onogi et. al., Kolloid-Z, Z Polymere, ***222***, 110 (1968)

[108] D.J. Ferry, *J. Chem. Phys.,* ***67***, 2297 (1963)

[109] J.P.Ibar, *SPE, ANTEC, Technical Papers,* ***45***, 1310 (1999)

[110] G. Locati, M. Pegoraro, and D. Nichetti, *Polym. Eng. Sci*, ***39***, 741 (1999)

[111] M. Kontopoulou, *"A Study of the Parameters Involved in Rotational Molding of Plastics"*, M.Eng. Thesis, Mc.Master University (1995)

[112] M. Kontopoulou, M. Bisaria, and J.Vlachopoulos, *Int. Polym. Process,* ***12***, 165 (1997)

[113] J. Vlachopoulos, C.T. Bellehumeur, and M. Kontopoulou, Proc. 12th Int. Congr. on Rheology, Quebec, 693 (1996)

[114] J.R. Street, *Trans. Soc. Rheol.,* ***12***, 103 (1968)

[115] K.W. Suh and D.D. Webb, Encyclopedia of Polymer Science and Technology, V.3, 2nd Ed., pp. 1-59, John Wiley and Sons, USA (1985)

[116] J.J. Morad, *SPE, ANTEC, Technical Papers*, ***41***, 783 (1995)

[117] E.P. Moore, Polypropylene Handbook, Hanser/Gardner Publications Inc. (1996)

[118] R. Pop-Iliev, G.M. Rizvi, and C.B. Park, *"The Importance of Timely Polymer Sintering While Processing Polypropylene Foams in Rotational Molding", Polym. Eng. Sci*, accepted (June 2002)

[119] H.C. Lau, S.N. Bhattacharya, and G.J. Field, *Polym. Eng. Sci*, ***38***, 1915 (1998)

[120] J.M. Dealy and K.F. Wissbrun, *Melt Rheology and Its Role in Plastic Processing,* Van Nostrand Reinhold, New York (1990)

[121] R. Wolf, *Polymer Process Engineering,* ***4***, 97 (1986)

[122] A. Ghijsels, J.J.S.M. Ente, and J.Raadsen, *Intern. Polymer Processing,* ***5***, 284 (1990)

[123] P. Micic, S.N. Bhattacharya, and G.J. Field, *Intern. Polymer Processing,* ***11***, 14 (1996)

[124] A. Ghijsels and J. De Clippeleir, *Intern. Polymer Processing,* ***9***, 252 (1994)

[125] X.C. Wang, C. Tzoganakis, and G.L. Rempel, *SPE, ANTEC, Technical Papers,* ***43***, (1997)

[126] A.S. Scheibelhoffer, A.S. Wimolkiatisak, B.L. Leonard, and D. Chundury, *SPE, ANTEC, Technical Papers,* ***39***, 629 (1993)

[127] B.J. Sheve, J.W. Mayfield, and A.J. DeNicola Jr., *"High Melt Strength Polypropylene Polymer, Process for Making It, and Use Thereof"*, U.S. Pat. 4,916,198 (April 10, 1990)

[128] E. Takacs, M. Kontopoulou, D. Annechini, and J. Vlachopoulos, *SPE, ANTEC, Technical Papers,* ***46***, 1331 (2000)

[129] N. Callan, M.P Kerns, M. Spenser, and R.J. Crawford, *SPE ANTEC, Technical Papers,* ***48***, (2002)

[130] M.C. Cramez, M.J. Oliveira, and R.J. Crawford, *SPE, ANTEC, Technical Papers,* ***44***, 1137 (1998)

[131] M.C. Cramez, M.J. Oliveira, and R.J. Crawford, *SPE, ANTEC, Technical Papers,* ***46***, 1351 (2000)

[132] M.A Rao and J.L. Throne, *Polym. Eng. Sci,* ***12***, 237 (1972)

[133] J.L. Throne, *Polym. Eng. Sci,* ***16***, 257 (1976)

[134] P.J. Nugent, *"A Study of Heat Transfer and Process Control in the Rotational Molding of Polymer Powder",* Ph.D. Thesis, Queen's University of Belfast (1990)

[135] R.J. Crawford and P.J. Nugent, *Plast. Rubb. Proc. Appl.,* **11**, 107 (1989)

[136] P.J. Nugent, R.J. Crawford, and L. Xu, *Adv. Polym. Tech.,* ***11***, 181 (1992)

[137] D.-W. Sun and R.J. Crawford, *Polym. Eng. Sci,* ***33***, 132 (1993)

[138] S. Bawiskar and J.L. White, *Intern. Polym. Proc,* ***10,*** 62 (1995)

[139] G. Gogos, L.G. Olson, X. Liu, and V.R. Pasham, *Polym. Eng. Sci,* ***38***, 1387 (1998)

[140] J.L. Throne, *Polym. Eng. Sci,* ***12***, 335 (1972)

[141] G. Gogos, X. Liu, and L.G. Olson, *Polym. Eng. Sci,* ***39***, 617 (1999)

[142] L.G. Olson, R. Crawford, M. Kearns, and N. Geiger, *Polym. Eng. Sci,* ***40***, 1758 (2000)

[143] C. T. Bellehumeur, *"Polymer Sintering and Its Role in Rotational Molding"*, PhD Thesis, Mc Master University (1997)

[144] C.T. Bellehumeur, *SPE, ANTEC, Technical Papers, **44***, 1112 (1998)

[145] C.T. Bellehumeur, M. Kontopoulou, J. Vlachopoulos, *Rheol. Acta, **37**,* 270 (1998)

[146] C.T. Bellehumeur and J.S. Tiang, *Polym. Eng. Sci*, ***42***, 215 (2002)

[147] C.T. Bellehumeur, *SPE RETEC, Technical Papers*, Independence, Ohio, 51 (2002)

[148] J. Frenkel, *J. Phys.*, ***9***, 385 (1945)

[149] S. Mazur, "Coalescence of polymer particles", in Polymer Powder Technology, p. 157, M. Narkis and N. Rosenzweig, eds., John Willey & Sons, New York (1995)

[150] F. Orgaz-Orgaz, *J. Non-Cryst. Solids, **100**,* 115 (1988)

[151] M. Kontopoulou, *"Polymer Melt Formation and Densification in Rotational Molding"*, PhD Thesis, Mc Master University (1999)

[152] M. Kontopoulou, E. Takacs, and J. Vlachopoulos, *SPE, ANTEC, Technical Papers, **45***, 1428 (1999)

[153] M. Kontopoulou, E. Takacs, and J. Vlachopoulos, *SPE RETEC, Technical Papers*, Strongsville, Ohio, 7 (1999)

[154] M. Kontopoulou and J. Vlachopoulos, *Polym. Eng. Sci*, ***41***, 155 (2001)

[155] M.A. Rao and J.L. Throne, "Theory of Rotational Molding-Part III; Sinter Melting and Degradation", *SPE,* 759 (1972)

[156] R.C. Progelhof, G. Cellier, and J.L. Throne, "New Technology in Rotational Molding; Powder Densification", SPE, Annual technical engineering conference, 762 (1982)

[157] R.J. Crawford and J.A. Scott, *Plast. Rubber. Process. Appl., 7,* 85 (1987)

[158] R.W. Hopper, *J. Fluid Mech., **243**,* 171 (1992)

[159] O. Pokluda, C.T. Bellehumeur, and J. Vlachopoulos, *AIChE J., **43***,3253 (1997)

[160] S. Mazur and D.J. Plazek, *Prog. Org. Coat., **24**,* 225 (1994)

[161] G.W. Scherer, *J. Am. Ceram. Soc., **67**,* 798 (1984)

[162] M. Kandis and T.L. Bergman, *J. Heat Transfer, Trans. ASME, **119**,* 824 (1997)

[163] C.T. Bellehumeur, *SPE, ANTEC, Technical Papers, **45***, 1446 (1999)

[164] R.J. Crawford and L. Xu, *Material Science, **28***, 2067 (1993)

[165] A.G. Spence, *"Analysis of Bubble Formation and Removal in Rotationally Molded Products",* PhD Thesis, Queen's University of Belfast (1994)

[166] S.-T. Lee., *"Foam Nucleation in Gas-Dispersed Polymeric Systems"*, 81, in Foam Extrusion Principles and Practice, S.-T. Lee., ed., Technomic Publishing Company Inc., Lancaster, Pennsylvania (2000)

[167] J.H. Saunders, *"Fundamentals of Foam Formation"*, 5 in Handbook of Polymeric Foams and Foam Technology, Klempner D. and Frisch K.C., eds., Hanser Publishers, New York (1991)

[168] C.W. Stewart, *J. Polym. Sci.*, ***A-28***, 937 (1970)

[169] M. Blander and J.L. Katz, *AlChE J.*, ***21***, 833 (1975)

[170] R. Cole, *Adv. Heat Transfer*, ***10***, 85 (1974)

[171] T. Pontiff, *"Foaming Agents for Foam Extrusion"*, 251, in Foam Extrusion Principles and Practice, S.-T. Lee., ed., Technomic Publishing Company Inc., Lancaster, Pennsylvania (2000)

[172] M. Amon and C. Denson, *Polym. Eng. Sci*, ***24***, 1026 (1984)

[173] M. Amon and C. Denson, *Polym. Eng. Sci*, ***26***, 255 (1986)

[174] W.-J. Yang and H.-C.Yeh, *AlChE J.*, ***12***, 927 (1965)

[175] J.R Street, A.L. Fricke and L.P. Reiss, *Ind. Eng., Fund.*, ***10***, 54 (1971)

[176] J.R. Street, *Trans. Soc. Rheo.*, ***12***, 103 (1968)

[177] C.B. Park, *"Manufacturing of Cellular and Microcellular Polymers"*, Course Lecture Notes, Department of Mechanical and Industrial Engineering, University of Toronto (2000)

[178] S.P. Levitskiy and Z.P. Shulman, Bubbles in Polymeric Liquids: Dynamics and Heat-Mass Transfer, Technomic Publishing Co., Lancaster, PA, 44 (1995)

[179] R.B. Bird, R.C. Armstrong and O. Hassager, Dynamics of Polymeric Liquids: Volume I: Fluid Mechanics, John Wiley & Sons, 458 (1977)

[180] C.B. Park, University of Toronto, personal communication (1997-2002)

[181] S. D'Uva, Ingenia Polymers Corp., Canada, personal communication (1997-2002)

[182] J.L. Throne, Sherwood Technologies, personal communication (1999,2002)

[183] G.L. Beall, Glenn Beall Plastics Ltd., personal communication (2002)

[184] ExxonMobil Chemical, Escorene® Data Sheets (2000)

[185] Nova Chemicals, Novapol® Data Sheets (1999)

[186] Millenium Petrochemicals Inc., Polypropylene Technical Tips, Cincinnati (1998)

[187] Montell Polyolefines, Data Sheets (1998)

[188] Uniroyal Chemical, Celogen Physical Properties Guide (1998)

[189] Rheometric Scientific, RS200 manuals (1995)

[190] J.M. Margolis, Instrumentation for Thermoplastics Processing, Hanser Publishers, Oxford University Press, Canada (1988)

[191] Seymour W. B., Modern Plastics Technology, Reston Publishing Company, Inc. (1975)

[192] TA Instruments Inc, TA 2910 DCS manuals (1996)

[193] TA Instruments Inc, TA 2050 TGA manuals (1996)

[194] C.H. Murphy, Handbook of Particle Sampling and Analysis Methods, Verlag Chemie International Inc. (1984)

[195] CARD® PRO Ver. 5.1, Documentation & Tutorials, S-Matrix Corporation (1999)

[196] Linkam Scientific Instruments Ltd, HFS 91 manuals (1997)

[197] R.G. Griskey, Polymer Process Engineering, Chapman & Hall, London, UK (1995)

[198] C.B. Park and N.P. Suh, *Polym. Eng. Sci.*, ***36***, 34 (1996)

[199] C.B. Park, A.H. Behravesh, and R.D. Venter, *Polym. Eng. Sci.*, ***38***, 1812 (1998)

[200] A. Dreiblatt and K. Eise, in Mixing in Polymer Processing, C. Rauwendaal, 241, Marcel Dekker Inc., New York (1991)

[201] A.W. Adamson, Physical Chemistry of Surfaces, 5th Ed., John Wiley & Sons, New York (1990)

[202] S.K. Goyal, *Plast. Eng.*, February, 25 (1995)

[203] D.F. Baldwin, C.B. Park, and N.P. Suh, *Polym. Eng. Sci.*, **36**, 1437 (1996)

[204] V. Kumar and N.P. Suh, *SPE, ANTEC, Technical Papers*, ***34***, 715 (1988)

[205] F. Liu, *"Processing of Polyethylene and Polypropylene Foams in Rotational Molding"*, M. A. Sc. Thesis, University of Toronto (1998)

[206] J. McDaid and R.J. Crawford, *SPE ANTEC, Tech. Papers*, ***44***, 1152 (1998)

[207] R. Pop-Iliev, G. Liu, F. Liu, and C.B. Park, *"Rotational Foam Molding of Polypropylene with Control of Melt Strength"*, *Adv. Polym. Tech.*, submitted June 2002

[208] K. Joshi, J.G. Lee, M.A. Shafi, and R.W. Flumerfelt, *J. Appl. Polym. Sci.*, ***67***, 1353 (1998)

[209] S.-T. Lee, N.S. Ramesh, and G.A. Campbell, *Polym. Eng. Sci*, ***36***, 2477 (1996)

[210] R. Pop-Iliev, G.M. Rizvi, and C.B. Park, *SPE, ANTEC, Technical Papers*, ***47***, 1598 (2001)

[211] R.B. Bird, W.E. Stewart, and E.N. Lightfoot, Transport Phenomena, Wiley, New York (1960)

[212] M.A. Shafi, J.G. Lee, and R.W. Flumerfelt, *Polym. Eng. Sci*, ***36***, 1950 (1996)

[213] D.C. Venerus, N. Yala, and B. Bernstein, *J. Non-Newtonian Fluid Mech.,* ***75***, 55 (1998)

[214] N.S. Ramesh, D.H. Rasmussen, and G.A. Campbell, *Polym. Eng. Sci*, ***31***, 1657 (1991)

[215] R. Zheng, P. Kennedy, J. Xu and L. Kishbaugh, *SPE ANTEC, Technical Papers*, ***48*** (2002)

[216] S.-T. Lee, ed., Foam Extrusion: Principles and Practice, Technomic Publishing Company Inc., Lancaster, Pennsylvania (2000)

[217] P. Zoller and D. Walsh, Standard Pressure-Volume-Temperature Data for Polymers, Lancaster, Technomic (1995)

[218] C.D. Han and H. J. Yoo, *Polym. Eng. Sci*, ***21,*** 518 (1981)

[219] C.D. Han, Rheology in Polymer Processing, Academic Press, New York (1976)

[220] P.J. Carreau, D.C.R. Kee, and R.P. Chhabra, Rheology of Polymeric Systems: Principles and Applications, Hanser / Gardner Publications (1997)

[221] R.G. Larson, Constitutive Equations for Polymer Melts and Solutions, Butterworths, Boston (1988)

APPENDIX 1

CALCULATING THE τ_{rr} AND $\tau_{\theta\theta}$ STRESSES USING THE DEWITT MODEL

The Dewitt Model [218, 219,221]:

$$\underset{\approx}{\tau} + \lambda \frac{D \underset{\approx}{\tau}}{Dt} = 2\eta_0 \underset{\approx}{d} \tag{1}$$

Differential Equation Group in spherical coordinate system [218]:

$$\begin{aligned} \tau_{rr} + \lambda\left(\frac{\partial \tau_{rr}}{\partial t} + v_r \frac{\partial \tau_{rr}}{\partial r}\right) &= 2\eta_0 \frac{\partial v_r}{\partial r} \\ \tau_{\theta\theta} + \lambda\left(\frac{\partial \tau_{\theta\theta}}{\partial t} + v_r \frac{\partial \tau_{\theta\theta}}{\partial r}\right) &= 2\eta_0 \frac{v_r}{r} \end{aligned} \tag{2}$$

Using a new variable defined by $y = \frac{\left(r^3 - R^3\right)}{3}$, the differential equations may be rewritten as follows:

$$\begin{aligned} \tau_{rr}(y,t) + \lambda \frac{\partial \tau_{rr}(y,t)}{\partial t} &= -4\eta_0 \frac{R^2 \dot{R}}{3y + R^3} \\ \tau_{\theta\theta}(y,t) + \lambda \frac{\partial \tau_{\theta\theta}(y,t)}{\partial t} &= 2\eta_0 \frac{R^2 \dot{R}}{3y + R^3} \end{aligned} \tag{3}$$

Where, the coefficient λ and η_0 can be determined by the following equation [220]:

$$\eta = \frac{\eta_0}{1 + (\lambda \dot{\gamma})^2} \tag{4}$$

Using experimentally obtained data for LL8556 at 190 °C we can find the value of the coefficient λ :

$$\begin{aligned} \eta_0 &= 1431.99[Pa \cdot s] \\ \lambda &= 0.00634[s] \end{aligned}$$

APPENDIX 2

SIGNIFICANCE OF THE POLYMER MELT PRESSURE PROFILE FOR THE ACCURACY OF THE MODEL PREDICTION

Since the dynamics of the growth and collapse of a single spherical gas bubble in an infinite polymer melt are governed by the conservation of momentum in the radial direction, and since it is assumed that the polymer is a highly viscous fluid so that the inertia items can be neglected, the momentum equation can be written as follows [48]:

$$-\frac{\partial P}{\partial r}+\frac{1}{r^2}\frac{\partial}{\partial r}(r^2\tau_{rr})-\frac{\tau_{\theta\theta}+\tau_{\varphi\varphi}}{r}=0 \tag{1}$$

Taking into account spherical symmetry $(\tau_{\theta\theta}=\tau_{\varphi\varphi})$, an integration of Equation (1) from the bubble wall to a certain arbitrary located boundary within the polymer melt, S, (or ultimately to infinity), relates the stresses within the fluid to the gas pressure inside the bubble and the ambient pressure as given in Equation (2):

$$P(R)-P(S)+\tau_{rr}(S)-\tau_{rr}(R)+2\int_R^S\frac{\tau_{rr}-\tau_{\theta\theta}}{r}dr=0 \tag{2}$$

A force balance at the bubble-liquid interface gives the following relationship:

$$2\pi R\sigma+\pi R^2\left[P(R)-\tau_{rr}(R)\right]_{Liquid}=\pi R^2\left[P_g+\tau_{rr,g}\right]_{Gas} \tag{3}$$

However, due to the low gas viscosity, the member including the gas normal stress in Equation (3) can be neglected, i.e., $\tau_{rr,g}=0$, and thus it reduces to the relationship presented in Equation (4):

$$P(R)=\tau_{rr}(R)+P_g-\frac{2\sigma}{R} \tag{4}$$

By substituting Equation (4) into Equation (2) the following relationship could be derived:

$$P_g - P(S) + \tau_{rr}(S) - \frac{2\sigma}{R} + 2\int_R^S \frac{\tau_{rr} - \tau_{\theta\theta}}{r} dr = 0$$

It could be further rewritten as given by Equation (5):

$$P_g = P(S) - \tau_{rr}(S) + \frac{2\sigma}{R} - 2\int_R^S \frac{\tau_{rr} - \tau_{\theta\theta}}{r} dr \tag{5}$$

Hence, the pressure profile in the polymer melt takes the following form:

$$P_g = P(S) - \tau_{rr}(S) + \frac{2\sigma}{R} - 2\int_R^S \frac{\tau_{rr} - \tau_{\theta\theta}}{r} dr = P(\infty) + \frac{2\sigma}{R} - 2\int_R^\infty \frac{\tau_{rr} - \tau_{\theta\theta}}{r} dr - \tau_{rr}(\infty)$$

If assuming: $r = \infty \Rightarrow \tau_{rr} = 0$, then:

$$P(S) = P(\infty) - 2\int_S^\infty \frac{\tau_{rr} - \tau_{\theta\theta}}{r} dr + \tau_{rr}(S) \tag{6}$$

For a Newtonian fluid, the stress components depend on the rate of deformation. Hence, the above calculation can be simplified as follows:

$$\tau_{ij} = \mu \Delta_{ij} \tag{7}$$

Where, τ_{ij}, represents the ij-th components of the stress tensor [Pa], whereas, Δ_{ij}, represents the ij-th components of the rate of deformation tensor [s^{-1}].

For a spherical coordinate system:

$$\tau_{rr} = -\frac{4\mu R^2 \dot{R}}{r^3} \tag{8a}$$

$$\tau_{\theta\theta} = \frac{2\mu R^2 \dot{R}}{r^3} \tag{8b}$$

Thus:

$$P(S) = P(\infty) - 4\mu \frac{R^2 \dot{R}}{r^3} \Big|_S^\infty - 4\mu \frac{R^2 \dot{R}}{S^3} \tag{9}$$

By substituting Equation (8a) in Equation (4) we obtain:

$$P(R) = P_g - \frac{2\sigma}{R} - 4\mu \frac{\dot{R}}{R}$$

By neglecting the inertia terms from Equation (9) due to high fluid viscosity, we obtain:

$$P(S) \cong P(\infty) \tag{10}$$

Equation (10) shows that the pressure throughout a Newtonian fluid is almost equal to its pressure in infinity (atmospheric pressure in the present case) and that taking into account the pressure profile would not improve the accuracy of the model prediction [48,218].